MATHEMATICAL MODELLING OF *PSEUDOMONAS AERUGINOSA*: CONSIDERING THE ANTIBIOTIC-INDUCED MORPHOLOGICAL TRANSITION TO IMPROVE TREATMENT STRATEGIES

by

CHLOE SPALDING

A thesis submitted to
The University of Birmingham
for the degree of
DOCTOR OF PHILOSOPHY

Supervisor: Dr Sara Jabbari
Co-Supervisor: Professor David J. Smith
Experimental collaborator: Dr Anne-Marie Krachler

School of Mathematics
College of Engineering and Physical Sciences
The University of Birmingham
January 2019

Abstract

Antimicrobial resistance is an urgent global health threat. It is critical that we understand how bacteria respond to antibiotics in order to formulate alternative treatment strategies to combat bacterial infections. β-lactam antibiotics are known to induce a morphological transition in *Pseudomonas aeruginosa* populations; the bacteria shed the cell wall and make the reversible transition from the native rod shape to a fragile spherical shape, consequently evading the effects of the antibiotic.

Through the formulation and analysis of mathematical models, this thesis investigates the impact of the morphological transition during the growth of *P. aeruginosa* infections. Our results suggest that the immune system may play a vital role in clearing persistent spherical populations. By analysing suitable parameter spaces, we show that the interplay between the immune response and the spherical cells could determine the success of combined treatments. We investigate the use of genetic algorithms to obtain tailored treatment strategies and show the need to consider the morphological transition when applying this method to *P. aeruginosa* infections. We advocate the use of an antivirulence drug in combination with antibiotics or antimicrobial peptides as a sequential therapy to eliminate *P. aeruginosa* infections in which the morphological transition occurs.

Dedicated to my beloved Nanna Maureen,

for always inspiring me with your

determination and sass, LOL x

ACKNOWLEDGEMENTS

First and foremost, I would like to thank my supervisor Dr. Sara Jabbari. Words cannot express how fortunate I feel to have had the opportunity to work with you for the last 5 years. Thank you for your guidance, constant encouragement and optimism. I truly appreciate all that you have taught me and the opportunities that you have provided.

I would like to express my gratitude to the University of Birmingham mathematics department with a special mention to my co-supervisor Professor David Smith and Michael Grove for all their advice and support. I would like to thank EPSRC for funding this research and to our experimental collaborators Dr. Anne-Marie Krachler and Emma Keen, it was a pleasure working with you both.

To my wonderful family, thank you for the encouragement, support and for showing (feigning?) an interest when I try to explain my research. Thanks to all of my friends in Birmingham and especially my twin Dr. Gemma Cupples; you have all made the last 4 years fly by. Sophie and Jack, thank you for the constant support and for all of the jokes that I never understand. To all of the Bandits and Lads Lads Lads, thank you for the endless entertainment over the last 4 years; you are the best group of friends anyone could ever ask for. Finally, a huge thank you to Ethan for teaching me to always believe in myself, you are officially the world's best hypeman.

CONTENTS

1 Introduction **1**

1.1 Antimicrobial Resistance 1

1.2 *Pseudomonas aeruginosa* and meropenem 4

1.3 Mechanisms of resistance and persistence 5

1.3.1 Resistance mechanisms used by *P. aeruginosa* 5

1.3.2 Persistence mechanisms 10

1.3.3 Cell wall deficient bacteria 12

1.4 Novel approaches to treating *P. aeruginosa* infections 14

1.4.1 Understanding the role of selective pressure in the development of AMR 14

1.4.2 Antibiotics vs. antivirulence drugs 17

1.4.3 Antivirulence drug resistance 18

1.4.4 Target mechanisms for antivirulence drug strategies 21

1.4.5 Combination therapies 25

1.4.6 Optimising antimicrobial usage 26

1.5 Mathematical modelling of bacterial infections 28

1.5.1 Formulating an ODE population dynamics model to describe bacterial growth 29

1.6 Project overview 40

2 Modelling the growth of *P. aeruginosa* in isolation with meropenem **44**

2.1 Model formulation 45

2.2 Parametrisation data and methods . . . 51
2.3 Results . . . 53
2.3.1 Model parametrisation . . . 53
2.3.2 Parameter testing . . . 59
2.3.3 Manipulating the morphological transition . . . 64
2.4 Discussion . . . 69

3 Modelling resistance to meropenem via upregulation of efflux pumps 74
3.1 Model formulation . . . 76
3.2 Results . . . 82
3.2.1 Modelling limited or no antibiotic treatment . . . 82
3.2.2 Modelling a constant infusion of antibiotic . . . 84
3.2.3 Investigating parameter values attributed to a resistant strain . . . 94
3.3 Discussion . . . 97

4 An infection level model 99
4.1 Model formulation . . . 100
4.2 Bacterial growth in the absence of antibiotic . . . 105
4.2.1 Single strain infection . . . 105
4.2.2 Investigating the emergence of resistance . . . 107
4.3 Introducing the antibiotic . . . 108
4.3.1 Single strain infection . . . 111
4.3.2 Investigating the emergence of resistance . . . 113
4.4 Considering alternative treatments . . . 116
4.4.1 AMPs . . . 116
4.4.2 Antivirulence drugs . . . 121
4.4.3 Triple combinations . . . 127
4.5 Phagocytosis rate . . . 129
4.5.1 Antibiotic-susceptible infection . . . 129

4.5.2 Antibiotic-resistant infection . . . 132
4.5.3 Mixed strain . . . 136
4.6 Recruitment rate . . . 139
4.6.1 Antibiotic-susceptible infection . . . 139
4.6.2 Antibiotic-resistant infection . . . 145
4.6.3 Mixed strain . . . 146
4.7 Discussion . . . 148

5 Considering the morphological transition of *P. aeruginosa* to optimise antibiotic usage 155
5.1 Model formulation . . . 157
5.2 Detail of the genetic algorithm . . . 159
5.3 Results . . . 162
5.3.1 Investigating antibiotic dosing regimens for a rod-shaped population 162
5.3.2 Investigating antibiotic dosing regimens for a population that utilises the antibiotic-induced morphological transition . . . 164
5.4 Discussion . . . 170

6 Discussion 171

Appendix A: Materials and Methods 177
A.1 Staining and fluorescence microscopy . . . 177
A.1.1 Microscopy images for displaying transition . . . 177
A.1.2 Microscopy images for parameter testing . . . 178
A.2 Growth curves for model parametrisation . . . 179

List of References 180

LIST OF FIGURES

1.1 The cell structure of a typical prokaryotic cell. 1

1.2 The arrangement of proteins formulating an efflux pump system within the cell membrane. 9

1.3 The saturating term used to model antibiotic action. 33

2.1 Cells of the meropenem-susceptible *P. aeruginosa* PA1008 strain transitioning between a rod and spherical shape. 45

2.2 Schematic representation of the transitions of *P. aeruginosa* in response to exposure to meropenem. 46

2.3 The solution to Model I, with $A_0 = 0$, using the parameters obtained by parametrising with Data set 1. 54

2.4 The solution to Model I using parameter sets Θ_1 and Θ_2, plotted along with the data points from Data set 1. 57

2.5 The long term solution to Model I, with $A_0 = 2$, using parameter sets Θ_1 and Θ_2. 58

2.6 Individual variable solutions to Model I, with $A_0 = 2$, using parameter sets Θ_1 and Θ_2. 59

2.7 The solution to Model I, with $A_0 = 0$, using the parameters in (2.10) and plotted with the additional test data for the growth curve of *P. aeruginosa* (Data set 2). 60

2.8 The solution to Model I using parameter sets Θ_1 and Θ_2, plotted with the additional test data (Data set 2). 61

2.9 Comparing the predicted variable solutions (to Model I) to the data obtained from the microscopy images. 65
2.10 Simulations displaying predictions of bacterial growth with variations to key parameter values. 66

3.1 Cells of the partially meropenem-resistant *P. aeruginosa* PA1004 strain transitioning between a rod and spherical shape. 75
3.2 Schematic representation of the transitions of *P. aeruginosa* in response to exposure to meropenem with the inclusion of active efflux. 77
3.3 The solution to Model II, using the default parameter set, with no antibiotic or a single dose of $10\mu g\,ml^{-1}$ of antibiotic. 85
3.4 The solution to Model II with a constant dose treatment, with $A_0 = 10\,\mu g\,ml^{-1}$, using the default parameter set. 88
3.5 The individual variable steady state solutions to Model II with a constant dose treatment, with $A_0 = 10\,\mu g\,ml^{-1}$, using the default parameter set and varying the growth rate, r. 91
3.6 The individual variable steady state solutions to Model II with a constant dose treatment, with $A_0 = 10$, using the default parameter set and varying the internalisation rate, ν. 92
3.7 The solution to Model II with a constant dose treatment, with $A_0 = 10\,\mu g\,ml^{-1}$, using the default parameter set with $\omega = 0$ and variations to key parameter values. 94
3.8 The solution to Model II with a constant dose treatment, with $A_0 = 10\,\mu g\,ml^{-1}$, using the default parameter set and varying the efflux pump upregulation constant, ω. 95
3.9 The solution to Model II with a constant dose treatment, with $A_0 = 10\,\mu g\,ml^{-1}$, using the default parameter set, with $\omega = 0.5$ and variations to keys parameter values. 96

3.10 The solution to Model II with a constant dose of antibiotic, with $A_0 = 10\,\mu\text{g}\,\text{ml}^{-1}$, using the default parameter set, with $\omega = 0.5$ and varying the fitness cost, c. 97

4.1 Transitions of a mixed strain *P. aeruginosa* infection in response to antibiotic action and host defences. 101

4.2 Growth of a single strain infection of *P. aeruginosa* at a site of infection in the absence of treatment. 107

4.3 Investigating how the initial condition and fitness cost influence the emergence of resistance during the growth of a mixed strain population of *P. aeruginosa* in the absence of antibiotic. 109

4.4 Investigating how resistance-attributed parameters influence the emergence of resistance during the growth of a mixed strain population of *P. aeruginosa* in the absence of antibiotic. 110

4.5 Growth of a single strain population of *P. aeruginosa* at a site of infection during a constant infusion of antibiotic. 112

4.6 Investigating how resistance-attributed parameters influence the steady state population of resistant bacteria after a continued dose of antibiotic is used to treat a mixed strain infection of *P. aeruginosa*. 115

4.7 Administering a continuous combined dose of antibiotic and AMPs to a susceptible population of *P. aeruginosa* with identical immunogenic properties for all cell types. 118

4.8 Investigating the effects of AMP efficacy on treatment duration needed for the combined therapy of antibiotics and AMPs. 119

4.9 Administering a continuous combined dose of antibiotic and AMPs to an antibiotic-resistant population of *P. aeruginosa* with identical immunogenic properties for all cell types. 120

4.10 Administering a continuous combined dose of antibiotic and AMPs to a mixed strain population of *P. aeruginosa* with identical immunogenic properties for all cell types. 122
4.11 Administering a continuous dose of an antivirulence drug to an antibiotic-susceptible population of *P. aeruginosa* with identical immunogenic properties for all cell types. 123
4.12 Administering a continuous combined dose of the antibiotic and an antivirulence drug to an antibiotic-susceptible population of *P. aeruginosa* with identical immunogenic properties for all cell types. 125
4.13 Administering a continuous combined dose of the antibiotic and an antivirulence drug to an antibiotic-resistant population of *P. aeruginosa* with identical immunogenic properties for all cell types. 126
4.14 Administering a constant dose of a triple combination of antibiotics, AMPs and an antivirulence drug to a single strain population of *P. aeruginosa* with identical immunogenic properties for all cell types. 128
4.15 Administering a constant dose of a triple combination of antibiotics, AMPs and an antivirulence drug to a mixed strain population of *P. aeruginosa* with identical immunogenic properties for all cell types. 128
4.16 Varying the phagocytosis rate of the spherical cells in an antibiotic-susceptible population of *P. aeruginosa* during a continued dose of antibiotic. 131
4.17 Administering a constant dose of a triple combination of antibiotics, AMPs and an antivirulence drug to a susceptible population of *P. aeruginosa* containing a spherical subpopulation with a default or slow phagocytosis rate. 132
4.18 Varying the phagocytosis rate of the spherical cells in an antibiotic-resistant population of *P. aeruginosa* during a continued dose of antibiotic. 133

4.19 Administering a continuous combined dose of antibiotic and AMPs to an antibiotic-resistant population of *P. aeruginosa* containing a spherical subpopulation with a slow phagocytosis rate. 135
4.20 Varying the phagocytosis rate of the spherical cells in a mixed strain population of *P. aeruginosa* during a continued dose of antibiotic. 137
4.21 Administering a continuous combined dose of antibiotic and AMPs to a mixed strain population of *P. aeruginosa* containing a spherical subpopulation with a slow phagocytosis rate. 138
4.22 Administering a continuous combined dose of antibiotic and an antivirulence drug to a mixed strain population of *P. aeruginosa* containing a spherical subpopulation with a slow phagocytosis rate. 140
4.23 Administering a constant dose of a triple combination of antibiotics, AMPs and an antivirulence drug to a single strain population of *P. aeruginosa* containing a spherical subpopulation with a slow phagocytosis rate. 141
4.24 Varying the phagocyte recruitment rate of the spherical cells in a antibiotic-susceptible population of *P. aeruginosa* during a continued dose of antibiotic. 142
4.25 Administering a constant dose of antibiotic and AMPs to an antibiotic-susceptible population of *P. aeruginosa* containing a spherical subpopulation with a slow phagocyte recruitment rate. 143
4.26 Administering a constant dose of antibiotic and an antivirulence drug to an antibiotic-susceptible population of *P. aeruginosa* containing a spherical subpopulation with a slow phagocyte recruitment rate. 144
4.27 Administering a constant dose of a triple combination of antibiotics, AMPs and an antivirulence drug to an antibiotic-susceptible population of *P. aeruginosa* containing a spherical subpopulation with a slow phagocyte recruitment rate. 145
4.28 Varying the phagocyte recruitment rate of the spherical cells in a mixed strain population of *P. aeruginosa* during a continued dose of antibiotic. . 147

4.29 Administering a constant dose of antibiotic and AMPs to a mixed strain population of *P. aeruginosa* containing a spherical subpopulation with a slow phagocyte recruitment rate. 148
4.30 Administering a constant dose of a triple combination of antibiotics, AMPs and an antivirulence drug to a mixed strain population of *P. aeruginosa* containing a spherical subpopulation with a slow phagocyte recruitment rate. 149

5.1 Dynamics of Model IV over 20 days with a 10 day traditional treatment regimen with a constant daily dose of $14\mu g\,ml^{-1}$. 163
5.2 Populations of rod-shaped and spherical cells after a traditional treatment regimen of varied antibiotic doses. 165
5.3 Simulating a sequential treatment strategy consisting of a tailored antibiotic treatment strategy followed by a constant dose of AMPs. 169

LIST OF TABLES

1.1 Review of mathematical models I-IV. 43

2.1 Definitions and units for the variables in Model I, described by equations (2.1)-(2.5). 50

2.2 Definitions and units for the parameters in Model I, described by equations (2.1)-(2.5). 50

2.3 Parameter sets Θ_1 and Θ_2, estimated using Model I and Data set 1. 55

2.4 Estimated initial conditions for Model I. 56

2.5 The average proportions of each bacterial subpopulation, obtained using the microscopy images. 63

3.1 Definitions and units for the variables in Model II, described by equations (3.6)-(3.10). 82

3.2 Definitions, units and default values for the parameters in Model II, described by equations (3.6)-(3.10). 83

4.1 Definitions and units for the variables in Model III, described by equations (4.1)-(4.9). 104

4.2 Definitions, units and default values for the parameters used in Model III, described by equations (4.1)-(4.9). 106

4.3 A review of the results for the treatments considered in Chapter 4. 150

5.1 Definitions and units for the variables in Model IV, described by equations (5.1)-(5.4). 159

5.2 Definition, units and default values for the parameters in Model IV, described by equations (5.1)-(5.4). 160
5.3 Comparison of the dosage vectors chosen by the GA to treat an infection that does not utilise the morphological transition ($\gamma = 0$ day^{-1}). 163
5.4 Comparison of the dosage vectors chosen by the GA to treat an infection that utilises the morphological transition ($\gamma = 1$ day^{-1}). 166
5.5 Comparison of the dosage vectors chosen by the GA to treat an infection that utilises the morphological transition ($\gamma = 1$ day^{-1}) but does not revert back to the rod-shape ($\delta = 0$ day^{-1}) 168

GLOSSARY OF TERMS

Apoptosis The process of programmed cell death..

Bactericide An agent that kills bacteria.

Bacteriostat An agent that prevents bacteria from growing.

Gram positive Used to describe bacteria that have a cell wall comprising a thick peptidoglycan layer.

Gram negative Used to describe bacteria that have a cell wall comprising a thin peptidoglycan layer that is surrounded by a thick plasma membrane.

Hydrolysis The chemical breakdown of a compound due to reaction with water.

Nosocomial Acquired or occurring in a hospital.

Phagocyte A type of cell within the body capable of engulfing and absorbing bacteria and other small cells and particles.

Phagocytosis The engulfment of bacteria and other small cells or particles by phagocytes.

Pleomorphic The ability of a micro-organism to alter its size or shape in response to environmental conditions.

Quorum sensing A process of cell-to-cell communication that enables allows bacteria to detect and to respond to cell population densities by gene regulation.

ABBREVIATIONS

AMPs Antimicrobial peptides.

CWDB Cell wall deficient bacteria.

GA Genetic algorithm.

HDTD High dose tapered doses.

HGT Horizontal gene transfer.

MDR Multi-drug resistance.

MIC Minimum inhibitory concentration.

OMP Outer membrane protein.

PAMPs Pathogen-associated molecular patterns.

PBP Penicillin-binding proteins.

PD Pharmacodynamics.

PDD Pathogen-density dependent.

PDI Pathogen-density independent.

PK Pharmacokinetics.

QS Quorum sensing.

RND Resistance-nodulation-division.

ROS Reactive oxygen species.

T3SS Type 3 secretion system.

UTI Urinary tract infection.

VGT Vertical gene transfer.

CHAPTER 1

INTRODUCTION

1.1 Antimicrobial Resistance

Pathogenic bacteria are prokaryotic cells that are able to reproduce asexually through the process of binary fission; the basic structure of a prokaryote can be seen in Figure 1.1. Bacterial infections occur when pathogenic bacteria enter the body and disrupt the cellular processes of the host cells or kill the host cells. Once the bacterial population is detected, the immune system can initiate an immune response in an attempt to eliminate the infection. The immune response can subsequently cause many symptoms as it attempts to clear the infection.

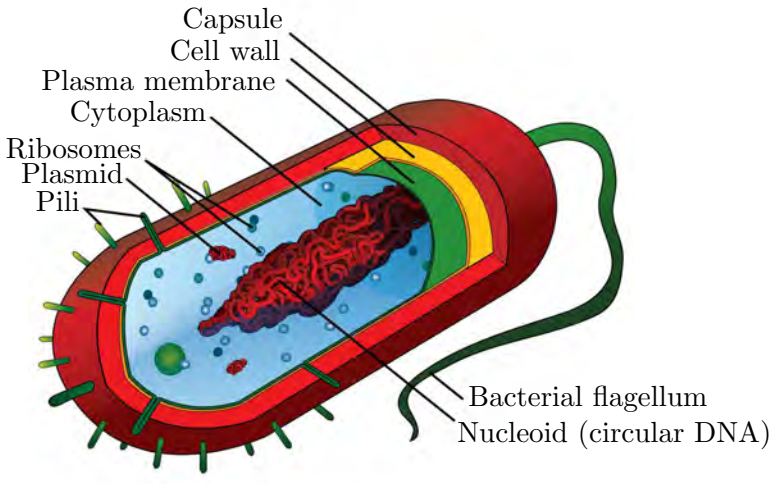

Figure 1.1: The cell structure of a typical prokaryotic cell. Public domain image adapted from [71].

In cases where the immune response is unable to eliminate the infection, further treatment is necessary. Over the last century we have managed to treat bacterial infections using multiple classes of antibiotics. However, the use of antibiotics has placed an evolutionary pressure on bacterial species and as a result, pathogenic bacteria have adapted and mutated to become less susceptible to antibiotics. Antimicrobial resistance (AMR) is now acknowledged as an urgent global health threat and the severity of the situation was highlighted by the World Health Organization 2014 report that discusses the increasing incidence of resistance-induced health problems in every region of the world [84]. A "post-antibiotic" era is described, where even a simple infection can become fatal as current drug strategies fail to ameliorate previously manageable infections.

It was Paul Ehrlich's idea of a "magic bullet" that first sparked the concept of a drug that would only target pathogenic microbes and not the host cell. His ideas led him to systematically screen different derivatives of the toxic drug Atoxyl in search for a drug that would cure syphilis without causing unwanted side effects. The screening process, which took place between 1904 and 1909, was a success and is often credited for the change in drug research strategies within the pharmaceutical industry. This systematic approach was similar to that of the most famous antibiotic advancement, the discovery of penicillin by Alexander Fleming in 1929 [37]. Howard Florey and Ernest Chain (1945) [21] followed Fleming's work and published a paper describing the purification strategies needed to enable scientists to clinically test penicillin and subsequently mass produce and distribute the first globally acknowledged antibiotic. The following decades between 1950 and 1970 are referred to as the golden era of antibiotic discovery, with many novel classes of antibiotics being discovered in this time [4]. However, since then, there have been few advancements in novel antibiotic discovery and substantial resistance to most classes has been observed [24]. Resistance was identified even in the earliest stages of antibiotic discovery but the positive impact of using the drugs was assumed to outweigh the possible threat of resistance. This is no longer the case, and the potential of resistance to become a worldwide epidemic is becoming more appreciable, as an increase in resistant strains

and phenotypic changes within common bacteria means our ability to cure infections with antibiotics alone becomes increasingly more challenging.

Many bacterial populations also display persistent characteristics that make it very difficult to completely clear bacterial populations. *Persistence*, is a result of heterogeneity and describes the ability of a subpopulation of a bacterial population to survive antibiotic exposure by adapting their functionality [18]. This subpopulation of persister cells form due to environmental pressure, such as antibiotic exposure, and can lay dormant until more favourable conditions occur, at which point the possibility of reversion results in persistent infections that do not necessarily rely on resistance genes. Persistence differs from resistance, the second of these can be defined by the ability of a bacterial species to grow at high concentrations of antibiotic and can be quantified using the minimum inhibitory concentration (MIC) value [18]. Whilst antibiotic-susceptible and -resistant bacteria have distinct differences in their genetic make-up, it is important to note that persistent bacteria are genetically identical, yet phenotypically different, to the rest of their population. Both phenomenon are examples of survival modes that bacteria can use to survive antibiotic action; as these strategies become more prevalent in bacterial species, humans and animals become more vulnerable.

Since the report by the World Health Organization, more pressure is being placed on governments and pharmaceutical companies to invest in the fight against AMR. The wide interpretation of how to tackle the problem of AMR has resulted in a wealth of research from a vast number of scientific areas from chemistry to social science and interdisciplinary work has proven essential in harnessing new ideas and techniques. A constitutive area in which we can help make those advances is with involvement of mathematical modelling. Identifying and understanding the population dynamics of bacterial growth can provide insight into the behaviour of the bacteria under different drug strategies. If it is possible to predict the effects of a drug using mathematical analysis, we can corroborate existing experimental advances and direct future laboratory work, helping to cut down the time and money needed to make further advances.

It is crucial that we find new ways to cope with bacterial infections and that we not only understand the pathogenesis of a bacterial infection but also how the mechanisms of antibiotics work, the bacterial responses that occur due to the threat of antibiotic action and how this results in the emergence and maintenance of resistance within bacterial populations. The more we discover about bacteria, the better chance we have of formulating novel treatment strategies. Additionally, as we increase our understanding of currently used treatments, we increase our ability to optimise them in order to try and minimise the development of resistance.

1.2 *Pseudomonas aeruginosa* and meropenem

Pseudomonas aeruginosa is a Gram-negative pathogenic bacteria that shows notable levels of resistance to many antibiotics. This extremely versatile, opportunistic pathogen is able to acquire nutrients from a wide range of organic matter, meaning that it can easily infect damaged tissues in animals and humans. *P. aeruginosa* is a leading cause of nosocomial infection and can thrive in moist environments and on hospital instruments such as catheters. Infections are often found in airways, urinary tracts and in burns and wounds and can often be asymptomatic until a biofilm forms. Biofilm formation can overwhelm the immune system, cause bacteraemia, pneumonia and sepsis, and can ultimately lead to death; this makes *P. aeruginosa* especially threatening to those who are immunocompromised, including in particular patients with cystic fibrosis [62].

In comparison to other pathogens, *P. aeruginosa* is relatively hard to eradicate, due to its capability to survive under extreme stresses, including antibiotic action. *P. aeruginosa* bacteria can readily adjust physiological processes in response to environmental cues and employ a diverse range of resistance mechanisms.

There are several antibiotics that still have activity against *P. aeruginosa* including some classes of β-lactams, the most widely used group of antibiotics. β-lactams are identified by possessing a β-lactam ring in the molecular structure and this class of antibiotics,

also including penicillin derivatives and cephalosporins, inhibits cell wall synthesis by binding to penicillin binding proteins (PBPs). Inhibition of cell wall synthesis results in structural changes to the bacteria and ultimately leads to lysis. Carbapenems are a class of β-lactams that exhibit a broader spectrum of activity to other classes within the β-lactam family and include imipenem and meropenem. Meropenem has enhanced activity against Gram-negative bacilli compared to other carbapenems due to its affinity for both PBP2 and PBP3 enzymes, which lead to inhibition of peptidoglycan synthesis at different regions of the bacterial wall [101]. Meropenem has been shown to induce morphological changes within populations of *P. aeruginosa* with both large spheroplasts and long filamentous cells observed [104].

In addition to the multi-drug resistant strains of *P. aeruginosa* that cannot be treated using traditional antimicrobial therapies, there is also evidence that some genetically susceptible strains are able to tolerate the presence of many β-lactams, including meropenem, for periods of time. We will now discuss some of the characteristics and mechanisms that can permit *P. aeruginosa* to survive antibiotic exposure.

1.3 Mechanisms of resistance and persistence

1.3.1 Resistance mechanisms used by *P. aeruginosa*

There are multiple mechanisms that, when expressed, permit bacteria to resist antibiotics; some resistance mechanisms are intrinsic whilst others are acquired and enable previously susceptible bacteria to develop resistance. Intrinsic resistance mechanisms are part of the genetic make-up of a bacteria and can incur a basic level of resistance to certain classes of antibiotics. Bacteria can also acquire resistance via chromosomal mutation or by obtaining new genetic material.

Intrinsic resistance can be defined as the innate ability of a bacterial species to resist or tolerate antibiotic through features of its inherent structure or characteristics. Intrinsic

resistance mechanisms can be found in common strains of bacteria and lead to high MICs. Occurring irrespectively of antibiotic exposure, these mechanisms render many classes of antibiotics ineffective in clearing bacterial infections.

In addition to the chromosomal encoded resistance mechanisms, bacteria can easily acquire additional genes that can increase the efficacy of the intrinsic mechanisms and result in further resistance. Genetic resistance involves the acquisition of new information via vertical gene transfer (VGT) or horizontal gene transfer (HGT). VGT refers to mutational events that occur during bacterial proliferation and can enhance intrinsic mechanisms. The mutational frequency rate will differ depending on the bacteria and antibiotic and mutations can cause various levels of resistance in bacteria. A single mutation could have a limited effect on bacterial resistance or it could cause the bacteria to be completely untreatable by certain antibiotics. Additionally it is possible that a number of mutations could work synergistically to cause much higher levels of resistance than if the mutations occurred in isolation.

Bacteria may also acquire genetic resistance from other bacteria. HGT is often plasmid-mediated; the plasmid (or other DNA element) acts as a vehicle and delivers the genetic material to the recipient, usually via conjugation. Plasmids that carry multiple resistance genes can induce multidrug resistance and it is possible for broad host plasmids to transfer genes to other bacterial species.

Additionally, unfavourable conditions, such as sub-inhibitory antibiotic concentration levels, can induce adaptive resistance. Adaptive resistance is relatively poorly understood, yet it can lead to higher antibiotic tolerance of bacteria. Resistance of this type is unstable and not inherited; the bacteria express the resistance genes whilst the environmental stresses are unfavourable and revert to the wild-type and regain susceptibility once conditions become more favourable.

P. aeruginosa is known for its decreased susceptibility to multiple classes of antibiotics; high levels of intrinsic resistance and an array of adaptive mechanisms allow even clinically susceptible strains to persist and survive. In combination with acquired mechanisms of

resistance or due to mutations, *P. aeruginosa* is able to achieve clinical resistance and can become extremely difficult to treat. Here we introduce some of the main resistance mechanisms used by *P. aeruginosa* to evade antibiotic effects.

Low membrane permeability

P. aeruginosa strains can be intrinsically resistant to many classes of antibiotics and genetically susceptible strains often have lower antibiotic susceptibility than other bacteria. One mechanism that is often credited to the inherently reduced susceptibility of *P. aeruginosa* is its low membrane permeability [43].

The cell envelope of a Gram-negative bacteria is characteristically comprised of a cytoplasmic membrane and an additional outer membrane. The outer membrane itself is made up of a lipid bilayer that acts as a hydrophobic barrier around the cell and is impermeable to large charged molecules. Embedded within the outer membrane are outer membrane proteins (OMPs) that mediate diffusion of molecules across the membrane. There are multiple types of OMPs, including porins, water filled channels that allow diffusion of hydrophilic molecules, such as nutrients or β-lactams, across the hydrophobic core. Porin channels differ in size and specificity and therefore successful translocation will often depend on the size and type of the molecule.

The outer membrane of *P. aeruginosa*, which is 12-100 times less permeable than that of *Escherichia coli*, imposes a restriction on the level of antibiotic uptake compared to other bacterial species [79]. In addition to low intrinisic permeability, *P. aeruginosa* down-regulates porin expression to further decrease membrane permeability. By decreasing the number and size of non-specific porin channels, the bacteria are able to slow down the transportation of antibiotic molecules into the cell. Specifically, the uptake of carbapenems, including meropenem, occurs through the OprD porin; it has been shown that many strains that show resistance to these antibiotics are OprD deficient mutants [105].

Whilst low membrane permeability does restrict antibiotic uptake within a cell, it does not permit resistance to all classes of antibiotics. For significantly high levels of

intrinsic resistance, the bacteria depend on secondary intrinsic and adaptive resistance mechanisms, such as efflux and enzyme production, that benefit from the decrease in intracellular antibiotic caused by low membrane permeability.

Efflux pumps

Active efflux systems provide an additional mechanism to decrease the intracellular antibiotic concentration and contribute to resistant properties of bacteria. In Gram-negative bacteria, such as *P. aeruginosa*, multidrug resistance (MDR) efflux systems often form tripartite systems comprising of three proteins. Specifically, the efflux of antipseudomonal antibiotics is mediated by efflux systems belonging to the resistance-nodulation-division (RND) family [67, 66]. The arrangement of these proteins can be seen in Figure 1.2; the first protein, located in the cytoplasmic membrane, acts as the pump with wide substrate specificity. There is a second membrane fusion protein that links the membrane proteins and finally a gated outer membrane protein. Together, these proteins combine to produce a pump system that can remove antibiotic molecules and other toxic molecules from within the cytoplasmic membrane or periplasm of a bacterium.

Efflux systems are ubiquitous in all living cells and efflux expression at low levels can contribute to intrinsic resistance. It was initially thought that the naturally low susceptibility of *P. aeruginosa* was a result of low membrane permeability but it is now accepted that active efflux is a codeterminent of intrinsic resistance, along with membrane impermeability. Upregulation of efflux systems often occurs due to mutations in the bacterial genome; overexpression of RND efflux systems can increase multidrug resistance and decrease susceptibility to antibiotics that were previously effective, including meropenem [66].

It is also believed that efflux pumps assume additional roles in bacterial physiology that augment bacterial virulence. It is thought that they can be highly influential in the quorum sensing systems due to their ability to translocate quorum sensing signal molecules across the cellular membrane [2]. The impact of these molecules on bacterial virulence

suggests that efflux pumps may not only be associated with resistance but influential in the expression of the virulent characteristics of the bacteria.

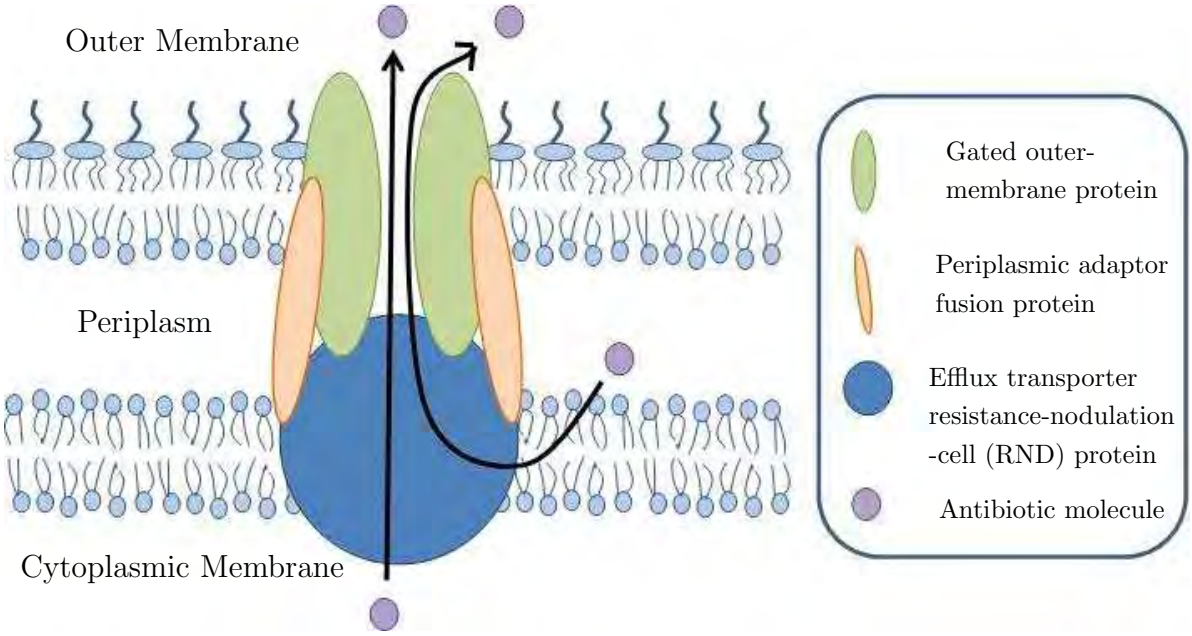

Figure 1.2: The arrangement of proteins formulating an efflux pump system within the cell membrane. Antibiotics that have been successful in crossing the membrane can be effluxed out along with molecules in the periplasm.

β-lactamases

In addition to decreasing the level of antibiotic within a cell, bacteria produce enzymes that are capable of modifying antibiotics, rendering them inactive and therefore allowing the bacteria to resist antibiotic effects. Different bacterial species can produce an array of enzymes that may be used to target a certain class of antibiotic or a specific antibiotic within that class. As we are interested in the resistance mechanisms of *P. aeruginosa* in response to β-lactams, and particularly meropenem, we focus on the β-lactamase class of enzymes.

There are multiple β-lactamases that are effective against multiple classes of antibiotics including penicillins, cephalosporins and carbapenems. The mode of action of these enzymes involves hyrodlysing the β-lactam ring, found in all β-lactam molecules, rendering it ineffective at binding to the bacteria. In Gram-negative bacteria, these enzymes

are often found in the periplasm and hydrolyse antibiotic molecules that have managed to traverse the cell wall. Therefore, in *P. aeruginosa* bacteria enzymes can take full advantage of the low intracellular antibiotic concentrations that occur due to low membrane permeability.

The chromosomal-encoded AmpC β-lactamase confers intrinsic resistance to some β-lactam antibiotics and the genes for enzyme production are expressed upon exposure to the antibiotic. Baseline levels of AmpC have been shown not to deter the effects of broad range β-lactams including meropenem, which has shown high levels of resistance to β-lactamases. Nevertheless, it is possible that extended mutational derepression of AmpC production may cause resistance to most classes of antibiotics, including meropenem.

In addition to the intrinsically encoded production, and possible overproduction, of AmpC β-lactamase, *P. aeruginosa* can resist more classes of antibiotic by acquiring genetic information via HGT. Additionally, pre-exposure to sub-inhibitory levels of antibiotics can cause an increase in β-lactamase. An example of adaptive resistance, this mechanism enables the bacteria to survive further exposure to antibiotics. Of particular clinical importance is the spread of plasmids that encode extended-spectrum β-lactamases (ESBLs), which are effective against multiple classes of β-lactam antibiotics. An increase in bacteria carrying EPBL genes resulted in an increase in the use of carpabenems. Consequentially, an increase in isolates carrying carpabenem-specific β-lactamases has increased and although initially chromosomal, these genes are now plasmid-mediated [88, 89, 107]. The prevalence of these enzymes within multiple bacterial species threatens the clinical efficacy of all antibiotic classes.

1.3.2 Persistence mechanisms

As with adaptive resistance, persistence arises in response to environmental stimuli that threaten bacterial survival. However, persistence differs to resistance in that not all bacteria in the population display the same characteristics that allow them to survive. Instead, only a small subpopulation of a clonal population display persistent characteristics. The

persistent subpopulation will adapt in order to survive environmental stresses such as nutrient limitation, oxidative stresses and antibiotic exposure. Under the stress of antibiotic exposure, the subpopulation of persister cells will survive for longer whilst the remaining non-persisting bacteria are quickly killed.

Persistence can occur due to a range of adaptations by the bacteria and the underlying mechanisms of persistence are not fully understood. Persister cells may reduce metabolic processes, such as virulence factor expression and proliferation, and lay dormant until environmental stresses subside. It is widely hypothesised that persistence is often characterised by a slower growth rate or an extended lag phase. Both of these characteristics reduce the susceptibility of the bacteria since many bactericidal antibiotics, such as β-lactams, target actively growing cells.

Persisters may sacrifice bacterial growth and development in order to survive and once more favourable environmental conditions occur, they can revert back to their original form and regain susceptibility in the process. The persister cells have not acquired resistance and as with adaptive resistance, decreased susceptibility is non-inheritable. It was shown that if a subpopulation of persister cells is initially grown in the absence of antibiotic and then re-exposed to antibiotic, the same heterogeneous response was recorded. Instead of the total population of daughter cells also displaying persistent characteristics, only a subpopulation of cells formed a persister population [15].

Many bacterial species display persistence-led survival including *E. coli*, *Staphylococcus aureus* and *P. aeruginosa*. Dealing with persistence is of great clinical importance and *P. aeruginosa* strains with high levels of persister cells have been shown as a major threat to the eradication of infection in cystic fibrosis patients [78]. Additionally, it has been suggested that persistence could be the cause of the disparity between *in vitro* MIC values and *in vivo* efficacy of antibiotics [43]. Although little is known about the underlying mechanisms that cause persistence in *P. aeruginosa*, persistence genes that have been identified could hint towards prospective targets for novel treatments [31]. New treatment strategies must be designed to not only cope with multiple strains, including

resistant strains, but also to acknowledge heterogeneous populations that include persister populations.

1.3.3 Cell wall deficient bacteria

The cell wall is a critical component of the cell structure and we have previously reviewed the role of the outer membrane in controlling the translocation of molecules across the cell envelope. The semi-permeability of the cell wall protects the bacteria from external influences and bacterial division also relies heavily on cell wall machinery. Additionally, cell shape and integrity are determined by the cell wall as it counteracts the outward pressure from within the cell and maintains the balance of turgor pressure. As an integral constituent of the bacterial structure, the cell wall has become an attractive target for antimicrobials, including the cell wall synthesis inhibiting β-lactams. Furthermore, the cell wall is also recognizable to the immune system, making it a target to host defence cells such as neutrophils and macrophages, collectively referred to as phagocytes.

Despite the importance of the cell wall, many bacterial species, including *P. aeruginosa*, can convert to a cell wall-deficient form in the presence of an inducing agent [35]. These cell wall-deficient bacteria (CWDB) can have no or little intact cell wall; the consequent imbalance of internal pressure will often cause the cell to change shape and form a large round cell. These pleomorphic forms have altered characteristics to the wild-type (WT) and characteristics such as viability will depend on several decisive factors such as the nutrient availability and external pressure.

Originally discovered in 1935 by Emmy Klieneberger [57] these bacteria were named L-forms, in honour of the Lister Institute where Klieneberger worked. Following this discovery there has developed some uncertainty surrounding the terminology used to describe cells that shed the cell wall in this way with terms such as L-forms, spheroplasts and protoplasts all being used to describe cells with varying characteristics. Often L-forms are described as CWDB that can proliferate, albeit at a much slower rate than walled bacteria and under specific osmoprotective conditions [35]. An L-form that is unstable is

assumed to be able to revert back to the cell-walled form whereas a stable L-form cannot and will stay in the spherical shape [35]. Additionally, protoplast and spheroplasts are described by their inability to proliferate and are distinguished by whether the bacteria is Gram-positive or -negative respectively [28, 36]. The controversy surrounding the correct nomenclature for these cells may have arisen due to the difficulty to accurately grow and identify these cells *in vitro* and because of the varying characteristics of CWDB in different bacterial species. Throughout this work we will refer to these pleomorphic forms as CWDB and we focus our interest on the CWDB that emerge in *P. aeruginosa* populations.

CWDB can be induced *in vitro* and have also been extracted from multiple bacterial infections. They have intrigued scientists for years and whilst the clinical relevance of these cells is often queried the potential threat and consequences of these aberrant forms should be appreciated [35, 83]. CWDB pose the potential to evade antibiotic effects and the possibility of reversion suggests that CWDB could permit the persistent characteristics of many bacterial species.

The work of Monahan et al. [75] investigates the tolerance of *P. aeruginosa* to β-lactam antibiotics, including meropenem, and suggests that the ability of the bacteria to withstand high concentrations of β-lactams can be attributed to a rapid transition of the population to a cell-wall deficient state. The experimental results show that antibiotic exposure induces a transition in morphology that produces a subpopulation of spherical CWDB. Whilst it was first thought that the cell wall deficient spherical cells would lyse due to the delicate structure of the cell, it was found that not only did the whole population of cells transition from rod-shaped to spherical within 24 hours, but also 84% of these cells were viable and able to transition back to rod-shaped cells in the absence of the meropenem [75].

This study suggests that the morphological transition of the WT bacteria to CWDB could be described as a survival strategy that enables the bacteria to evade antibiotic effects. Conversely, in [28], the formation of spheroplasts is accredited to the cell-wall

inhibiting properties of β-lactam antibiotics, such as meropenem, with no mention of CWDB. Whilst spheroplasts are acknowledged, it is suggested that the formation of these CWDB merely confirm the mechanism of action of the drug. Whether this large scale transition is an observation of the mechanistic interactions between the drug and the bacteria or a mechanism used as a defensive strategy controlled by the bacteria, the viability of these cells and the possibility of a reverse transition could explain some of the persistent characteristics of *P. aeruginosa* infections. In [75], it is proposed that the CWDB can lay dormant until more favourable, antibiotic-free conditions occur, at which point they possess the ability to transition back into rod-shaped cells and resume proliferation. Although this shift in morphology does not indicate persistence as described in Section 1.3.2, the varying characteristics of the subpopulations we see when meropenem is added to *P. aeruginosa* form an analogous environment.

1.4 Novel approaches to treating *P. aeruginosa* infections

1.4.1 Understanding the role of selective pressure in the development of AMR

P. aeruginosa is ubiquitous and due to its arsenal of intrinsic and acquired resistance mechanisms, strains have developed that can evade traditional treatment methods. It is imperative that we try to gain a deeper understanding of currently used drug treatments and formulate new approaches to tackle the threat of multi-drug resistant strains. Moreover, we must consider the possibility of resistance to new strategies and understand the role of persistent populations, including the transition of CWDB, in population survival.

Before we discuss some of the novel approaches that are being considered to deal with the threat of resistant bacteria, it is necessary to understand why resistant populations emerge and what drives the evolution of resistance. We have previously discussed the adaptations that permit bacteria to survive antibiotic action yet we have not considered

why a resistant strain may flourish in a multi-strain environment.

Selective pressures are factors that drive selection for characteristics in an organism, The consequences of selective pressure can be directly linked to natural selection; organisms that express genes that provide an advantage under a certain selective pressure will be selected for since the organisms that do not express those genes will be at a disadvantage and may not survive. At a bacterial level, selective pressures include the site of infection, host responses and antibiotic concentration. All of these pressures will determine the survival of a pathogen and influence its pathogenesis, which is dictated by its virulent properties.

In the work of Levin and Svanborg Edén [63] we see that a clear distinction must be made between two types of selective pressure, those that lead to direct selection and others that lead to coincidental expression. Firstly, and most simply, direct selection represents characteristics or genes which, when expressed, result in a reward by some benefit to the species. In a bacterial species, expression of these genes can result in increased transmission or can strengthen its ability to proliferate, invade and survive at a within host site. For example, *S. aureus* faces the threat of being killed by reactive oxygen species (ROS) at a site of infection; in order to protect themselves from this they produce CrtM, an enzyme responsible for the production of a golden pigment called staphyloxanthin, which provides the bacteria with protection from ROS [3]. The expression and maintenance of the virulence factor results in increased bacterial fitness and enables the population to continue with their invasive pathogenicity, inferring that these genes will be directly selected [63].

Alternatively, many bacterial characteristics are believed to be expressed as a result of coincidental selection. These factors do not benefit the pathogen in a parasitic sense but are often the by-products of selection for other non-pathogenic adaptations that coincidentally result in virulence [19, 63]. In other words, expression of these factors is positively correlated with host damage but will not benefit the bacterial fitness (via increased growth or transmission for example) at the site of infection. They may be the

coincidental result of an adaptation required to promote survival or proliferation at an extra-host site or at a within-host site at which they are not symptomatic. To give a clear example we look to the expression of P pili adhesins by extraintestinal pathogenic *E. coli* (ExPEC) strains. These are opportunistic pathogenic strains of *E. coli* that are often found in the healthy intestinal microbiota but become virulent and cause disease in specific extraintestinal sites such as the brain or urinary tract. In the commensal site of the intestine, the expression of these adhesins leads to persistence; implying a directly positive impact on the bacterial fitness. Similarly, in urinary tract inections (UTI) the expression of P pili adhesins facilitates colonization, however, the inflammatory response to these adhesins, which cause the painful syptoms of a UTI, can result in clearance of the bacteria. This raises the question of whether there are measurable benefits to bacterial fitness at these extraintestinal sites and it is therefore believed that selection for this virulence factor in extraintestinal sites is not a result of direct selection at the site of infection but alternatively arises coincidentally from the direct selection at the intestinal site, where the factor is beneficial to bacterial fitness [3].

We can directly translate these ideas of selective pressure within pathogenesis to the pressures that surround the emergence and sustainment of drug-resistant strains. The consequences of antibiotic action on mortality and growth result in direct selection for strains that hold an advantage i.e. resistance to the antimicrobial. The continued use, or pressure, of antimicrobials has led to the development of multi-drug resistant strains that have been selected for as they are able to survive exposure to multiple drugs.

As we place pressure on pathogens, in the form of antimicrobials, we are supporting the selection for phenotypes that can evade antibiotic action and therefore it is essential to understand in which situations selective pressure will promote these phenotypes. When investigating novel treatments, it is critical that we consider the effects of this pressure on the bacterial population and acknowledge the varying phenotypes within a population. Additionally, by optimising currently used treatment strategies, it may be possible to limit the pressure placed on pathogens and thus limit the emergence of resistance.

1.4.2 Antibiotics vs. antivirulence drugs

The mechanism of any antibiotic compound is to be either bactericidal, which means to kill the bacteria, or bacteriostatic; here the aim is to inhibit growth or reproduction and interrupt population growth. All mechanisms involve targeting processes that are crucial for microbial survival and therefore the presence of any antibiotic incurs a fitness cost to the population of susceptible bacteria [20]. The resistant population is ultimately rewarded by not being affected by the antibiotic and there will be direct selection for these resistant characteristics [3]. Consequently, with a diminished susceptible population, a competitor-free environment will arise. There is decreased competition for essential nutrients and as a result of this the resistant strain thrives.

New alternative strategies being developed involve disarming the pathogen using antivirulence drugs; instead of targeting the survival of the bacteria, these would target its pathogenic characteristics or virulence factors [3]. Virulence, although defined in varying ways depending on the context, can be typically understood as harm or mortality to a host. Without virulence, a pathogen is no longer able to harm a host and it is these so-called virulence factors, characteristics of the pathogen resulting in virulence, that drive pathogenicity. Each pathogen has a wide array of virulence factors, all of which may be contributory or instrumental in completing pathogenic goals such as colonization or immunosuppression.

The mode of action of antivirulence drugs is to inhibit the mechanisms within the micro-organism that cause harm to the host, promote infection or enable the bacteria to evade the effects of the host immune system. If this has no or little effect on the fitness of the bacteria then the limited fitness cost will reduce the selection pressure for resistance. These drugs should theoretically initiate the evolution of a new population of bacteria that will not damage its host and are under less evolutionary pressure to develop resistance. An additional advantage of this is the likely preservation of the host microflora, a complex and vital biosystem that can be significantly disturbed by administration of antibiotics [91]. Whilst the potential of this concept has been studied, a great deal of

further screening and clinical testing is needed before this antivirulence approach can be employed.

1.4.3 Antivirulence drug resistance

The concept of a drug which disarms bacteria but does not attempt to affect the net growth of a pathogen seems logical, but we should also study the likelihood of bacteria developing resistance to antivirulence drugs. However, it is necessary to redefine the meaning of *resistance* in this context. Antibiotic resistance is defined as a micro-organism's ability to resist the effects of an antibiotic drug that would have previously eradicated the population. Resistance in this context refers to an adaptation that helps the pathogen population recover, following exposure to antibiotics. Since antivirulence drugs do not attempt to diminish the population directly we need to define resistance to antivirulence drugs in terms of the virulence factor that it targets, instead of growth recovery. We can define resistance in this sense as the recovery of the virulence factor, following the exposure of the pathogen to antivirulence drugs [3].

Identifying target factors for antivirulence compounds involves screening a pathogen for non-essential genes that do not affect bacterial growth in rich *in vitro* media, yet cause increased virulence during infection. It is then necessary to understand the consequences of virulence expression on pathogen fitness *in vivo*; a factor may or may not be beneficial to the pathogen at the site of infection, or it can be collectively beneficial to the whole population. Here, we can refer back to the introduction of direct and coincidental pressure introduced in Section 1.4.1. The consequences which lead to the expression of a virulence factor can help infer whether or not resistance would develop, should the factor be targeted.

If a virulence factor is non-beneficial at the site of infection or in rich *in vitro* media then there may be no selective advantage for resistance. This suggests that this type of virulence factor would provide an ideal target for antivirulence strategies. In Section 1.4.1 we introduced coincidental virulence factors, which in sites of infection can often be

non-beneficial. These are factors found in opportunistic pathogens that usually exploit distinct environments. These factors are coincidentally selected for, due to the natural environment of the pathogen. This would imply that if an antivirulence drug was to target the site of infection then it may be successful in removing the virulence without imposing selection for resistance. If we refer back to the example of P pili expression in ExPEC strains then we can hypothesise the effects of an antivirulence drug at an exclusive ExPEC site of infection in comparison to a general within-host application. If the drug were to directly target a site infection such as the urinary tract (where P pili expression does not confer a direct benefit) then we could expect both a decrease in pathogenicity and that there would be no selection for resistance. However, if the drug was not so specific in its target site and was applied to the intestine as well then we would presume that resistance would be selected for as the drug would infer a direct decrease in bacterial fitness due to P pili being necessary for bacterial progression in the intestine.

Although antivirulence drugs attempt to decrease the virulence of a bacterial population, instead of reducing the population itself, it has still been shown that some antivirulence drugs can aid clearance [45]. This may only be in the presence of an intact immune response or whilst in combination therapy with antibiotics, but it still gives evidence that the virulence factors targeted by these drugs must be beneficial to the pathogen, at the site of infection, in some way and supports the theory of direct selection. A result of this is that if the pathogen fitness and virulence factor are positively correlated then a resistant mutant would be strongly selected for as this would recover the pathogen fitness. Again we can refer back to Section 1.4.1; if an antivirulence factor were to suppress the ability of *S. aureus* to produce the protective enzyme CrtM then this would result in it becoming defenceless to reactive oxygen species (ROS). Consequently, if a resistant strain emerges then this strain will be invulnerable to the ROS and this will lead to strong selection for the recovery of the virulence factor.

It is important here to discuss the class of beneficial virulence factors, which not only affect the fitness and benefit the focal bacterium but are collectively beneficial to the

population of bacteria. These virulence factors become 'public goods' which may come as a costly contribution for the individual, but are beneficial to their neighbours. In this case, we must explore the effects of social cheating and cooperative behaviour within the bacterial population. Social evolution theory suggests that non-producers may become social cheats, exploiting their neighbours that are able to produce the goods. The resulting possibility of resistance developing in this type of environment will largely depend on how the population is structured. For example, in a well mixed environment, antivirulence drugs targeting a collectively beneficial virulence factor would cause susceptible bacteria, unable to contribute, to become social cheats [72]. Resistant bacteria will be the subpopulation who can still produce the virulence factor. This subpopulation will be exploited by the social cheats; the cheats will be able to use the virulence factor produced by the resistant bacteria without having to pay the high metabolic cost of producing it. This may result in strong selection against resistance in a well mixed environment [3]. This example highlights how structure, environment and fitness benefits need to be considered when choosing a target virulence factor.

Antivirulence resistance has already been reported, however, this does not necessarily mean that resistance will hinder the efficiency of these drugs [68]. There is no doubting that resistance mechanisms exist, but it is important to distinguish between the existence of these mechanisms and whether these resistance mechanisms will develop and be selected for. If the evolution of the pathogen chooses against selection of the resistant strain then the efficiency of the drug will not be affected. For example, many pathogens rely on adhesion mechanisms to efficiently bind with host cells in order to deploy virulence factors and effector proteins into the cell. Anti-adhesion drugs target these mechanisms and inhibit the ability of the bacteria to bind to the host. Resistance to these drugs is possible but any resistant mutations to specific binding mechanisms would directly impact the ability of the bacteria to bind to the host and negatively impact the fitness of the pathogen. In the following section we review some of the relevant biological mechanisms that could be used as targets for novel antivirulence strategies.

1.4.4 Target mechanisms for antivirulence drug strategies

When targeting virulence, there are several pathogenic characteristics that we may attempt to inhibit. These virulence factors are often non-essential to bacterial growth but cause harm to the host during infection. In Allen et al. [3] several factors were identified and investigated to decide whether each targeted virulence factor provided a selective advantage to the pathogen in an *in vivo* site of treatment. In the following sections we discuss some examples of possible targets.

Microbial attachment

In order for a bacterium to infect a cell it firstly needs to attach itself to the cell via adhesion. It produces an adhesin which mediates the interaction between the pathogen and the cell-surface ligand on the host cell. Pathogens are able to present multiple adhesins depending on the site or time so it is unlikely that a universal class of anti-adherence drugs will be developed. However, several adhesive strategies have emerged as hallmark requirements for virulence thus becoming targets for antivirulence drugs. The importance of adhesion in the early stages of the infectious process means that this represents an ideal strategy to hinder bacterial pathogenesis. Impairing bacterial adhesion would directly impede the ability of the bacteria to successfully infect cells and hence prevent growth of the bacterial infection.

Most adhesins are incorporated into extracellular fibres called fimbriae or pili; these fibriae are not only required for the attachment to host cells, but they are also crucially involved in the fitness and formation of intracellular bacterial communities (IBCs) [115]. An example of this can be seen in the importance of pilus adhesion in biofilm formation of *E. coli* in the pathogenesis of UTIs. The IBCs formed by Uropathogenic *E. coli* (UPEC) provide protection from the host defences of the urinary tract and antibiotics, meaning that UTIs can become recurrent and chronic. Whilst adhesion may facilitate colonisation, it does not confer a direct benefit to individual cell viability. Therefore, due to the importance of the pilus in IBC formation and adhesion, these fimbriae are ideal candidates

for an antivirulence drug target [60].

There are three main strategies in targeting pilus-mediated function; the first involves physically preventing the pathogen binding to the host cell. This approach is adhesion specific and involves blocking the adhesive properties of already formed pilus. This can be achieved by various competitive binding strategies. For example, FimH is the adhesive subunit of type 1 pili in fimbriated UPEC that binds to mannosides on the host cell via mediation by carbohydrates. FimH antagonists, such as biphenyl mannosides have been shown to successfully bind to the FimH subunit before it is able to bind to the host receptors rendering the bacteria unable to bind with the host [42].

Alternatively, peptide-based inhibitors can inhibit adhesion by binding to the host receptors before the bacteria. The bacterial surface protein multivalent anti-adhesive molecule 7 (MAM7) has shown potential for inhibiting adhesion and therefore infection, in several pathogenic species such as *E. coli*, *Vibrio cholerae* and *P. aeruginosa* [58, 59].

The third strategy involves preventing the initial formation of the pilus via inhibitory action towards the chaperone-usher systems involved in pilus assembly. This approach, in comparison to the first approach, could lead to a broader range of drugs and could also impact on the ability of pathogens to form IBCs [20]. It is this approach that has been taken in the attempt to inhibit P pili production in *E. coli*. Bicylic 2-pyridones are able to bind to the PapD chaperone thus preventing further interaction of the chaperone-pilus subunit with the usher unit, located in the membrane [87].

One of the advantages of anti-adhesion strategies that makes them so appealing as an alternative approach to antibiotics and other conventional antimicrobials is that their use may not induce resistance. This is because they inhibit adhesion, which is beneficial to the population as it facilitates colonisation but it does not always directly benefit pathogen fitness. Therefore, this may infer little to no selective pressure for resistance mechanisms. It is theoretically possible that a resistance mutation could occur, however, it is possible that resistance to the anti-adhesion drug could also render the mutant unable to bind to the host. We consider the MAM7 anti-adhesion therapy as an example. If a resistant

bacterium appeared it would need to produce an entirely new receptor protein to bind to the host cell in an alternative way. The energy required for this could negatively impact the pathogenic fitness and may not be selected for as a result of this. An additional advantage of this type of antivirulence drug is that they would be unaffected by efflux pumps due to their extracellular nature.

Toxin secretion systems

Another potential focus when looking for antivirulence targets are bacterial secretion systems. Pathogenic bacteria can secrete toxins and molecules in a number of ways and the effects of these secretions can lead to severe symptoms.

Toxins are usually exported by type II secretion systems and an example of the effects of these toxins can be seen in the severe dehydration and diarrhoea symptoms of the cholera toxin produced by *V. cholerae* and the shiga toxins associated with *E. coli*. Possible ways of targeting this type of virulence factor include gene expression inhibition and neutralising toxins using antibodies.

Type III secretion systems (T3SS) are another type of secretion system used by many Gram-negative pathogens, such as *E. coli* and *Yersinia pseudotuberculosis*. They allow pathogens to translocate macromolecules, known as effector molecules, across the bacterial envelope into the host. These molecules could be enzymes, proteins or toxins and after entering the host cell, they are able to adjust and regulate the host's defence response. This increases the survival rate of the pathogen and can decrease the presence and effect of the host's immune response. Small-molecule inhibitors have been found that inhibit the T3SS systems of both *Y. pseudotuberculosis* and *Chlamydia trachomatis* and this is attributed to conserved elements that are found in the T3SS machinery of many pathogens. The idea that many T3SS systems include these elements gives reason to believe that broad range T3SS inhibitors could be developed [20, 55, 80, 95, 114].

Finally, type IV secretion systems also allow for the translocation of molecules, resulting in similar effects to those of T3SS but they also allow for the mediation of transmis-

sion of genetic material, such as resistance genes, to other cells [14, 23]. This results in a twofold contribution to virulence. Both of these functions have an additional contribution to pathogenicity and resistance respectively and therefore make these systems attractive targets for novel drugs.

Many of the molecules and drugs that target the secretion systems of pathogens bind extracellularly and this is beneficial when considering resistance via efflux pumps [14].

Quorum sensing

Quorum sensing (QS) is the term to describe the chemical signalling that occurs between bacteria. It can be seen as a way for the bacteria to communicate with one another. Occurring via the production and recognition of small molecule signals called autoinducers, it can coordinate gene expression and regulate many processes that are involved in community behaviour, cell growth and also virulence. Only a subpopulation of signals are directly involved in virulence and although some of these signals are not necessarily virulence factors themselves, they can induce the expression of many other virulence factors.

This area has received a lot of attention as a possible therapeutic target due to its role in many inter-cell processes. There are two types of possible drugs: signal-response and signal-supply inhibitors. Signal response inhibitors will render susceptible bacteria "signal-blind" and there will be a subsequent reduction in the production of the quorum sensing virulence factors. Resistant bacteria will therefore be a subpopulation that can still detect the signal and produce the virulence factors. Selection for resistance will therefore be dependent on the beneficiaries of the virulence factors and will follow the ideas outlined in Section 1.4.3.

Signal-supply inhibitors will inhibit the bacteria from supplying the quorum sensing signals, thus causing a decrease in the amount of signal produced in the population. Resistant bacteria will be those who can still produce the signals. In this situation "social cheating", as discussed in Section 1.4.3, may arise. If the resistant population is initially

small then there will still be a small amount of signal supplied in the environment. In a mixed environment, this will be available to all bacteria, meaning that quorum sensing-controlled virulence factors will be expressed by all bacteria to an equal extent, if there is enough signal. The antibiotic-susceptible bacteria become social cheats and remain virulent. However, in a structured environment, the signal will be detected only by resistant bacteria, meaning that resistance will be selected for if that virulence factor is beneficial to the individual. Quorum sensing is extremely influential in bacterial populations, which makes it an attractive target for antivirulence drugs. However, there are concerns that changing such an integral part of a cell's function may automatically promote resistance mechanisms [3].

1.4.5 Combination therapies

Formulating novel therapies, such as antivirulence treatments, will help to combat the ever-growing threat that antimicrobial resistance poses to humans and animals. However, new approaches may take years to develop and test until they become clinically available and antibiotic-resistant bacteria are already present. Strategies to use current antibiotics more effectively are being developed to minimise the emergence of resistance.

Combination therapy and sequential therapy involve the administration of multiple drugs to a patient, either simultaneously or in succession. This strategy, which has become common practice in hospitals, aims to exploit the varying mechanisms of action of drugs with the hope that they will act synergistically to minimise the rate of evolution of resistance within bacterial populations. If a strain emerges that is resistant to one antibiotic, it may remain susceptible to the other drug. Multi-drug resistance is feasible and the efficacy of combination treatment may be limited if drug interactions are not well researched [117]. A common combination therapy for treating *P. aeruginosa* bacteremia and sepsis is the administration of the β-lactam-aminoglycoside pairing. Whilst studies report conflicting results regarding the advantages of combination therapy over monotherapy using this antibiotic pairing [16, 47, 70], it has been stressed that the results of these

studies are often not comparable due to different study designs [22].

In [75], the combination of meropenem and antimicrobial peptides (AMPs) is investigated as a potential therapy for *P. aeruginosa* infections. AMPs are relatively inactive against rod-shaped *P. aeruginosa* as they induce cell death by creating pores in the cytoplasmic membrane, which remains unexposed in normal bacillary cells. However, it was found that spherical cells displayed large areas of exposed cytoplasmic membrane which gave reason to believe that the CWDB would be more susceptible to the bactericidal effects of AMPs. This hypothesis was supported by experimental data that saw a combination therapy of meropenem and AMPs leading to lower bacterial load *in vitro*. In spite of these results, it is unclear whether this combination would have any effect on the emergence of a resistant strain. Before novel combinations are used it is crucial that we investigate how resistance would be affected by any combination of drugs and also, as in the case of the β-lactam-aminglycoside pairing, that the drug combination is in fact effective.

1.4.6 Optimising antimicrobial usage

The use of combination therapy could, in theory, help prevent the emergence of resistance, unless a strain emerges that is resistant to both treatments. In some cases the use of combination therapy may not be an option, for example in countries where antibiotics are not readily available (making cycling through multiple antibiotics unviable). Vast amounts of research must also must be done to investigate compatibility of drug combinations. Another strategy to prolong the lifetime of currently used antibiotics is to optimise their usage.

It is clear that the development of antibiotic resistance can be affected and accelerated by several factors, some of which are bacteria-specific such as mutation rate and biological fitness. In [82] the authors highlight the need to consider the antibiotic-induced impact on these bacteria-specific factors, and specifically the impact on bacterial fitness, when choosing a suitable antibiotic. For example, a suitable antibiotic would be one that may

induce an increased fitness cost for resistant bacteria or for which mutations are rare [82].

Research has also indicated that the inappropriate use of antibiotics and sub-optimal dosing strategies could impact the spread of resistance [12, 32]. The WHO defines the appropriate use of antimicrobials as "the cost-effective use of antimicrobials which maximizes clinical therapeutic effect while minimizing both drug-related toxicity and the development of antimicrobial resistance" [85]. Whether a single antibiotic is used or a combination, the concentration of antibiotic at the site of infection and the dose duration will determine the extent to which resistance develops. Traditional dosing regimens involve a fixed number of the same dose and it is now widely accepted that these regimes may be sub-optimal and could in fact perpetuate the emergence of resistant strains. It is crucial that we find new ways to optimise regimens so that infections can be cleared without involving a level of pressure that could perpetuate the spread of resistance. Mathematical approaches can be used to pinpoint suitable concentrations and doses that could minimise the development of resistance and some of these will be discussed in Chapter 5.

In addition to investigative work into optimal treatment strategies, the general use of antibiotics must be improved. To successfully implement the appropriate use of antibiotics, educative campaigns have been used to target both physicians and the general public and increase awareness of the threat of resistance. In [49] an extensive review into national and regional campaigns in high-income countries is undertaken. It is suggested that campaigns do have a positive impact on antimicrobial usage, however, it is unclear whether the observed decrease in usage is because of a change in the prescribing behaviour of physicians or the behaviour of the public. Finding data to support any hypothesis surrounding the results of these campaigns would also prove difficult.

We have reviewed the characteristics of *P. aeruginosa*, the mechanisms that enable the bacteria to evade antibiotic effects and some potential strategies to overcome resistance. The task of providing new treatment strategies and exploring the interactions between drugs and bacteria has traditionally fallen to the pharmaceutical industry but with the waning effectiveness of classic antibiotic strategies, it is imperative that we can

harness ideas and techniques from other disciplines in order to explore how we can control antibiotic resistance. The following sections aim to give a brief overview of the role of mathematical modelling in combating AMR, with a specific focus on the formulation of population dynamics models and their applications.

1.5 Mathematical modelling of bacterial infections

Mathematical models are used to investigate biological systems in an abstract manner. The biological processes and characteristics of a system can be translated into mathematical formulae that are used to predict the behaviour of the system. The model can be validated by comparing the model predictions to observed biological behaviour or experimental data; if a model does not match the expected behaviour then this indicates that some process is missing from the model. If the results from the model provide a successful approximation to the expected biological outcome then this provides support to use the model as an analogous system to obtain predictions of unknown biological behaviour. Whilst a mathematical model can often be a simplification of the respective biological system, the potential to investigate complex systems and produce useful conclusions is compelling.

There are numerous approaches and methods used to formulate mathematical models and the type of model will depend on the system that it is describing. Models can be continuous or discrete depending on the objects that are being modelled; large scale events such as fluid flow or population growth are often modelled as continuous, whilst micro-scale systems are often described using discrete models. Models can be deterministic, where the outcome will be dependent on the pre-determined parameter values in the model and the initial conditions, or stochastic, where randomness is incorporated into the model. A deterministic model will produce the same results for a given set of initial conditions, however, a stochastic model may produce varying results as the variable states are defined by probability distributions instead of given values.

Mathematical modelling is increasingly being used to study the changes in growth of bacterial populations, the effects of antibiotics and the emergence of resistance. By incorporating mathematical models into the research strategy, it is possible to connect concepts from areas such as epidemiology, microbiology and pharmacology and meld existing hypotheses and conclusions in order to understand the biological processes involved in the emergence and development of resistance. Mathematical modelling can simulate lengthy and expensive experiments relatively quickly and provide predictions that can guide experimental design.

Throughout this thesis we assume that the population is large enough to ignore stochastic effects and we exclude spatial effects as we assume the population to be well-mixed. Therefore, we focus our attention to deterministic population dynamics models, which are commonly used to model populations of humans, animals and microorganisms. Population dynamics models generally use mass action kinetics to assign rates of biological processes to the species involved. In the remainder of this chapter we will explore terms that are used within ODE models to describe some of the relevant biological processes involved in the evolution of a bacterial infection.

1.5.1 Formulating an ODE population dynamics model to describe bacterial growth

Modelling bacterial growth

Before considering the effects of an antibiotic or any other influential factors, we consider how bacterial growth can be described mathematically. If we consider the growth of a homogeneous population of bacteria *in vitro*, there are well established mathematical terms that can be used to successfully describe the experimentally observed characteristics of bacterial growth. Bacterial growth, or proliferation, occurs by the asexual process known as binary fission and results in one parent cell splitting into two daughter cells. If a single bacterium was to grow without regulation then we would expect the population to

continue proliferation indefinitely. The bacterial population, B, would grow exponentially and this can be described using a linear differential equation,

$$\frac{dB}{dt} = \eta B, \tag{1.1}$$

with a constant growth rate, η. The growth rate will be specific to the species and strain of bacteria and the environment in which it grows. The environment will also dictate other factors that may limit growth, such as space or nutrient. These growth limiting factors mean that in many environments bacterial growth occurs at a non-constant rate. The logistic growth term, proposed by Verhulst in 1845, is frequently used to model population growth as it incorporates resource limitations. The logistic equation describes the growth of a population, B, using an equation of the form

$$\frac{dB}{dt} = \eta B \left(1 - \frac{B}{k}\right). \tag{1.2}$$

Here, η is the maximal bacterial growth rate and k is the carrying capacity or saturation number. When using (1.2), population growth is dependent on the population size; the initial growth stage is approximately exponential and as the population grows the rate of growth slows until the carrying capacity is reached. Once the population has reached its carrying capacity, growth will stop. Other nonlinear growth functions include the Gompertz equation [41] and Richards' model [93]. These sigmoidal models incorporate competition of resources phenomenologically instead of explicitly considering the amount of substrate or resources; one way to incorporate the amount of substrate available is to use Monod kinetics [76]. Monod kinetics describe growth of bacteria and depletion of nutrient using the following equations

$$\frac{dB}{dt} = \left(\frac{\eta S}{K_{50} + S}\right) B. \tag{1.3}$$

$$\frac{dS}{dt} = -\frac{1}{y}\frac{dB}{dt}, \tag{1.4}$$

with initial conditions,

$$B(0) = B_0, \quad S(0) = S_0. \tag{1.5}$$

Here, S is the concentration of substrate, η is the maximum growth rate, K_{50} is the saturation constant, the concentration of substrate for which half maximum growth rate is achieved and y is the yield factor. Monod kinetics are similar to Michaelis-Menten kinetics as the rate of growth is dependent on the concentration of substrate. The equations can be solved under the assumption that the yield factor is constant to obtain,

$$B_\infty = B_0 + yS_0, \tag{1.6}$$

where B_∞ is the limit of the bacterial population as $t \to \infty$. Equation (1.6) indicates that the limiting population is dependent on the initial amount of substrate and the initial bacterial load. This differs to the logistic equation where the limiting population value depends entirely on the carrying capacity k.

Both the logistic equation and monod equation are used to model *in vitro* data and specifically batch growth experiments. The Monod equation is more mechanistic compared to the phenomenological sigmoidal models that include mathematical parameters that may have limited biological interpretation. However, following Zwietering et al., it is possible to reparameterise models such as the logistic equation, to reflect microbial growth parameters such as lag time and maximum growth rate [118]. Furthermore, in Kargi et al. the monod and logistic equations are shown to be theoretically related, with the logistic equation being a special case of the Monod kinetics, thus making it a suitable choice in certain cases [54].

Incorporating a treatment

We are interested in how the addition of a treatment will affect the overall growth of a bacterial population and therefore look towards terms that can describe this process. In order to describe the effects of a treatment we must consider how the treatment interacts

with the bacteria and include a suitable term within the model. If the concentration of antibiotic changes over time then this must also be included within the model.

To include the concentration and effects of an antibiotic in a model we introduce concepts from pharmacokinetics (PK), the study of drug absorption and elimination, and pharmacodynamics (PD), the study of the response of the bacteria in the presence of the drug. Previously, PK models have been used to obtain suitable treatment regimes that are effective and limit toxicity; they can be used to quantify information about the concentration of a drug at the site of infection, which will depend on how and when the drug was administered. The concentration of a drug at a specific time point, $A(t)$, will depend on the initial amount of antibiotic administered and how much has been eliminated. Drug elimination is commonly assumed to follow first order kinetics (exponential decay) and the concentration of antibiotic at any given time is determined by the equation,

$$\frac{dA}{dt} = -bA, \tag{1.7}$$

with decay rate b. The decay rate can be calculated using the half-life, which can be obtained experimentally.

We may then employ PD to integrate ideas from PK into our population model. Equation (1.7) determines the concentration of the antibiotic and we can then use mass action laws to incorporate the effect it has on the bacterial population. A commonly used term for the impact of an antibiotic on a bacterial population is a saturating hyperbolic function:

$$E(A) = \frac{E_{MAX} A^n}{A_{50}^n + A^n}, \tag{1.8}$$

where $E(A)$ defines the total antibiotic effect on the rate of change of the bacteria, which is dependent on the antibiotic concentration A [8, 48, 64, 69]. Here, E_{MAX} represents the maximum effect rate, A_{50} is the concentration for half maximal effect and n dictates the slope of the curve. Equation (1.8) is a Hill function and n is the Hill coefficient; if $n = 1$ then we have an equation that is similar to the Monod kinetics, discussed previously as a

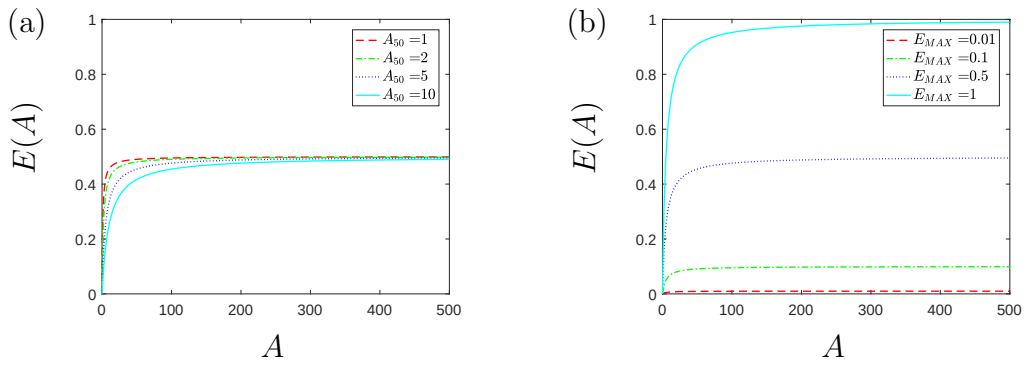

Figure 1.3: Graphs displaying the saturating term, equation 1.8 used to model antibiotic action with $n = 1$. (a) shows varying values of A_{50} with $E_{MAX} = 0.5$ and (b) has fixed $A_{50} = 5$ and varying values of E_{MAX}.

suitable function to model bacterial growth.

Figure 1.3 shows how this term behaves for varying values of A_{50} and E_{MAX}. As A increases, the overall effect will tend to the maximum rate representing a saturating effect. In Figure 1.3 (a), the antibiotic effect tends to the maximum rate for all values of A_{50} but as A_{50} increases more antibiotic is needed to reach E_{MAX}. Conversely, if we fix A_{50}, shown in Figure 1.3 (b), then the antibiotic effect tends to the different values of E_{MAX} with the same slope. This saturation model approach can represent biological processes such as reactions involved in metabolism and the finite number of binding sites to which drugs must bind in order to initiate antibiotic effects.

When considering the effects of bactericidal antibiotics that aim to kill the bacteria, the saturating term can be used with mass action laws to create a separate antibiotic-induced death term. For bacteriostatic antibiotics, it may be more suitable to use a different approach when modelling antibiotic action. Bacteriostatic antibiotics aim to stop the bacteria proliferating which may not necessarily kill them and the effects of these antibiotics can be incorporated via a decrease in overall bacterial growth. In Baker et al. [10], antibiotic effects are modelled as a reduction in growth and a Hill-function (similar to the saturating term above) is used to determine the extent to which growth is hindered by the antibiotic. In D'Agata et al. [29] the impact of the antibiotic on bacterial growth is assumed to be constant and the antibiotic concentration is not considered.

In Abel zur Weisch et al. [1], to incorporate antibiotic effects, the model includes the number of intracellular binding sites available to the antibiotic. This explicitly incorporates the cohesion of binding kinetics, an intracellular mechanism, into a population dynamics model. The results give biological insight into the specific mechanisms involved in various previously unexplained antibiotic effects, such as post antibiotic growth suppression, a phenomenon witnessed in bacterial populations after exposure to antibiotics. Obtaining a detailed understanding of this type of phenomena is key in devising optimal treatment strategies and investigating the emergence of resistance.

The mathematical terms used to model antibiotic effects are relatively consistent. Antivirulence drugs represent a new treatment approach and therefore there are fewer models that incorporate their effects. However, there has been some modelling of the target mechanisms discussed in Section 1.4.4, in particular regarding QS. Ward et al. [111] and Dockery and Keener [34] both produced ODE models to describe the signalling processes involved in QS in *P. aeruginosa* and a subsequent model incoporating QS inhibitors supported the idea that this could be a practicable treatment strategy that should be investigated further [6]. Additional research in this area led to similar models describing the QS system of *S. aureus* [51] and also a spatial model that aimed to predict the effects of QS inhibitors and antibiotics on a biofilm poulation of *P. aeruginosa* [5]. A more general framework was produced in Ternent et al. [102] to investigate the effects of using a combined treatment of both antibiotic and an antivirulence drug that increased bacterial susceptibility to the host immune system. Results then suggested that the efficiency of antivirulence treatments would depend largely upon the host's immune system.

Host cells

Until now we have only considered mathematical terms used to describe bacterial growth and the effects of a treatment. Simple models that only consider these interactions are useful when describing bacterial growth *in vitro* but in order to investigate the growth of an infection *in vivo*, it is important to consider host defences.

The immune system is extremely complex and many models have been formulated to describe the initial dynamics of the immune response. These models do not consider antibiotic effects and instead focus on the specific regulatory mechanisms involved in the immune response such as inflammatory responses, cytokine production and different types of immune cells [38, 113]. Other notable models of the initial immune response can be seen in [53, 98]; both studies attempt to formulate simpler models of the initial dynamics of the immune response, whilst maintaining a focus on specific aspects of the immune system such as the individual components of the immune response involved in a lung infection [98] or the interactions between the bacteria and immune response with respect to inflammatory damage [53].

Detailed studies are useful to investigate the specific interactions that may cause the initial immune response to succeed or fail in clearing an infection. However, our interest lies in modelling the bacterial infection over the time course of a treatment and hence we can assume that the initial immune response has been ineffective in clearing the bacteria alone. Whilst the immune response may not succeed in clearing the infection alone, it can dictate whether a treatment is successful or not. For example, the immune system can have a considerable impact when the antimicrobial in use is bacteriostatic as it can work synergistically with the drug [44]. Similarly, it was suggested that the immune response could support antibiotic action when a persistent population was present [7]. For that reason, it is important that we include host defences within models that attempt to analyse suitable treatment methods and notable examples can be seen in [7, 29, 39, 44, 64, 102].

Studies that have investigated the role of host defences during antibiotic treatment have used various approaches when including the immune response within the mathematical model. In some cases, host defences are considered implicitly; in Lipsitch and Levin [64], the effects of the immune response are incorporated into the model via a decrease in bacterial growth. Similarly, in [29], the number of activated phagocytes is assumed to be at equilibrium and thus taken as constant. Here, a Monod term is used to include the effects of phagocytosis and the authors formulate a simple multi-strain model that can

investigate the impact of dosing regimens on the emergence of resistant bacteria, through HGT, without having to add another equation for the phagocyte population.

If we assume that the immune response may vary over the course of the infection or treatment period, then it could be unsuitable to include it implicitly within the model. Instead, the immune response can be included explicitly; an additional equation can be formulated to describe the strength or number of immune cells alongside the bacterial population. In Handel et al. [44] the strength of the immune response, normalised to be between 0 and 1, is modelled. Modelling the strength of the immune response indicates a more phenomenological approach and could be a suitable strategy if there are multiple types of immune cells involved within the immune response. An alternative approach would be to model the number of immune cells, whether that be a combined immune cell population or multiple subpopulations of specific immune cells [7, 9, 39].

Following the principles of population dynamics, the equation to describe the immune response will include terms to describe the growth and decay of the immune cell population The population of immune cells will increase due to recruitment, which occurs when the immune system detects that a pathogen is present in the body. Pathogen-associated molecule patterns (PAMPs) are molecules that are present in the pathogen and can be recognized by receptors, thus inducing an influx of immune cells into the environment. A suitable term must be chosen to describe the process of recruitment, which can vary depending on the type of immune cell. We consider two scenarios: recruitment is pathogen density-dependent (PDD) or pathogen density-independent (PDI) [7]. For the former, a term that includes the bacterial population must be chosen and for a PDI response the bacterial population will not appear within the term. Both PDD and PDI terms are investigated in Handel et al. [44] and Ankomah et al. [7]; both studies compare different recruitment terms to investigate the effects of different immune responses on the emergence of resistance and different treatment methods. Additionally, many studies choose to use a saturating term for recruitment under the assumption that there will be limitations on the strength of the immune response [7, 44, 102].

To model the clearance of phagocytes from the environment, we focus our attention to two processes: natural clearance and pathogen-induced apoptosis, which occurs when the engulfed bacteria excrete toxins that induce immune cell death. Whilst some models only consider natural clearance ([7, 39, 44]) and assume that the rate of clearance is constant, others include a term for each of the two processes. In Ternent et al. [102] natural clearance is assumed to occur at a constant rate and a mass-action type term is chosen to describe the density dependent process of bacteria-induced apoptosis.

We have considered the dominant processes that will characterise the growth of the immune response. Finally, we must integrate the effects of the immune system on bacterial growth into the model. In many models it is assumed that immune-mediated killing bacteria occurs at a rate that is directly proportional to the size of the immune response and a mass-action term is added to the equations that describe the bacterial populations [7, 102]. However, in Handel et al. [44] they considered a saturating term in addition to the mass-action term. It was acknowledged that immune cells may take time to complete phagocytosis and that under this condition, the mass-action term would break down for high bacterial load.

Introducing host defences into a mathematical model provides the opportunity to model bacterial growth *in vivo* and we shall see in later chapters that it is crucial to consider the effects of the immune system when investigating ways to optimise treatment strategies. Similarly, in order to explore the emergence and development of resistant strains or persistent subpopulations, we must include these species within the model. We will now discuss some notable studies that include multi-strain models of bacterial populations and consider the methods of differentiating between subpopulations.

Modelling heterogeneous populations

The focus of this project surrounds the growth of *P. aeruginosa* and the impact of the morphological transition that occurs under the influence of β-lactam antibiotics. There are multiple ways to model a transition between subpopulations and the term used will

depend on the system that is being described. If we consider models of persistence then the wild-type bacteria may be able to transition to and from the persistent form. A simple example can be seen in the persistence model used by Balaban et al. where the bacteria will transition between a normal and persistent state at a constant rate [11]. A more complex transition is used to model the transition to a peristent population in Cogan et al. [25]. Here, the transition is dependent on both the antibiotic concentration and the growth rate, which is modelled using Monod kinetics. This approach incorporates the dependence of persister formation on the growth stage of the bacteria and the pressure exerted onto the bacteria by antibiotic exposure. However, reversion from the persistent population is dependent on the antibiotic concentration only. A later model of persister formation by Cogan et al. [26] assumes that the transition from a normal to persistent state is proportional to the concentration of a toxin that is produced in response to environmental stress. Reversion back to the susceptible population occurs at a constant rate and it is assumed that this is small in comparison to the transition to the persistent form and negligible when considering constant doses.

Modelling the emergence of a resistant strain is similar to the methods used to model persistence in that we must understand the mechanism through which bacteria gain resistance and formulate a mathematical interpretation of the inter-population transition. Acquisition of resistance genes can either be a result of genetic mutation or via HGT. Lipsitch and Levin [64] developed a deterministic compartmental ODE model that described the growth of an antibiotic-susceptible strain of bacteria and a strain with reduced susceptibility. An additional equation was used to describe the dynamics of antibiotic concentration. They incorporated the emergence of resistance due to mutation using a stochastic component that modelled the appearance of resistant mutants using a Poisson distribution every time the susceptible population replicated. Another way of integrating a resistant mutant population could involve introducing the resistant population manually at a time point during the numerical simulation. It is possible to choose the size of the initial resistant population and hence this approach can be used to simulate the

appearance of a mutated bacterium or an influx of resistant bacteria, which could occur in the case of cross contamination.

If a resistance mechanism is more likely to be passed via HGT then the number of bacteria that transition from the susceptible to resistant population, B_R, will no longer only be dependent on the susceptible population, B_S (as is the case with mutation models). A frequency dependent term,

$$\beta(B_S, B_R) = \beta \frac{B_S B_R}{B}, \tag{1.9}$$

where β is the gene transfer rate and $B = B_S + B_R$, is commonly used in models of HGT [10, 29, 110]. We notice that instead of using a typical mass action kinetics term, the transmission rate, β, is normalised by the total population. By normalising the transmission rate it is possible to preserve the expected behaviour of transmission when one population is much larger than the other. Modelling HGT in this way fixes the gene transfer rate as a constant, however, in Novozhilov et al. [81] the evolution of horizontally transferred genes was investigated using a deterministic ODE model with an additional stochastic counterpart.

In addition to acquiring resistance via HGT, it is also possible to lose the plasmid and gain susceptibility. Some studies have assumed that plasmid loss occurs over such a lengthy time frame that it need not be included within the model [10]. In D'agata at el. plasmid loss is assumed to occur during replication and modelled using a reversion term that depends on the replication rate and a probability parameter [29].

Biological processes and the speed that they occur will be individual to the strain and phenotype of the bacteria. Therefore it is reasonable to assume that the rates used to describe these processes may differ between subpopulations. Growth rates are especially specific and will vary depending on the strain, phenotype and environment. For example, some persistent bacteria enter a dormant state and do not proliferate. Additionally, resistant bacteria are assumed to proliferate at a slower rate due to the fitness cost that is

attached to carrying resistance. It is possible to model a fitness cost by including separate growth terms for the susceptible and resistant strains ([64]), which we define as η_S and η_R respectively. Alternatively, the fitness cost can be incorporated explicitly into the model by introducing a fitness cost parameter, c. The resistant growth term becomes

$$\eta_R = (1 - c)\eta_S, \tag{1.10}$$

where c can take values between 0 and 1 [10, 64, 102]. By including a fitness cost parameter we can easily explore different growth rates for the resistant strain as a proportion of the growth rate of the susceptible bacteria.

In addition to the growth rate, each bacterial population will have distinctive rates of death, whether that be natural death or antibiotic-induced death. Specifically, antibiotic-resistance enables bacteria to survive antibiotic effects and in mathematical models this effect is often identified by individual antibiotic-induced death rates or PD properties [10, 29, 44, 102]. Other rates that may differ between phenotypes, including visibility to immune cells and phagocytosis, can also be made individual to a subpopulation when formulating a population dynamics model.

1.6 Project overview

We have provided a detailed overview of the methods used to formulate a population dynamics model of a bacterial infection. Additionally, we have considered the terms that are used to incorporate a treatment, host defences and heterogeneity within a population. Throughout this thesis we will formulate various models for the growth of *P. aeruginosa* with varying levels of complexity. For reference, we include Table 1.1, which includes a brief description and the assumptions used to formulate the models herein. Our approach will be to parametrise models using experimental data where possible, to obtain rates that are specific to *P. aeruginosa* and the β-lactam antibiotic meropenem. If data is not

available then we will explore the feasible parameter space to investigate the possible qualitative behaviour of the system. We will investigate novel treatment options by varying the rates of key processes and investigate the optimisation of currently used treatments using a genetic algorithm (GA).

In Chapter 2 we formulate a mechanistic model (Model I) to describe the growth dynamics of *P. aeruginosa* in isolation with meropenem. The model is mechanistic in the sense that carrying capacity is taken into account through the dynamics of nutrient availability rather than via logistic growth. Using *in vitro* data of growth curves of *P. aeruginosa* in the presence of varying concentrations of the antibiotic meropenem, we obtain parameter estimates for the model that enable it to reproduce experimentally observed behaviour. The analysis of two parameters sets, that produce different long term behaviour, allows us to manipulate the system theoretically in order to explore the advantages of the shape transition and simulate the effects of a combined dose of meropenem and AMPs. The work in Chapter 2 has been published in [99].

In Chapter 3 we formulate Model II to describe the growth dynamics of *P. aeruginosa* in isolation with meropenem and incorporate the possibility of efflux pump upregulation, i.e. antibiotic resistance. Due to limited data, we obtain a parameter set using values from our previous parametrisation attempts and literature. We explore the feasible parameter space to investigate the impact of the morphological transition on the growth of a meropenem-susceptible and -resistant strain of *P. aeruginosa* and explore the parameters associated with the resistance mechanism.

In Chapter 4, we extend Model II to formulate a mixed strain infection level model (Model III). We analyse the potential impact of the immune response on the growth of a *P. aeruginosa* infection during different treatment combinations. By altering the immunogenic properties of the spherical cells *in silico*, we identify scenarios in which the relationship between the immune response and the spherical population may determine treatment success.

Finally, in Chapter 5 we apply a GA to Model IV to obtain optimised dosing regimens

for a single antibiotic-susceptible strain of *P. aeruginosa*. Initially we assume that the bacteria do not transition during antibiotic exposure to show that the GA chooses dosing strategies that consist of a high initial dose that tapers off as the treatment progresses. We then include the morphological transition to show that the presence of spherical cells may impact the tailored treatment strategies suggested by the GA.

Table 1.1: Review of mathematical models formulated to describe the growth of *P. aeruginosa*.

Model	**Description**
I	Model I describes the growth of a single meropenem-susceptible strain in isolation with meropenem. Model assumptions include: • only rod-shaped cells proliferate • nutrient-dependent growth of rod-shaped cells • bacteria transition freely between the rod and spherical shape (i.e. the reverse transition occurs independently to antibiotic concentration) • spherical cells evade the effects of meropenem • all cells die naturally
II	Model II describes the growth of a single strain in isolation with meropenem. We include the possibility of resistance via active efflux. Model assumptions include: • only rod-shaped cells with no bound antibiotic proliferate • bacterial growth described by logistic growth • rod-shaped cells become internalised by antibiotic when the antibiotic binds within the cell • efflux reduces the rate of internalisation • spherical cells are immune from antibiotic effects • natural death of rod-shaped cells is negligible • spherical cells only revert back to rods at low antibiotic concentrations
III	Model III describes the growth of a mixed strain population at the site of infection. We include antibiotic effects and host defences. The model is formulated using the assumptions from Model II and the following: • density-dependent immune response • immunogenic properties may differ between cell morphologies • immune cells are subject to natural clearance and bacteria-induced apoptosis • resistant bacteria appear due to mutation or through cross contamination
IV	Model IV describes the growth of a single meropenem-susceptible strain in isolation with meropenem. Model assumptions include: • only rod-shaped cells proliferate • bacterial growth described by logistic growth • spherical cells only revert back to rods at low antibiotic concentrations • spherical cells evade the effects of meropenem • spherical cells die naturally due to fragility

CHAPTER 2

MODELLING THE GROWTH OF *P. AERUGINOSA* IN ISOLATION WITH MEROPENEM

In [75] they attribute the survival of *P. aeruginosa* cells after exposure to meropenem to a shape transition that results in the formation of viable yet fragile spherical cells. In this chapter we develop a system of differential equations to describe the bacterial growth of *P. aeruginosa* in the presence of the antibiotic meropenem with the inclusion of a morphological transition that is activated by the presence of the antibiotic. Whether this transition is a result of direct antibiotic action or attributable to an intrinsic survival mechanism, we assume that the cell wall deficient spherical cells evade antibacterial effects, as evidenced by the data in [75] and our own data. Using growth data we obtain estimates for the parameters used in the model and analyse the results to changes in these parameter values.

We note that our investigation in this chapter will focus solely on a meropenem-susceptible strain of *P. aeruginosa*; initially our concern is not with the mechanisms of resistance that are often attributed to *P. aeruginosa*, such as the upregulation of efflux pumps. Rather, we wish to investigate a shape transition that permits meropenem-susceptible strains of *P. aeruginosa* to tolerate the presence of antibiotics.

The work in this chapter has been published in PLOS Computational Biology [99]. The experimental data used in this chapter was obtained by the Krachler group at the

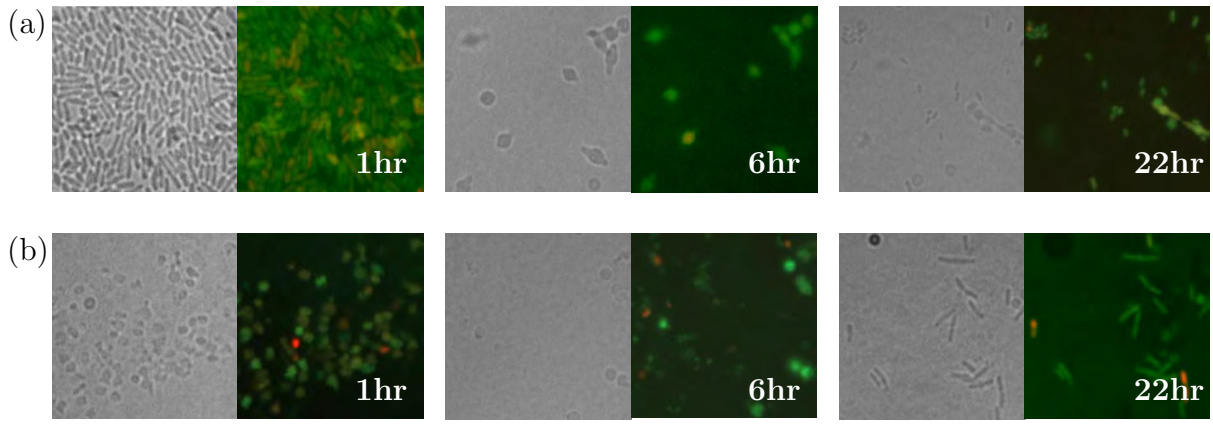

Figure 2.1: Cells of the meropenem-susceptible *P. aeruginosa* PA1008 strain rapidly convert to a spherical shape after adding (a) $0.5\,\mu g\,ml^{-1}$ and (b) $2\,\mu g\,ml^{-1}$ of meropenem before reverting back to a bacillary form. Microscopy images were taken after 1, 6 and 22 hours. Left panels: transmitted light, right panels: fluorescence microscopy. In fluorescence images, green and red colouring indicates viable and lysed cells respectively.

University of Birmingham and University of Texas Health Science Center at Houston. Note that we have changed some variable notation from the paper for consistency with the remainder of this thesis. In the published version of this work we refer to the spherical cell population as S whereas in the following chapters we refer to this population as L.

2.1 Model formulation

The assumptions made for the model are based upon the results in [75], which we have reproduced experimentally, with our results displayed in Figure 2.1 (see Appendix A.1 for experimental Materials and Methods). The images indicate changes to cell morphology shortly after exposure to the antibiotic; spherical shaped cells can be seen after only one hour. After 22 hours we see rod-shaped cells that are in the process of dividing (Figure 2.1 (b)) and this indicates that the cells can revert back from the spherical form and continue proliferation. Additionally, the fluorescence microscopy images support the results of [75]; most of the cells stained green, indicating that these spherical forms were viable.

In accordance with these findings, our compartmental model follows the interactions described in Figure 2.2. We introduce variables (defined in Table 2.1) for rod-shaped

bacteria (H) and spherical bacteria (L). Here, we assume that the rod-shaped cell population consists of all those cells that are susceptible to the antibiotic, this may include cells that have shown signs of localised swelling or filamentation. In this model we will refer to this population as rod-shaped whereas the spherical cell population is made up of cells that have transitioned into this form due to antibiotic exposure. Experimental data has shown that the spherical cells are susceptible to lysis due to internal turgor pressure and that this causes the cells to expand before they lyse. For this model we will contain all spherical cells, regardless of their size, in the same population.

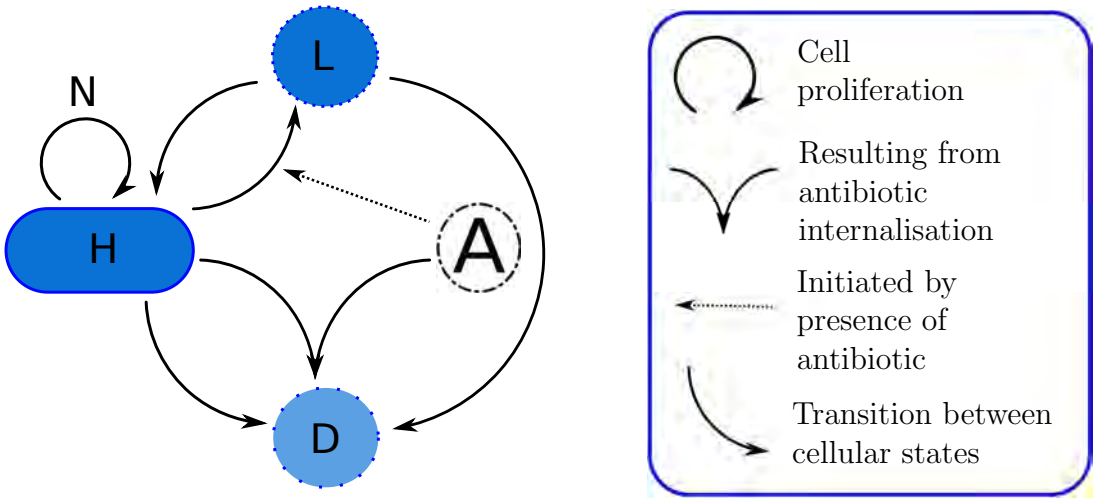

Figure 2.2: Schematic representation of the transitions of *P. aeruginosa* in response to exposure to meropenem. The species shown are defined as follows: H are rod-shaped cells, L are spherical cells and D represent dead cells. When the antibiotic, A, is introduced, rod-shaped cells can make the reversible transition to a spherical shape. The antibiotic is assumed to be effective at killing rod-shaped cells but not spherical cells due to a depleted cell wall. Rod-shaped cells lyse naturally as do spherical cells. Rod-shaped cells can proliferate if there is enough nutrient, N.

In addition to these variables we define the antibiotic concentration to be A and the proportion of nutrient remaining in the system, N. Including a nutrient dependent growth term, instead of the commonly used logistic growth term, will allow us to formulate a mechanistic model. Figure 2.2 also includes a population of dead cells, however we do not include this variable in the model or results. Any lysed cells will quickly disappear from the culture, we can therefore assume that the contribution made to the optical density by

the lysed cells can be considered negligible. This assumption is supported by Figure 2.1; with only a minority of cells in the image fluorescing red (indicating a dead cell) we can assume that the majority of dead cells have completely lysed and disappeared.

We assign parameters for the rates of growth, death and transition as defined in Table 2.2. Nutrient dependent growth will occur at the rate r and proliferation will concurrently incur a decrease in nutrient that occurs at the rate $\tilde{r}$. Nutrient growth and depletion are both modelled using a constant rate; we could use a monod expression to describe both of these processes, however, we choose this linear term as the bacteria are growing in a nutrient rich growth medium. For this model we assume that only rod-shaped cells can proliferate. This assumption is based on existing literature, experimentally characterising the proliferation of usually rod-shaped bacteria that have undergone conversion to spherical cells as a result of shedding the cell wall [73]. The experiments demonstrated that although proliferation of spherical cells was possible, it was only possible under specific osmoprotective conditions and even then proceeds in only a very small subset of spherical cells, with a doubling time 10-fold higher than that of the rod-shaped cells. Conventional proliferation becomes impossible due to the compromised integrity of the spherical cell wall; bacterial proliferation is heavily dependent on correct positioning of the cell wall and without this it is unlikely that a cell will successfully divide. Although *P. aeruginosa* was not included in these experiments, it was suggested that similar proliferation occurs across all bacteria; due to the high doubling time we will assume that spherical growth is negligible.

Meropenem is bactericidal hence its action is modelled via a death term distinct from natural death [50]. This additional term differs from some models that absorb the antibiotic effects into the model by means of a reduction in bacterial growth, yet this approach would be more suited to bacteriostatic antibiotics [8, 29]. The antimicrobial effects on the rod-shaped population is modelled using a density dependent term to incorporate a saturating effect. Attempts at using a linear term for this resulted in unsuccessful parameter fits (results omitted) and a saturating term was found to be more suitable in describing

the effects of the antibiotic; this is in keeping with previous models of antibiotic treated bacteria [8, 10, 102]. We assume that the meropenem only inhibits rod-shaped cell survival as experimental results indicate that transitioning to a spherical form mediates tolerance to lethal β-lactam antibiotic concentrations for multiple bacterial species [73, 75]. We assign ρ to be the maximum death rate of rod-shaped cells due to antibiotic and A_{50} to be the antibiotic concentration needed for half maximal killing. For simplicity, we set the Hill coefficient to 1 (i.e. $n = 1$ in (1.8)). We assume that the meropenem molecules will enter the cell and bind to the PBPs in order to inhibit cell wall synthesis. In this model we assume that this binding is irreversible due to the mode of action of β-lactams. The antibiotic molecules covalently modify PBPs upon binding [112] and therefore when a bacterium lyses, any bound antibiotic is unlikely to be released back into the extracellular domain. The irreversibility of the antibiotic results in antibiotic decay and we will take this to happen at a rate, $\tilde{\rho}$. Again, we choose not to have a specific Hill coefficient for simplicity. Investigation into the value of $\tilde{\rho}$ has shown that relaxing this parameter and setting $\tilde{\rho} = 0\,\mu\mathrm{g\,ml^{-1}\ OD^{-1}\ min^{-1}}$ does not affect the results significantly (results omitted) yet we include this assumption as it has an impact on long-term model predictions of bacterial growth. In addition to this, we take antibiotic decay to follow first order kinetics at a rate α. In concordance with [75], we assume that spherical cells evade the effects of the antibiotic.

The primary objective of this model is to investigate whether we can describe the population dynamics of *P. aeruginosa* in the presence of meropenem by including the morphological transition witnessed in experimental data. We model this transition from rod-shaped cells to spherical cells with a saturating term, similar to that used for the bactericidal effects of the antibiotic on the rod-shaped cell population. Following exposure to the meropenem the rod-shaped cells transition to a spherical form at a maximum rate γ and T_{50} defines the concentration for which we get the half maximal transition rate and again we assume that the Hill coefficient is 1. Following [73, 75] we include the process of reversion within our model: antibiotic is removed from samples in order to experimentally

show that spherical cells can transition back to the bacillary form, implying that this occurs independently from the presence of the antibiotic. Previous models of persister populations have assumed that reversion does not occur when a constant dose of antibiotic is administered [25, 26]. However, in our model, antibiotic may degrade out of the system and even when present the spherical cells may not be directly exposed to antibiotic at all times. Reversion will be independent from the antibiotic concentration and we define δ to be the rate at which this occurs. Supported by the microscopy results in Figure 2.1, this reverse transition also lends weight to the assumption that antibiotic decays as it suggests that the pressure on the bacteria from the antibiotic has decreased.

Finally, following our own fluorescence microscopy data, we assume that both types of cell will lyse naturally. In our microscopy results we witnessed lysed (red) rod-shaped cells even in the absence of antibiotic, indicating that some level of natural death must occur. Subsequently, we assume that spherical cells also lyse naturally due to the increased fragility of the cell structure. Lysed cells degraded sufficiently quickly that we may assume they do not contribute to the OD settings in our experimental set-up. The spherical cells lyse at a rate ψ, whilst rod-shaped bacteria lyse at a rate ϕ. Due to the availability of nutrient and general fitness of the rod-shaped cells we would expect ϕ to be small and due to the compromised integrity of the cell wall in spherical cells we expect $\phi < \psi$. We also expect natural rod-shaped cell death to happen at a slower rate than death due to antibiotic action.

Following mass action kinetics we produce Model I:

$$\frac{dH}{dt} = rNH - \left(\frac{\gamma A}{T_{50}+A}\right)H + \delta L - \left(\frac{\rho A}{A_{50}+A}\right)H - \phi H, \tag{2.1}$$

$$\frac{dL}{dt} = \left(\frac{\gamma A}{T_{50}+A}\right)H - \delta L - \psi L, \tag{2.2}$$

$$\frac{dA}{dt} = -\alpha A - \left(\frac{\tilde{\rho} A}{A_{50}+A}\right)H, \tag{2.3}$$

$$\frac{dN}{dt} = -\tilde{r}NH, \tag{2.4}$$

with initial conditions

$$H(0) = H_0, \quad L(0) = 0, \quad A(0) = A_0, \quad N(0) = 1. \tag{2.5}$$

As N is defined to be the proportion of initial nutrient remaining instead of a concentration we can specify $N(0) = 1$. All variables and parameters are defined in Tables 2.1 and 2.2 respectively.

Table 2.1: Definitions and units for the variables in Model I, described by equations (2.1)-(2.5).

Variable	**Definition**	**Units**
H	Antibiotic-susceptible rod-shaped cells	OD
L	Spherical shaped cells	OD
N	Nutrient proportion of initial concentration	dimensionless
A	Antibiotic concentration	μg ml^{-1}

Table 2.2: Definitions and units for the parameters in Model I, described by equations (2.1)-(2.5).

Parameter	**Description**	**Units**
α	Antibiotic decay rate.	min^{-1}
r	Growth rate of rod-shaped bacteria.	min^{-1}
$\tilde{r}$	Decay rate of nutrient due to consumption by rod-shaped bacteria.	OD^{-1} min^{-1}
γ	Transition rate from rod to spherical shape.	min^{-1}
δ	Transition rate from spherical to rod shape.	min^{-1}
ρ	Death rate of rod-shaped bacteria due to antibiotic.	min^{-1}
$\tilde{\rho}$	Decay rate of antibiotic due to irreversible binding to bacteria.	μg ml^{-1} OD^{-1} min^{-1}
ϕ	Death rate of rod-shaped bacteria.	min^{-1}
ψ	Death rate of spherical bacteria.	min^{-1}
T_{50}	Antibiotic concentration required for half maximal killing effect	μg ml^{-1}
A_{50}	Antibiotic concentration required for half maximal transition effect	μg ml^{-1}

2.2 Parametrisation data and methods

Parametrisation data

In order to successfully parametrise Model I we have used two sets of data, which we will refer to as Data set 1 and Data set 2. Single colonies of the *P. aeruginosa* strain PA1008, a meropenem susceptible isolate derived from a hospital burn unit [90], were inoculated in LB broth and grown overnight. The following day, meropenem was added to the bacteria culture at different concentrations. The optical density of each sample was recorded every 30 minutes for 24 hours to obtain growth curves for the population. A complete guide to the materials and methods used to obtain this data can be found in Appendix A.2. The first data set is used as parametrisation data; this consists of three biological replicates, each with three technical repeats. The meropenem concentrations used for this data set were $0\,\mu\mathrm{g\,ml^{-1}}$, $2\,\mu\mathrm{g\,ml^{-1}}$, $4\,\mu\mathrm{g\,ml^{-1}}$, $10\,\mu\mathrm{g\,ml^{-1}}$, $20\,\mu\mathrm{g\,ml^{-1}}$, $40\,\mu\mathrm{g\,ml^{-1}}$ and $200\,\mu\mathrm{g\,ml^{-1}}$. For each concentration we display the mean of the nine resulting growth curves. The error bars are formulated by calculating the standard deviation of the means of the three biological replicates.

Data set 2 is also referred to as the test data and includes one biological replicate with three technical repeats; the meropenem concentrations used for Data set 2 were $0\,\mu\mathrm{g\,ml^{-1}}$, $0.5\,\mu\mathrm{g\,ml^{-1}}$, $1\,\mu\mathrm{g\,ml^{-1}}$, $5\,\mu\mathrm{g\,ml^{-1}}$, $50\,\mu\mathrm{g\,ml^{-1}}$ and $100\,\mu\mathrm{g\,ml^{-1}}$. For each concentration, we calculate the mean value of the three resulting growth curves at each time point and the standard deviation error bars for this data set represent the standard deviation over the three technical repeats.

Parameter fitting methods

The parameter estimates were obtained using the MATLAB function *fminsearch*, which uses the Nelder-Mead algorithm as described in [61]. The *fminsearch* function fits parameters that minimise a specified objective function given some initial estimates. We

employ the following objective function,

$$R = \frac{1}{n}\left(\frac{||\left(\boldsymbol{H} + \frac{\boldsymbol{L}}{2}\right) - \boldsymbol{y}||_2}{||\boldsymbol{y}||_2}\right). \tag{2.6}$$

The vectors $\boldsymbol{H}$ and $\boldsymbol{L}$ are the solutions for rod-shaped and spherical cells respectively at the time points used in the experiments. The vector $\boldsymbol{y}$ consists of the OD values obtained in the experiment and n is the number of data values. This equation evaluates the mean relative error of the difference between the data and the solution to the system at each time point. We use the relative error in our objective function as unlike the absolute error the relative error should not be skewed by large or anomalous data points. We note here that the contributions of rod and spherical shaped cells to the OD differ in the objective function. OD is a measurement of the absorbency of a material; it measures how much light can pass through a sample and therefore reflects the total number of cells present in the inoculum. Rod and spherical cells will contribute differently to the OD measurement as they differ in size and absorbency. Therefore, rather than attempt to scale OD to obtain a total cell number, we work in OD and based on our biological insight we have assumed that spherical cells contribute half the absorbance of rod cells to the OD measurements.

When using the MATLAB function *fminsearch* to parametrise we also apply a constraint that restricts parameter values to non-negative values. To do this we apply a penalty to the objective function that increases its value significantly if a parameter is less than zero; we simply multiply the objective function value by 1000 (i.e. we make the penalised objective function much larger than we anticipate the relative error using the fitted parameters to be).

2.3 Results

2.3.1 Model parametrisation

Parametrisation without meropenem

We first fit the non antibiotic-associated parameters that we expect to remain fixed in the presence of antibiotic. By removing the antibiotic from the system we are left with the following pair of equations

$$\frac{dH}{dt} = H(rN - \phi), \tag{2.7}$$
$$\frac{dN}{dt} = -\tilde{r}NH, \tag{2.8}$$

with initial conditions

$$H(0) = H_0, \quad N(0) = 1. \tag{2.9}$$

The initial guess for r is $1 \times 10^{-3}\,\mathrm{min}^{-1}$ and for $\tilde{r}$ we choose $1 \times 10^{-1}\,\mathrm{OD}^{1}\,\mathrm{min}^{-1}$. The natural death rate, ϕ, is assumed to happen at a slower rate than growth; a bacterial population would not thrive if growth and death occurred at the same magnitude and we therefore choose an initial parameter guess for ϕ of $1 \times 10^{-5}\,\mathrm{min}^{-1}$. Including the initial condition, H_0, in our estimation allows for the incorporation of error, whether it be systematic or random, within the initial data values. The initial guess for H_0 is chosen to be the initial data value. We attain the results shown in Figure 2.3 parametrised by the resulting final estimates,

$$[r,\ \tilde{r},\ \phi,\ H_0] = [5.1 \times 10^{-3}\,\mathrm{min}^{-1},\ 8.9 \times 10^{-3}\,\mathrm{OD}^{-1}\mathrm{min}^{-1},$$
$$7.8 \times 10^{-6}\,\mathrm{min}^{-1},\ 0.17\,\mathrm{OD}]. \tag{2.10}$$

All parameters are given to two significant figures and the mean relative error is 7×10^{-4}. Figure 2.3 indicates that these parameters produce a good fit and that this model

with nutrient dependent growth can describe the growth dynamics of the bacteria in the experiment. We note that the model is unable to reproduce the slight lag phase (see papers by, for example, Zwietering et al. and Biranyi et al. for developments of the logistic model that can achieve this [13, 118]) and instead underestimates the initial condition; we do not anticipate that this will alter any of the findings of this study and therefore choose not to include further parameters to obtain the lag phase. We also notice that the death rate is much lower than the growth rate; this supports the hypothesis that the natural death rate of the rod-shaped bacteria will be low.

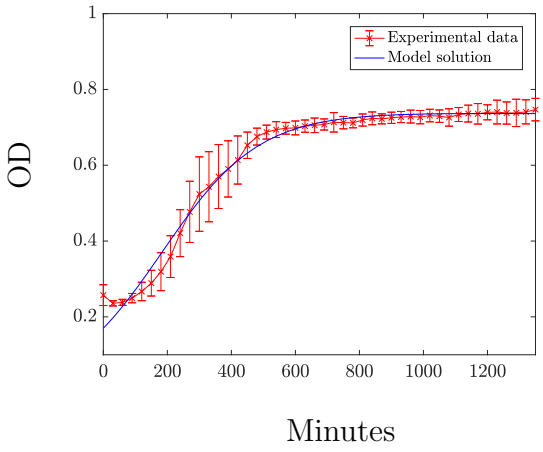

Figure 2.3: The solution to the system (2.7)-(2.9) using the parameters in (2.10), plotted with the experimental data for the growth curve of *P. aeruginosa* (Data set 1). Data points are plotted with errorbars representing the standard deviation of the means of the three biological replicates.

Parametrisation with meropenem

Fixing the parameters given by equation (2.10), we use the killing curves to estimate the remaining parameters that are attributed to the presence of antibiotic. This data includes the addition of meropenem at multiple concentrations and therefore the full system, equations (2.1)-(2.5), is used. Early parametrisation attempts provided initial parameter guesses for the optimiser and these values are shown in Table 2.3 along with the estimated parameter values obtained.

The optimiser estimated the values of all but two parameters, α and $\tilde{\rho}$, which were

Table 2.3: Estimated parameter values (EPVs) for Model I. We define two parameter sets, one that results in population elimination for all concentrations of meropenem (Θ_1) and another that displays population recovery of the bacteria when $2\mu g\,ml^{-1}$ is added, Θ_2 (only α and $\tilde{\rho}$ differ between the two sets). Units for each parameter are shown in Table 2.2. R represents the sum of the relative errors for each of the data sets in Data set 1. Early parametrisation attempts were used to gauge reasonable initial parameter guesses (IPGs).

Parameter	IPG	EPV	
		Parameter set that incurs population elimination Θ_1	Parameter set that incurs population recovery Θ_2
r	1×10^{-3}	5.1×10^{-3}	5.1×10^{-3}
$\tilde{r}$	1×10^{-3}	8.9×10^{-3}	8.9×10^{-3}
ϕ	1×10^{-5}	7.8×10^{-6}	7.8×10^{-6}
α	1×10^{-3}	1.4×10^{-8}	5.5×10^{-6}
γ	3×10^{-3}	5.4×10^{-3}	5.4×10^{-3}
δ	1×10^{-3}	1.8×10^{-3}	1.8×10^{-3}
ψ	9×10^{-5}	1.2×10^{-5}	1.2×10^{-5}
ρ	1×10^{-3}	1.7×10^{-3}	1.7×10^{-3}
$\tilde{\rho}$	1×10^{-3}	2.9×10^{-3}	8.2×10^{-3}
T_{50}	0.5	0.47	0.47
A_{50}	0.5	0.13	0.13
R	-	3.47×10^{-3}	3.56×10^{-3}
OD when $A_0 = 2$ at $t = 5000$		0.069	0.37

determined to be unidentifiable. These two parameters represent the natural decay rate and the rate of decay due to internalisation of the antibiotic; both are rates of decay of a species for which we do not have data explicitly and thus it is unsurprising that they cannot be identified. Latin hypercube sampling was used to investigate the possible values of the two unidentifiable parameters and the results of this concluded that multiple pairings of values can be used to successfully describe the population dynamics of all concentrations. Further investigation into these feasible parameter pairings revealed two qualitatively different predictions for population growth when the model is simulated over a longer time period than used in experimental procedure. We choose two parameter sets Θ_1 and Θ_2 to represent each of these outcomes, see Table 2.3. The estimated initial condition H_0 obtained for each parameter set can be found in Table 2.4.

Table 2.4: Estimated initial condition H_0 for each experimental data set in Data set 1. Initial antibiotic concentration is fixed. The initial experimental data values are chosen as the IPGs. EPVs obtained by treating the initial condition as a parameter and simultaneously fitting all data sets from Data set 1, with parameters fixed, using the built in MATLAB function *fminsearch*.

Antibiotic concentration	IPG	EPV	
		Parameter set Θ_1	Parameter set Θ_2
2	0.25	0.23	0.22
4	0.26	0.23	0.23
10	0.26	0.23	0.23
20	0.26	0.23	0.23
40	0.26	0.24	0.24
200	0.25	0.24	0.24

Using parameter sets Θ_1 and Θ_2 we obtain the results shown in Figure 2.4; both parameter sets successfully fit the model to all of the experimental data in Data set 1. The total errors of these data fits over all concentrations are 3.47×10^{-3} and 3.56×10^{-3} respectively and if taken as an indicator of goodness of fit, along with the visual fits shown, we cannot distinguish between the two parameter sets when using Data set 1. However, in future tests we find that there are slight differences in the ability of the two parameter sets to describe the growth of the population at low antibiotic concentrations (in Data set 2 and cell count data - see Section 2.3.2.

The qualitative differences between Θ_1 and Θ_2 emerge when we use the model to predict the population growth over a longer time only for the case when $2\mu\text{g ml}^{-1}$ is added (for higher concentrations population eradication occurs for both parameter sets). Figure 2.5 (a) displays the model solution for the predicted growth of the bacterial population over a time of approximately 10 days using parameter set Θ_1: the model predicts the eventual elimination of the population due to antibiotic effects and an exhausted nutrient supply. In contrast, if we simulate the experiment for this time using Θ_2, we get the results shown in Figure 2.5 (b). The results indicate that instead of the population dying out, we would expect a large growth recovery period shortly after the time of the experiment, with

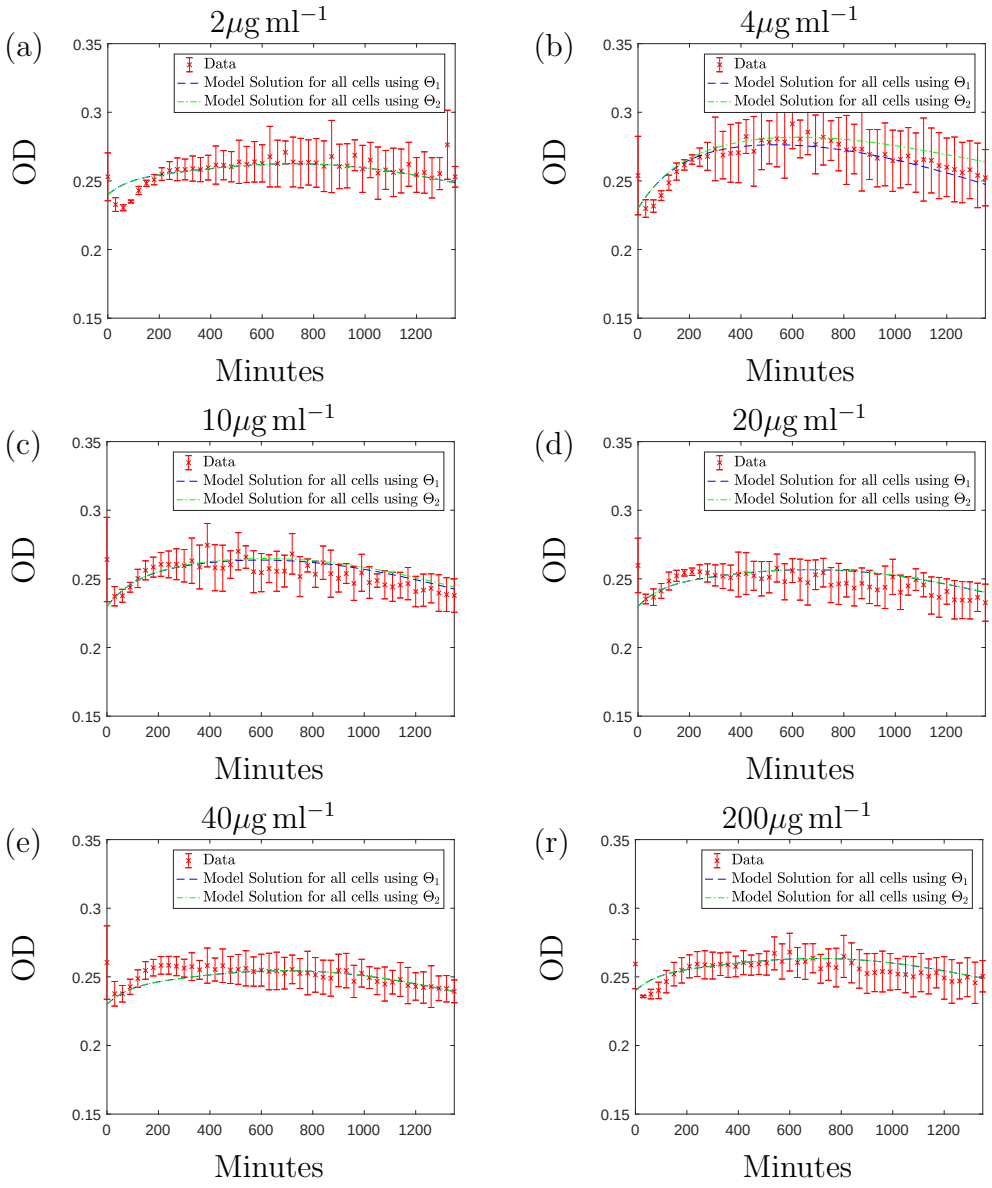

Figure 2.4: The solution to the system (2.1)-(2.5) with Θ_1 (blue dashed line) and Θ_2 (green dotted line). Initial conditions are taken from Table 2.4, for (a) $2\,\mu g\,ml^{-1}$, (b) $4\,\mu g\,ml^{-1}$, (c) $10\,\mu g\,ml^{-1}$, (d) $20\,\mu g\,ml^{-1}$, (e) $40\,\mu g\,ml^{-1}$ and (f) $200\,\mu g\,ml^{-1}$ of meropenem. These results are plotted along with the data points (red crosses) from Data set 1 with errorbars displaying the standard deviation of the means of three biological replicates. Data values are measured in optical density (OD); we formulate the solution for OD using the equation $OD(t) = H(t) + \frac{S(t)}{2}$.

the optical density levels surpassing those measured in the experiments. This is followed by a slow, natural death phase caused by nutrient depletion. To explain this, we break down the solution in Figures 2.6 (a)-(d). These single variable solutions show that when

using Θ_2, the antibiotic degrades at a higher rate than under parameter set Θ_1. Due to the higher antibiotic depletion rate, we predict that the antibiotic will be unsuccessful in killing off the bacteria and growth resumes until around 5000 minutes when nutrient supply depletes and slow natural death dominates. The nutrient levels predicted using Θ_1 indicate that the nutrient is almost completely used up before the antibiotioc has fully degraded from the system. Consequently, bacterial growth cannot exceed death and this results in the population being eradicated by the antibiotic. We also notice, when modelling the system using Θ_2, that the population of spherical cells depletes entirely, shortly after the antibiotic is expended: the cells revert back to the native bacillary morphotype, as witnessed in the results in [75] and our microscopy results in Figure 2.1.

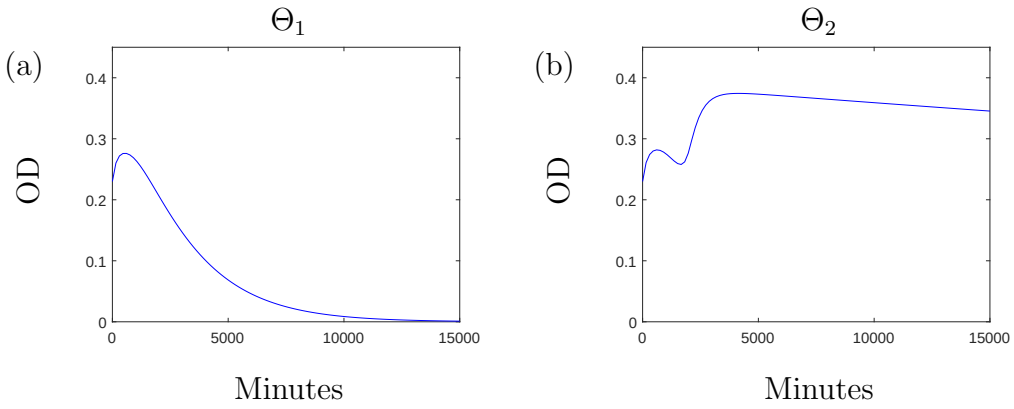

Figure 2.5: The long term solution to the system (2.1)-(2.5), using parameter sets (a) Θ_1 and (b) Θ_2 from Table 2.3, with $A_0 = 2$. Parameter set Θ_2 has a faster rate of antibiotic loss due to internalisation and this results in the antibiotic degrading from the system before it can sufficiently eliminate the bacteria. For higher concentrations of antibiotic we see the bacteria being eliminated by the antibiotic for both parameter sets (results omitted).

These qualitatively different characteristics result from varying values of only two parameters and indicate the sensitivity of the model solution to these parameters. Furthermore, the differences in parameter values indicate that it is the value of $\tilde{\rho}$ that determines whether we predict population eradication or recovery. Θ_1 has a slower rate of natural antibiotic degradation, α, yet it is possible to use a higher value for this parameter and this still results in the population dying out sooner (results omitted). The difference in

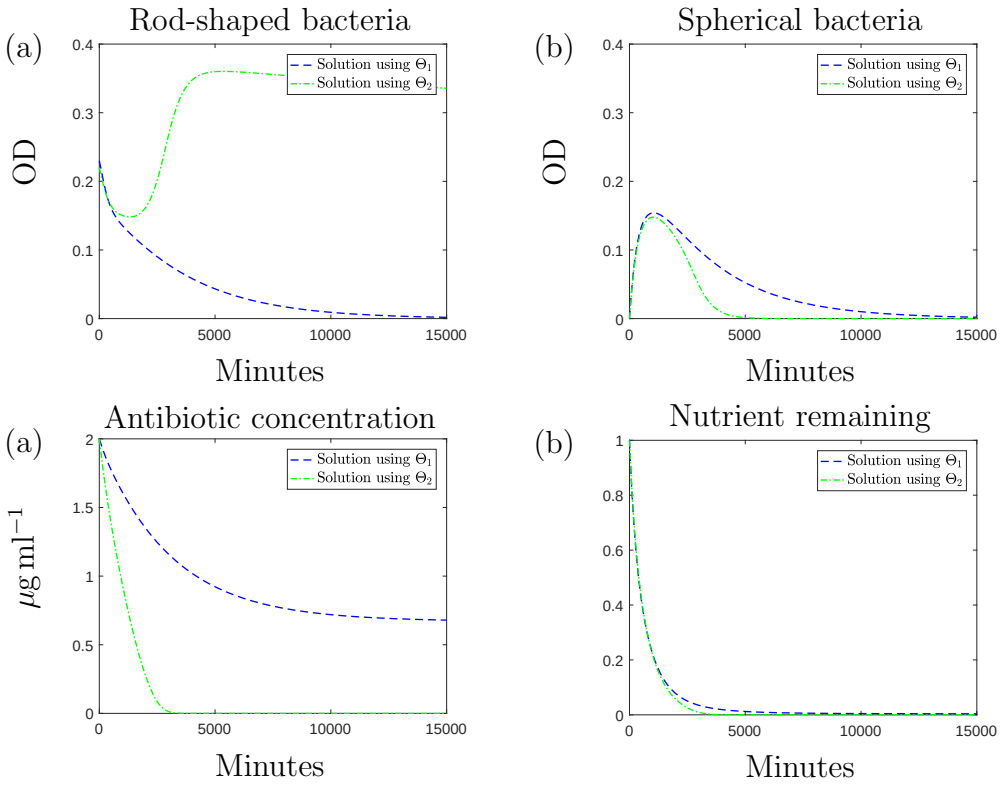

Figure 2.6: The individual variable solutions to system (2.1)-(2.5) with $A_0 = 2$. The solution using Θ_1 is represented with a blue dashed line and the green dashed-dotted line represents the solution using Θ_2 for (a) rod-shaped cells, (b) spherical shaped cells, (c) antibiotic concentration and (d) nutrient. We note that these solutions are simulated over a longer time series than the experiments. The results for higher concentrations of antibiotic follow the trend of Θ_1 for each variable when using either parameter set. The only exception to this is the predicted growth of H when using Θ_2; here the population of H is eradicated to low OD values for all higher values of A_0.

our values of $\tilde{\rho}$ is less significant numerically than that for α yet drastically changes the estimated growth characteristics of the bacteria.

2.3.2 Parameter testing

Testing OD predictions

To test our parametrisation results, we use Data set 2 to examine whether the parameters obtained can successfully fit the data acquired from an additional biological replicate, with differing initial antibiotic concentrations. Initially we tested the parameters obtained

using the growth curve in the absence of meropenem; by fixing these parameters yet allowing the initial condition to be fitted to the new data, we are able to successfully describe the growth curve of the new data. The results, shown in Figure 2.7, show that although we are not able to capture all the detailed dynamics of growth, the growth rates found for the initial data set are able to predict the overall behaviour of the new data set when no antibiotic is added.

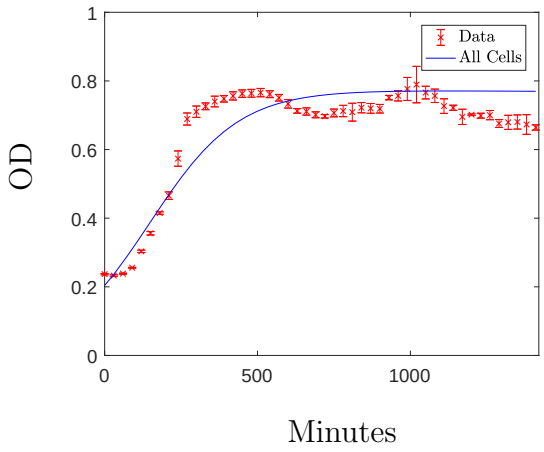

Figure 2.7: The solution to the system (2.1)-(2.5) using the parameters in (2.10), plotted with the additional test data for the growth curve of *P. aeruginosa* (Data set 2). Using *fminsearch* we get a relative error value of $R = 0.002$ with an estimated initial condition $H_0 = 0.2$ when using growth rates (2.10).

After testing Θ_1 and Θ_2 against the new data set that includes the addition of antibiotic we obtain the results displayed in Figure 2.8. Although both parameter sets are suitable in describing the general trend of the curves for the higher concentrations of antibiotic ($\geq 2\,\mu\text{g}\,\text{ml}^{-1}$), Θ_1 appear to describe the dynamics of the new kill curve data at the lower concentration more successfully. Θ_1 gives a relative error value of $R = 0.014$ and the model captures the general trend of each curve at the earlier and later timepoints but does miss some qualitative behaviour at intermediate timepoints (the dip in OD prior to regrowth observed in Figures 2.8 (a)-(c) does not emerge). Nevertheless the model fits the test data (including new concentrations) sufficiently well to proceed to the subsequent analysis of the parametrised model. We note that the initial conditions have been fitted

to the data; fixing the initial conditions results in a similar prediction for Θ_1 and using Θ_2 the model overestimates growth.

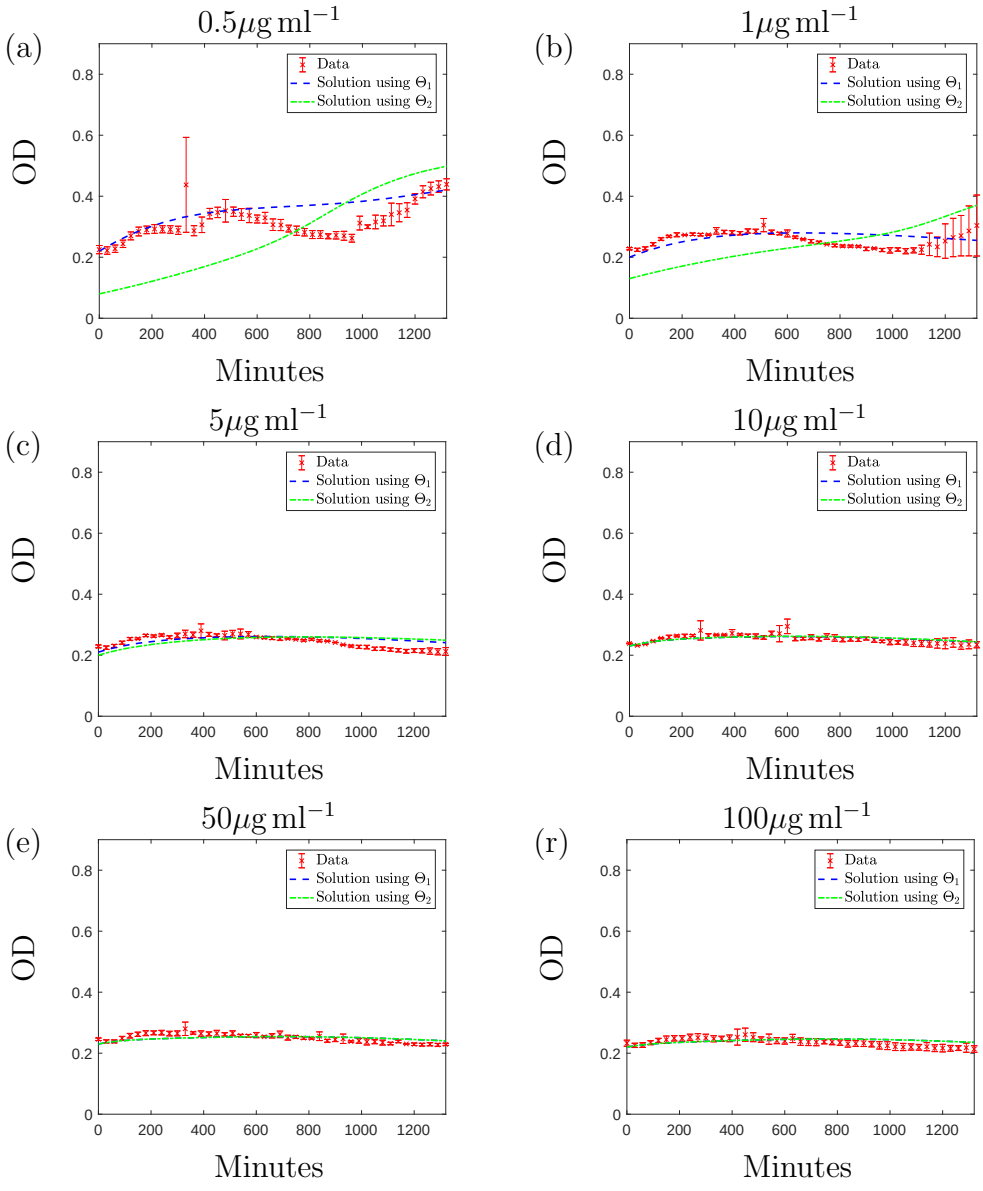

Figure 2.8: The solution to the system (2.1)-(2.5) with Θ_1 (blue dashed line) and Θ_2 (green dashed-dotted line). These results are plotted along with the data points from Data set 2 (along with standard deviation errorbars) with initial antibiotic concentrations of (a) $0.5\,\mu g\,ml^{-1}$, (b) $1\,\mu g\,ml^{-1}$, (c) $5\,\mu g\,ml^{-1}$, (d) $10\,\mu g\,ml^{-1}$, (e) $50\,\mu g\,ml^{-1}$ and (f) $100\,\mu g\,ml^{-1}$ meropenem. The initial conditions were estimated using the initial data points as initial estimates. Data values are measured in optical density (OD); we formulate the solution for OD using the equation $OD(t) = H(t) + \frac{L(t)}{2}$.

Additionally, we notice that the experimental results using $0.5\,\mu g\,ml^{-1}$ and $1\,\mu g\,ml^{-1}$

display periods of population regrowth at later timepoints, a result that is also seen in the microscopy results at 22 hours (see Figure 2.1). The model predicts this behaviour (over a longer timeframe) when using Θ_2 for an initial concentration of $2\,\mu g\,ml^{-1}$. Using antibiotic concentrations from Data set 2, Θ_1 can also successfully describe the post-antibiotic regrowth phase for lower concentrations, as well as predicting the eradication of the population using higher concentrations.

Testing the parameter sets against this new data suggests Θ_1 may be a more viable parameter set but importantly we reiterate the dependence of these fits on the values of the unidentifiable parameters related to antibiotic decay. Furthermore, we shall see below that when comparing against a different experiment, Θ_2 may match the data better.

Using Data set 2 has enabled us to test the OD predictions of the model, however, the OD measurements provide no insight into the proportions of rod-shaped and spherical cells within the total population. In order to validate our model predictions further we use microscopy results to estimate the contribution of each subpopulation to the overall OD value.

Calibration against microscopy images

The images in Figure 2.1 give glimpses of the bacterial population at 3 time points of the experiment and we can clearly see that a shape transition is occurring during the experiment. The proportion of different phenotypes visible in further images under 3 conditions and at 3 timepoints were obtained using the cell counter plug-in for Fiji [96, 97]. Visible in many of the images were cells that were of an intermediate form or filamentous and following the assumptions of the model, bacteria of all phenotypes that were not completely spherical were contained in the rod-shaped population. For each concentration and time point we obtained up to 7 images; Table 2.5 displays the mean proportions of each of the subpopulations over the various images used.

To compare the cell count results to the model solutions, the model solutions must be scaled from OD to cell number. We use the scaling given in [56] where an OD measurement

Table 2.5: The average proportions of each bacterial subpopulation, obtained using the microscopy images. The values in this table were obtained by counting the number of cells in each subpopulation in each slide. The proportions were then calculated by dividing the number of cells in a each subpopulation by the total number of cells in the image. The mean proportion was then taken.

Antibiotic concentration	Subpopulation	Time *(Number of images)*		
		1 hour	6 hours	22 hours
$0\,\mu\mathrm{g\,ml^{-1}}$	H	1 *(5)*	1 *(6)*	1 *(7)*
	L	0 *(5)*	0 *(5)*	0 *(5)*
$0.5\,\mu\mathrm{g\,ml^{-1}}$	H	0.981 *(6)*	0.781 *(6)*	0.989 *(6)*
	L	0.019 *(6)*	0.219 *(6)*	0.011 *(6)*
$2\,\mu\mathrm{g\,ml^{-1}}$	H	0.95 *(5)*	0.411 *(5)*	0.953 *(6)*
	L	0.05 *(5)*	0.589 *(5)*	0.047 *(6)*

of 1 is given as equivalent to 2.04×10^8 cells. Comparing the model predictions to the cell count data gives the results displayed in Figure 2.9. For the case when no antibiotic is added we see that the microscopy results match the model predictions exactly; since no antibiotic is in the system we would not expect the bacteria to transition and therefore we only see and predict rod-shaped cells. As we add antibiotic, we find that the microscopy counts match the model predictions well for the majority of timepoints, especially when using Θ_2. Qualitatively, for both parameter sets (and quantitatively for Θ_2), we get a good comparison for the lower concentration of $0.5\mu\,\mathrm{g\,ml^{-1}}$; less than half of the bacteria transition to the spherical form over the first few hours of the experiment before the population becomes almost entirely comprised of rod-shaped cells towards the end of the experiment. As we increase the antibiotic concentration we get a very good comparison over the first two timepoints but at the final timepoint we notice some disparity between the cell counts and the model solutions. Qualitatively, the solution using Θ_2 is equivalent to the microscopy result. Θ_1 predicts different qualitative behaviour with a long-term persistent population of spherical cells. At higher concentrations of meropenem, both parameter sets predict this and this is reflected in the killing curve data where significant growth does not occur at these higher concentrations. Qualitatively the experimental data shows the spherical cells transitioning back to rod-shaped more quickly than that captured by Θ_2. However, the fragility of the spherical cells will influence the experimental

result: in [75] it was found that spherical cells would easily burst when placed directly between the slide and coverslip. It is likely that this also would have occurred during our experiments, thus leading to fewer spherical cells being visible in the images. It is therefore possible that the population appears to transition back to fully rod-shaped quicker than it actually would since many of the spherical cells in the sample could burst before the image was taken.

Given the good qualitative and quantitative agreement between the data sets and either Θ_1 or Θ_2 (depending on the type of data), we proceed our analysis using both parameter sets. Recall that the difference between the two data sets results from two unidentifiable parameters; continuing with both parameter sets we can ensure a comprehensive range of plausible qualitative behaviour is explored.

2.3.3 Manipulating the morphological transition

Our primary interest in formulating this model is to investigate the proposed morphological change observed in our experimental data of *P. aeruginosa*. This shape transition has been associated with the ability of the bacteria to withstand high levels of antibiotic and using suitable parameters we can reproduce the bacterial regrowth witnessed in our experimental data. We can now manipulate the system by changing parameters associated with the transition mechanism to investigate the impact the shape transition has on bacterial susceptibility and produce predictions that could facilitate treatment design.

Figures 2.10 (a)-(f) display numerical simulations used for the analysis in this section. We note here that the results using Θ_1 are qualitatively the same regardless of the initial antibiotic concentration and these are also similar to the results when using Θ_2 with initial antibiotic doses of $> 2\,\mu\mathrm{g\,ml^{-1}}$. The results for Θ_2 differ for higher ($> 2\,\mu\mathrm{g\,ml^{-1}}$) and lower ($2\,\mu\mathrm{g\,ml^{-1}}$) antibiotic concentrations and therefore we only include simulations using Θ_2 for brevity (i.e. the Θ_1 results are equivalent to the Θ_2 results at $10\,\mu\mathrm{g\,ml^{-1}}$). We have chosen to display simulations using the initial antibiotic dose of $A_0 = 2\,\mu\mathrm{g\,ml^{-1}}$ as the results in this case differ from the other concentrations and $A_0 = 10\,\mu\mathrm{g\,ml^{-1}}$ as this

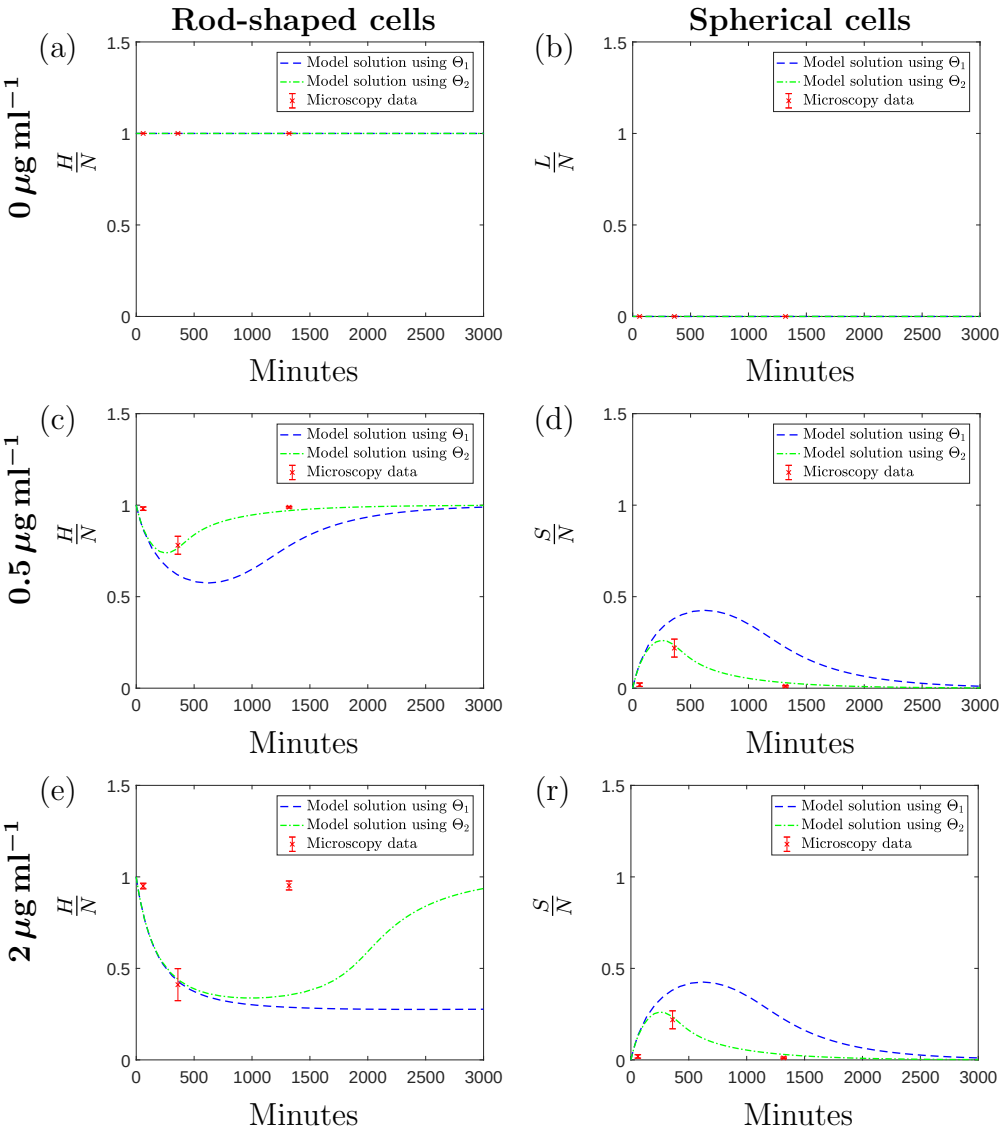

Figure 2.9: The variable solutions with respect to total population for H with (a) $A_0 = 0$, (c) $A_0 = 0.5$, (e) $A_0 = 2$, and L with (b) $A_0 = 0$, (d) $A_0 = 0.5$ and (f) $A_0 = 2$. Solutions were obtained by solving the system (2.1)-(2.5) using Θ_1 (blue dashed) and Θ_2 (green dashed-dotted). The red markers show the proportion of each subpopulation with respect to the total number of cells counted in the microscopy images. The errorbars indicate the standard deviation over the multiple images used.

case represents a clinically relevant antibiotic concentration.

Inhibiting the change from rod-shaped to spherical cells

To propose that the morphological transition is a defensive mechanism that occurs due to antibiotic exposure would imply that inhibition of this mechanism would be detrimental to

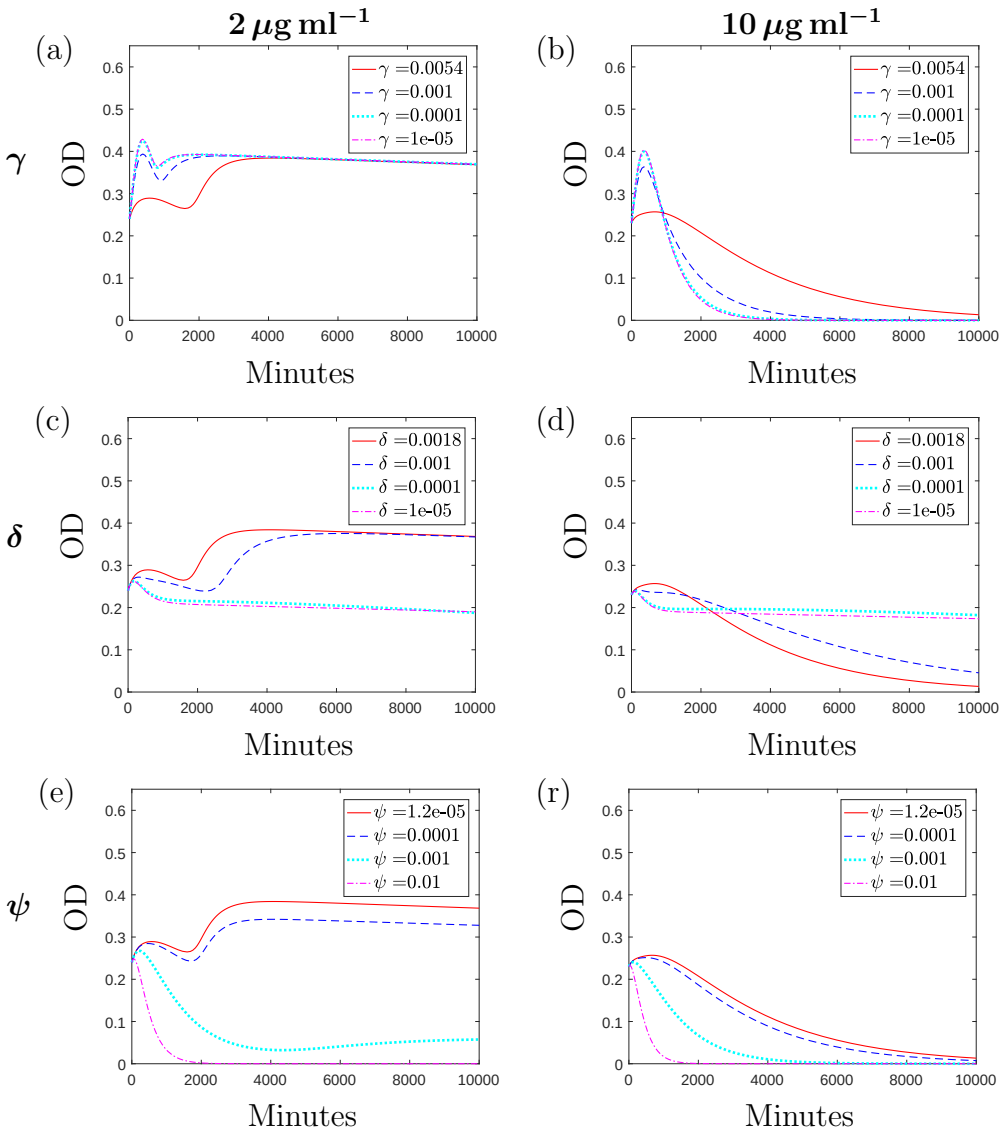

Figure 2.10: The solution to the system (2.1)-(2.5) using Θ_2 and varying the parameters (a) γ for the case where $A_0 = 2$, (b) γ for the case where $A_0 = 10$, (c) δ for the case where $A_0 = 2$, (d) δ for the case where $A_0 = 10$, (e) ψ, when $A_0 = 2$ and (f) ψ when $A_0 = 10$. The default values, found via paramterisation, are depicted by the red solid lines. Values for all varied parameters have units min^{-1}.

the bacteria. By decreasing the transition rate γ we can examine whether inhibition may lead to enhanced antibiotic action and scrutinise the impact of the transition mechanism.

Figures 2.10 (a)-(b) illustrate numerical simulations of the experiment varying γ using Θ_2 and initial antibiotic doses of $2\,\mu\text{g}\,\text{ml}^{-1}$ and $10\,\mu\text{g}\,\text{ml}^{-1}$ respectively. At $10\,\mu\text{g}\,\text{ml}^{-1}$, these simulations imply that inhibiting the transition to a spherical morphology would

initially lead to higher OD levels but in all cases we ultimately achieve increased antibiotic action with the bacterial population being eradicated faster than when we use the default value of γ from the respective parameter set. The higher initial OD levels are a consequence of having more rod-shaped cells in the system as they have a higher contribution to the OD than the spherical cells.

A different result is obtained in Figure 2.10 (a). In this case we see that though a decrease in γ will result in an increase in OD levels initially (as above), the population will grow to the same value regardless of the decrease in transition rate. This population value is reached once the antibiotic dose of $2\,\mu\mathrm{g\,ml^{-1}}$ has been exhausted and the system is reduced to equations (2.7)-(2.8). Bacterial growth once again becomes dependent on the proportion of nutrient remaining in the system and as this depletes, bacterial growth is unable to exceed bacterial death, resulting in a post-antibiotic, post-nutrient death phase. Thus the transition to spherical cells may be considered a long-term defence mechanism only at higher concentrations of antibiotic.

Inhibiting the reverse transition

Our microscopy results support the conclusion made by Monahan et al. that *P. aeruginosa* bacteria are able to transition back to rod-shaped cells after transitioning to a spherical form [75]. This reverse transition grants the bacteria the ability to resume growth and in Figure 2.6 (a)-(b) we saw results that indicate the impact of this mechanism on restoring the bacterial population size. Decreasing δ, the transition rate from spherical to rod-shaped bacteria, from its estimated value illustrates how inhibiting this mechanism would impact the survival of the bacteria.

Figure 2.10 (c)-(d) show the results of these simulations. Our variable solutions (omitted) indicate that for all initial antibiotic concentrations and using both parameter sets, decreasing the rate of the reverse transition predicts a higher population of spherical cells and fewer rod-shaped cells, as might be anticipated. If we inhibit the transition sufficiently ($\delta < 1 \times 10^{-4}\,\mathrm{min^{-1}}$), the model predicts similar overall population levels (OD_{600} values

of around 0.2), that are made up entirely of spherical cells, regardless of the parameter set used or the initial antibiotic concentration (compare the blue and pink lines in Figures 2.10 (c)-(d)). Since we have assumed that the spherical cells cannot proliferate but do evade antibiotic effects, the larger spherical cell population results in prolonged antibiotic and nutrient availability. Consequently, this predicts a system where though spherical cells can transition back to a rod-shape at a much slower rate, in doing so they become exposed to the effects of the unused antibiotic. Alternatively, they die naturally due to their inherent fragility and this produces an extended death phase that ultimately leads to population eradication, but over a much extended period of time than simulated. Conversely, if the level of inhibition is not sufficient then we predict lower population levels initially than with default parameters, although behaviour is the same over the prolonged period of time.

In cases where the antibiotic was previously unable to eradicate the population (for example when we simulate the case of $2\,\mu\mathrm{g\,ml^{-1}}$ using Θ_2), inhibiting the transition at which spherical cells can revert back to the bacillary form is advantageous to us as it extends the efficacy of the antibiotic. This is reflected in Figure 2.10 (c) where we see that the population level predicted through sufficient inhibition is less than that predicted when using the default value. However, Figure 2.10 (d) displays the results when we use parameter set Θ_2 and let $A_0 = 10\,\mu\mathrm{g\,ml^{-1}}$; this represents a system that would have previously predicted population eradication and by inhibiting the transition, we see that the total population level achieved through sufficient inhibition is larger than we predicted when using the default parameter value. Restricting the reverse transition interferes with the antibiotic action and prevents the antibiotic from killing the bacteria. This result is reiterated when using Θ_1 for all initial concentrations and Θ_2 for concentrations above $2\,\mu\mathrm{g\,ml^{-1}}$.

Investigating the use of antimicrobial peptides

In addition to investigating and establishing the existence of the transition mechanism, Monahan et al. experimented with the use of antimicrobial peptides (AMPs) as an additional antimicrobial agent. These AMPs are relatively inactive against rod-shaped *P. aeruginosa* as they induce cell death by creating pores in the cytoplasmic membrane, which remains unexposed in normal bacillary cells. However, they found that spherical cells displayed large areas of exposed cytoplasmic membrane which gave reason to believe that they would be more susceptible to the bactericidal effects of AMPs. This hypothesis was supported by experimental data that saw a combination therapy of meropenem and AMPs leading to lower bacterial load [75].

We can reproduce this theoretically by increasing the death rate of spherical cells, ψ. Increasing the death rate ψ is equivalent to administering AMPs; these results are shown in Figures 2.10 (e)-(f). An expected increase in spherical cell death and consequently a decrease in rod-shaped cells results in faster population suppression for all concentrations and both parameter sets. The depleted spherical cell population means that fewer cells transition back to their native bacillary form and lower OD levels are achieved overall. We note that for the case of $2\,\mu\mathrm{g\,ml^{-1}}$ using Θ_2 ψ must be increased from its default value more than is required for the other cases for the AMPs to successfully assist the meropenem in killing off the bacteria population, in comparison to cases with higher initial antibiotic concentration or using Θ_1. However, under all parameter conditions, any increase in spherical cell death results in lower OD predictions and this reinforces the results of Monahan et al. and advocates the use of meropenem in combination with AMPs as a potential therapy for treating *P. aeruginosa*.

2.4 Discussion

Following the conclusions made by Monahan et al. [75] and supported by our own data, we have formulated a model that describes the growth dynamics of *P. aeruginosa* in the

presence of meropenem, with the inclusion of a subpopulation of cells with an incomplete cell wall that results in an altered shape and size. We have made assumptions regarding the inducement of this morphological shift and by successfully fitting it to experimental data we obtained two parameter sets that successfully fit the data yet result in qualitatively different predictions of the long-term bacterial dynamics and different predictions when we investigate the values of some of the model parameters. The values of the antibiotic-attributed parameters were found to determine whether the bacterial population survived antibiotic action when the initial antibiotic concentration was $2\mu\mathrm{g\,ml}^{-1}$. We notice that this is around the MIC value for meropenem when used to treat *P. aeruginosa* and this could describe the system sensitivity to the antibiotic parameters at this antibiotic concentration.

By formulating a mechanistic model we have obtained parameter values that are not only potentially measurable but are also more meaningful and directly relate to the amount of nutrient in the experiment. The model can successfully describe the overall trends witnessed in the growth curves and although the model does not capture the growth dynamics over the first few hours of the experiment perfectly, the impact of this on the applications of this model is arguable as our interests lie with the long term predictions of population growth, which are accurately predicted. The error over this region increases for the higher antibiotic doses yet we note these are much higher than the recommended clinical dose of $10-20\,\mu\mathrm{g\,ml}^{-1}$, therefore any discrepancies obtained for these concentrations should have no clinical relevance. We also take note of the large error bars for the initial condition: the high level of variance between the measurements taken at this time point means it could be difficult to achieve a fit of high confidence in this region regardless. Furthermore, having parametrised the model from total bacterial load (OD measurements) the model is then able to correctly predict the underlying dynamics of the individual rod-shaped and spherical populations (calculated from the microscopy data).

Manipulation of the parameters obtained allows us to investigate the impact of inhibiting the transition mechanism. Our results suggest that inhibiting the spherical transition

would be detrimental to bacterial populations in most cases with inhibition leading to faster depletion and lower OD levels over a long time scale. An exception to this is when we use parameter set Θ_2 and initial antibiotic concentration of $2\,\mu\mathrm{g\,ml}^{-1}$; in this case, inhibition is only detrimental to growth in the short term, whereas long term predictions are the same regardless of the level of inhibition. In most cases (including all antibiotic concentrations for Θ_1) the results imply that inhibition of the spherical transition would be desirable in treating a *P. aeruginosa* infection and thus support the hypothesis that this may be an intrinsic defence strategy of the bacteria.

When the transition to spheres was inhibited, the simulations also displayed a characteristic of higher OD levels over the first few hours than with no inhibition; if these results were to be directly translated to an *in vivo* infection, this could imply a higher level of bacterial virulence. However, in order to formulate biological conclusions based on these results we must consider the virulent properties of the different cell types we include in the model. A higher OD value does not automatically signify a higher level of virulence since we cannot assume that the virulence of spherical cells is half that of the rod-shaped cells, an assumption we make for the OD. Virulence in *P. aeruginosa* is to a large extent based on the Type III secretion system and secreted toxins; both of which depend on outer membrane components for successful secretion. It is probable that the spherical cells are less virulent than the rod-shaped cells due to their compromised outer membrane. If this assumption is correct then although inhibition of the shape transition predicts higher antibiotic action over the total time, a higher initial bacterial load would not be a desirable effect of a treatment when these are predominantly rod-shaped cells. Increased virulence could be threatening to a patient's health and this would be especially dangerous when treating immunocompromised patients.

An alternative strategy would be to target the reverse reaction and our results indicate that this approach could be beneficial, depending on the virulent properties of the spherical cells. By inhibiting this reaction we predict a higher proportion of spherical cells and this enables successful suppression of a lower proportion of remaining rod-shaped cells

without exhausting the antibiotic supply. Following this phase of rod-shaped cell death, the model predicts that for sufficient inhibition, the bacteria attains similar spherical-only population levels regardless of the parameter set used or initial antibiotic concentration. Though in many cases the estimated population level is higher than we would predict using the default parameter values, this would not be an undesirable outcome under the assumption that spherical cells are not as virulent as rod-shaped cells due to the compromised cell membrane.

Owing to the high proportion of spherical cells we predict when inhibiting the spherical to rod transition, we could consider the combination therapy of meropenem and AMPs with a drug that would inhibit the reverse transition. Simulations suggest that if we sufficiently inhibit the reverse transition rate then any increase in spherical cell death would result in faster killing of the bacterial population and extended antibiotic presence regardless of the parameter set used or initial antibiotic concentration (results omitted for brevity). Here we define sufficient inhibition of the reverse transition to be when we choose a value for δ that predicts population levels comprised of mostly spherical cells.

If we do not attempt to inhibit the morphological transition and instead pursue the application of a drug that increases the death rate of spherical cells alone, we predict lower OD levels. This supports the results detailed in [75] that promote the use of AMPs as a supplementary agent in combination therapy with the meropenem and empiric studies have also found that β-lactam and AMPs act synergistically to inhibit growth [116]. In Chapter 4 we extend the investigation into the use of AMPs in order to explore whether they maintain a synergistic relationship with meropenem at the site of infection.

We have formulated a model to predict the growth dynamics of *P. aeruginosa* witnessed *in vitro*. In order to make conclusions in a clinical setting we would have to translate the model to an *in vivo* model and extend it to include antibiotic dosing instead of the single antibiotic application used in our experiments. We would also need to consider how nutrient availability would differ *in vivo*. Nutrient availability *in vivo* is likely to be lower than in the nutrient rich growth media used in experiments, but it may be re-

plenished over time. Numerical simulations (omitted) indicate that if nutrient-abundance is maintained for longer, the bacteria may withstand higher concentrations of antibiotic.

In conclusion, by formulating a model based on biological mechanisms, including a morphological transition, into a mathematical model for population growth, we have successfully obtained parameters values that describe the rates of the mechanisms involved. Crucially, extending this model will allow for a better prediction of how these potential therapies may impact the emergence and development of drug resistance and parameter analyses could hint at strategies to combat the threat of resistance. Our analysis suggests that inhibition of the morphological transition could be a suitable target for a treatment strategy.

In the following chapter we extend Model I to include active efflux. By incorporating the upregulation of efflux, we formulate a model that is capable of describing the growth dynamics of a susceptible and a resistant strain.

CHAPTER 3

MODELLING RESISTANCE TO MEROPENEM VIA UPREGULATION OF EFFLUX PUMPS

P. aeruginosa infections can be remarkably hard to treat, along with other nosocomial infections, due to the ability of *P. aeruginosa* to express intrinsic resistance mechanisms and acquire further resistance via mutation or HGT.

Monahan et al. obtained experimental data that exhibited the population wide shape transition of a meropenem-susceptible strain of *P. aeruginosa*. Using microscopy, we reproduced these results with the meropenem-susceptible PA1008 strain (see Figure 2.1) and the partially resistant PA1004 strain. The microscopy results for the PA1004 strain, shown in Figure 3.1, indicate that the meropenem-resistant *P. aeruginosa* cells transition from a rod to spherical shape (as the susceptible PA1008 strain does), yet the higher number of viable cells in these images, compared to the images for PA1008, indicate resistance to meropenem.

In Section 1.3 we discussed the main resistance mechanisms that are attributed to resistance in *P. aeruginosa*. Along with restricted porin channels, the upregulation of efflux and the overproduction of β-lactamase are the most commonly encountered resistance mechanisms of *P. aeruginosa*. Whilst porin channel restrictions and active efflux both reduce the intracellular uptake of antibiotic molecules, β-lactamases act to inactivate antibiotic molecules that manage to translocate into the periplasmic space. These mechanisms can work simultaneously to reduce the successful binding of antibiotic molecules to

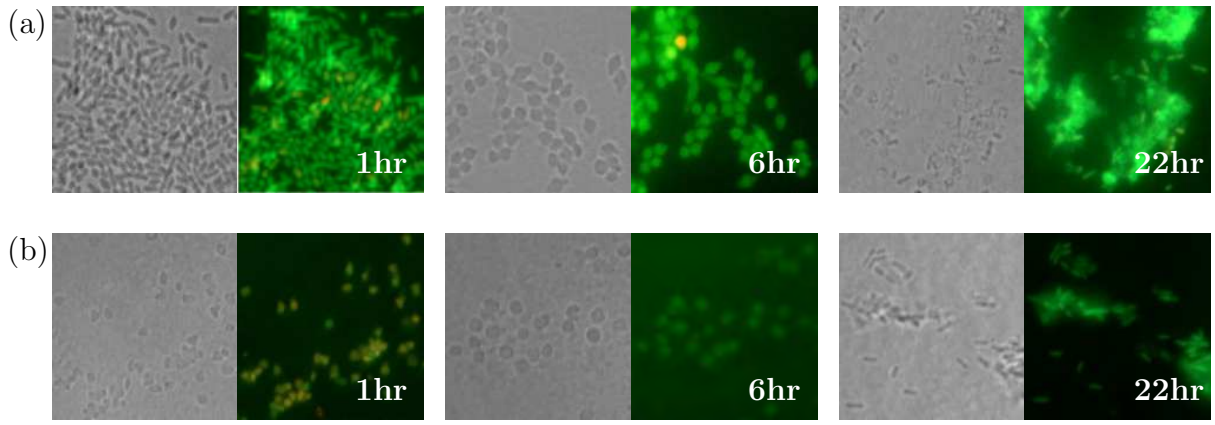

Figure 3.1: Cells of the partially meropenem-resistant *P. aeruginosa* PA1004 strain rapidly convert to a spherical shape after adding (a) $0.5\,\mu g\,ml^{-1}$ and (b) $2\,\mu g\,ml^{-1}$ of meropenem before reverting back to a bacillary form. Microscopy images were taken after 1, 6 and 22 hours. Left panels: transmitted light, right panels: fluorescence microscopy. In fluorescence images, green and red colouring indicates viable and lysed cells respectively.

PBPs and enable *P. aeruginosa* populations to survive antibiotic exposure. Meropenem resistance by PA1004 is assumed to be as a result of the action of efflux pumps and although other mechanisms, such as β-lactamase production, may play a role in resistance, we will focus on active efflux as being the primary resistance mechanism.

Mathematical models of antibiotic resistance often incorporate the effects of resistance via a change in pharmacodynamic properties of the antibiotic. Often, these models describe the growth of a susceptible and resistant strain simultaneously. For example, in [10], the resistant and susceptible bacterial populations are assumed to have different MICs. A general approach is also taken in [29], with the different strains possessing different mortality rates depending on whether they bear a resistance plasmid. Similarly, in [44, 102], antibiotic effects are modelled using a density dependent term, identical to the term used in Model I; the effects of antibiotic resistance are modelled using different maximum kill rates and half-maximal antibiotic concentrations for the two strains. Both of these examples do not specify a resistance mechanism and instead focus more on the resultant effects of resistance on bacterial growth or death.

Mechanistic representations of antibiotic resistance are somewhat rarer. In [74] a

model was formulated to describe the efflux of a drug in and out of a cell. The intercellular model comprises two ODEs and a PDE that incorporates efflux via facilitated diffusion. The energy-dependent efflux mechanism is modelled using a PDE that explicitly depends on binding between the drug substrate and energy levels within the cell; the enzyme kinetics of this reaction produces an ODE model using Michaelis-Menten kinetics. In [33], the finite difference method is applied to a reaction-diffusion model for biofilm growth. Diffusion of β-lactamases into the extracellular domain is investigated and the results suggest that the release of β-lactamases upon bacterial lysis should be considered as it could decrease the extracellular antibiotic concentration and aid biofilm growth.

We wish to extend Model I to include efflux of intracellular antibiotic; we will extend this model in later chapters to include a mixed population of susceptible and resistant bacteria, similar to those in [10, 30, 44, 102].

3.1 Model formulation

We formulate a model that describes the growth of a single strain of *P. aeruginosa* in isolation with meropenem in which efflux of meropenem can be accounted for. Following the microscopy results we continue to include a shape transition and we extend Model I by including the possibility of resistance via active efflux. Our model follows the interactions described in Figure 3.2.

To include active efflux within our model we will differentiate between cells that have internalised bound antibiotic and those that do not. Bacteria do not lyse due to antibiotic effects unless the antibiotic has successfully bound to the penicillin binding proteins (PBPs) within the cell, and therefore we introduce a new variable I to represent the rod-shaped cells with internalised bound antibiotic. Note that the term 'internalised' is used throughout and refers to the antibiotic successfully entering and binding within the cell.

In accordance with this new variable, we amend the definition of H to be the population of rod-shaped cells with no internalised antibiotic. Following from Model I, the

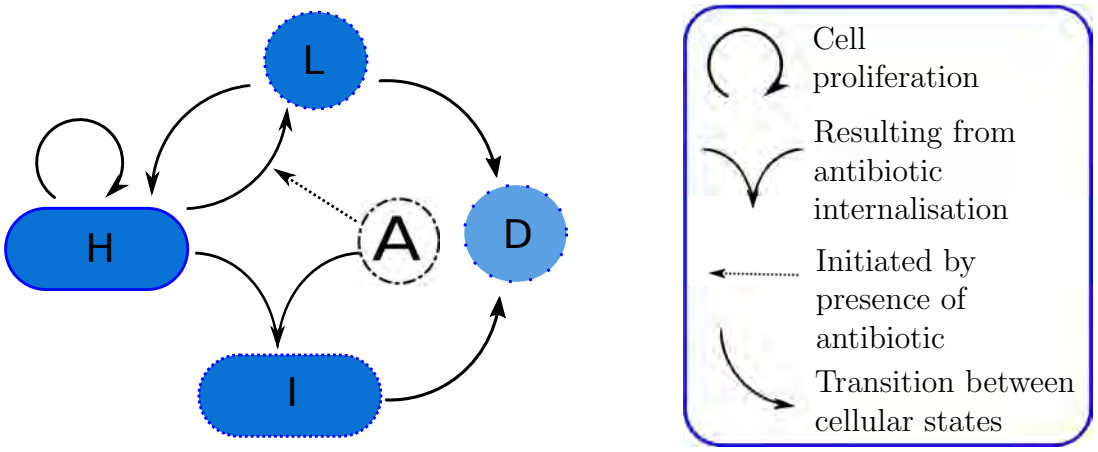

Figure 3.2: Schematic representation of the transitions of *P. aeruginosa* in response to exposure to meropenem with the inclusion of active efflux. The species shown are defined as follows: H are rod-shaped cells with no bound antibiotic, I are rod-shaped cells with bound internalised antibiotic and L are spherical cells. When the antibiotic, A, is introduced, rod-shaped cells can make the reversible transition to a spherical shape. The antibiotic can internalise within the bacteria and bind to the PBPs, causing the bacteria to transition to the I population and quickly lyse. The antibiotic is assumed to be effective at killing rod-shaped cells but not spherical cells due to a depleted cell wall. Rod-shaped cells can proliferate but we assume that spherical cells cannot proliferate and that proliferation of the I population will be negligible. Spherical cells can lyse naturally due to the fragile nature of these cells. Active efflux results in a decrease in successful binding of antibotic molecules within a cell and its effects are incorporated into the arrow fom H to I. Note that we do not include natural death of the rod-shaped cells with no internalised antibiotic as this is assumed to be negligible using the parametrisation results in Chapter 2.

spherical cell population is described by L and we omit the equation for lysed cells. Bacteria that lyse will disappear from the culture and we assume that their contribution to the bacterial population will be negligible. The rod-shaped bacterial subpopulations are now separated by whether they contain bound antibiotic and therefore we define the variable A to be the concentration of unbound antibiotic. We wish to investigate total population growth in addition to the growth of the bacterial subpopulations and hence we define B to be the total bacterial population such that,

$$B = H + I + L. \tag{3.1}$$

As we hope to extend this model in later chapters to include a host response it is important to consider how nutrient availability would differ at a site of infection and *in vitro*. Although we can assume that *in vivo* nutrient availability could be less abundant than the nutrient rich broth used *in vitro*, it is also likely that there would be some influx of nutrient at the site of infection. Subsequently, we may expect to see a low but constant level of nutrient availability *in vivo*, compared to the nutrient rich broth used in experiments. Following this, and since we have limited insight into nutrient availability, a nutrient dependent growth term, similar to the term used in equation (2.1), would be unsuitable to use. As nutrient levels *in vivo* are unknown, and would ultimately depend on the site of infection, we choose here to model growth using a term that does not depend explicitly on nutrient availability. It is expected that bacterial growth would saturate over time, due to limitations of space and nutrient and therefore we use a logistic term to model bacterial growth as this provides the model with a means of growth that is not dictated by an unknown level of substrate. We use the growth function,

$$G(H) = (1-c)rH\left(1-\frac{H}{k}\right), \tag{3.2}$$

where $G(H)$ defines the growth of the rod-shaped bacteria with no internalised antibiotic, r is the maximum growth rate, k is the carrying capacity and c is the fitness cost. The upregulation of efflux, along with the expression of multiple resistance mechanisms, can compromise bacterial growth. Hence we attach a fitness cost to the bacterial growth term so that we can consider the effects of resistance on bacterial growth when modelling a resistant strain. It is possible to model a fitness cost by including separate growth terms for the different strains or by incorporating a fitness cost explicitly into the model by introducing a fitness cost parameter, c, that can take values between 0 and 1 [10, 64, 102]. By including a fitness cost parameter we can easily explore different growth rates for the resistant strain as a proportion of the growth rate of the susceptible bacteria. Introducing a fitness cost parameter will incur a penalty to the growth that can be set equal to zero

when modelling a susceptible strain and vary when simulating a resistant strain.

Note that our growth term is specific to the population of rod-shaped cells with no internalised antibiotic. We assume that following successful internalisation, the antibiotic molecules will inhibit cell wall synthesis, which will disrupt the proliferation process. We assume that proliferation of the bacteria with bound antibiotic will be severely limited by the antibiotic and successful proliferation will be negligible in comparison to the rate of antibiotic-induced death. Following from Chapter 2, we assume that the cell wall deficient spherical cells lack the machinery needed to successfully proliferate and subsequently we only include proliferation of the rod-shaped cells with no internalised antibiotic within the model.

Antibiotic internalisation is modelled using the function,

$$B(A, H) = (1 - \omega)\frac{\nu A}{A + A_{50}}H, \tag{3.3}$$

where $B(A, H)$ defines the internalisation of the antibiotic in the rod-shaped cells, ν is the maximum internalisation rate, A_{50} is the concentration needed for half maximal internalisation and ω is defined as the efflux pump upregulation parameter.

We use a density-dependent term as attempts at using a linear term to model internalisation were unsuccessful (results omitted) and it is likely, due to the inherently low membrane permeability of *P. aeruginosa*, that antibiotic molecule translocation across the cellular membrane would saturate quickly. We assume that prior to the antibiotic successfully binding, the bacteria will not be susceptible to antibiotic-induced death and hence the population of internalised bacteria, I, are assumed to have bound antibiotic within the cell.

We choose to model the upregulation of efflux via a decrease in internalisation (i.e. we assume that antibiotic is effluxed sufficiently rapidly that it can be assumed to be effectively instantaneous) and hence the efflux upregulation parameter, ω, can take values between 0 and 1; as ω increases the internalisation rate will decrease. Modelling resis-

tance via a decrease in internalisation differs from the models in [10, 30, 44, 102], where resistance results in a direct effect on antibiotic action. We assume that efflux will affect antibiotic-induced death indirectly; once an antibiotic molecule has bound within the cell, bacterial lysis will occur at the same rate regardless of efflux. Efflux directly decreases the intracellular antibiotic concentration and thus decreases the rate of antibiotic binding. Hence by including the internalisation term within the model and assuming that efflux affects the binding process, a more mechanistic approach is used. Furthermore, this approach facilitates future model developments that will include regulation of the genetic network involved in efflux.

Before the antibiotic successfully internalises, the bacteria may transition to a spherical shape. We define the transition of the rod-shaped bacteria with no internalised antibiotic to spherical cells as $T(A, H)$ and describe this process using the function,

$$T(A, H) = \frac{\gamma A}{A + T_{50}} H. \tag{3.4}$$

A density dependent term is used to describe the morphological transition, with maximum transition rate γ and antibiotic concentration needed for half maximal transition, T_{50}.

We continue to assume that the bacteria can transition back to the rod-shape but we now assume that the reverse transition only occurs when the concentration of unbound antibiotic is low. We model the reverse transition, $R(A, L)$, using a hyperbolic tangent function,

$$R(A, L) = \frac{\delta}{2}\left(1 + \tanh\left(\frac{A_c - A}{b}\right)\right) L, \tag{3.5}$$

with slope parameter b, critical antibiotic threshold A_c and maximum reverse transition rate, δ. Once the antibiotic concentration reaches the critical threshold, the cell wall deficient bacteria will transition back to the rod shape and resume proliferation.

Our parametrisation results in Chapter 2 indicated that the rate of natural death of the rod-shaped cells with no internalised antibiotic may be low. Here, we assume that natural death of the H population will be negligible when compared to the rates of

internalisation and transition and hence we do not include a separate natural death term for these rod-shaped cells. If we wished to include natural death then this could easily be absorbed into the logistic growth term. Similarly, we assume that natural death of the rod-shaped cells with bound antibiotic will be negligible when compared to the rate of antibiotic-induced death. We continue to assume that whilst in the spherical form, the bacteria will completely evade antibiotic effects. However, the spherical cells may lyse naturally, due to fragility, at a rate ψ. Additionally, the rod-shaped cells with internalised antibiotic may lyse due to antibiotic effects and we model antibiotic action using a linear death term with death rate, ρ.

Antibiotic decay is modelled using a natural degradation term that follows first order kinetics, with decay rate α. Additionally, we include a degradation term for the antibiotic that is lost due to successful binding within bacteria. We define $\tilde{\nu}$ as rate of antibiotic loss due to internalisation and this is assumed to be proportional to the rate of internalisation, ν.

Following mass action kinetics we produce the following model:

$$\begin{aligned}
\frac{dH}{dt} &= (1-c)rH\left(1-\frac{H}{k}\right) - (1-\omega)\frac{\nu A}{A+A_{50}}H - \frac{\gamma A}{A+T_{50}}H \\
&\quad + \frac{\delta}{2}\left(1+\tanh\left(\frac{A_c-A}{b}\right)\right)L, \qquad (3.6)\\
\frac{dI}{dt} &= (1-\omega)\frac{\nu A}{A+A_{50}}H - \rho I, \qquad (3.7)\\
\frac{dL}{dt} &= \frac{\gamma A}{A+T_{50}}H - \frac{\delta}{2}\left(1+\tanh\left(\frac{A_c-A}{b}\right)\right)L - \psi L, \qquad (3.8)\\
\frac{dA}{dt} &= -\alpha A - \frac{\tilde{\nu} A}{A+A_{50}}H, \qquad (3.9)
\end{aligned}$$

with initial conditions

$$H(0) = 10^4 \quad I(0) = 0 \quad L(0) = 0 \quad A(0) = A_0. \qquad (3.10)$$

Variable definitions are given in Table 3.1 and parameter definitions and default parameter

values are shown in 3.2 (these choices will be justified in Section 3.2), although a range of values are used throughout. Unless otherwise specified, we use an initial antibiotic concentration of $10\mu g\,ml^{-1}$ as this represents a clinically relevant *in vivo* meropenem concentration [77, 103]. We choose a relatively small initial population of 10^4 cells and assume that no bacteria will transition to the spherical form prior to treatment.

Table 3.1: Definitions and units for the variables in Model II, described by equations (3.6)-(3.10).

Variable	Definition	Units
B	Total bacterial population	cells cm^{-3}
H	Rod shaped cells with no bound antibiotic	cells cm^{-3}
I	Rod shaped cells with internalised bound antibiotic	cells cm^{-3}
L	Spherical shaped cells	cells cm^{-3}
A	Unbound antibiotic	$\mu g\,ml^{-1}$

It is worth noting here that by separating the bacterial populations into those that do contain antibiotic and those that do not, we find that antibiotic-induced cell death is represented by a term that does not explicitly depend on the level of unbound antibiotic. Whilst this may appear surprising at first, the unbound antibiotic concentration does affect cell death indirectly via the presence of internalised antibiotic. This differs from Model I; now only the transitions from H to I and H to L depend explicitly on the external antibiotic concentration.

3.2 Results

3.2.1 Modelling limited or no antibiotic treatment

Figure 3.3 displays the model solutions using the default parameters for the case when no antibiotic is added and when we simulate the administration of one dose of meropenem. Note that we are simulating the growth of a susceptible strain and hence we set both the efflux pump upregulation parameter and fitness cost to 0. When no antibiotic is added, we see bacterial growth of the rod-shaped population until it reaches carrying capacity; since

Table 3.2: Definitions, units and default values for the parameters in Model II, described by equations (3.6)-(3.10).

Parameter	Definition	Units	Default parameter value	Source
r	maximum growth rate of rod-shaped cells	day^{-1}	3	[94]
c	deduction in growth due to fitness cost attached to carrying resistance	dimensionless	0.15	[100, 109]
k	carrying capacity of rod-shaped bacteria	cells cm^{-3}	10^6	[94]
ν	maximum antibiotic internalisation rate	day^{-1}	1.57	-
ω	decrease in internalisation due to upregulation of efflux	dimensionless	0.5	-
A_{50}	antibiotic concentration needed for half maximal internalisation	$\mu\text{g ml}^{-1}$	0.47	Chapter 2
γ	maximum transition rate of rod-shaped cells	day^{-1}	1.57	-
T_{50}	antibiotic concentration needed for half maximal transition	$\mu\text{g ml}^{-1}$	0.47	-
ρ	antibiotic-induced cell death rate for rod-shaped cells	day^{-1}	100	-
ψ	spherical cell death rate	day^{-1}	0.017	Chapter 2
δ	transition rate from spherical to rod shape	day^{-1}	10	-
A_c	critical antibiotic concentration threshold for reversion of spherical cells	$\mu\text{g ml}^{-1}$	0.5	
b	smoothed step function slope parameter	$\mu\text{g ml}^{-1}$	1	-
α	antibiotic decay rate	day^{-1}	10	[77, 103]
$\tilde{\nu}$	antibiotic decay rate due to internalisation in rod-shaped cells	$\mu\text{g ml}^{-1}\text{day}^{-1}$ $(\text{cells cm}^{-3})^{-1}$	1×10^{-3}	-

the transition is antibiotic-dependent we see no spherical cells and clearly no antibiotic becomes internalised. When one dose is administered we see some bacteria transitioning to the cell wall deficient state, resulting in an increase in L, and the antibiotic internalises within some rod-shaped bacteria, resulting in an increase in I. Once the antibiotic is exhausted the spherical bacteria transition back to the rod shape, the internalised bacteria

lyse and the model is reduced to the antibiotic free system,

$$\frac{dH}{dt} = rH\left(1 - \frac{H}{k}\right). \tag{3.11}$$

From equation (3.11) we find two steady states: the trivial unstable bacteria-free steady state,

$$(H^*,\, I^*,\, L^*,\, A^*) = (0,\, 0,\, 0,\, 0)\,, \tag{3.12}$$

and the stable steady state with the bacterial load at carrying capacity,

$$(H^*,\, I^*,\, L^*,\, A^*) = (k,\, 0,\, 0,\, 0)\,. \tag{3.13}$$

In the absence of antibiotic we would expect to reach the stable steady state if the initial population size is nonzero. Similarly, if any bacteria remain after a dose of antibiotic has degraded, we would also expect the population to reach the stable steady state. The true values of the parameters in the model may vary from those in our default parameter set and it is likely that these parameter values will vary by bacterial strain and site of infection. However, it is unlikely that one dose of antibiotic would cause the bacterial population to reach a level at which it would die off completely, especially with the initial population size used in our simulations. Therefore, in agreement with the model predictions, we expect that if a single dose of antibiotic was added, the population would still reach the carrying capacity steady state. If we use the resistant strain parameters then the results are in agreement with the susceptible strain; a single dose is ineffective and the population would grow to the steady state (results omitted).

3.2.2 Modelling a constant infusion of antibiotic

The model suggests that the effects of one dose of antibiotic would be insignificant and this is in line with typically used dosing strategies; it is unlikely that one bolus dose of antibiotic would be given as we would not expect this limited amount of antibiotic

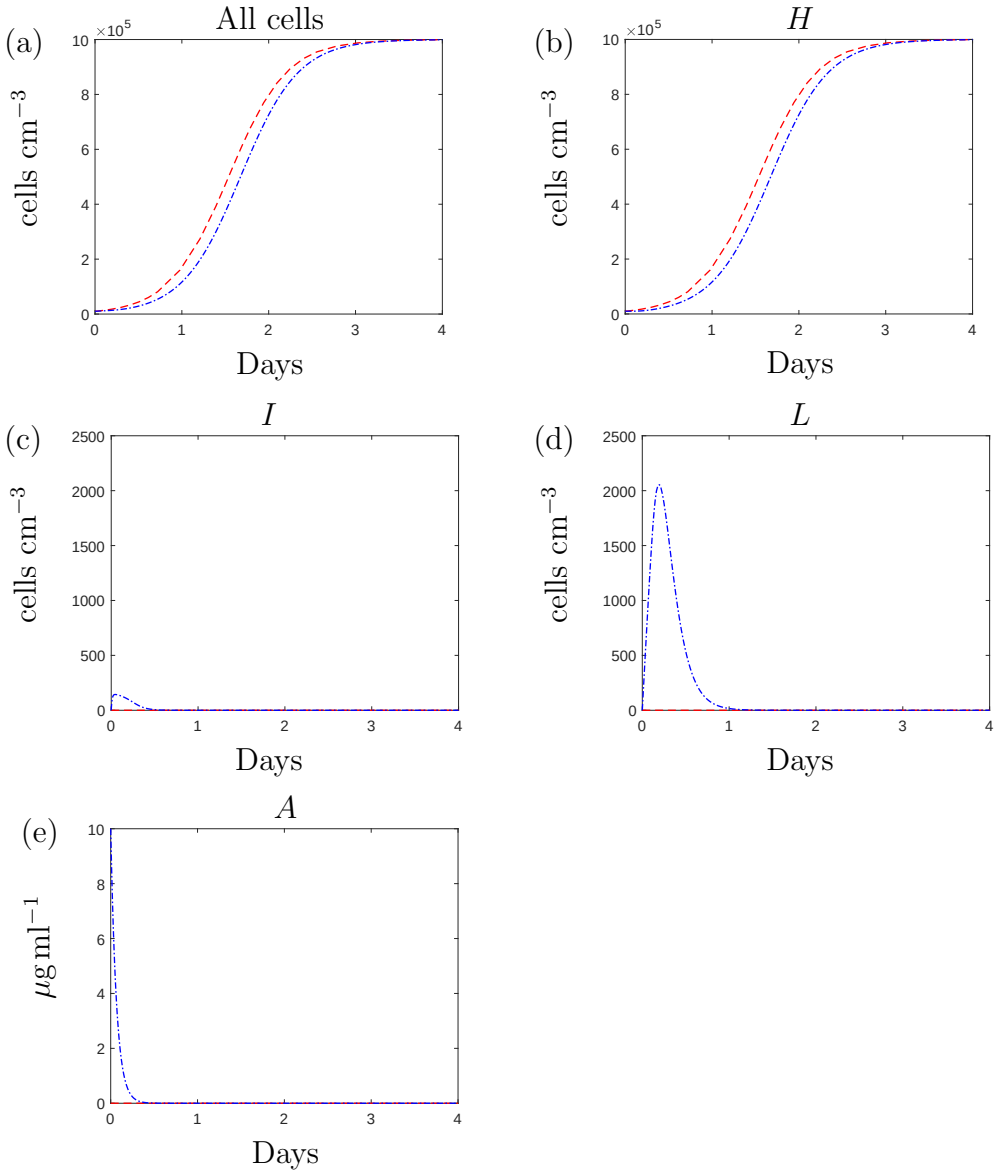

Figure 3.3: The solution to the system (3.6)-(3.10), using default parameter values shown in Table 3.2, with $A_0 = 0\mu\text{g}\,\text{ml}^{-1}$ (red dashed lines) and $A_0 = 10\mu\text{g}\,\text{ml}^{-1}$ (blue dashed-dotted lines).

exposure to eradicate a bacterial population. Instead a number of repeated doses or a continuous infusion of meropenem is more likely to be administered. For this model we focus on the latter case, of a continuous dose and we continue to use a clinically relevant steady state antibiotic concentration of $10\,\mu\mathrm{g\,ml^{-1}}$ [77, 103].

If the constant antibiotic concentration is higher than the critical antibiotic threshold, A_c, then we would expect the spherical cells to remain dormant for the duration of the dosing regimen. Our microscopy images suggest that the bacteria transition when $A_0 = 0.5\,\mu\mathrm{g\,ml^{-1}}$, but we do not know whether the transition would occur at lower antibiotic concentrations. Therefore, we use $A_c = 0.5\,\mu\mathrm{g\,ml^{-1}}$ as an upper bound for the critical threshold value for the reverse transition. The continuous infusion dose of $10\,\mu\mathrm{g\,ml^{-1}}$ is much greater than the default critical threshold antibiotic concentration and therefore we assume that the effects of the reverse transition on the population solutions will be negligible. We amend the equations, (3.6)-(3.10) to obtain our continuous dose model,

$$\begin{aligned}
\frac{dH}{dt} &= (1-c)rH\left(1-\frac{H}{k}\right) - (1-\omega)\frac{\nu A}{A+A_{50}}H - \frac{\gamma A}{A+T_{50}}H, && (3.14)\\
\frac{dI}{dt} &= (1-\omega)\frac{\nu A}{A+A_{50}}H - \rho I, && (3.15)\\
\frac{dL}{dt} &= \frac{\gamma A}{A+T_{50}}H - \psi L, && (3.16)\\
\frac{dA}{dt} &= 0, && (3.17)
\end{aligned}$$

with initial conditions

$$H(0) = 10^4 \quad I(0) = 0 \quad L(0) = 0 \quad A(0) = A_0. \tag{3.18}$$

Solving this system, with the default parameter values produces the solutions shown in Figure 3.4. The rod shaped cell population with no internalised antibiotic decreases over time as the bacteria become internalised by the antibiotic or transition to spheres. We have assumed that the bacteria will not transition back from the spherical form whilst the antibiotic is present and hence we see the spherical population increases over time.

As the population of rod-shaped cells decreases, the spherical population reaches a peak and following this we see a decline due to spherical cell death. Similarly, we see the same behaviour in the population of rod-shaped cells with internalised antibiotic. A sharp increase occurs until the H population depletes and the antibiotic-induced death term dominates the behaviour and causes a decrease in I until the steady state is reached.

Solving equations (3.14)-(3.17) at steady state, we obtain the bacteria-free steady state,

$$(H^*,\, I^*,\, L^*,\, A^*) = (0,\, 0,\, 0,\, A_0)\,, \tag{3.19}$$

and a second steady state,

$$(H^*,\, I^*,\, L^*,\, A^*) = \left(\frac{k}{(1-c)r}X,\ \frac{(1-\omega)\nu kY}{(1-c)\rho r}X,\ \frac{\gamma kZ}{(1-c)\psi r}X,\ A_0\right), \tag{3.20}$$

where,

$$X = ((1-c)r - (1-\omega)\nu Y - \gamma Z)\,, \tag{3.21}$$

$$Y = \frac{A_0}{A_0 + A_{50}} \tag{3.22}$$

and

$$Z = \frac{A_0}{A_0 + T_{50}}. \tag{3.23}$$

We see that the second steady state is dependent on the value of (3.21). For all values of $X < 0$ we find that only one non-negative steady state is possible; this is the bacteria-free steady state (3.19) and it is stable in this region. When $X = 0$ we find that there is a transcritical bifurcation and two steady states exist for values $X > 0$. Firstly we have (3.19), which now becomes unstable, and secondly we have (3.20), which is stable for all $X > 0$ (e.g. see results in Figures 3.5-3.6, which were generated using XPPAUT v8.0).

Using these steady state expressions we are able to gain insight into suitable values for the estimated parameters for which we do not have any prior information. Firstly, note that we initially set the fitness cost, c, and upregulation of efflux, ω, parameters to 0 to represent an antibiotic-susceptible strain. All of the subpopulation steady state

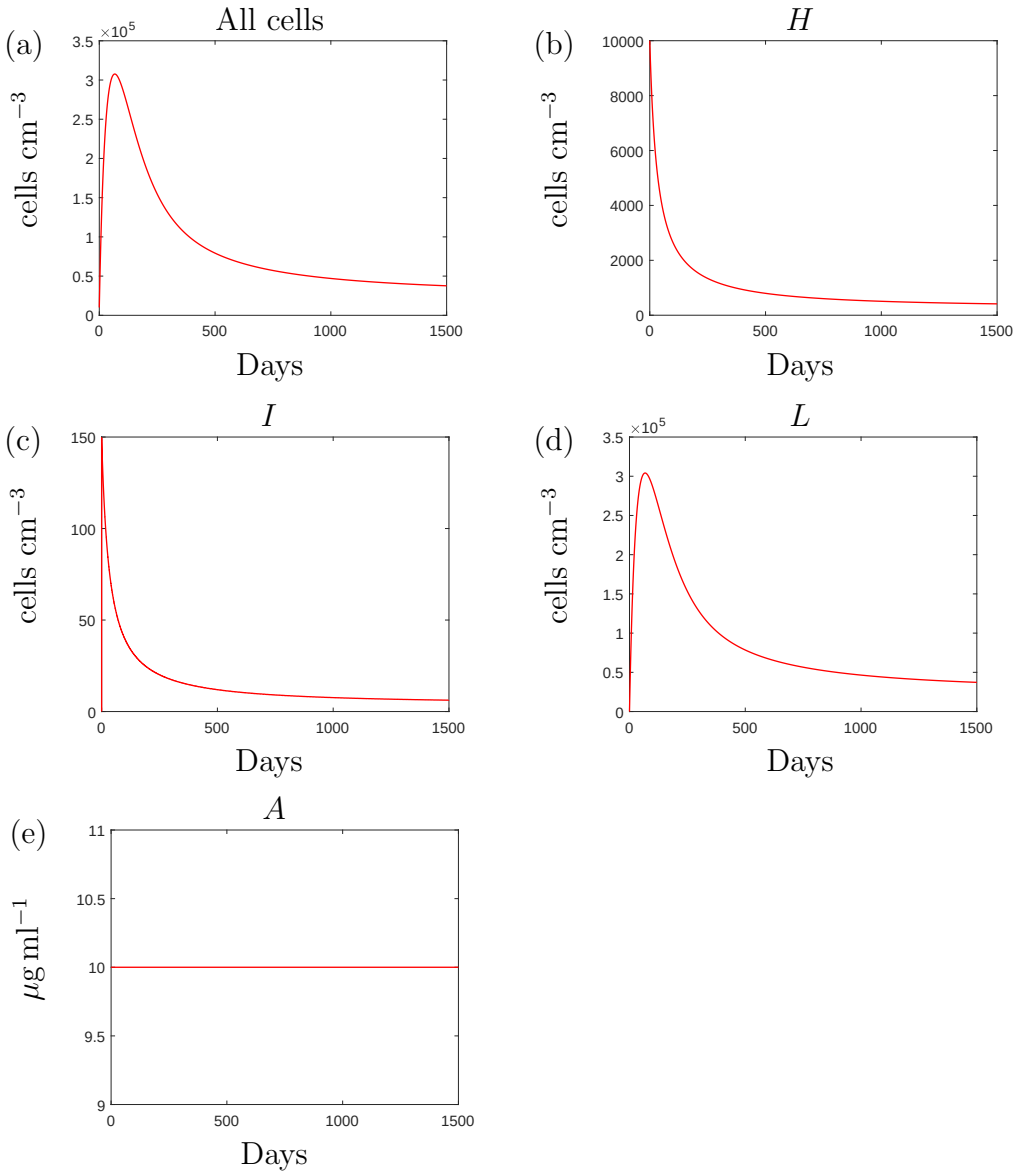

Figure 3.4: The solution to the system (3.14)-(3.18), using default parameter values shown in Table 3.2, with $A_0 = 10\,\mu\text{g}\,\text{ml}^{-1}$.

expressions depend on the value of (3.21), which is dependent on the growth rate, r, and the internalisation and transition parameters: γ, A_{50}, ν and T_{50}.

Firstly, the growth rate and carrying capacity, k, were chosen from a suitable range of values obtained via parametrisation attempts in [94] where a bacterial growth model of *P. aeruginosa* was fitted to *in vivo* experimental data taken from burn wounds in rats. We would expect a continuous infusion of antibiotic to suppress the population of rod-shaped bacteria with no internalised antibiotic and result in a low steady state value. In order to obtain a positive steady state value we require a positive value of X and from this we can infer that,

$$r \;>\; \nu Y + \gamma Z. \tag{3.24}$$

For simplicity, we assume that $A_{50} = T_{50}$ and choose $T_{50} = 0.47\,\mu\mathrm{g\,ml^{-1}}$, following the parametrisation results in Chapter 2. Subsequently, by substituting the chosen values of A_{50}, T_{50} and r into (3.24), along with the initial antibiotic concentration $A_0 = 10\mu\mathrm{g\,ml^{-1}}$, we can deduce the following inequality,

$$3.141 > (\nu + \gamma)\,. \tag{3.25}$$

From condition (3.25), we can infer biologically feasible values for the maximum rates of internalisation and transition for a nonzero steady state to be feasible. This inequality is obtained using the default parameter values, yet a similar inequality could be found if the growth-attributed parameter values were to vary. The parameters used to obtain this inequality are potentially all measurable and provide us with insight into the combined rates of internalisation and transition. For our default parameter set, for simplicity we will assume that the maximum rate of transition, γ, is equal to the maximum antibiotic internalisation rate, ν.

Using the steady state expressions, we can explore the parameter values used and confirm that changes to the parameter values result in the expected biological result.

Firstly, we investigate changes to the two death rates: the natural death rate of the spherical cells, ψ, (which could be altered using AMPs) and the antibiotic-induced death rate of the rod-shaped cells, ρ (which would change for different antibiotics). By inspection of (3.20), increasing either death rate results in a decrease in the respective population. The steady state values of the non-affected populations remain unchanged.

We recall that the carrying capacity, k, defines the maximum size to which the population can grow and illustrates the limitations of resource availability on population growth. If, for example, nutrient availability increased, we would expect the carrying capacity to increase, allowing for higher population levels. Similarly, if resources were further restricted, the carrying capacity may decrease from the default value and we would expect lower population levels. The steady state expressions are in accordance to the expected results with k featuring in the numerator of each of the population expressions.

Next, we investigate the effects that changes to the growth rate have on the steady state population levels. Figure 3.5 displays the results when we vary the growth rate, r (note that we have omitted the solution for antibiotic concentration as this remains unchanged). We vary the growth rate over a range of values taken from parametrisation efforts in [94]. Figure 3.5 indicates that an increase in growth rate would result in higher populations for all subpopulations, as we would expect. An increase in growth rate would lead to more rod-shaped cells that are able to transition and evade antibiotic effects, resulting in a higher total population. In contrast, we find that even a small decrease in growth rate from the default value leads to predictions of the population dying off completely. Since we have chosen default values for the rate of transition, ν, and internalisation, γ, based on the default growth rate, the model solution then becomes dependent on the condition that $X > 0$. If the inequality is not met then the system reaches the bacteria-free steady state.

Following the results of changes to the growth rate, we obtain similar results if we make changes to the internalisation rate, ν, or the transition rate, γ. Figure 3.6 displays the steady state values when we vary the internalisation rate; as expected, a decrease

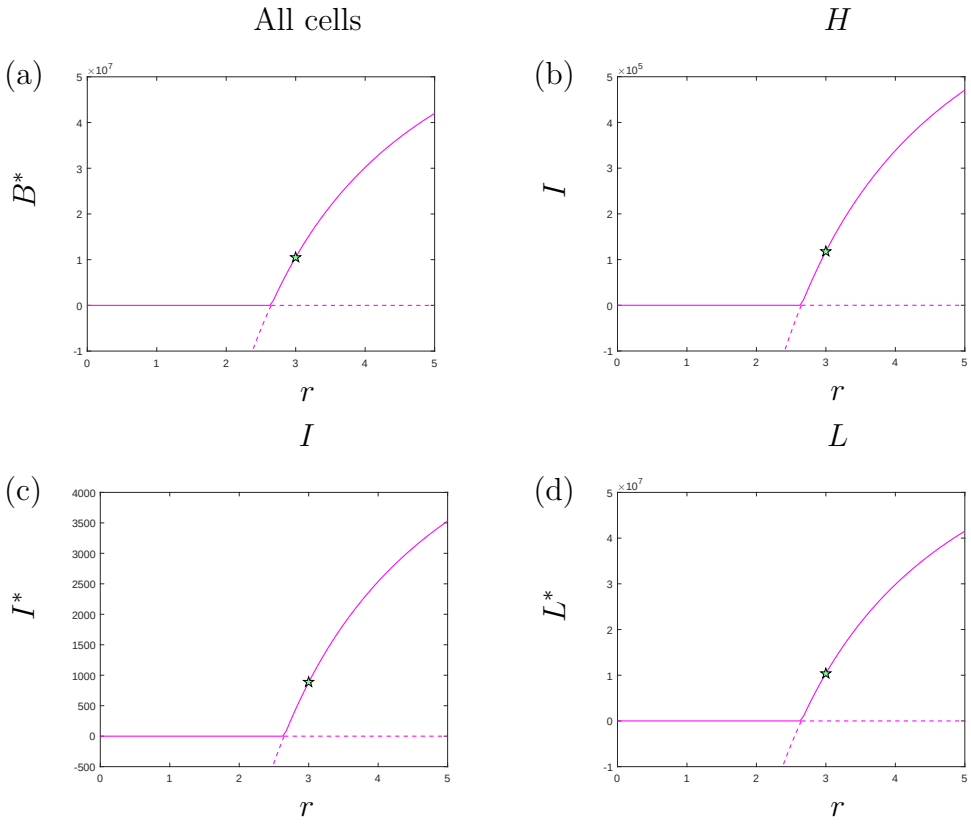

Figure 3.5: The steady state solutions to the system (3.14)-(3.18) using the default parameter values shown in Table 3.2, with $A_0 = 10\,\mu\text{g}\,\text{ml}^{-1}$ and varying the growth rate, r, from the default value of $3\,\text{day}^{-1}$. The solid lines represent the region in which the steady state is stable and the dotted lines show where the steady state is unstable. B is the total number of bacteria, such that $B = H + I + L$.

in the internalisation rate leads to higher populations of rod-shaped cells that have no internalised antibiotic. Subsequently, a higher H population leads to more spherical cells. The interesting results seen in Figure 3.6 (c) occur due to a balance between the growth rate of the antibiotic-free bacteria and the internalisation rate. The results indicate that if we decrease the internalisation rate from the default value then we would expect a higher steady state for the population of bacteria with bound antibiotic. This could seem counter-intuitive as we would expect to have fewer bound bacteria if the antibiotic internalises less efficiently. However, as fewer bacteria have antibiotic binding within them, there is a larger population of rod-shaped cells that can proliferate and this causes the higher steady state value for I^*. Decreasing ν sufficiently eventually has the more

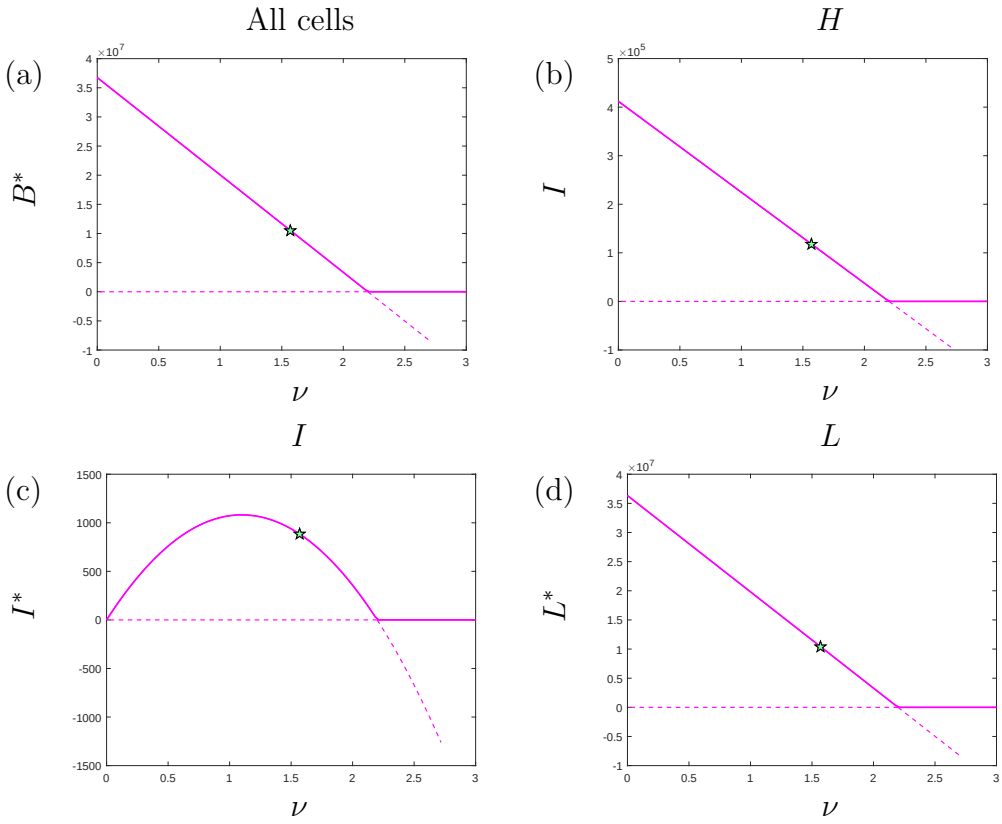

Figure 3.6: The steady state solutions to the system (3.14)-(3.18) using the default parameter values shown in Table 3.2, with $A_0 = 10\,\mu\text{g}\,\text{ml}^{-1}$ and varying the internalisation rate, ν from the default value of $1.57\,\text{day}^{-1}$. The solid lines represent the region in which the steady state is stable and the dotted lines show where the steady state is unstable. B is the total number of bacteria, such that $B = H + I + L$.

intuitive effect of lowering I^*.

If we increase the internalisation rate, even by a small amount, we see the system reaches the bacteria-free steady state. This is similar to the effects of decreasing the growth rate, r, and occurs due to the inequality condition, (3.25), not being met. If the internalisation rate is increased then bacterial growth no longer outweighs the effects of the antibiotic and the population will die out.

Varying the transition rate, γ, gives similar predictions to those obtained when we vary ν (results omitted for brevity); the internalisation and transition rates have similar effects on the system and this is supported by their relative contributions to the steady state expressions. Following from these results, we find that if we increase the transition

rate, from the default value, then we would expect the population to die out. If the transition rate increases then higher numbers of bacteria transition to the spherical form and the remaining rod-shaped cells do not proliferate at a rate that would outweigh antibiotic effects. As the spherical cells do not contribute to population growth, the total population will die out.

Rather than varying the transition and internalisation rates individually, as previously shown, we can also investigate the relative sizes of these parameters. Figure 3.7 displays the results when we consider different parameter pairings for the two rates of internalisation and transition; for each parameter pairing, the combined sum of the two rates is fixed to be 0.314. As the combined value of ν and γ does not differ, the population of rod-shaped cells with no bound antibiotic does not change. As we increase the internalisation rate we witness an increase in the number of bound bacteria, as expected, since the numerator of the steady state expression increases. Subsequently, we predict fewer spherical cells as an increase in ν results in a decrease in the transition rate γ. As a result of the model set up and (3.25), we would expect to obtain nonzero steady state values for all of the parameter pairings considered. However, our results suggest that the population would be significantly affected if we set the transition rate to 0 as we predict a very small steady state population (≈ 300 cells cm^{-3}).

The parameter surveys performed have indicated the dependency of the steady state expressions, and hence the model solutions, to the expression (3.21). We have used some parameter estimates in the analysis which could, of course, vary in reality. However, our analysis indicates a method that can be used to obtain relative parameter values required for a trivial or nontrivial steady state and is easily adaptable for alternative parameter choices.

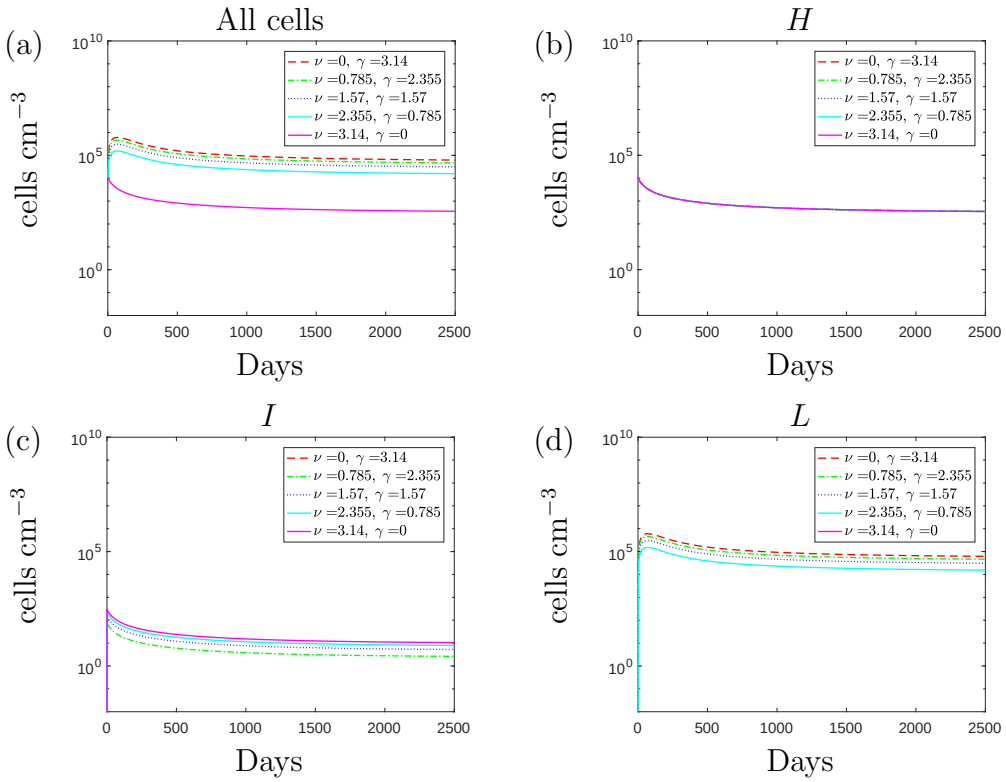

Figure 3.7: The solutions to the system (3.14)-(3.18) using the default parameter values shown in Table 3.2 with $\omega = 0$ and $A_0 = 10\,\mu\text{g}\,\text{ml}^{-1}$. We vary the maximum rate of internalisation, ν, and the maximum rate of transition, γ, whilst keeping the combined sum of these rates to be 0.314. Both ν and γ have a default value of $1.57\,\text{day}^{-1}$ and hence the default solution is represented by the blue-dotted lines.

3.2.3 Investigating parameter values attributed to a resistant strain

We have used the model, described by equations (3.14) - (3.18) to describe the growth dynamics we would expect from a susceptible strain of *P. aeruginosa* and we have explored how changes to the parameter values affect bacterial growth. We now wish to investigate how changes to the parameters attributed to resistance affect the model solutions.

Firstly, we investigate whether we can produce the growth dynamics we would expect from a resistant strain by increasing the efflux pump upregulation parameter, ω. Efflux pumps remove antibiotic molecules from the cytoplasm and periplasm of the bacterium and cause a lower antibiotic concentration within the cell. Subsequently, the effects of efflux pump upregulation result in a decrease in successful antibiotic internalisation.

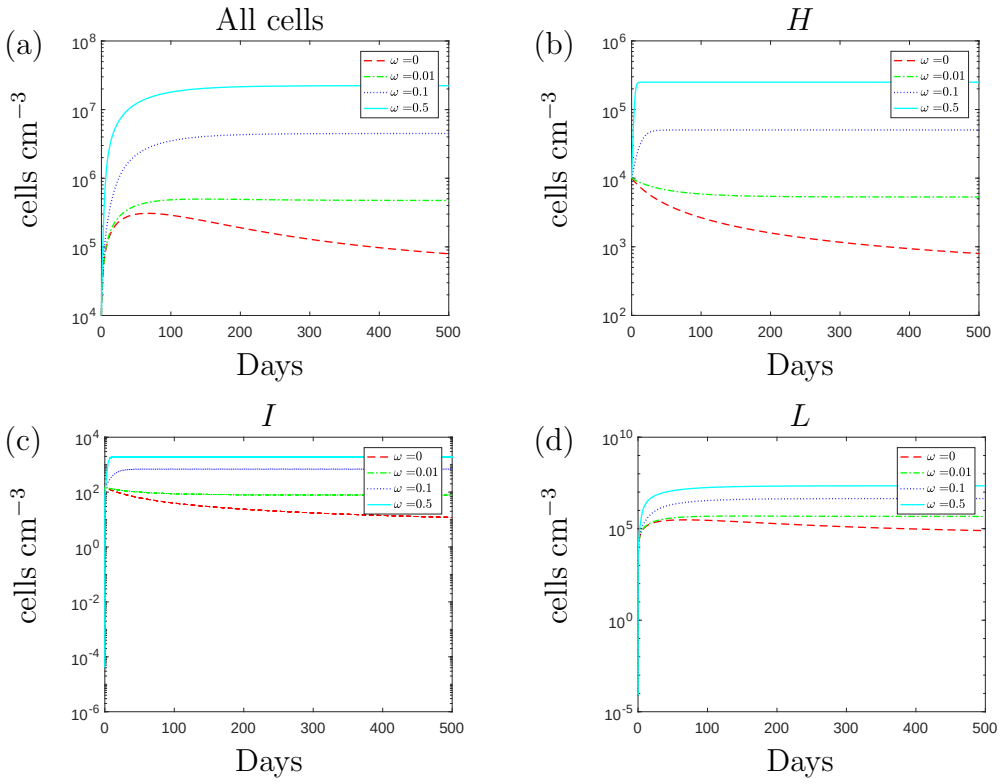

Figure 3.8: The solution to the system (3.14)-(3.18) using the default parameter values shown in Table 3.2, with $A_0 = 10\,\mu\text{g}\,\text{ml}^{-1}$ and varying the efflux pump upregulation constant, ω from the default value of 0.5.

Increasing the efflux efficacy parameter, ω, produces the results displayed in Figure 3.8. It is clear to see that even a small increase in ω causes significant increases in all of the bacterial subpopulations. If the bacteria are able to inhibit the successful binding of the antibiotic by just 10% then we see the total population exceed values of the carrying capacity. It is possible for the population to exceed the carrying capacity as logistic growth is only limited by the rod-shaped population with no internalised antibiotic since we have assumed that neither of the remaining subpopulations proliferate.

Figure 3.7 indicated that the susceptible population would be significantly reduced if the rod-shaped cells were unable to transition to spheres. Figure 3.9 shows a similar investigation into the relative sizes of the transition and internalisation rates. We see that the resistant bacterial population successfully survives antibiotic exposure with each parameter pairing, including the case when the transition rate is set to zero. If we compare

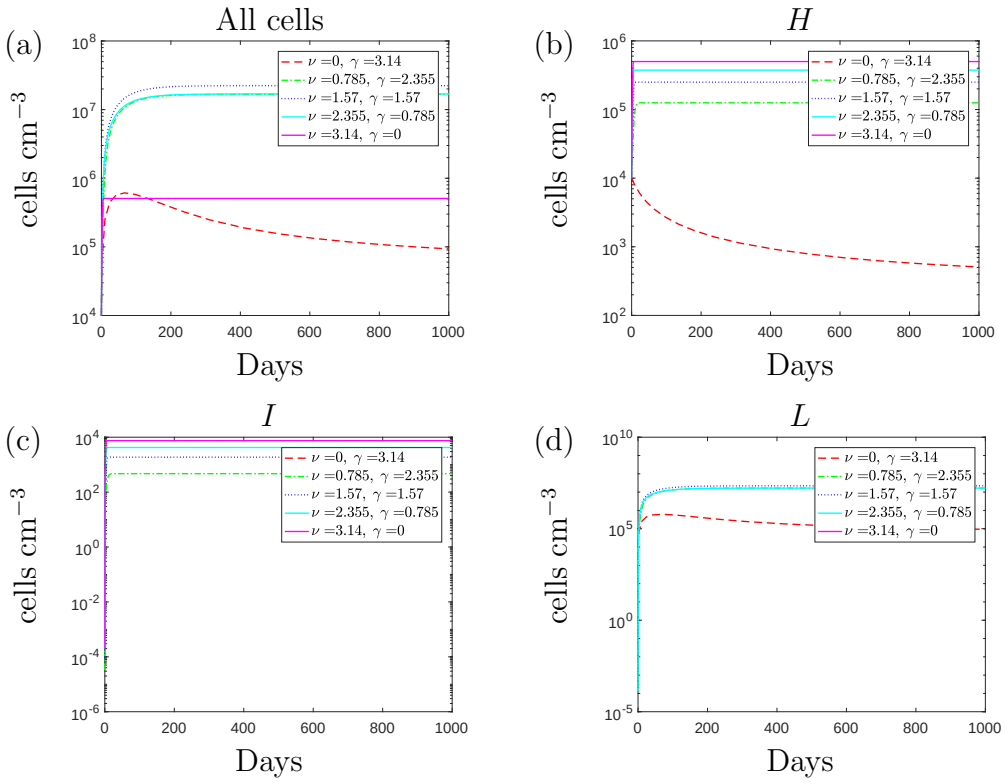

Figure 3.9: The solution to the system (3.14)-(3.18) using the default parameter values shown in Table 3.2 with $\omega = 0.5$ and $A_0 = 10\,\mu\text{g}\,\text{ml}^{-1}$. We vary the maximum rate of internalisation, ν, along with the maximum rate of transition, γ, whilst keeping the combined sum of these rates to be 0.314. Both ν and γ have a default value of $1.57\,\text{day}^{-1}$ and hence the default solution is represented by the blue-dotted lines.

the cases of $\gamma = 3.14\,\text{day}^{-1}$ (red dashed lines, no internalisation) and $\nu = 3.14\,\text{day}^{-1}$ (pink lines, no transition), the results suggest that the resistant strain could benefit from not utilising the morphological transition. During a constant dose of antibiotic, the resistant spherical bacteria are still susceptible to natural death whereas the rod-shaped cells are susceptible to internalisation yet they can proliferate. However, due to the upregulation of efflux, the rate of internalisation is decreased and hence the benefits of maintaining the cell wall could outweigh the benefits of transitioning to the spherical form.

Finally, we investigate how including a fitness cost to the growth of a resistant strain would affect the model predictions. It has been shown that various resistant plasmids can incur a fitness cost to the host bacteria that can vary from 0.09 to 0.25 as a proportion of non-plasmid bearing growth [100]. We assume that the energy costs associated with

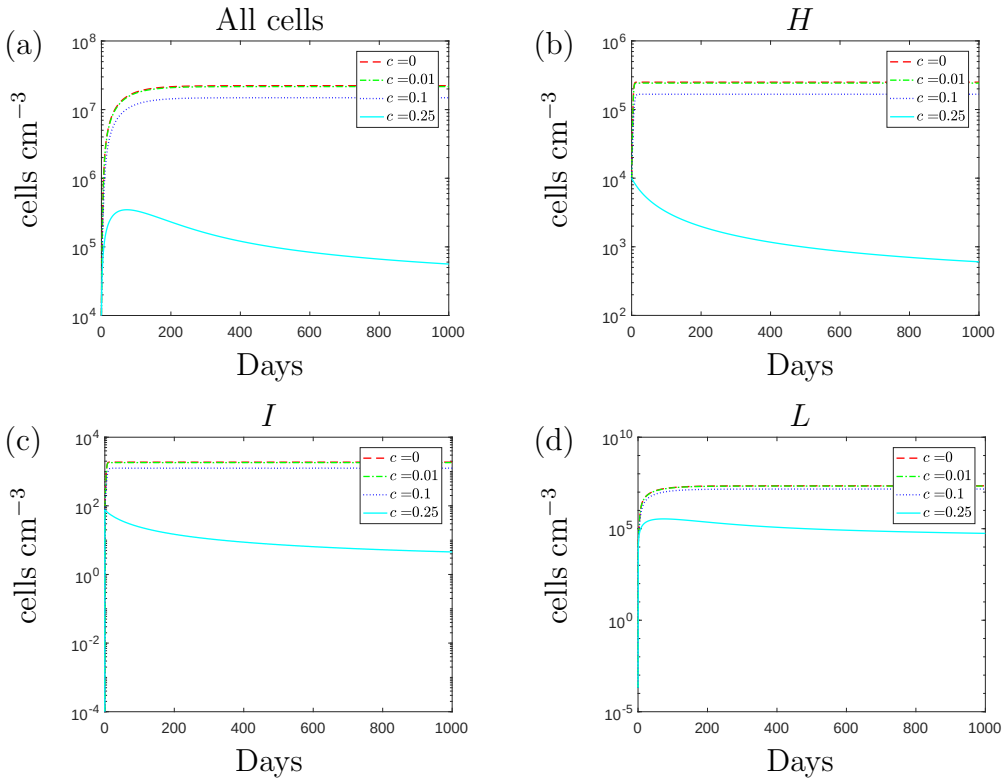

Figure 3.10: The solution to the system (3.14)-(3.18) using the default parameter values shown in Table 3.2, with $\omega = 0.5$ and $A_0 = 10\,\mu\text{g}\,\text{ml}^{-1}$ and varying the fitness cost, c, from the default value of 0.15.

the overexpression of efflux would incur similar fitness costs. Figure 3.10 displays the results when we vary the fitness cost parameter c; an increase in c results in a reduction of the growth rate of the rod-shaped cells. As the growth rate decreases, we predict lower population levels, as expected. As the fitness cost reaches 0.25, population growth is significantly inhibited and the population reaches similar levels to the susceptible strain. However, the effects of a high fitness cost could be countered with a sufficiently high increase in efflux (results omitted).

3.3 Discussion

The models, described by equations (3.6)-(3.10) and (3.14)-(3.18) are able to successfully produce the population dynamics of a susceptible and resistant strain of *P. aeruginosa*

after exposure to a single dose or constant infusion of antibiotic respectively. Using a suitable parameter set, the models predict that both strains would survive a single dose of antibiotic and grow to the carrying capacity. Whilst the susceptible strain relies on the morphological transition to flourish, the results suggest that the transition could potentially obstruct bacterial growth in a resistant strain. If the efflux pumps are suitably effective then we predict that the benefits of efflux pump upregulation could outweigh the potential benefits of the morphological transition and the burden of the fitness cost that could occur as a result of expressing the resistance mechanism.

In the following chapter we extend Model II to an infection level model. We investigate the growth of a multi-strain infection, the effects of the host response and the role of the morphological transition *in vivo*.

CHAPTER 4

AN INFECTION LEVEL MODEL

Throughout Chapters 2-3, we have only considered the growth of a single strain of *P. aeruginosa* in isolation with the antibiotic meropenem. In Chapter 3, we introduced an efflux parameter and chose a suitable parameter set to successfully predict the growth dynamics of an antibiotic-susceptible and -resistant strain. By extending Model II, to include an immune response, we can formulate a model to investigate the role of the shape transition during the growth of an infection *in vivo* and to explore the effects of the immune system on the different bacterial subpopulations. Additionally, we can model a susceptible and resistant strain simultaneously and explore the conditions in which a resistant strain would emerge.

Mixed strain models have been used to investigate the emergence of resistance under different antibiotic regimens ([29, 64]) and to explore how the immune response can affect the resistant population [44]. In [102] a general model was developed to describe the population dynamics of a local bacterial infection. The model was used to investigate the effects of a single antibiotic treatment and a combined antibiotic and antivirulence treatment. Suitable treatment strategies were discovered that could eliminate the bacterial population and prevent the emergence of resistance, thus providing support for research into antivirulence drugs. We will conduct a similar investigation but with the inclusion of morphological heterogeneity within the bacterial population.

4.1 Model formulation

The model will describe the growth dynamics of a multi-strain *P. aeruginosa* population with the influences of antibiotic action and an immune response. The compartmental model follows the interactions described in Figure 4.1. In accordance with Model II, we introduce the variable (defined in Table 4.1) H_i, where $i = \{S, R\}$, for rod-shaped bacteria with no internalised bound antibiotic; the subscripts S and R refer to the susceptible and resistant strains respectively. Similarly, we define I_i and L_i, with $i = \{S, R\}$, to be the populations of rod-shaped bacteria with internalised bound antibiotic and spherical cells respectively, for the susceptible and resistant strains. We define the concentration of unbound antibiotic, A, and introduce the phagocyte population, P.

As we are modelling growth *in vivo* we continue to use the logistic growth term, with maximum growth rate r and carrying capacity, k. We choose to use logistic growth, instead of nutrient dependent growth as nutrient availability is unknown and likely to vary between infection types. Therefore we choose a growth term that will describe growth yet does not depend explicitly on nutrient levels. Following from Model II we assume that only rod-shaped bacteria with no internalised bound antibiotic will proliferate. As soon as the antibiotic binds within the cell, proliferation will be inhibited and become negligible compared to the high antibiotic death rate. Similarly, as bacteria shed the cell wall and transition to spheres, they may lack essential machinery needed to successfully proliferate. Since we are using a logistic growth term we do not include a separate natural death term for the rod-shaped cells with no bound antibiotic. Additionally, we assign a fitness cost parameter, c, to the growth of a resistant strain.

We assume that the resistant strain is only partially resistant to the antibiotic effects and hence the antibiotic can bind to penicillin-binding proteins (PBPs) in both strains; we model internalisation using a non-linear saturating term with maximum transition rate, ν, and antibiotic concentration needed for half-maximal internalisation, A_{50}. We continue to assume that resistance to meropenem will occur via efflux pump overexpression. Resistance will result in a lower intracellular antibiotic concentration within resistant bacteria

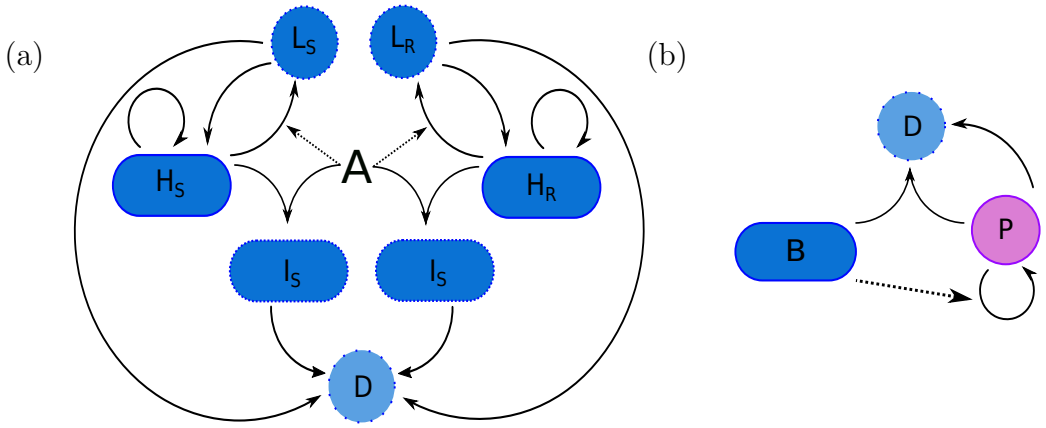

Figure 4.1: A diagram representing the transitions of a susceptible and resistant strain of *P. aeruginosa* in the presence of (a) meropenem and (b) host defences. The species are defined as follows: H_i are rod-shaped cells with no internal bound antibiotic, I_i are rod-shaped cells with internalised bound antibiotic, L_i are spherical cells, A is the external antibiotic concentration and P is the population of phagocytes. A subscript S or R indicates that the bacteria are susceptible or partially-resistant to the meropenem respectively. The effects of the antibiotic and the transitions between cell types are detailed in (a). We assume that proliferation is negligible if the antibiotic is bound within the cell or if the cell wall has been shed. In the presence of the antibiotic, rod-shaped cells transition to spherical cells or become have antibiotic internalised within the cell. Spherical cells can lyse naturally due to fragility and bacteria that have internalised antibiotic can die due to the effects of the meropenem. The effects of the immune response are detailed in (b). Phagocytes are recruited in response to all bacterial subpopulations, albeit at individual rates for the rod-shaped cells and spherical cells (here, B represents the bacterial population and the dashed arrow represents the influence of the bacteria on phagocyte recruitment). All bacterial species are susceptible to phagocytosis and phagocytes are removed via natural clearance and bacteria-induced apoptosis.

and a lower successful binding rate of the antibiotic within the cells. Therefore as before we model efflux pump upregulation as a decrease in the internalisation rate, ν, and define ω to be the efflux pump upregulation parameter that can take values between 0 and 1.

Rod-shaped bacteria with internalised antibiotic will lyse due to antibiotic effects as the antibiotic inhibits cell wall synthesis. We define ρ to be the death rate of rod-shaped cells due to antibiotic effects and assume that this death rate is the same for both strains since we are modelling resistance via a decrease in internalisation. We assume that natural death of the rod-shaped cells with bound antibiotic will be negligible when compared to the rate of antibiotic-induced death and therefore we do not include a separate natural

death term.

Following the microscopy images in Figures 2.1 and 3.1, we assume that both strains transition to spherical cells following exposure to the antibiotic. The transition is modelled using a saturating nonlinear term with maximum transition rate, γ, and concentration needed for half-maximal transition, T_{50}. We continue to assume that bacteria in both strains can transition back to the rod-shape once the extracellular antibiotic concentration depletes to a low critical threshold concentration. We model the reverse transition using a hyperbolic tangent function with slope parameter b and critical antibiotic threshold A_c. Once the antibiotic concentration reaches the critical threshold, the cell wall deficient bacteria will transition back to the rod shape and resume proliferation. If the spherical cells do not transition back to the rod shape they are susceptible to lysis due to their inherent fragility and we model this using a linear term with death rate, ψ.

To model an immune response, we assume that all bacterial subpopulations are susceptible to phagocytosis; the rate at which phagocytosis occurs will depend on the number of phagocytes available and the type of bacteria. The immunogenic properties of L-forms remain relatively unknown [35, 36, 83]. However, the cell envelope is highly immunogenic: both the outer membrane and peptidoglycan layer have constituents that act as pathogen-associated molecular patterns (PAMPs). These molecules are recognisable to the immune system and phagocytes will respond accordingly. Therefore, since the cell wall is disrupted in the spherical cells it is not clear whether or not the spherical cells will incur the same immune response as cells that harbour an intact cell wall. Following [98, 102], we model phagocyte recruitment using logistic growth and assume that the morphology of a bacterium could affect its immunogenic properties. We define the maximum recruitment rate κ_i, where $i = \{H, L\}$, with subscripts H and L referring to the rod-shaped and spherical bacteria respectively. The carrying capacity of phagocytes is defined as P_{MAX}. We assume that all bacteria, regardless of shape, are susceptible to phagocytosis. Similarly, since phagocytosis may depend on the outer membrane being intact, we assume that the susceptibility of the spherical cells to phagocytosis could vary

from that of the native rod shaped bacteria. Hence we introduce the parameter ϕ_i, where $i = \{H, L\}$, to be the phagocyte-induced death rate of rod-shaped bacteria and spherical bacteria respectively.

P. aeruginosa bacteria can produce toxins that induce apoptosis of neutrophils and other immune cells [108]. We model bacteria-induced apoptosis using a linear density dependent term with rate, μ. For simplicity, we assume that bacteria produce toxins at the same rate regardless of the strain or shape and hence apoptosis occurs at the same rate for all bacterial subpopulations. Additionally, we define the clearance rate of phagocytes, ξ.

Throughout our results we consider the introduction of resistance into the environement via gene acquisition or cross contamination. Bacteria can acquire resistance through HGT or as a result of mutations during proliferation. Overexpression of the genes that regulate efflux is thought to occur as a result of mutations and therefore for simplicity, we assume that this is the only way that a bacterium may gain reduced susceptibility [67]. Alternatively, through cross contamination, a population of resistant bacteria could appear within the environment. Throughout the simulations we incorporate the emergence of resistance into the model by introducing a resistant population at some point over the course of the simulated treatment. If we are considering a resistant population that has arisen due to mutation then our initial population size would be small, whereas a population that appears from cross contamination could be much larger. Our aim is to understand the conditions under which a resistant population would grow and to investigate how treatments could work in conjunction with the host response to control the emergence of resistance and clear the population.

Table 4.1: Definitions and units for the variables in Model III, described by equations (4.1)-(4.9).

Variable	Definition	Units
H_S	Antibiotic-susceptible rod-shaped cells with no internalised bound antibiotic	cells cm^{-3}
I_S	Antibiotic-susceptible rod-shaped cells with internalised bound antibiotic	cells cm^{-3}
L_S	Antibiotic-susceptible spherical cells	cells cm^{-3}
H_R	Antibiotic-resistant rod-shaped cells with no internalised bound antibiotic	cells cm^{-3}
I_R	Antibiotic-resistant rod-shaped cells with internalised bound antibiotic	cells cm^{-3}
L_R	Antibiotic-resistant spherical cells	cells cm^{-3}
P	Phagocytes	cells cm^{-3}
A	Extracellular antibiotic concentration	$\mu\mathrm{g\,ml}^{-1}$

Following these assumptions we formulate the following model:

$$\begin{aligned}
\frac{dH_S}{dt} &= rH_S\left(1-\frac{(H_S+H_R)}{k}\right)-\frac{\nu A}{A+A_{50}}H_S-\frac{\gamma A}{A+T_{50}}H_S \\
&\quad +\frac{\delta}{2}\left(1+\tanh\left(\frac{A_c-A}{b}\right)\right)L_S-\phi_H H_S P, && (4.1)\\
\frac{dI_S}{dt} &= \frac{\nu A}{A+A_{50}}H_S-\rho I_S-\phi_H I_S P, && (4.2)\\
\frac{dL_S}{dt} &= \frac{\gamma A}{A+T_{50}}H_S-\frac{\delta}{2}\left(1+\tanh\left(\frac{A_c-A}{b}\right)\right)L_S-\psi L_S-\phi_L L_S P, && (4.3)\\
\frac{dH_R}{dt} &= (1-c)rH_R\left(1-\frac{(H_S+H_R)}{k}\right)-(1-\omega)\frac{\nu A}{A+A_{50}}H_R-\frac{\gamma A}{A+T_{50}}H_R \\
&\quad +\frac{\delta}{2}\left(1+\tanh\left(\frac{A_c-A}{b}\right)\right)L_R-\phi_H H_R P, && (4.4)\\
\frac{dI_R}{dt} &= (1-\omega)\frac{\nu A}{A+A_{50}}H_R-\rho I_R-\phi_H I_R P, && (4.5)\\
\frac{dL_R}{dt} &= \frac{\gamma A}{A+T_{50}}H_R-\frac{\delta}{2}\left(1+\tanh\left(\frac{A_c-A}{b}\right)\right)L_R-\psi L_R-\phi_L L_R P, && (4.6)\\
\frac{dP}{dt} &= \kappa_H\left(H_S+I_S+H_R+I_R\right)\left(1-\frac{P}{P_{MAX}}\right)+\kappa_L\left(L_S+L_R\right)\left(1-\frac{P}{P_{MAX}}\right) \\
&\quad -\mu\left(H_S+I_S+H_R+I_R+L_S+L_R\right)P-\xi P, && (4.7)\\
\frac{dA}{dt} &= -\alpha A-\frac{\tilde{\nu}A}{A+A_{50}}\left(H_S+(1-\omega)H_R\right), && (4.8)
\end{aligned}$$

with initial conditions,

$$H_S(0) = H_{S0}, \quad I_S(0) = 0, \quad L_S(0) = 0, \quad H_R(0) = H_{R0}, \quad I_R(0) = 0,$$
$$L_R(0) = 0, \quad P(0) = 0, \quad A(0) = A_0. \tag{4.9}$$

Definitions for all variables and parameters are displayed in Tables 4.1 and 4.2 respectively. A default parameter set was chosen using suitable literature, the parametrisation results in Chapter II and the analysis in Chapter III. The default parameter values are also shown in Table 4.2, although a range of values is used throughout.

To produce the simulations in the remainder of this chapter we include the assumption that bacterial growth will cease when the population reaches a low critical threshold. It is likely that environmental pressure and the stochasticity of biological processes would cause the rod-shaped population to die out if the population decreased to a low level. When solving the model we include the assumption that growth will stop once the rod-shaped population reaches 50 bacteria and further assume that the rod-shaped bacteria will no longer transition to the spherical form. We assume that the reverse transition is still possible, as are the interactions of the immune system and antibiotic with the remaining cellular populations.

4.2 Bacterial growth in the absence of antibiotic

4.2.1 Single strain infection

Initially, we consider bacterial growth of a susceptible strain, prior to treatment, such that the initial conditions are,

$$H_S(0) = 10^4, \quad I_S(0) = 0, \quad L_S(0) = 0, \quad H_R(0) = 0, \quad I_R(0) = 0,$$
$$L_R(0) = 0, \quad P(0) = 0, \quad A(0) = 0. \tag{4.10}$$

Table 4.2: Definitions, units and default values for the parameters used in Model III, described by equations (4.1)-(4.9). We define $i = \{H, L\}$ where H and L imply that the rate is attributed to the bacillary (rod-shaped) or spherical bacteria respectively.

Parameter	Definition	Units	Default parameter value	Source
r	Rod-shaped bacterial growth rate.	day^{-1}	3	[94]
c	Fitness cost attached to carrying resistance genes.	dimensionless	0.15	[100, 109]
k	Carrying capacity of rod-shaped bacteria with no internalised bound antibiotic.	cells cm^{-3}	10^6	[94]
ν	Maximum antibiotic internalisation rate.	day^{-1}	1.57	-
ω	Efflux pump upregulation parameter.	dimensionless	0.5	-
A_{50}	Antibiotic concentration required for half maximal internalisation.	$\mu\text{g ml}^{-1}$	0.47	Chapter 3
γ	Maximum transition rate from rod to spherical shape.	day^{-1}	1.57	-
T_{50}	Antibiotic concentration required for half maximal transition effect.	$\mu\text{g ml}^{-1}$	0.47	Chapter 3
δ	Transition rate from spherical to rod shape.	day^{-1}	10	-
A_c	Critical antibiotic concentration threshold for reversion of spherical cells.	$\mu\text{g ml}^{-1}$	0.5	-
b	Smoothed step function slope parameter.	$\mu\text{g ml}^{-1}$	1	-
κ_i	Maximum recruitment rate of phagocytes by bacteria.	day^{-1}	0.5	-
P_{MAX}	Carrying capacity of phagocytes.	cells cm^{-3}	1.8×10^5	[98]
ψ	Death rate of spherical cells.	day^{-1}	0.017	Chapter 3
ρ	Death rate of rod-shaped bacteria due to antibiotic.	day^{-1}	100	-
ϕ_i	Death rate of bacteria by phagocytes.	$(\text{cells cm}^{-3})^{-1}$ day^{-1}	2.4×10^{-4}	[98]
μ	Death rate of phagocytes by bacteria-induced apoptosis.	$(\text{cells cm}^{-3})^{-1}$ day^{-1}	6×10^{-6}	[98]
ξ	Natural clearance rate of phagocytes.	day^{-1}	1.512	[98]
α	Extracellular antibiotic decay rate.	day^{-1}	15	[77]
$\tilde{\nu}$	Extracellular antibiotic decay due to internalisation in rod-shaped cells.	$\mu\text{g ml}^{-1}$ $(\text{cells cm}^{-3})^{-1}$ day^{-1}	1×10^{-3}	-

A suitable phagocyte recruitment rate, κ_H, is chosen to reflect an infection that cannot be cleared by the immune system alone. Figure 4.2 (a) displays the solutions of the model using the default parameter set with $A(0) = 0$. Since the immune response cannot clear the infection we see that both populations of rod-shaped bacteria and phagocytes reach nonzero steady state values.

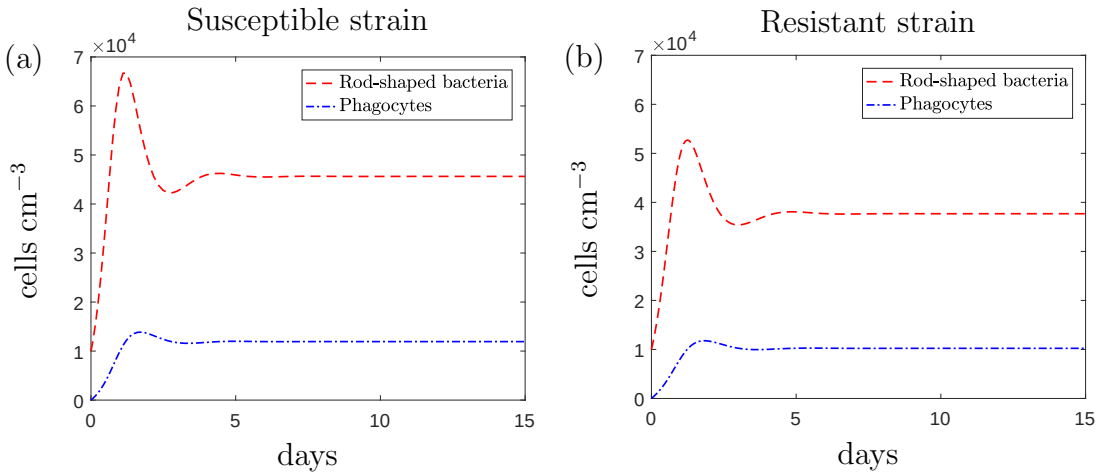

Figure 4.2: The solution to the system (4.1)-(4.8), using the default parameter values found in Table 4.2 and the initial conditions (a) (4.10) and (b) (4.11).

If we consider a single strain that is partially-resistant to the antibiotic and solve the model using the initial conditions,

$$H_S(0) = 0, \quad I_S(0) = 0, \quad L_S(0) = 0, \quad H_R(0) = 10^4, \quad I_R(0) = 0,$$
$$L_R(0) = 0, \quad P(0) = 0, \quad A(0) = 0, \tag{4.11}$$

then we obtain the results in Figure 4.2 (b). Before the antibiotic is added, the susceptible and resistant populations have similar growth dynamics and identical immunogenic properties as no bacteria transition to the spherical form. The only assumed difference between the two strains prior to antibiotic exposure is the fitness cost attributed to carrying resistance genes. The effects of the fitness cost are observed in the lower steady state value reached by the resistant population.

4.2.2 Investigating the emergence of resistance

It is possible that a resistant population may emerge via mutation or due to cross-contamination prior to treatment and hence the initial number of resistant bacteria that appear in the population, H_{R0}, could vary. In addition to the initial condition, the time

that the resistant population appears, which we refer to as T_R, could affect the size of the resistant population. Figure 4.3 displays the population levels of the resistant population when we vary the fitness cost against the initial condition. We note that the graphs show the size of the resistant population (not the steady state population sizes) at the specified time after introducing the resistant population at time $t = 0$. The results indicate time-dependent behaviour; the resistant population could survive with reduced fitness but the length of time that it can continue to grow will depend on the size of the fitness cost. The population will inevitably die out eventually unless the fitness cost is very low; further investigation indicates that if the fitness cost is less than 1×10^{-5} then we could expect the resistant population to persist for an extended time period. Fitness cost values of this size are extremely small in comparison to the interval of realistic values provided in [100, 109] and although these values are related to plasmid-mediated resistance, we can use them as an indication of the potential size of a fitness cost. This indicates that fitness costs of less than 1×10^{-5} could be considered as negligible and thus we conclude that unless the resistant strain has a negligible fitness cost, then we would not expect a resistant strain to emerge. If there is a negligible fitness cost then Figures 4.3 (a)-(b) indicate that the initial condition will determine the size of the resistant population.

Similarly, we can explore the effects of the time that the resistant population appears on whether a resistant population can establish itself. Figure 4.4 indicates that T_R does not significantly affect the population size of the resistant population when compared to the effects of the fitness cost and initial condition.

4.3 Introducing the antibiotic

In Chapter 3 we considered the effects of a single dose of antibiotic and predicted that the amount of antibiotic simulated would not successfully clear either a susceptible or resistant population. After incorporating an immune response we attain similar results using the default parameter set and conclude that even with the additional effects of an immune

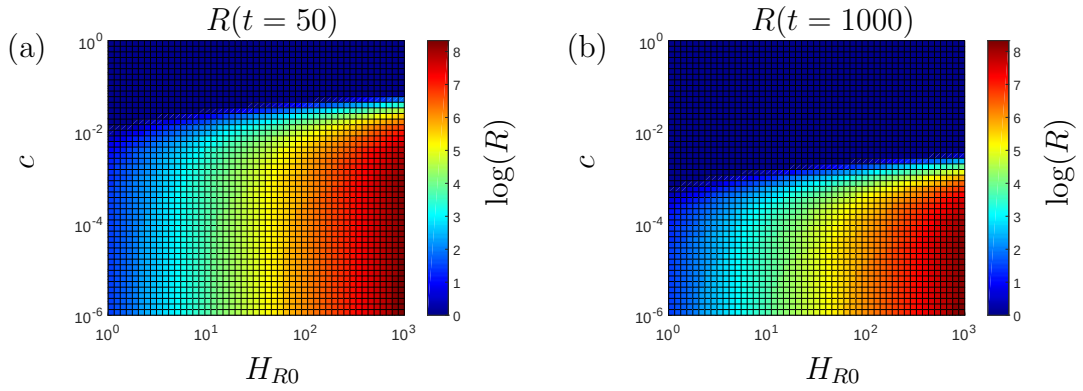

Figure 4.3: The population levels of resistant bacteria for varying values of fitness cost, c, and initial condition, H_{R0}. Note that these figures show the total resistant population after (a) 50 days and (b) 1000 days. Population growth is simulated by solving the equations (4.1)-(4.8), using the default parameter values found in Table 4.2 and initial conditions (4.10) with $H_R(0) = H_{R0}$, for the desired time frame. The total population of resistant bacteria, R, is calculated such that $R = H_R + I_R + L_R$. The total number of susceptible bacteria is not significantly affected, regardless of the characteristcs of the resistant population (results omitted).

response, a single dose of antibiotic would not be effective in clearing either a susceptible or resistant infection (results omitted for brevity). Furthermore, a similar investigation into the emergence of a resistant population indicates that as soon as the antibiotic is exhausted the conditions at the site of infection would return to the antibiotic-free state. If a resistant population emerges during the treatment then following from the results in Figure 4.3, the survival of this population after antibiotic exposure will be determined by the fitness cost. Unless there is a negligible fitness cost then we would expect the resistant population to die out following exhaustion of the antibiotic. A single dose treatment would be clinically irrelevant and consequently we continue to consider the effects of a continuous dose of antibiotic on the bacterial population.

For the following analysis we will consider a constant dose of antibiotic and assume that antibiotic exposure will prevent the spherical bacteria from rebuilding the cell wall for the duration of the treatment. After considering a constant dose of antibiotic and assuming that there is no reverse transition, we amend Model III and obtain the constant

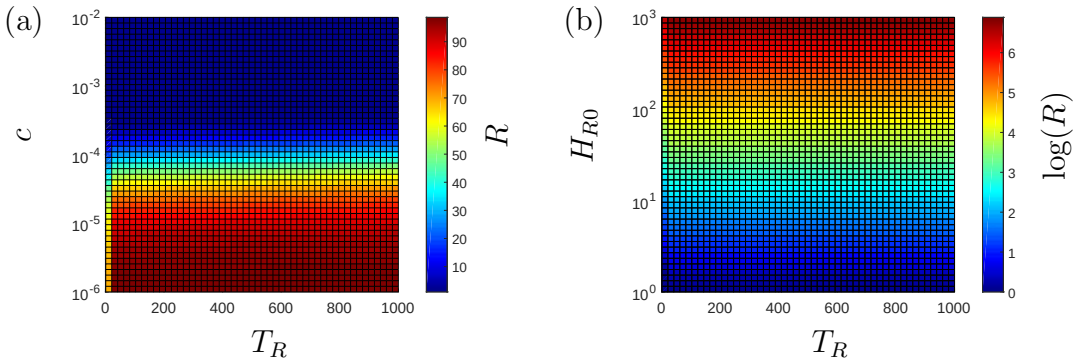

Figure 4.4: The population levels of resistant bacteria for varying values of (a) fitness cost and (b) initial condition against the time of population appearance, T_R. In (a), the initial resistant population size was taken as 100 bacteria and in (b) it was assumed that the resistant bacteria had no fitness cost. After simulating the emergence of the resistant population, the simulation is continued until (a) 5000 days (as the steady state is reached on a unrealistically long timescale) and (b) the steady state is reached; after this, the number of resistant bacteria, R, is calculated such that $R = H_R + I_R + S_R$. The total number of susceptible bacteria is not significantly affected, regardless of the characteristics of the resistant population (results omitted).

dose model,

$$\begin{aligned}
\frac{dH_S}{dt} &= rH_S\left(1-\frac{(H_S+H_R)}{k}\right)-\frac{\nu A}{A+A_{50}}H_S-\frac{\gamma A}{A+T_{50}}H_S \\
&\quad -\phi_H H_S P, && (4.12)\\
\frac{dI_S}{dt} &= \frac{\nu A}{A+A_{50}}H_S-\rho I_S-\phi_H I_S P, && (4.13)\\
\frac{dL_S}{dt} &= \frac{\gamma A}{A+T_{50}}H_S-\psi L_S-\phi_L L_S P, && (4.14)\\
\frac{dH_R}{dt} &= (1-c)rH_R\left(1-\frac{(H_S+H_R)}{k}\right)-(1-\omega)\frac{\nu A}{A+A_{50}}H_R-\frac{\gamma A}{A+T_{50}}H_R \\
&\quad -\phi_H H_R P, && (4.15)\\
\frac{dI_R}{dt} &= (1-\omega)\frac{\nu A}{A+A_{50}}H_R-\rho I_R-\phi_H I_R P, && (4.16)\\
\frac{dL_R}{dt} &= \frac{\gamma A}{A+T_{50}}H_R-\psi L_R-\phi_L L_R P, && (4.17)\\
\frac{dP}{dt} &= \kappa_H\left(H_S+I_S+H_R+I_R\right)\left(1-\frac{P}{P_{MAX}}\right)+\kappa_L\left(L_S+L_R\right)\left(1-\frac{P}{P_{MAX}}\right) \\
&\quad -\mu\left(H_S+I_S+H_R+I_R+L_S+L_R\right)P-\xi P, && (4.18)\\
\frac{dA}{dt} &= 0, && (4.19)
\end{aligned}$$

with initial conditions,

$$H_S(0) = H_{S0}, \quad I_S(0) = 0, \quad L_S(0) = 0, \quad H_R(0) = H_{R0}, \quad I_R(0) = 0,$$
$$L_R(0) = 0, \quad P(0) = 0, \quad A(0) = A_0. \tag{4.20}$$

Using the continuous dose model, we will investigate the population growth of both single strain infections and a mixed strain infection during multiple treatment combinations. We also consider varying immunogenic characteristics for the spherical populations. Table 4.3 is given at the end of this chapter and details the results obtained throughout; this can be used as a guide to the predictions made using the continuous dose infection level model.

4.3.1 Single strain infection

Initially, we consider a population of susceptible bacteria and assume no cross-contamination or breakthrough mutations occur during the time course of the treatment. We solve the model (4.12)-(4.19) using the default parameter set, with initial conditions,

$$H_S(0) = 10^4, \quad I_S(0) = 0, \quad L_S(0) = 0, \quad H_R(0) = 0, \quad I_R(0) = 0,$$
$$L_R(0) = 0, \quad P(0) = 0, \quad A(0) = 10, \tag{4.21}$$

and obtain the solutions displayed in Figure 4.5 (green dashed lines). Within the first few days we see a rapid decrease in rod-shaped bacteria with no bound antibiotic as the antibiotic binds within the bacteria or they shed the cell wall. The presence of the bacterial population initiates an immune response and we see a rise in phagocytes. As the antibiotic treatment continues we see all subpopulations decrease until the infection is cleared, albeit after a lengthy treatment period. We note that our results in Chapter 2 suggested that the morphological transition could enable the population to survive a constant dose of antibiotic (see Figure 2.6); the results in Figure 4.5 suggest that the

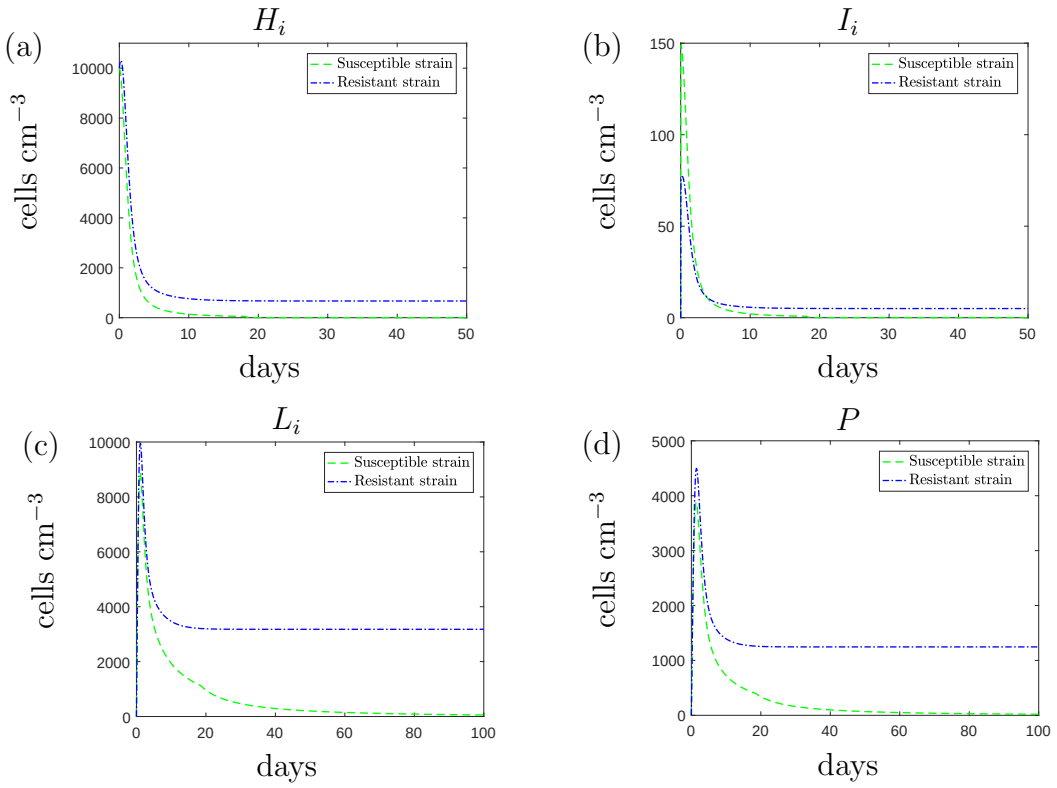

Figure 4.5: The solutions to the system (4.12)-(4.19) using the default parameter values in Table 4.2 and the initial conditions (4.21) (green dashed lines) and (4.22) (blue dashed-dotted lines).

additional effects of the immune response could aid the antibiotic and clear an antibiotic-susceptible infection.

We have predicted that the immune response could be a critical factor when predicting treatment success. This result can be directly related to the study by Ankomah et al. [7] in which they suggest that the presence of a subpopulation with phenotypic resistance (i.e. persister cells) would not cause treatment failure in cases where the rate of phagocytosis is sufficiently high. These results highlight the importance of acknowledging hosts defences when considering mechanisms of antibiotic evasion including the morphological transition.

We also consider the effects of a continuous dose of antibiotic on an infection that comprises a single antibiotic-resistant strain. Solving equations (4.12)-(4.19), with initial

conditions,

$$H_S(0) = 0, \quad I_S(0) = 0, \quad L_S(0) = 0, \quad H_R(0) = 10^4, \quad I_R(0) = 0,$$
$$L_R(0) = 0, \quad P(0) = 0, \quad A(0) = 10, \tag{4.22}$$

gives the results displayed in Figure 4.5 (blue dashed-dotted lines). As expected, the results suggest that the resistant bacteria would reach a non-zero steady state, even after continued exposure to the antibiotic and in the presence of an intact immune response. Active efflux enables the bacteria to resist antibiotic effects and an alternative treatment would be required in order to successfully clear the infection.

4.3.2 Investigating the emergence of resistance

In Section 4.2.2 we concluded that in the absence of antibiotic, a resistant population could only emerge if the fitness cost was small enough. Antibiotic effects will undoubtedly place pressure on the susceptible population and it is likely that this pressure will impact the conditions needed for a resistant population to emerge. There are four parameters that could affect the resistant population; we previously considered the fitness cost, c, initial condition, R_0, a time of emergence, T_R. In the presence of antibiotic, the efflux parameter, ω, must also be considered.

We assume that a resistant population could emerge, due to mutation, and avoid antibiotic exposure until the population has grown to the size of approximately 100 bacteria and therefore use an initial condition of $H_R(0) = 100$ (unless we are investigating the initial population size). Similarly, it is possible that a contaminant population of resistant bacteria could be of this size, or greater. Additionally, it is possible that a resistant population may already be present before the treatment is administered; following from the previous section we note that this will only occur if there is no fitness cost attributed

to carrying resistance. Thus we obtain the initial conditions,

$$H_S(0) = 10^4, \quad I_S(0) = 0, \quad L_S(0) = 0, \quad H_R(0) = 100, \quad I_R(0) = 0,$$
$$L_R(0) = 0, \quad P(0) = 0, \quad A(0) = 10. \tag{4.23}$$

Note that we have chosen an initial condition for the susceptible population that is much lower than the antibiotic free steady state. This initial condition was chosen to reflect an infection that was caught before the population reached its steady state value. In a hospital environment, it is possible that a *P. aeruginosa* infection could be detected and treated whilst in the early stages of infection.

Following from Figure 4.5 we find that a constant dose of antibiotic will clear the susceptible population in the absence or presence of a resistant subpopulation. Hence we only investigate changes to the steady state population of the resistant bacteria. Figure 4.6 (a) displays the steady state values for the resistant population when we vary the time of emergence against the initial number of resistant bacteria. The results indicate that neither variable has an effect on the steady state population. In an antibiotic free environment we predicted that the initial condition would affect the steady state population (see Figure 4.4 (b)), however, we now find that neither variable impacts the population size when a constant dose of antibiotic is added. After further investigation we find that neither T_R nor R_0 has any impact on the steady state population level when compared with the fitness cost, c, or the efflux parameter, ω (see Figure 4.6 (c)-(f)).

Figure 4.6 (b) displays the results if we vary the population determining parameters: the fitness cost, c, and efflux upregulation parameter, ω. Two clear regions of behaviour emerge for low and high values of c. When we have a low fitness cost ($c < 10^{-2}$), we find that changes to the efflux parameter have a large impact on the steady state whilst the fitness cost has little effect. For higher fitness costs ($c > 10^{-2}$), we find that the efflux parameter has less of an effect on the steady state compared to the fitness cost. For the highest values of the fitness cost and lowest values of the efflux parameter we find that

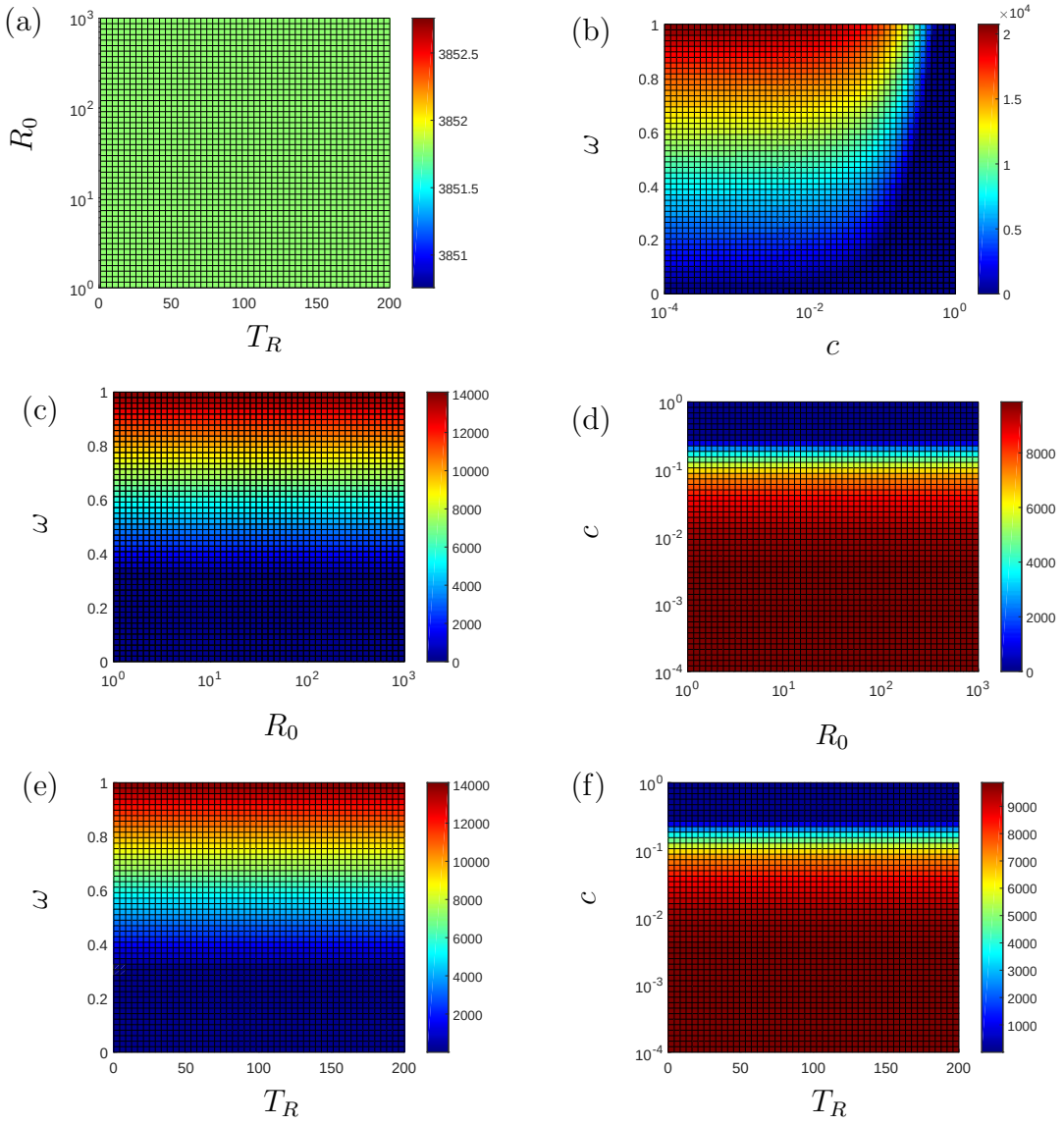

Figure 4.6: Steady state values of the resistant bacterial population after solving the system (4.12)-(4.19), with initial conditions (4.23) and default parameter values shown in Table 4.2. We vary the following parameter pairings: (a) initial condition, H_{R0}, and emergence time, T_R, (b) fitness cost, c, and efflux parameter, ω, (c) initial condition and efflux parameter, (d) initial condition and fitness cost, (e) efflux parameter and emergence time and (f) fitness cost and emergence time.

the population is cleared regardless of the size of the other parameter.

Note that Figure 4.6 (d) and (f) both suggest that bacteria with lower fitness can still establish a population in the presence of antibiotic compared to the antibiotic-free environment (see Figure 4.3). The higher allowance for reduced fitness in resistant bacteria arises due to the niche created by the mass killing of the susceptible bacteria by the

antibiotic. These results suggest that antibiotic exposure causes a selective pressure that could enable resistant populations to emerge that would not survive in an antibiotic-free system.

4.4 Considering alternative treatments

The results in Figure 4.5 predicted that a constant dose of antibiotic could successfully clear an antibiotic-susceptible strain infection with the support of the immune response. However, we are considering a parameter choice that requires a lengthy treatment time of around 200 days. A treatment of this length is clinically infeasible as not only would it be costly, it would provide an ideal environment for resistance to develop and leave the patient vulnerable to more threatening infections.

In [75] antimicrobial peptides were suggested as a suitable therapy to target cell wall deficient bacteria (CWDB) and our results in Chapter 2 supported the use of antibiotics and AMPs when the bacteria was in isolation with the antibiotic. Additionally, the combined use of antibiotics and an antivirulence drug was considered in [102]. We will continue to explore the effects of AMPs and an antivirulence drug on the growth of a single and mixed strain infection.

4.4.1 AMPs

Firstly, we do not consider the use of AMPs as a single treatment for a *P. aeruginosa* infection. AMPs target the spherical cells that form during antibiotic exposure; if no antibiotic is added then AMPs can have no effect. Rather, we still consider the use of AMPs in conjunction with antibiotics. We recall that the use of AMPs is simulated by increasing the death rate of the spherical cells.

Antibiotic-susceptible infection

Figure 4.7 displays the results when we simulate a combined treatment of antibiotic and AMPs on an antibiotic-susceptible infection. The model predicts that an increase in the spherical death rate, caused by the AMPs, would result in fewer spherical cells. The effect this has on the total population consequently depends on whether the decrease in the spherical population causes a substantial difference in the number of phagocytes recruited. These results suggest that there is a non-monotonic relationship between the effectiveness of the AMPs and the success of this combined treatment. If the AMPs increase the spherical cell death rate by approximately 5-fold ($\psi = 0.1$ day^{-1}, green dashed-dotted lines) then the persistent population of spherical cells is cleared faster without impacting the initial immune response. However, a more substantial increase in spherical cell death ($\psi = 10$ day^{-1}, cyan solid lines), from the default value, causes a substantial decrease in spheres and subsequently significantly fewer phagocytes are recruited initially. With fewer phagocytes at the site of infection, the rod-shaped cells are able to proliferate and grow to greater numbers. As the rod-shaped population increases, the immune response reacts accordingly and eventually the rod-shaped population is cleared but the treatment duration is no less than if we were to use the antibiotic alone.

If the antibiotic is administered alone (red dashed lines) then we predict that the population comprises only spherical cells towards the end of the treatment. Therefore, the application of the antibiotic at the later stages is not necessary for bactericidal purposes but instead as a requirement to keep the spherical cells from reverting back to rods. The remaining spherical cells are then cleared through natural clearance and phagocytosis. The AMPs have the ability to clear this population of spherical cells' faster, if their effectiveness does not significantly impact the immune response. However, if the AMPs are too potent then they have little impact on the overall population and instead they alter the composition of the population because of the indirect effect they have on the immune response. For higher values of ψ, the population towards the end of the treatment comprises mostly rod-shaped cells with no internalised antibiotic and the antibiotics are

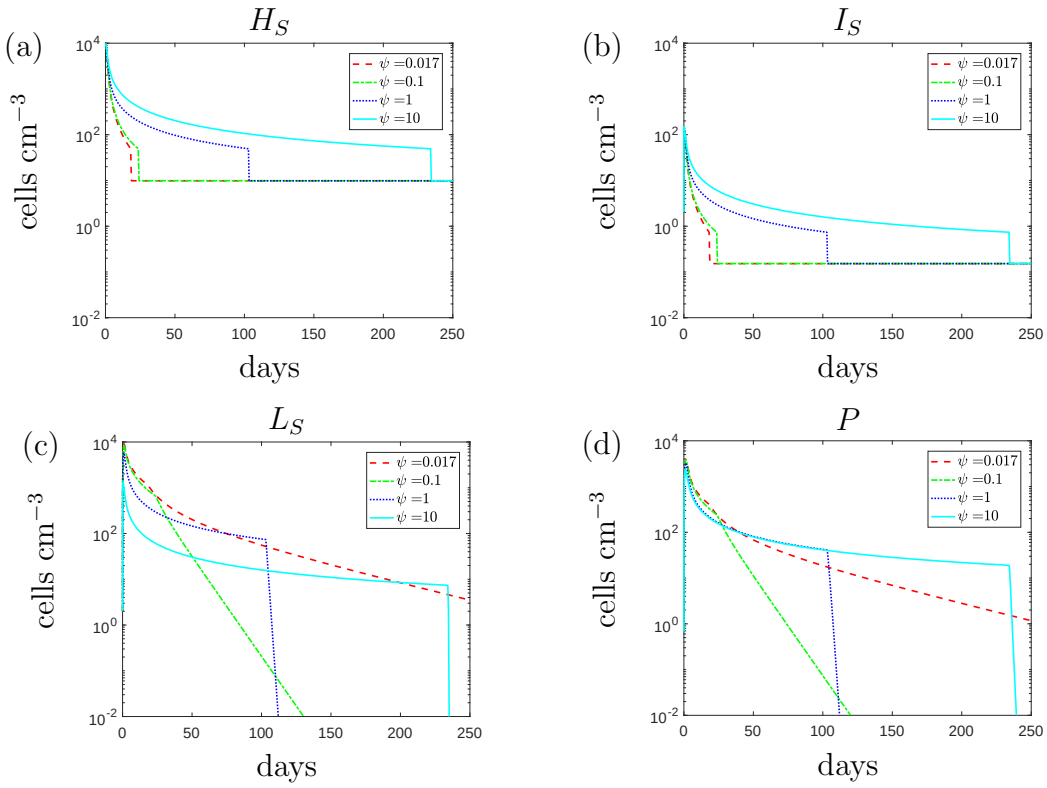

Figure 4.7: The variable solutions to the system (4.12)-(4.19), with initial conditions (4.21), default parameter values shown in Table 4.2 and varying the spherical cell death rate, ψ, from the default value of $1.7 \times 10^{-2}\,\text{day}^{-1}$. An increase in ψ represents the addition of antimicrobial peptides.

necessary for bactericidal purposes. We recall that due to the compromised cell membrane the spherical cells could be less virulent than the rod-shaped cells. If so, an increase in the proportion of rod-shaped cells would be an undesirable outcome and using AMPs could result in a more threatening infection.

Overall we predict that there could be a synergistic relationship between the AMPs and the antibiotic but this ultimately depends on the AMPs having a specific level of effectiveness. If we consider the parameter space for the spherical cell death rate, ψ, then we can attempt to find an optimal value of ψ, for which we predict the shortest necessary treatment time. If we vary the value of ψ and calculate the minimum time needed to eradicate the population then we obtain the results in Figure 4.8. We estimate the optimal death rate of the spherical cells to be $\psi \approx 0.25\,\text{day}^{-1}$, which relates to an

eradication time of approximately 61 days for our default parameter set. Beyond this synergistic potency level, the AMPs could become ineffective and possibly detrimental to treatment efforts.

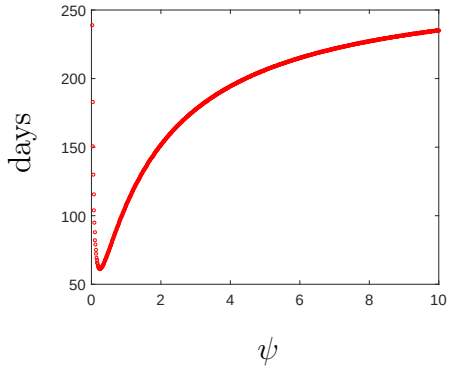

Figure 4.8: The time taken to clear an infection for various values of the spherical cell death rate, ψ. These results represent the administration of a continuous dose of antibiotics and AMPs; an increase in ψ represents an increase in the addition of AMPs. The variable solutions to the system (4.12)-(4.19), with initial conditions (4.22), default parameter values shown in Table 4.2 were calculated with various values of the spherical cell death rate, ψ. The time taken to clear the total bacterial population was then obtained and plotted against the values of ψ.

Antibiotic-resistant infection

If we simulate a combined dose of antibiotics and AMPs as a treatment for an antibiotic-resistant strain then the results, detailed in Figure 4.9, suggest similar findings to those obtained for the susceptible strain. As we increase the spherical cells death rate from the default parameter value we predict fewer spherical cells and a larger rod-shaped bacteria population. Overall, the total population is not altered substantially and the steady state of the total population is similar, regardless of the efficacy of the drug and its influence on the immune response. Using AMPs in addition to the AB does not affect the total population but instead alters the composition of the population. If we use antibiotics alone then we predict that the largest subpopulation will be the spherical cells. If we add the AMPs then the rod-shaped bacteria make up the dominant subpopulation. The

antibiotic alone was unable to treat the resistant infection and we find that the use of AMPs does not change the treatment outcome.

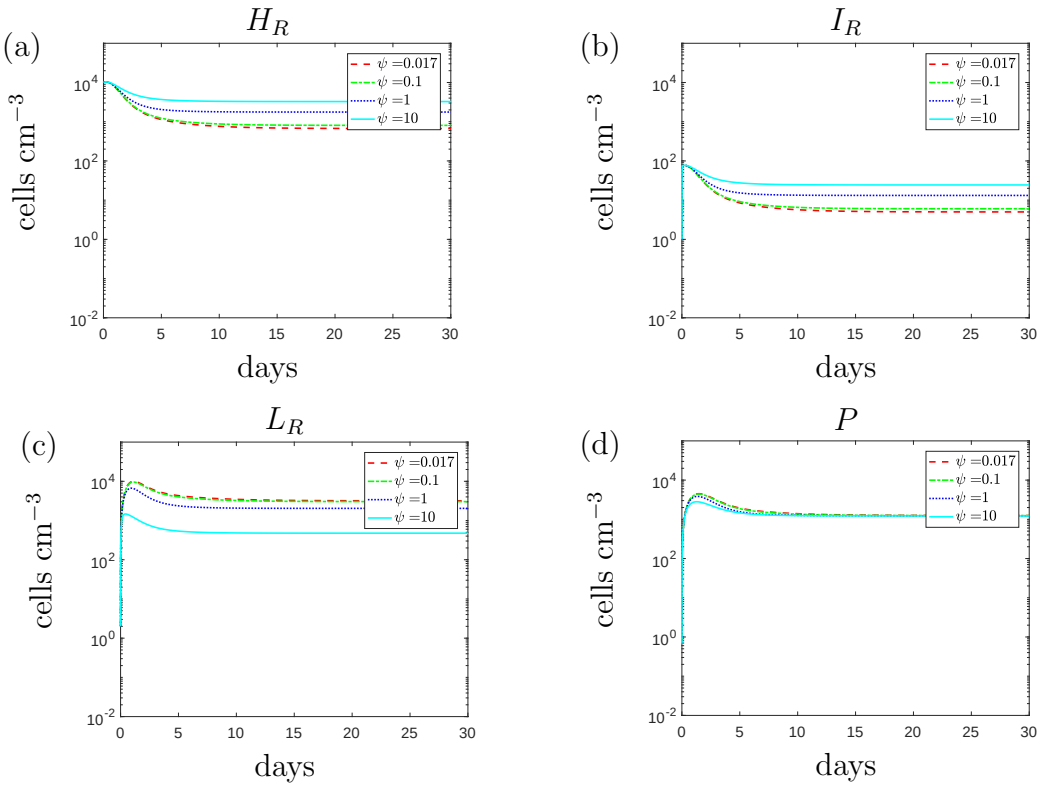

Figure 4.9: The variable solutions to the system (4.12)-(4.19), with initial conditions (4.22), default parameter values shown in Table 4.2 and varying the spherical cell death rate, ψ, from the default value of $1.7 \times 10^{-2}\,\text{day}^{-1}$. An increase in ψ represents the addition of antimicrobial peptides.

Mixed strain infection

Finally, we consider the use of the antibiotic and AMP combination on a mixed strain infection. From the results in Figure 4.6 we concluded that the initial condition and time that the resistant population first appears does not affect the steady state population for the resistant bacteria. Following these results, we only consider an initial population of 100 resistant bacteria in the following simulations and assume that this population is present at time $t = 0$.

Figure 4.10 displays the results if we simulate a combined dose of antibiotic and AMPs

on a mixed population. The results are similar to those obtained for the resistant strain infection; the AMPs alter the composition of the infection but do not alter the outcome of the treatment. Overall we find that the susceptible population is cleared marginally faster if we use the combined treatment. However, a large resistant population remains and grows to the same steady state for all tested values of ψ. Furthermore, by adding AMPs we could expect a more threatening resistant infection due to the increased proportion of rod-shaped cells.

4.4.2 Antivirulence drugs

Administering the antivirulence drug as a single treatment

Antivirulence drugs work by disarming the pathogen of a specific virulent property and each pathogen will display an array of these factors. Therefore we must specify a target virulence factor in order to suitably incorporate the administration of an antivirulence drug within the model. Some antivirulence drugs will increase the efficacy of the host immune system by weakening pathogenic properties that counteract immune effects. In [102], the effect of the antivirulence drug was modelled by an increase in the phagocytosis rate; a saturating term was used to incorporate the concentration of the drug and its PK properties. We will assume that a continuous dose of antivirulence drug is added and hence the increase in the rate of phagocytosis can be modelled as constant. It is unclear how an antivirulence drug would affect the spherical cells and hence we assume that only the rod-shaped bacteria are affected.

Initially, we consider the use of an antivirulence drug on its own. In Figure 4.11 the model predictions suggest that using a single antivirulence treatment could clear a bacterial infection (of both rods and spheres) in a few days if sufficiently potent. Further investigation indicates that a 60-fold increase in rod-shaped cell phagocytosis, from the default value of ϕ_H, would be required for an antivirulence drug to clear the infection in a week if used as a single treatment. Note that a similar increase in phagocytosis would

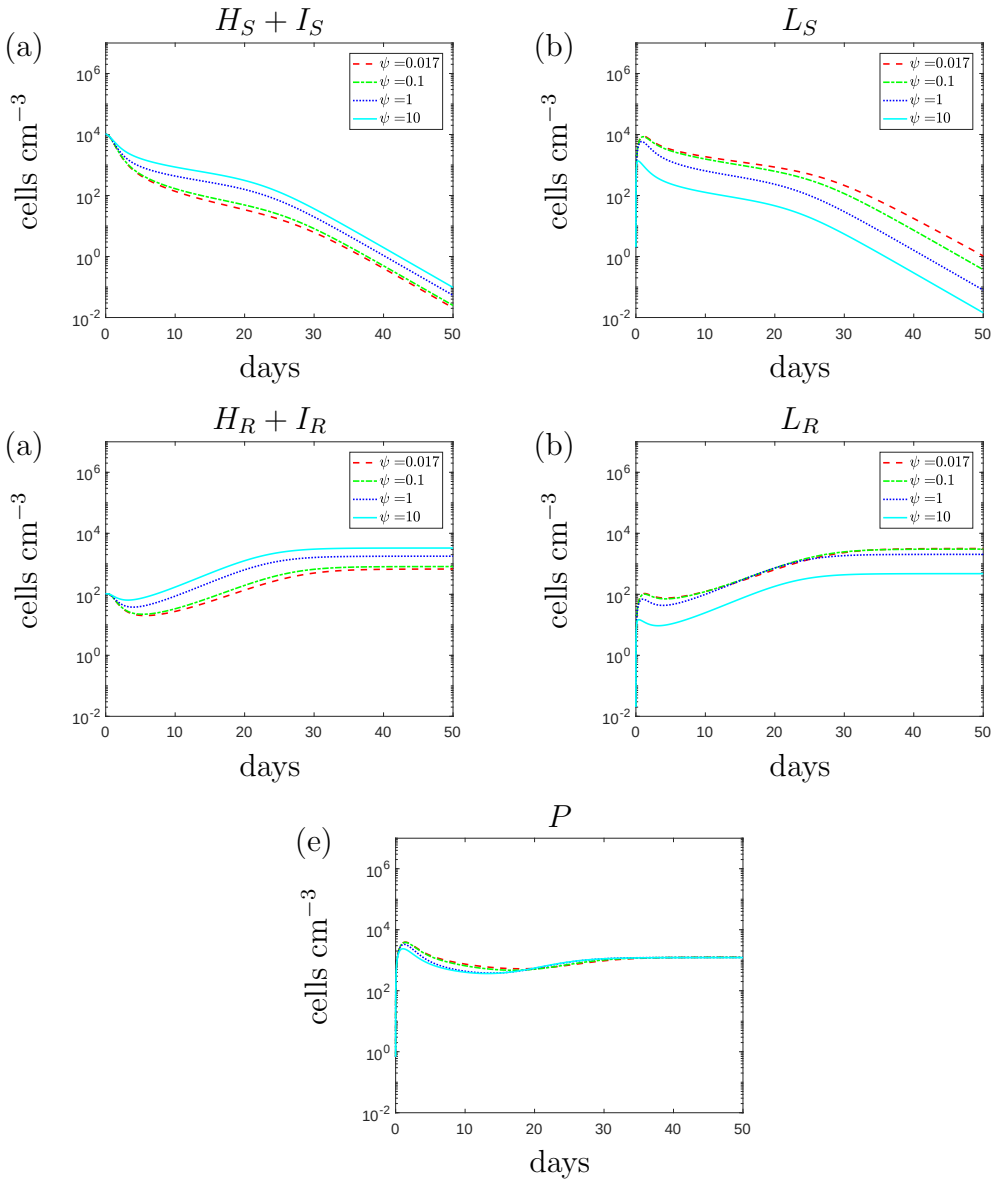

Figure 4.10: The variable solutions to the system (4.12)-(4.19), with initial conditions (4.23), default parameter values shown in Table 4.2 and varying the spherical cell death rate, ψ, from the default value of $1.7 \times 10^{-2}\,\text{day}^{-1}$. An increase in ψ represents the addition of antimicrobial peptides.

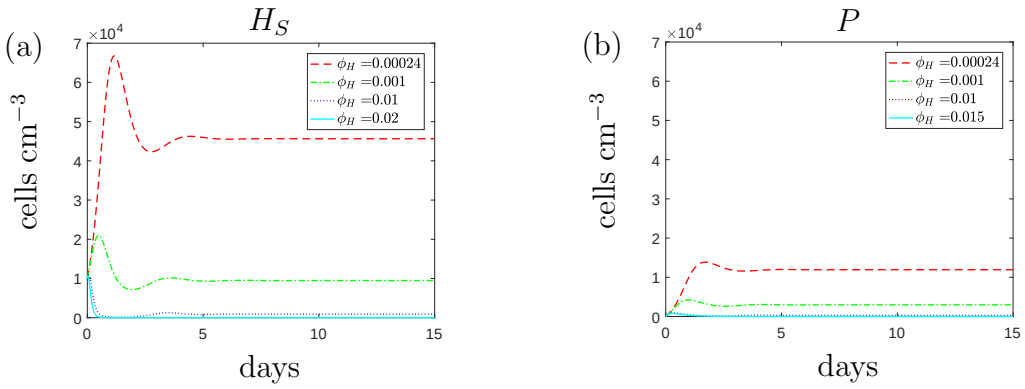

Figure 4.11: The variable solutions to the system (4.12)-(4.19), with initial conditions (4.20), default parameter values shown in Table 4.2 and varying the rod-shaped cell phagocytosis rate, ϕ_H, from the default value of $2.4 \times 10^{-4}\,(\text{cells}\,\text{cm}^{-3})^{-1}\,\text{day}^{-1}$. An increase in ϕ_H represents the addition of an antivirulence drug that increases susceptibility of the rod-shaped bacteria to host defences. It is assumed that the antivirulence drug is the only treatment and hence $A_0 = 0$.

be needed for an antivirulence drug to clear a single antibiotic resistant strain of bacteria (results omitted).

If we consider a mixed strain infection then our results suggest that the antivirulence drug would have the same effect on a mixed and single strain population. Furthermore, we conclude that the antivirulence drug would require the same level of effectiveness to clear the susceptible subpopulation in the absence and presence of a resistant subpopulation. As we previously predicted, the fitness cost could prevent the emergence of the resistant population if no treatment is administered. By adding an antivirulence drug, we are able to clear the resistant population faster than without treatment.

Antivirulence drugs are still being investigated and sufficient data is not available to obtain pharmacodynamic properties. Therefore it is not possible to quantify their efficacy using experimental data and we cannot conclude whether an antivirulence drug would be effective enough to clear an infection when used as a single therapeutic agent (though in the majority of *in vivo* studies, antivirulence drugs have attenuated but not cleared infections [27, 46, 52, 65, 92]). However, if the level of efficacy achieved by the antivirulence drug was sufficiently high that it could clear an antibiotic susceptible strain then our

results also suggest that it could clear an antibiotic resistant infection (unsurprisingly since the only difference here is that the resistant strain grows more slowly). Conversely, if the antivirulence drug was found to have limited efficacy when used alone (a 60-fold increase in the phagocytosis rate is likely to be unrealistic), it could be considered as a potential component of a combined treatment.

Administering the antivirulence drug in combination with the antibiotic

Following from Figure 4.11, we predict that the rod-shaped phagocytosis rate, ϕ_H, would need to increase above 10^{-2} in order to clear the infection using the antivirulence drug alone. In the following simulations and subsequent sections we consider the combined use of an antibiotic-antivirulence drug pairing. We limit the parameter space for the phagocytosis rate of rod-shaped cells to $\phi_H \in [0 \quad 10^{-2}]$ so that we only consider antivirulence drugs that cannot be used alone.

Firstly, we consider the use of the antibiotic and an antivirulence drug for the treatment of an antibiotic-susceptible infection. The results shown in Figure 4.12 indicate that as the effectiveness of the antivirulence drug increases, the rod-shaped population is cleared faster and subsequently a smaller population of spherical cells appears. Once the rod-shaped population has been cleared, the remaining spherical population enters a slow death phase where the cells are susceptible to natural death and phagocytosis (recall that the antivirulence drugs are assumed to not have any effect on the phagocytosis rate of the spheres). Since the rod-shaped cells are cleared faster using the antivirulence drug, the spherical cells enter the death phase sooner and are subsequently cleared faster than if the antibiotic was added alone. Antibiotic exposure is crucial during the death phase as it prevents the spherical cells from transitioning back to the rod-shape.

If we simulate the growth of an antibiotic-resistant strain with the antibiotic-antivirulence treatment we obtain a similar result to the antibiotic-susceptible strain. The results, displayed in Figure 4.13 indicate that if the antibiotic is used alone ($\phi_H = 2.4 \times 10^{-4}$ (cells cm^{-3})$^{-1}$ day^{-1}, red dashed lines) then we would expect the rod-shaped populations to

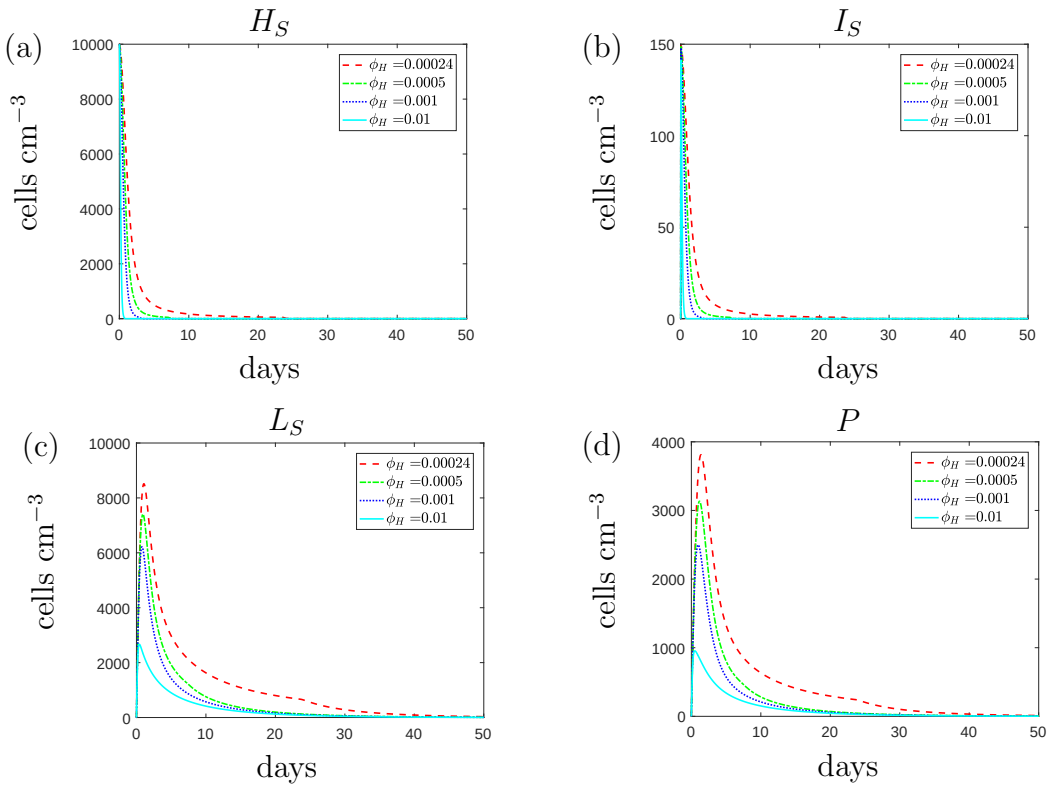

Figure 4.12: The variable solutions to the system (4.12)-(4.19), with initial conditions (4.21), default parameter values shown in Table 4.2 and varying the rod-shaped cell phagocytosis rate, ϕ_H, from the default value of $2.4 \times 10^{-4}\,(\text{cells}\,\text{cm}^{-3})^{-1}\,\text{day}^{-1}$. An increase in ϕ_H represents the addition of an antivirulence drug.

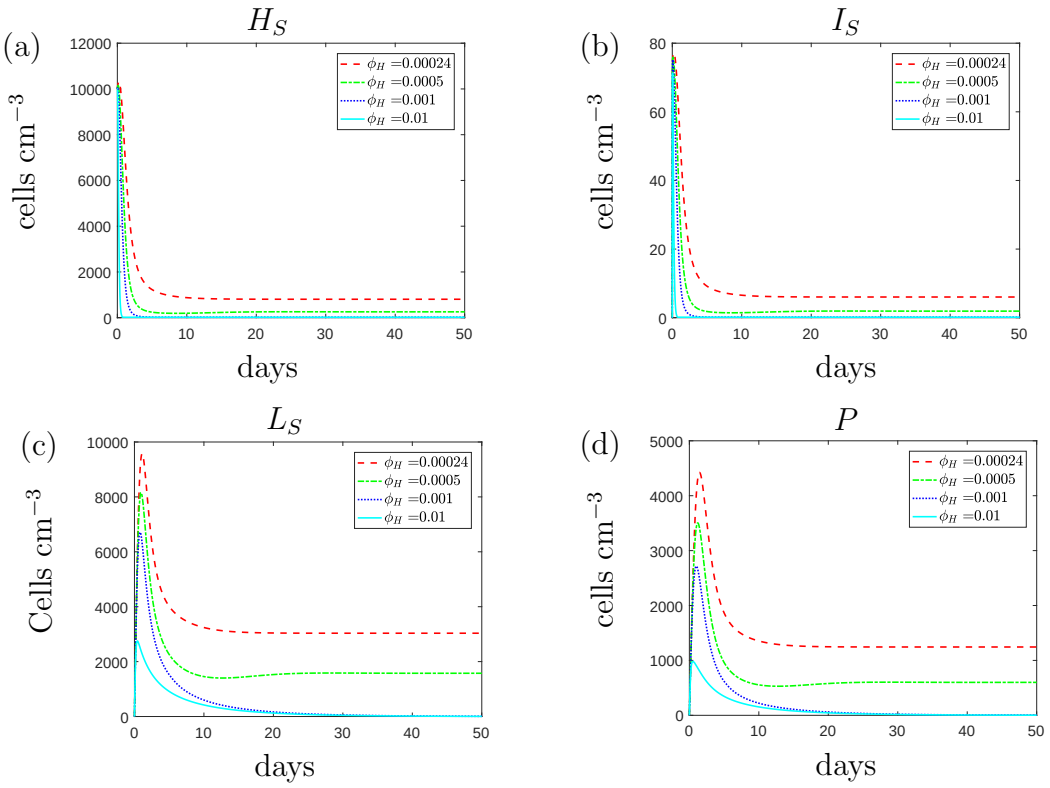

Figure 4.13: The variable solutions to the system (4.12)-(4.19), with initial conditions (4.22), default parameter values shown in Table 4.2 and varying the rod-shaped cell phagocytosis rate, ϕ_H, from the default value of $2.4 \times 10^{-4}\,(\text{cells}\,\text{cm}^{-3})^{-1}\,\text{day}^{-1}$. An increase in ϕ_H represents the addition of an antivirulence drug.

reach nonzero steady state values. If we increase the rod-shaped cell phagocytosis rate from the default value, our results suggest that using an antivirulence drug could help clear the rod-shaped population and increase the success of the antibiotic treatment. As with the susceptible-only strain, the spherical population enters a death phase, once the rod-shaped population has cleared and it is crucial that we clear this population in order to achieve treatment success.

If we simulate the effects of the combined antibiotic and antivirulence drug treatment on the growth of a mixed strain infection then our predictions are congruent to the single strain predictions (results omitted). The antivirulence drug enables clearance of all the rod-shaped cell subpopulation and the remaining spherical cells enter a slow death phase. Thus by combining antibiotics with an sufficiently potent antivirulence drug, the

model predicts that an antibiotic-susceptible (but persistent) infection can be cleared more quickly and an antibiotic-resistant infection can also be cleared.

4.4.3 Triple combinations

Our results thus far suggest that we could expect a lengthy treatment duration if antibiotics are used alone to treat a susceptible infection. If a resistant population is present then antibiotics become ineffective and cannot clear the infection. After considering two combination strategies we find that we could still expect a very lengthy treatment duration if we use a combination of antibiotics along with either AMPs or an antivirulence drug. The AMPs were found to help clear the spherical population whilst the antivirulence drugs support the immune system in clearing the rod-shaped cell population. If we simulate a triple drug combination treatment of the antibiotic, AMPs and an antivirulence drug then it may be possible to clear the infection in a much shorter time frame. If we simulate a triple combination of drugs on the single strain antibiotic-susceptible and antibiotic-resistant infections then we obtain the results displayed in Figure 4.14 (a) and (b) respectively. The graphs display the total population size after 14 days of continuous treatment and we predict that it could be possible to clear both infections within this clinically relevant time frame by using a combined therapy of antibiotic, antimicrobial peptides and an antivirulence drug. We notice two distinct regions in both plots of Figure 4.14. For low rod-shaped cell phagocytosis rates ($\phi_H < 1 \times 10^{-3}$ (cells cm^{-3})$^{-1}$ day^{-1}) the population cannot be cleared in the two week time period, regardless of the effectiveness of the AMPs. For faster rates of rod-shape cell phagocytosis ($\phi_H > 1 \times 10^{-3}$ (cells cm^{-3})$^{-1}$ day^{-1}) we find that the effectiveness of the antivirulence drug determines the population size but total clearance is only possible if the spherical cell death rate if sufficiently high ($\psi > 0.05$ day^{-1}). We note that a discontinuity arises in Figure 4.14 (b) and we see a rapid change in solution occurs around the region when $\phi_H < 1 \times 10^{-3}$ (cells cm^{-3})$^{-1}$ day^{-1}. We attribute this behaviour to a previous assumption regarding the behaviour of the population at low cell numbers; we have assumed that the bacteria will cease to

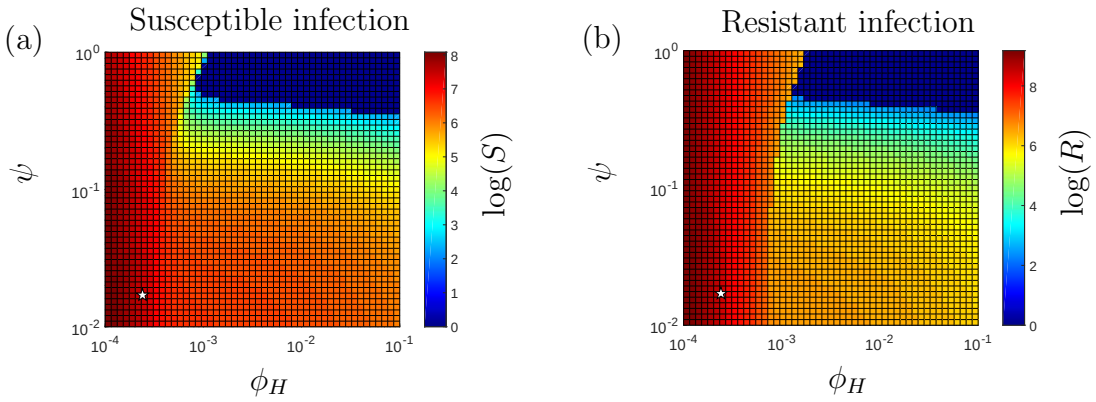

Figure 4.14: The population levels of (a) susceptible bacteria and (b) resistant bacteria after 14 days for varying values of the rod-shaped cell phagocytosis rate, ϕ_H, and spherical cell death rate, ψ. Increasing these parameters from their default values (marked with a star) simulates the effects of an antivirulence drug and antimicrobial peptide treatment respectively on the single strain infections. The total population of susceptible, S, and resistant bacteria, R, is calculated such that $S = H_S + I_S + L_S$ and $R = H_R + I_R + L_R$ respectively.

proliferate once the population reaches 50 bacteria.

We also simulate the triple combination on the mixed population and conclude from Figure 4.15 that if the AMPs and antivirulence drug can clear the susceptible strain then the resistant strain will also be cleared due to its small initial condition and fitness cost.

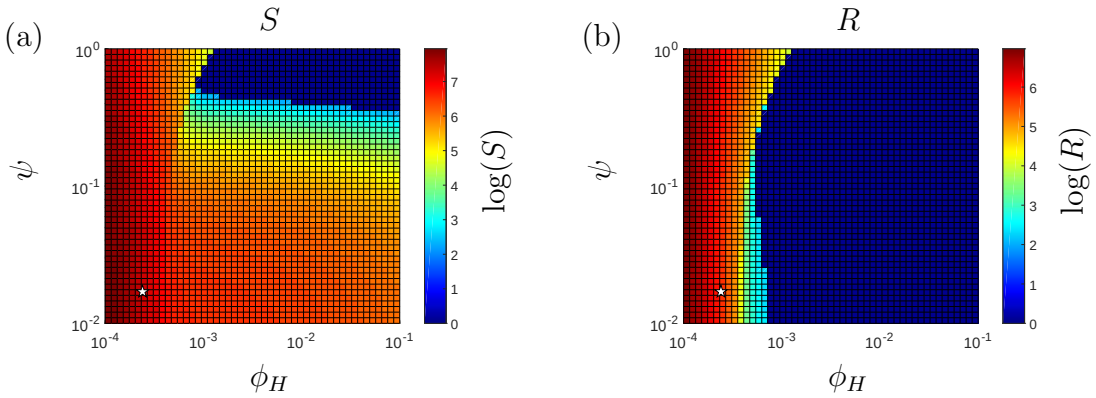

Figure 4.15: The population levels of (a) susceptible bacteria and (b) resistant bacteria after 14 days for varying values of the rod-shaped cell phagocytosis rate, ϕ_H, and spherical cell death rate, ψ. Increasing these parameters from their default values (marked with a star) simulates the effects of an antivirulence drug and antimicrobial peptide treatment respectively on the mixed strain infection. The total population of susceptible, S, and resistant bacteria, R, is calculated such that $S = H_S + I_S + L_S$ and $R = H_R + I_R + L_R$ respectively.

4.5 Phagocytosis rate

Until now we have assumed that the spherical bacteria have identical immunogenic properties to the rod-shaped cells and our default parameters were chosen such that the recruitment rate, κ and the phagocytosis rate, ϕ, are the same regardless of cell shape.

It has been suggested that the immunogenic properties of the spherical cells could differ to those of the rod-shaped bacteria [35, 36, 83]. Both the outer membrane and peptidoglycan layers have constituents that act as PAMPs and activate immune responses. If peptidoglycan is lost, spherical cells may actually be less immune stimulatory. With regards to phagocytosis, if the outer membrane is not intact then phagocytosis could also occur at a different rate for the spherical cells. By varying these parameters we can investigate how different immunogenic properties could affect the total bacterial load during treatment.

We begin by considering the case where phagocytosis rates differ between rod-shaped and spherical bacteria and assume that recruitment of phagocytes is the same regardless of the state of the cell wall.

4.5.1 Antibiotic-susceptible infection

Initially, we consider the impact of different phagocytosis rates for different cell types in an antibiotic-susceptible strain infection during a continuous treatment of antibiotic. The properties of the spherical cells suggest that phagocytosis may occur at a different rate to rod cells due to the damaged cell wall. It is unknown how well immune cells phagocytose spherical cells. Phagocytosis may occur at a faster rate since the cells have a depleted cell wall. However, the depletions may incur loss of targets for the immune cells and therefore phagocytosis could occur at a slower rate. Investigation into faster phagocytosis rates for the spherical cells indicated that in all cases the bacteria would be cleared faster for all treatment combinations (results omitted). Following this, we choose to investigate the casse where the spherical cell population has a slower phagocytosis rate than the

rod-shaped cells. If we decrease the spherical cell phagocytosis rate, ϕ_L, we obtain the results in Figure 4.16. As expected, we predict larger populations of spherical cells as we decrease the phagocytosis rate from the default value. The larger spherical population causes the total population of bacteria to increase and this initiates a stronger immune response as more phagocytes are recruited. Additionally, since fewer spherical cells are phagocytosed, fewer phagocytes undergo apoptosis. Consequently, due to the higher number of phagocytes, we predict that the rod-shaped populations would be cleared faster if the phagocytosis rate of the spherical cells decreases. The spherical cells are susceptible to natural death and replenishment depends on the size of the rod-shaped population. Hence we see a decline in the spherical population as soon as the rod-shaped population has depleted.

The qualitative result for the total population remains the same regardless of the phagocytosis rate; we predict total bacterial clearance, even if we assume that the spherical cells are immune to phagocytosis ($\phi_L = 0\,(\text{cells cm}^{-3})^{-1}\,\text{day}^{-1}$, cyan solid lines). The treatment duration needed to clear the infection increases as the phagocytosis rate decreases and we could expect a higher bacterial load over the course of the treatment.

After further investigation we find that the qualitative results of the combination therapies are the same regardless of the phagocytosis rate. The success of using AMPs alongside the antibiotic will be dependent on the effectiveness of the AMPs and using an antivirulence drug with the antibiotic could decrease the treatment time by a few days. We omit the results for the dual treatment combinations (which are qualitatively equivalent to those in Sections 4.4.1-4.4.2) but compare the results for a triple combination when $\phi_H > \phi_L$. Using Figure 4.16 we predicted that the rod-shaped population could die out faster if the spherical cell phagocytosis rate decreases. Consequently, when $\phi_H > \phi_L$ the antivirulence drug does not need to be as effective to clear the infection, compared to the case when $\phi_H = \phi_L$ - see Figure 4.17. Additionally, we observe a higher population at the end of the 14 day treatment for many of the parameter pairings in Figure 4.17 (b) compared to those in Figure 4.17 (a). The higher populations represent the

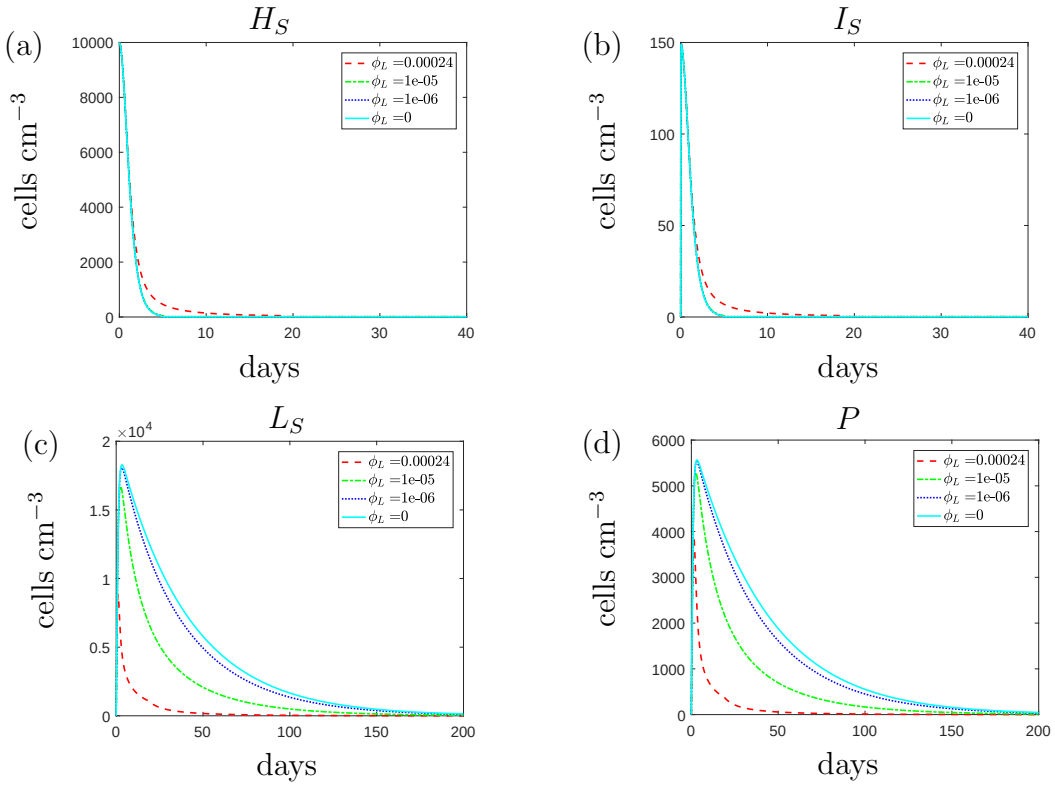

Figure 4.16: The variable solutions to the system (4.12)-(4.19), with initial conditions (4.21), default parameter values shown in Table 4.2 and varying the spherical cell phagocytosis rate, ϕ_L, from the default value of $2.4 \times 10^{-4}\,(\text{cells}\,\text{cm}^{-3})^{-1}\,\text{day}^{-1}$.

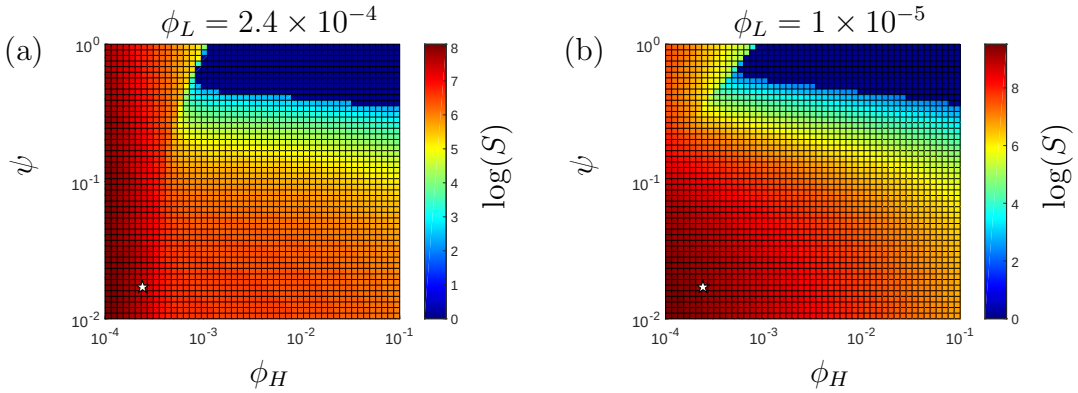

Figure 4.17: The population levels of total susceptible bacteria after 14 days for varying values of the rod-shaped cell phagocytosis rate, ϕ_H, and spherical cell death rate, ψ. Increasing these parameters from their default values (marked with a star) simulates the effects of an antivirulence drug and antimicrobial peptide treatment respectively. We have assumed that the spherical cell phagocytosis rate is (a) equal to the rod-shaped phagocytosis rate, (b) slower than the default rod-shaped phagocytosis rate (1×10^{-5}).

higher spherical cell population that occurs as we decrease the spherical cell phagocytosis rate; this indicates that a longer treatment period may be necessary if the spherical cell phagocytosis rate is lower than the default value.

4.5.2 Antibiotic-resistant infection

If the immunogenic properties are the same for all bacterial subpopulations then the model predicts that a partially antibiotic-resistant infection would be untreatable using antibiotics alone (see Figure 4.5). Figure 4.18 displays the model solutions if we vary the phagocytosis rate of the spherical cells, ϕ_L, assuming that $\phi_L < \phi_H$. The results suggest similar findings to the susceptible strain; as the spherical cell phagocytosis rate decreases from the default value, the spherical population increases and initiates a stronger immune response. If the bacterial infection is susceptible to the antibiotic then the increase in phagocytes results in faster clearance of the rod-shaped population. However, in the case of an antibiotic-resistant infection, the increase in phagocytes could kill off the rod-shaped population that would otherwise survive if the immunogenic properties were identical for all cell types. Therefore, we predict that a resistant strain infection could become treatable

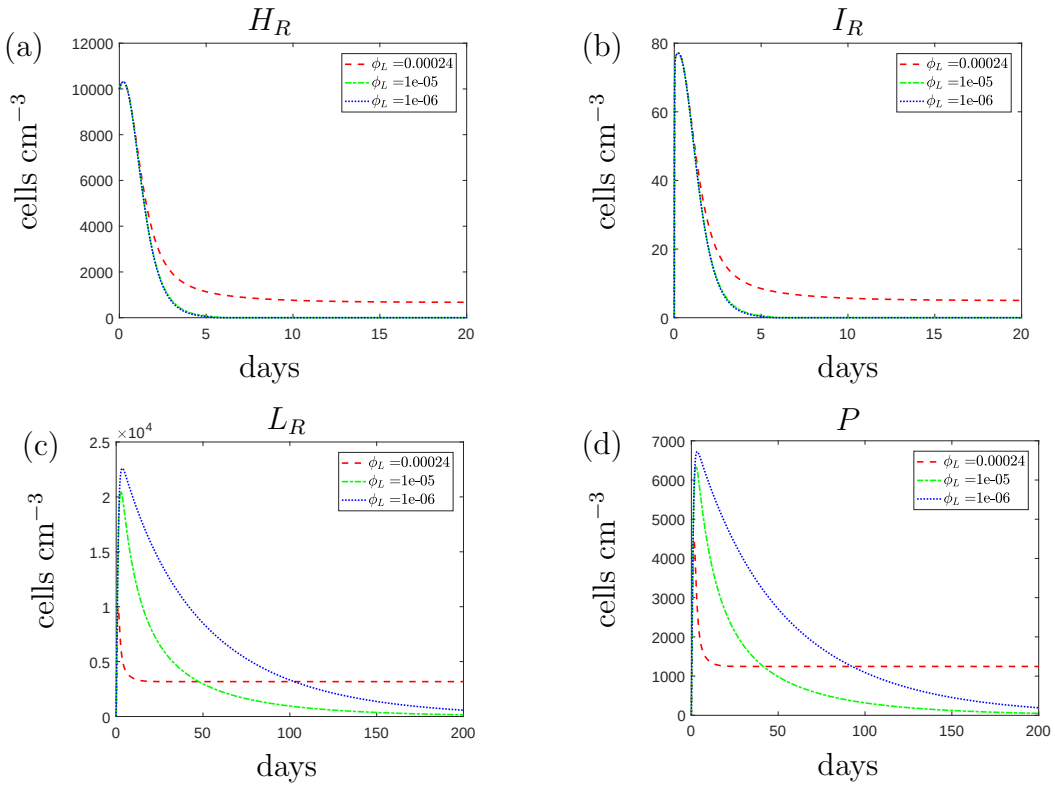

Figure 4.18: The variable solutions to the system (4.12)-(4.19), with initial conditions (4.22), default parameter values shown in Table 4.2 and varying the spherical cell phagocytosis rate, ϕ_L, from the default value of $2.4 \times 10^{-4}\,(\text{cells}\,\text{cm}^{-3})^{-1}\,\text{day}^{-1}$.

with antibiotics if the spherical cell phagocytosis rate is slower than the rod-shaped cells.

The results in Figure 4.18 are counter-intuitive and it is only through consideration of the immune response that we are able to obtain these predictions. The results suggest that it may not be beneficial for the resistant bacteria to activate the morphological transition at a site of infection if the spherical cells are phagocytosed slower than the rod-shaped cells. If the resistant population suffers as a result of transitioning to the spherical form then it is possible that they may not utilize this mechanism; we will consider this in the discussion section of this chapter.

If the model solutions do convey the true behaviour of a resistant only population then antibiotics alone could be sufficient to clear the infection if the spherical cells are phagocytosed slower than the rod-shaped cells. However, we continue to explore combined treatments with the view to cut down the lengthy treatment time needed to clear the

spherical population.

If we assume that the immunogenic properties between cell types are identical then our previous results suggested that the use of AMPs in conjunction with the antibiotic would not change the steady state value of the resistant population compared to the antibiotic-only treatment strategy (see Figure 4.9). If we assume that the spherical cell phagocytosis rate is lower than that for rods and simulate the use of AMPs along with the antibiotic we obtain the results in Figure 4.19. The AMPs initially cause a decrease in spherical cells and therefore there are fewer phagocytes recruited than when the antibiotic was added alone. Consequently, the rod-shaped population is not overwhelmed by the immune response and the population survives treatment. These results suggest that AMPs could provide a more favourable environment for the rod-shaped population and prove detrimental to treatment success.

If we simulate the use of an antivirulence drug alongside the antibiotic to treat a resistant infection with a low spherical cell phagocytosis rate then we predict identical results to those obtained for the susceptible infection when assuming identical immunogenic properties between bacterial phenotypes (see Figure 4.12). If we add an antivirulence drug then we decrease the time it takes to clear the rod-shaped population using the antibiotic alone. Consequently, the spherical populations enter a slow death phase and the time until total clearance marginally decreases as the effectiveness of the antivirulence drug increases.

To decrease the treatment duration we can investigate the administration of a triple drug combination. We find that the region of parameter pairings needed to clear the infection within 14 days are similar for both cases: when immunogenic properties are identical and when the phagocytosis rates of the cell types are different (see Figure 4.14 (b)).

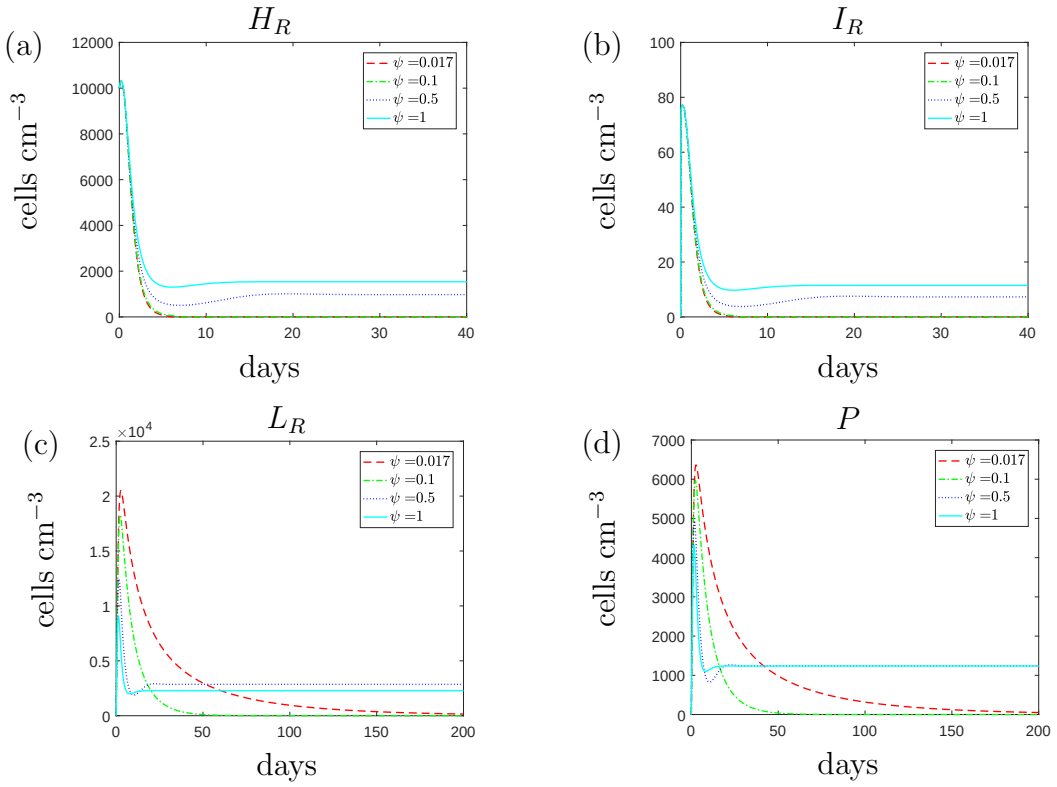

Figure 4.19: The variable solutions to the system (4.12)-(4.19), with initial conditions (4.21), default parameter values shown in Table 4.2, with $\phi_L = 1 \times 10^{-5}$ (cells cm^{-3})$^{-1}$ day^{-1} and varying the spherical cell death rate, ψ, from the default value of 1.7×10^{-2} day^{-1}. The rate of spherical cell phagocytosis, ϕ_L, is slower than the default rate as we are investigating the possiblity that spherical cells are less susceptible to phagocytosis than rod-shaped cells. An increase in ψ represents the addition of antimicrobial peptides.

4.5.3 Mixed strain

We now consider a mixed strain infection and assume that the spherical cells are phagocytosed slower than the rod-shaped cells. If we vary the phagocytosis rate for the spherical cells in a mixed strain infection then we obtain the results in Figure 4.20. For both strains, the results indicate similar findings to those obtained when considering single strain populations. As we decrease the spherical cell phagocytosis rate we predict a larger spherical population that comprises mostly antibiotic-susceptible spherical cells. The increased spherical population initiates a stronger immune response and subsequently the rod-shaped subpopulations die out faster as we decrease the spherical cell phagocytosis rate from the default value. Eventually the susceptible population is cleared after continued antibiotic usage. As previously witnessed in Figure 4.18, the rapid morphological transition could potentially suppress the emergence of resistance by boosting the phagocyte population. Whilst having a lower phagocytosis rate could be favourable for the spherical populations initially, it may be unfavourable for the other bacterial subpopulations. This result could potentially suggest an opportunity to exploit this natural suppression. However, we still estimate a lengthy treatment period and conclude that a successful treatment would need to clear the spherical populations to prevent either strain recovering after the treatment is stopped.

If we simulate the use of AMPs along with the antibiotic, we obtain the results in Figure 4.21. The effects of the AMPs cause a decrease in susceptible spherical cells and therefore there are fewer phagocytes recruited. When only antibiotics are used, the large phagocyte population (recruited due to the large susceptible spherical population) showed potential to delay the emergence of the resistant population. By adding AMPs we are providing a more favourable environment for the resistant strain and we see the resistant rod-shaped cell population flourish for sufficiently large ψ. The increase in spherical cell death should negatively impact both of the spherical populations but the rod-shaped resistant population becomes so large that the AMPS do not prevent growth of the resistant population. Our predictions indicate that in the case of a multi-strain

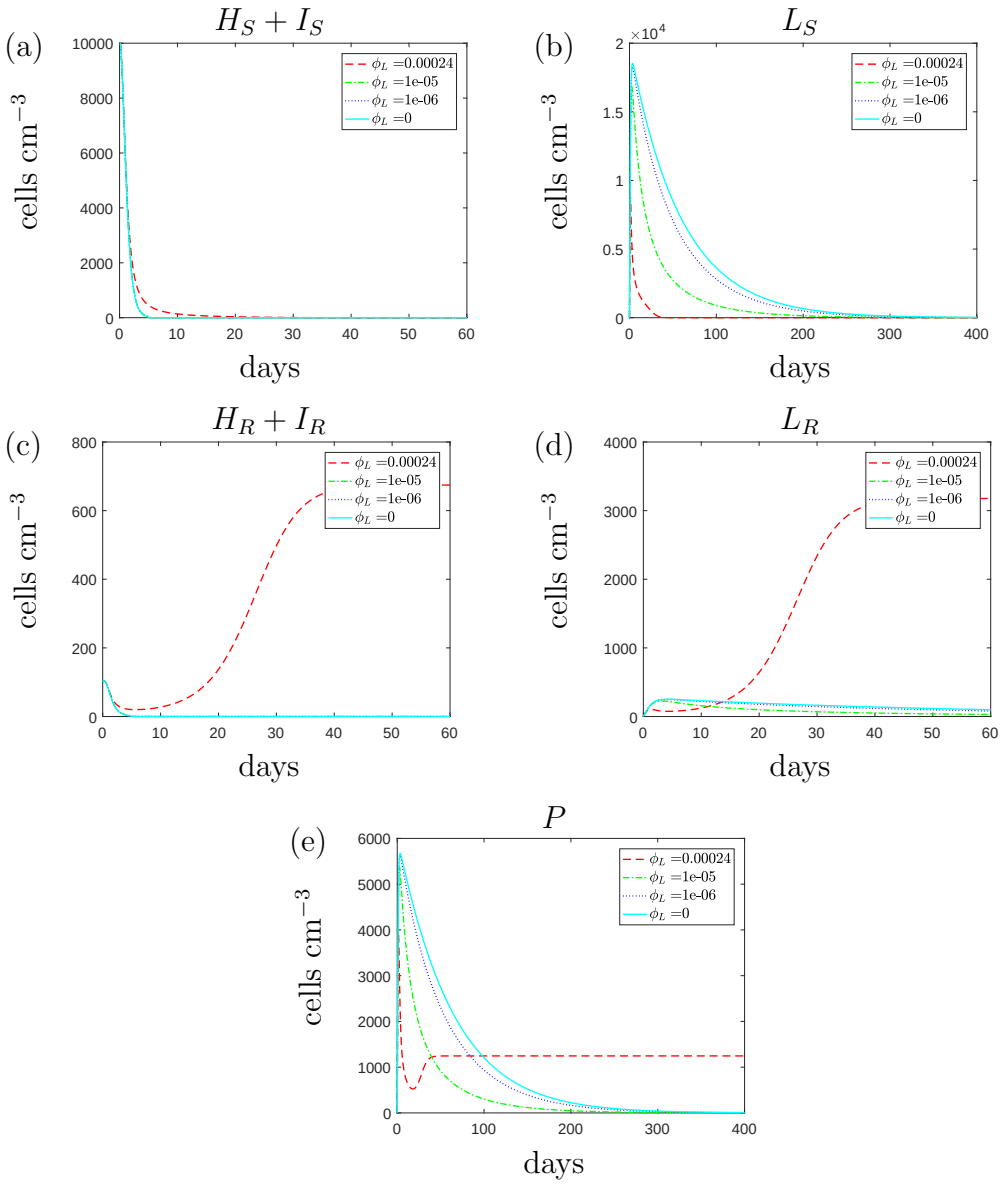

Figure 4.20: The variable solutions to the system (4.12)-(4.19), with initial conditions (4.23), default parameter values shown in Table 4.2 and varying the spherical cell phagocytosis rate, ϕ_L, from the default value of $2.4 \times 10^{-4}\,(\text{cells}\,\text{cm}^{-3})^{-1}\,\text{day}^{-1}$.

infection with a spherical population that is less susceptible to phagocytosis, the use of AMPs could be detrimental and would not pose a suitable treatment in combination with antibiotics.

Instead of considering a combination therapy of antibiotics and AMPs, we consider the combined use of an antivirulence drug with the antibiotic in order to clear the mixed infection faster. Simulating the use of this drug combination indicates the results shown

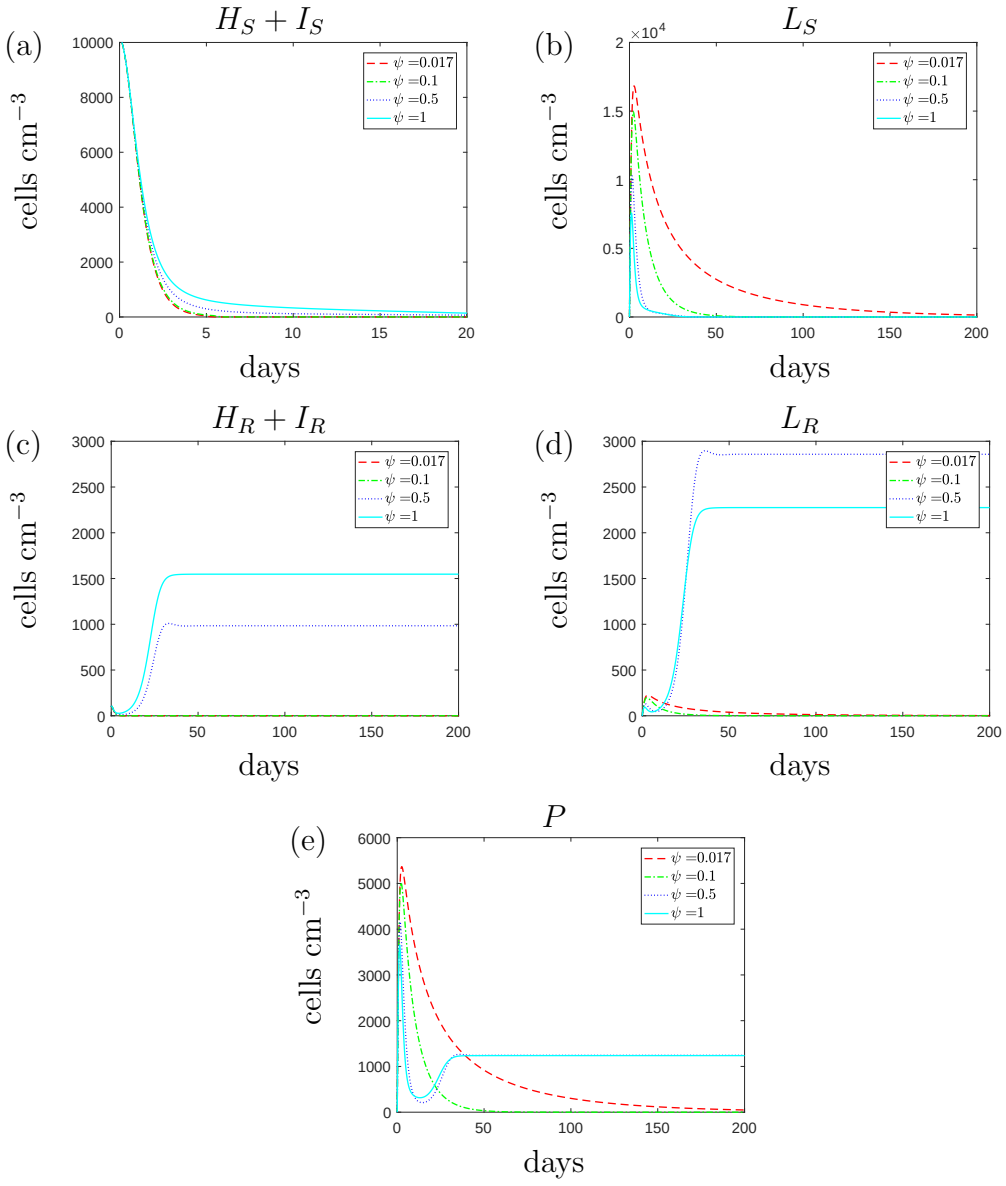

Figure 4.21: The variable solutions to the system (4.12)-(4.19), with initial conditions (4.23), default parameter values shown in Table 4.2, with $\phi_L = 1 \times 10^{-5}$ (cells cm^{-3})$^{-1}$ day^{-1} and varying the spherical cell death rate, ψ, from the default value of 1.7×10^{-2} day^{-1} to mimic the addition of AMPs. The rate of spherical cell phagocytosis, ϕ_L, is slower than the default rate as we are investigating the possiblity that spherical cells are less susceptible to phagocytosis than rod-shaped cells.

in Figure 4.22. If we increase the rod-shaped cell phagocytosis rate, ϕ_H, then both the susceptible and resistant rod-shaped cell populations are cleared faster. Subsequently, as we increase the rod-shaped cell phagocytosis rate, fewer spherical cells form. The length of treatment required to fully clear the infection (i.e. rods and spheres) is not substantially decreased as a result of adding the antivirulence drug. However, the antivirulence drug shows potential to further exploit the suppression of the resistant population, caused by the effects of the transition-inducing antibiotic, and decrease the time required to clear the rod-shaped cells, which may have increased virulence to the spherical cells.

If we simulate a triple combination therapy we can infer that as long as the additional drugs are effective enough to clear the susceptible population then they will also clear the resistant population (see Figure 4.23). If we compare Figure 4.23 (b) to Figure 4.14 (a) (where the immunogenic properties are assumed equal), we find that the resistant population becomes more susceptible to the antivirulence drug if the phagocytosis rate is slower for the spherical population.

4.6 Recruitment rate

As the outer membrane may still be intact in the spherical cells, it could be more reasonable to assume that shedding the cell wall is more likely to affect the recruitment rate. PAMPs are often found in the peptidoglycan layer of the cell membrane and the outer membrane and therefore it is very likely that the spherical cells will have fewer PAMPs and be less immune stimulatory.

4.6.1 Antibiotic-susceptible infection

If we decrease the recruitment rate of the spherical cells, κ_L, in an antibiotic-susceptible strain, we obtain the results in Figure 4.24. In the initial stages of treatment, the lower recruitment rate of the spherical cells causes fewer phagocytes to be recruited by the infection. As a result of the smaller phagocyte population, all bacterial subpopulations

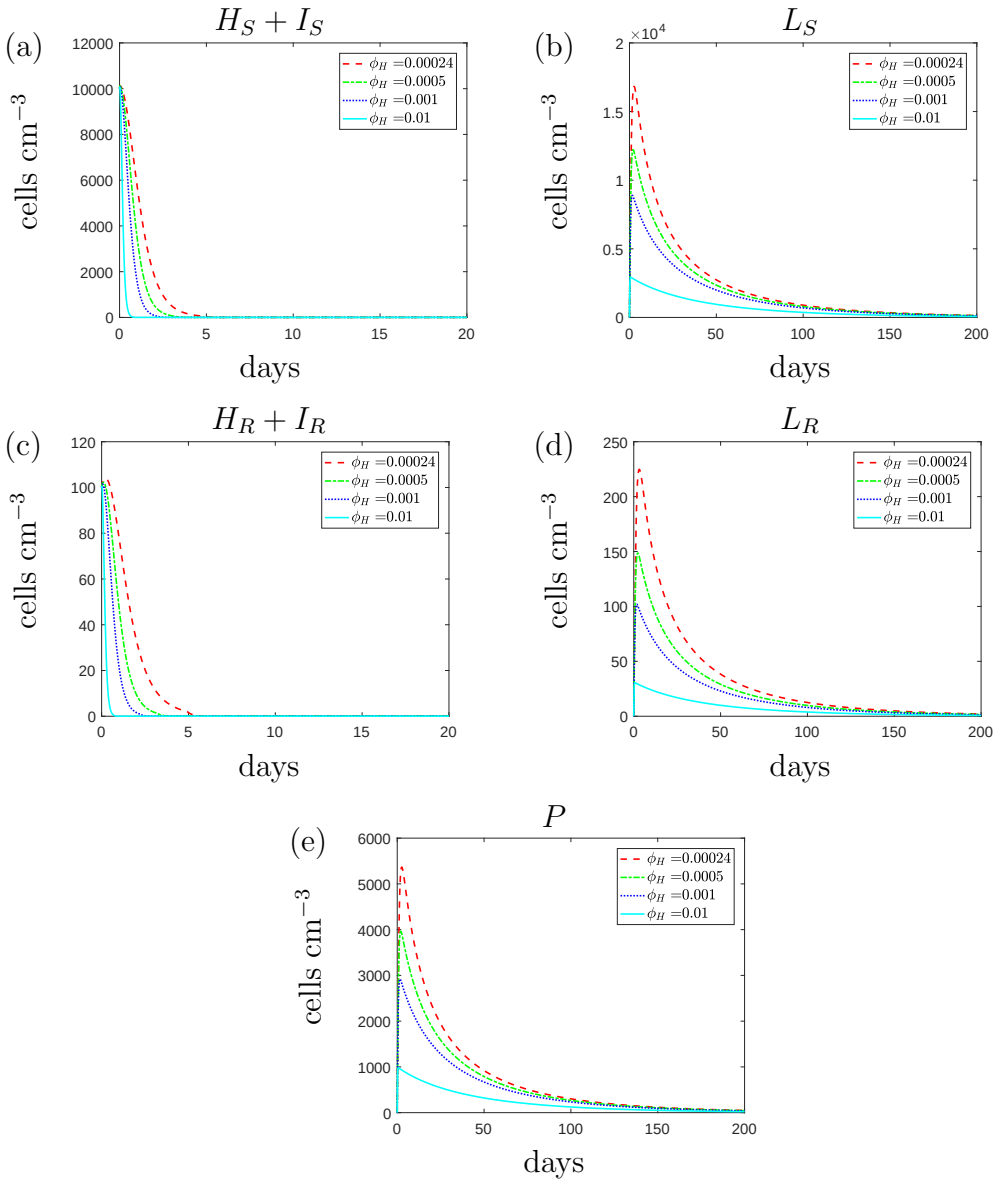

Figure 4.22: The variable solutions to the system (4.12)-(4.19), with initial conditions (4.23), default parameter values shown in Table 4.2, with $\phi_L = 1 \times 10^{-5}$ (cells cm^{-3})$^{-1}$ day^{-1} and varying the rod-shaped cell phagocytosis rate, ϕ_H, from the default value of 2.4×10^{-4} (cells cm^{-3})$^{-1}$ day^{-1}. The rate of spherical cell phagocytosis, ϕ_L, is slower than the default rate as we are investigating the possiblity that spherical cells are less susceptible to phagocytosis than rod-shaped cells. An increase in ϕ_H represents the addition of an antivirulence drug that increases susceptibility of the rod-shaped bacteria to host defences.

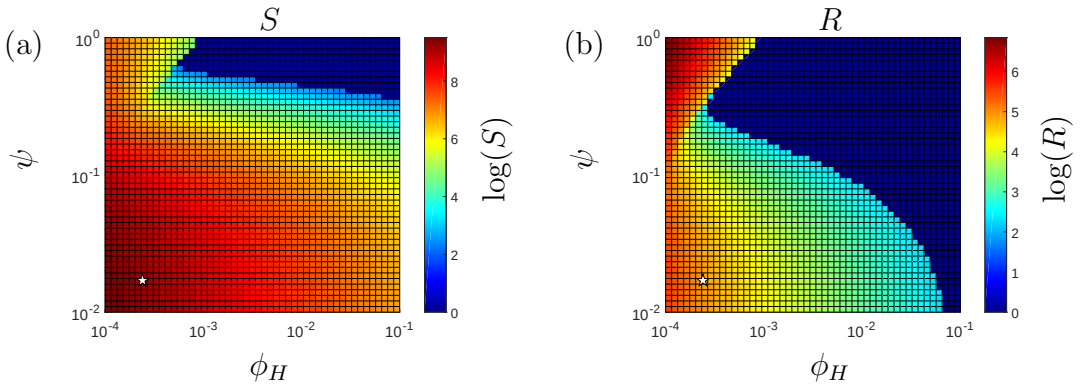

Figure 4.23: The population levels of (a) susceptible bacteria and (b) resistant bacteria after 14 days for varying values of the rod-shaped cell phagocytosis rate, ϕ_H, and spherical cell death rate, ψ. Increasing these parameters from their default values (marked with a star) simulates the effects of an antivirulence drug and antimicrobial peptide treatment respectively. We have assumed that the spherical cell phagocytosis rate is slower than the rod-shaped phagocytosis rate (1×10^{-5}). The total population of susceptible, S, and resistant bacteria, R, is calculated such that $S = H_S + I_S + L_S$ and $R = H_R + I_R + L_R$ respectively.

increase as the recruitment rate of the spherical cells decrease. If the spherical cell recruitment rate decreases to $\kappa_L = 1 \times 10^{-3}$ day^{-1} then we could expect the qualitative result of the treatment to change as the antibiotic treatment fails to clear the infection.

For Figures 4.25-4.27 we assume that the phagocyte recruitment rate of the spherical cells is $\phi_L = 1 \times 10^{-3}$ (cells cm^{-3})$^{-1}$ day^{-1}, since using this value we have predicted that the antibiotic treatment would become ineffective in clearing the antibiotic-susceptible infection alone. We investigate whether we can clear the infection using a combination therapy of antibiotic with AMPs or an antivirulence drug. We simulate the AMPs by varying the spherical cell death rate, ψ, and obtain the results in Figure 4.25. The results suggest that the addition of AMPs could lead to fewer spherical cells. However, as the AMPs only target the spherical cells and the spherical cells have a low phagocyte recruitment rate, we find that the remaining subpopulations are unaffected by the addition of AMPs. Adding AMPs could potentially help clear the infection but we predict that this could take over 200 days of constant therapy and hence we conclude that this would not be a suitable treatment strategy.

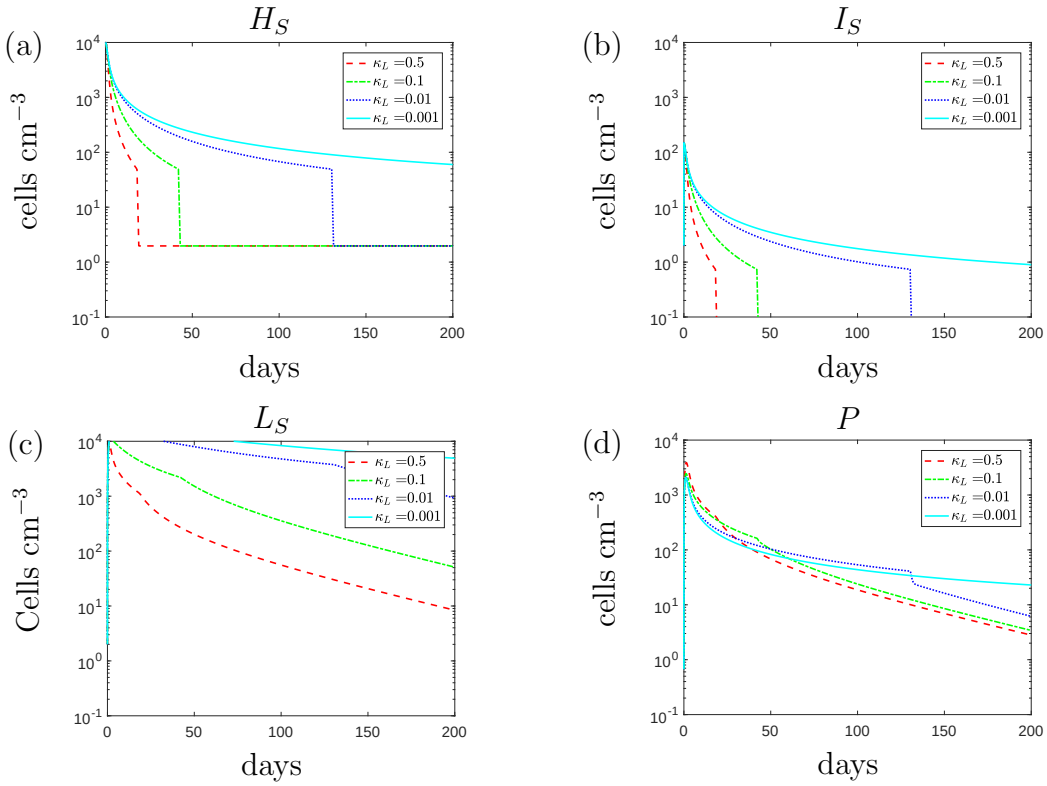

Figure 4.24: The variable solutions to the system (4.12)-(4.19), with initial conditions (4.21), default parameter values shown in Table 4.2 and varying the spherical cell phagocyte recruitment rate, κ_L, from the default value of 0.5 day^{-1}.

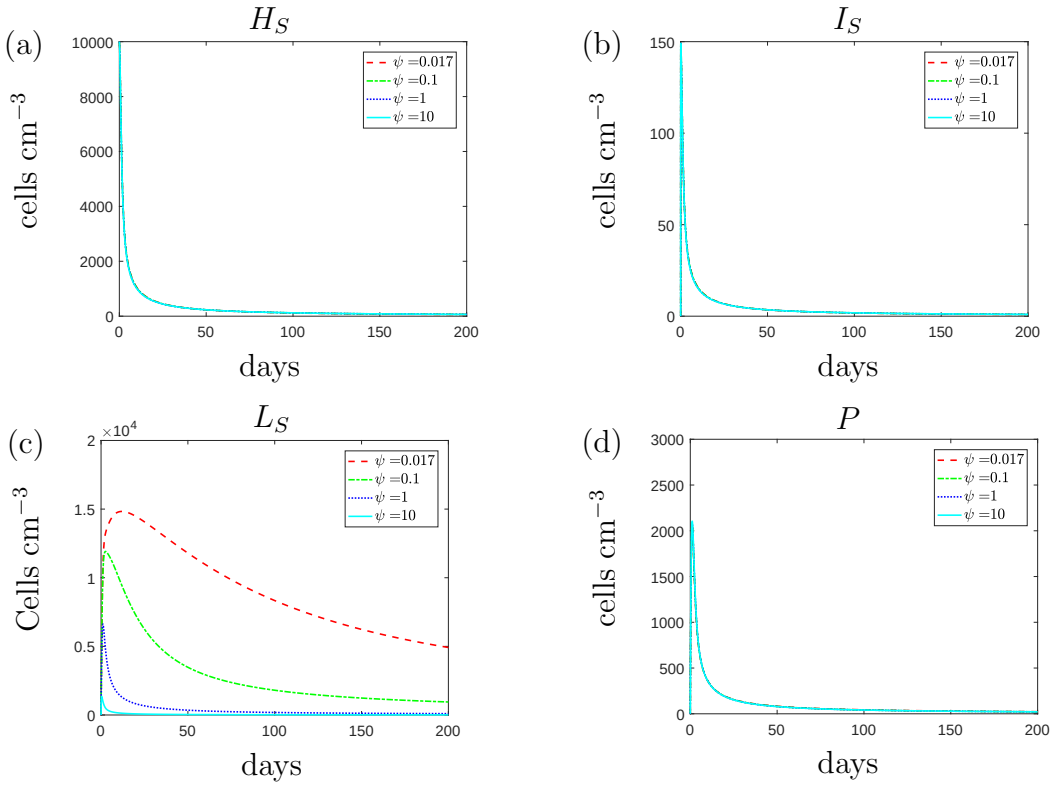

Figure 4.25: The variable solutions to the system (4.12)-(4.19), with initial conditions (4.21), default parameter values shown in Table 4.2, with $\kappa_L = 1 \times 10^{-3}$ day^{-1} and increasing the spherical cell death rate, ψ, from the default value of 1.7×10^{-2} day^{-1} to mimic the use of antimicrobial peptides. The rate of phagocyte recruitment by spherical cells, κ_L, is slower than the default rate as we are investigating the possiblity that spherical cells are less immune-stimulatory than rod-shaped bacteria.

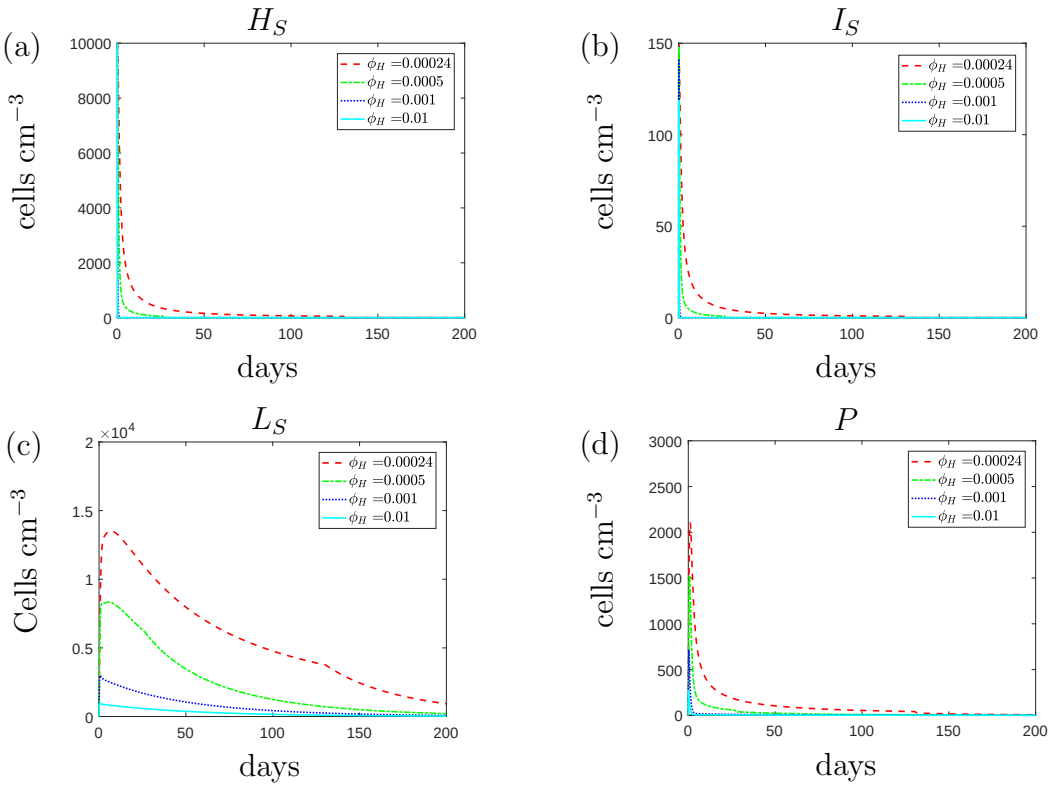

Figure 4.26: The variable solutions to the system (4.12)-(4.19), with initial conditions (4.21), default parameter values shown in Table 4.2, with $\kappa_L = 1 \times 10^{-3}$ day^{-1} and varying the rod-shaped cell phagocytosis rate, ϕ_H, from the default value of $2.4 \times 10^{-4}\,(\text{cells}\,\text{cm}^{-3})^{-1}\,\text{day}^{-1}$. An increase in ϕ_H represents the addition of an antivirulence drug that increases the susceptibility of the rod-shaped bacteria to host defences. The rate of phagocyte recruitment by spherical cells, κ_L, is slower than the default rate as we are investigating the possiblity that spherical cells are less immune-stimulatory than rod-shaped cells.

Similarly, we investigate the effects of an antibiotic-antivirulence drug pairing. Figure 4.26 suggests that a combined dose of antibiotics and antivirulence drug could be successful in clearing the infection, if the antivirulence drug was sufficiently effective. The antivirulence drug enables the phagocytes to limit bacterial growth and this prevents as many rod-shaped bacteria from transitioning to the spherical form. However, neither the antibiotic nor the antivirulence treatment directly affects the fitness of the spherical cells so we predict a slow death phase.

If we investigate a triple treatment combination we get the results in Figure 4.27. The results indicate that a combination therapy of all three drugs could clear the infection in

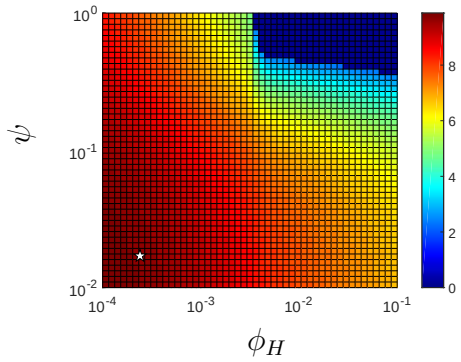

Figure 4.27: The population levels of susceptible bacteria after 14 days for varying values of the rod-shaped cell phagocytosis rate, ϕ_H, and spherical cell death rate, ψ. Increasing these parameters from their default values (marked with a star) simulates the effects of an antivirulence drug and antimicrobial peptide treatment respectively. We have assumed that the spherical cell recruitment rate (1×10^{-3}) is slower than the rod-shaped cell phagocytosis rate.

as little as 14 days if the drugs are sufficiently effective. We note that a higher level of efficacy is needed for the antivirulence drug in comparison to the results in Figure 4.17, where we have assumed that the phagocytosis rate is slower for the spherical cells but immune cells are recruited at the same rate to all types of cell. If the immune system is not as responsive to the spherical population then it is still possible to clear the infection if we boost the ability of the immune cells to kill the rod-shaped bacteria.

4.6.2 Antibiotic-resistant infection

Using the model we find that the consequences of the spherical cells having a lower phagocyte recruitment rate than the rod-shaped cells causes identical changes in both the antibiotic-susceptible and -resistant infections. For brevity we do not include the corresponding simulations but instead provide a short overview of the results.

A decrease in the spherical cell recruitment rate from its default value could result in higher populations for all types of bacteria. A combined dose of antibiotic and AMPs would only influence the spherical cell subpopulation and hence the treatment would remain unsuccessful. An alternative treatment of an antivirulence drug and the antibiotic

could help decrease all subpopulations and the results are akin to those obtained through simulating the same treatment on a resistant infection with identical immunogenic properties (Figure 4.13).

4.6.3 Mixed strain

We have shown that if the population consists of a single strain and the phagocyte recruitment rate of the spherical cells is slower than that of the rod-shaped cells then we could expect a more threatening infection that could evade antibiotic effects. If we consider the recruitment rate of the spherical cells and suppose that the population consists of both strains then we obtain the predictions in Figure 4.28. In a mixed strain infection, the model predicts similar dynamics to the single strain up to around day 20; all susceptible subpopulations grow to higher levels as we decrease spherical cell recruitment. Due to the lower recruitment rate, we initially predict a weaker immune response and as a result we see faster growth of the resistant population. However, as the resistant population grows, the immune response increases in response to the higher resistant rod-shaped cell population. Consequently, the antibiotic and increased immune response can clear the susceptible population that previously persisted in the single strain simulations. This predicted behaviour suggests that if recruitment is lower for the spherical cells then we could expect the presence of a resistant strain to impact the survival of the susceptible strain negatively whilst promoting the growth of the resistant strain.

If we simulate the combination of AMPs and antibiotics then we obtain the predictions in Figure 4.29. As expected, the AMPs are successful in clearing the spherical cells, however, they do not affect the rod-shaped cell populations and therefore we could still expect a dominant resistant population to emerge. The results indicate that an additional drug is necessary if we wish to clear the resistant population.

If we consider the use of an antivirulence drug in combination with the antibiotics then we obtain results similar to the single strain results. We predict that the antivirulence drug would lower the rod-shaped cell populations and consequently we also predict fewer

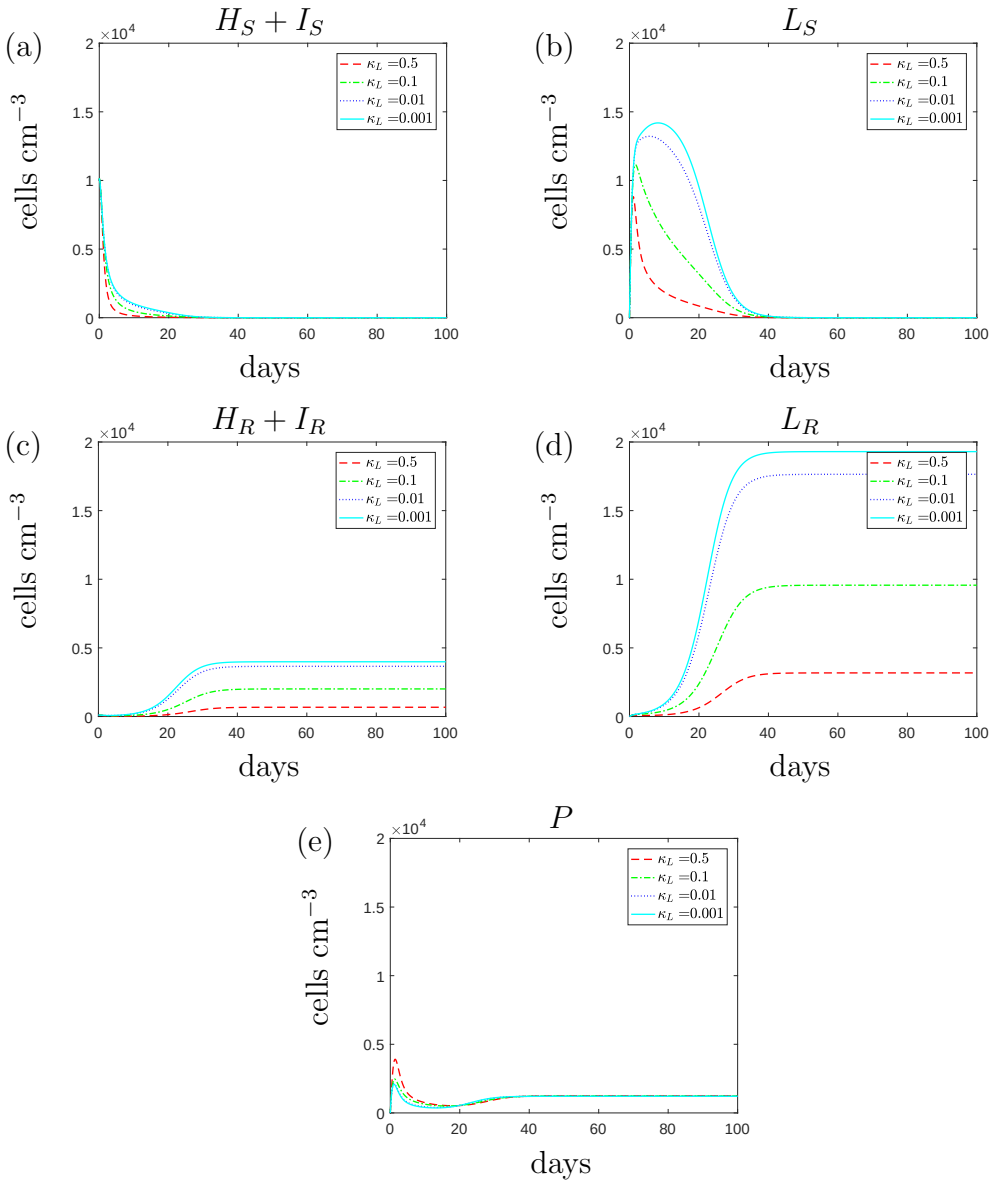

Figure 4.28: The variable solutions to the system (4.12)-(4.19), with initial conditions (4.23), default parameter values shown in Table 4.2 and varying the spherical cell phagocyte recruitment rate, κ_L, from the default value of $0.5\,\text{day}^{-1}$.

spherical cells. The spherical population takes some time to clear but it is possible to completely clear the infection eventually (results omitted). Finally, Figure 4.30 indicates that it is possible to clear the mixed strain infection within 14 days if the spherical cells recruit phagocytes at a slower rate than the rod-shaped cells. Following from our previous results we conclude that this would only be possible using both a triple combination of the antibiotic, AMPs and antivirulence drug.

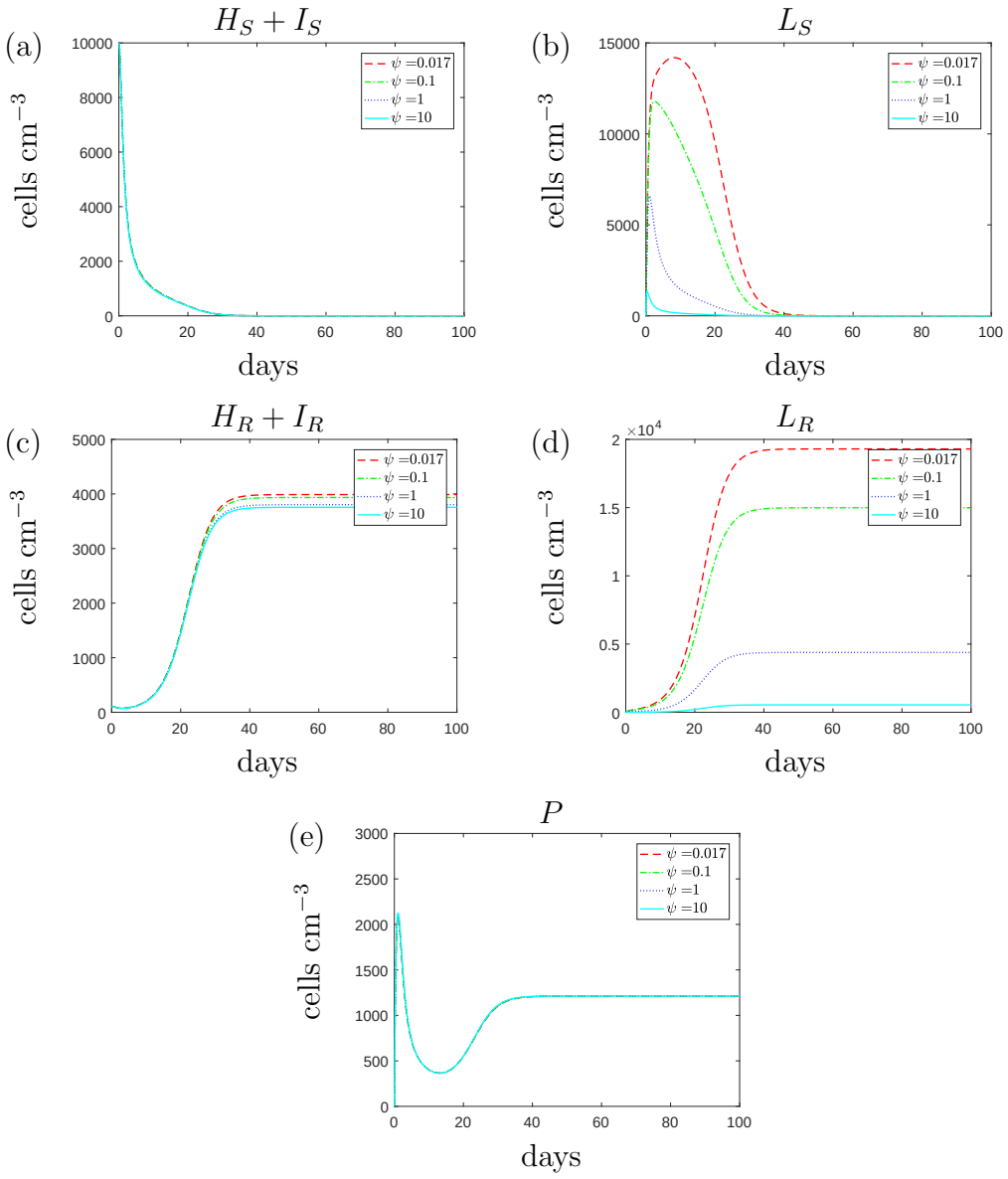

Figure 4.29: The variable solutions to the system (4.12)-(4.19), with initial conditions (4.23), default parameter values shown in Table 4.2, with $\kappa_L = 1 \times 10^{-3}$ day^{-1} and increasing the spherical cell death rate, ψ, from the default value of 1.7×10^{-2} day^{-1} to mimic the addition of antimicrobial peptides. The rate of phagocyte recruitment by spherical cells, κ_L, is slower than the default rate as we are investigating the possiblity that spherical cells are less immune-stimulatory than rod-shaped cells.

4.7 Discussion

Following from Model II, we have formulated a model that describes the growth dynamics of a multi-strain population of *P. aeruginosa* at the site of infection with the inclusion of a morphological transition, immune response and multiple treatment combinations.

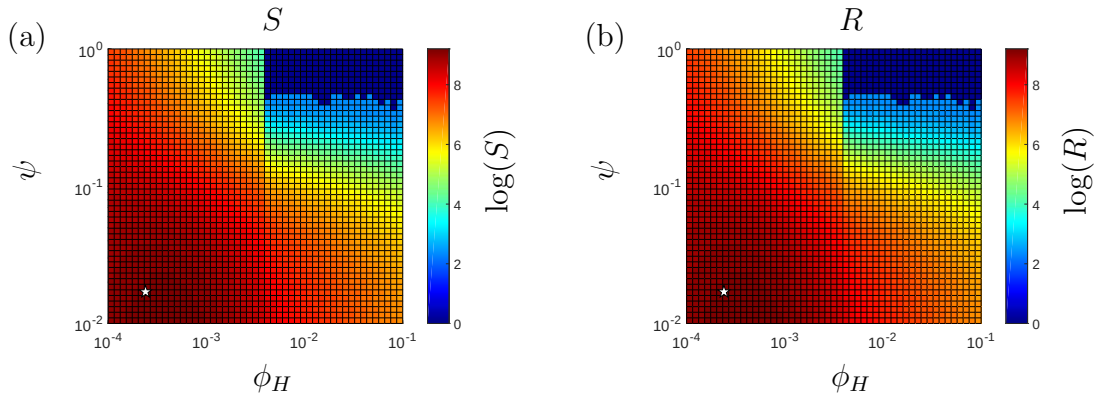

Figure 4.30: The population levels of (a) susceptible bacteria and (b) resistant bacteria after 14 days for varying values of the rod-shaped cell phagocytosis rate, ϕ_H, and spherical cell death rate, ψ. Increasing these parameters from their default values (marked with a star) simulates the effects of an antivirulence drug and antimicrobial peptide treatment respectively on the single strain infections. The total population of susceptible, S, and resistant bacteria, R, is calculated such that $S = H_S + I_S + L_S$ and $R = H_R + I_R + L_R$ respectively.

We summarise our results for all treatment combinations and all explored immunogenic characteristic settings in Table 4.3.

If we assume that the immunogenic properties are identical between cell types then the results suggest that antibiotic treatment could clear a *P. aeruginosa* infection only if it was purely susceptible to the antibiotic. In Chapter 3 we predicted that a continuous dose of antibiotic would not clear an infection and after including an immune response within the model we see that treatment success is now predicted. This result supports the conclusions in [7] and emphasises the importance of including the immune response when considering persistent populations as host defences may help determine the treatment outcome. If a resistant strain is present then we predict that the antibiotic treatment would fail, as expected.

After considering an antivirulence drug we conclude that it could be used as a single treatment and clear all infections if the drug is sufficiently potent. Whilst this conclusion strongly supports the use of antivirulence drugs we would require further experimental evidence to hint towards feasible levels of efficacy. As with any antivirulence strategy, the selective pressure placed on the population by the antivirulence drug would need to be

Table 4.3: A review of the results for treatments considered in Chapter 4. A single tick, ✔, indicates that treatment success is possible but the duration required is clinically infeasible. A double tick, ✔✔, infers that treatment success is possible in a clinically feasible time frame. A cross, ✘, indicates that treatment is not possible and if followed by (R) then the remaining infection is resistant to antibiotics. We highlight the effects of using an antivirulence treatment alone with a ✻ to note that bacterial clearance is possible but will depend on the effectiveness of the antivirulence drug. For the drug combinations we have assumed that the level of antivirulence efficacy is below the level needed to clear the infection in a feasible time frame.

		Single drug		Combined drugs		
		AB	AV	AB + AMP	AB + AV	AB + AV + AMP
$\phi_H = \phi_L$ $\kappa_H = \kappa_L$	Susceptible strain	✔	✔✔✻	✔	✔	✔✔
	Resistant strain	✘(R)	✔✔✻	✘(R)	✔	✔✔
	Mixed strain	✘(R)	✔✔✻	✘(R)	✔	✔✔
$\phi_H > \phi_L$	Susceptible strain	✔	✔✔✻	✔	✔	✔✔
	Resistant strain	✔	✔✔✻	✘(R)	✔	✔✔
	Mixed strain	✔	✔✔✻	✘(R)	✔	✔✔
$\kappa_H > \kappa_L$	Susceptible strain	✘	✔✔✻	✔	✔	✔✔
	Resistant strain	✘(R)	✔✔✻	✔	✔	✔✔
	Mixed strain	✘(R)	✔✔✻	✘(R)	✔	✔✔

analysed in order to anticipate resistance developing to the drug.

Our investigation into the effects of the different immunogenic cell properties has been extensive but not exhaustive. We also undertook preliminary investigations into the case where both of the immune-related rates are lower for the spherical cells (not included here). Whilst this is a plausible and likely scenario, we find that many of the results we obtained under this assumption were congruent with the results obtained in Sections 4.5 and 4.6 combined. Using the results in these sections we are able to make suitable predictions regarding bacterial growth and treatment success if both the spherical cell phagocytosis rate and phagocyte recruitment rate were both lower than the rod-shaped cells rates. Considering both of the immunogenic properties simultaneously requires the evaluation of a vast parameter space and hence predictions could be inconclusive; further investigation would benefit from experimental evidence that could hint towards suitable parameter values.

The varied results in Table 4.3 indicate that the immunogenic properties of the spherical population could affect the survival of an infection and change the treatment outcome. If we examine the predictions for bacterial growth during a single antibiotic treatment and vary the immunogenic properties then we recognise two interesting scenarios. Firstly, we predicted that the susceptible population could become untreatable with antibiotics alone if the recruitment rate was slower for the spherical cells but subsequent results showed that in this case we could apply additional treatments to increase the likelihood of treatment success.

Secondly, we found that a resistant infection could become treatable with antibiotics alone if the phagocytosis rate of the spherical cells is lower than the rod-shaped cells. The rapid transition of many of the resistant bacteria causes a large influx of phagocytes that enable total bacterial clearance. This compelling result seems counter-intuitive and leads us to question whether the resistant bacteria would utilise the morphological transition if it was detrimental to the overall population. It is likely that the resistant bacteria would adapt and remain as bacillary cells if the selective pressures of the immune response caused

by the antibiotic-induced morphological transition negatively impacted bacterial fitness. However, it is unclear whether the increased immune response explicitly causes a decrease in individual bacterial fitness. The morphological transition permits a bacterium to evade antibiotic effects, thus increasing its individual bacterial fitness. It could be argued that the increase in immune cells, caused by the large spherical population, damages the total bacterial population but not individual cell fitness.

If the resistant bacteria were to adapt and remain as bacillary cells in order to limit the immune response then they could once again become untreatable by antibiotics alone. If they do not transition to the spherical form then we would not consider the use of AMPs but we may still consider the use of an antivirulence drug in combination with the antibiotic; the success of this treatment would depend on the effectiveness of the antivirulence drug (see Figure 4.13).

Our results suggest that a susceptible strain could be cleared using antibiotic alone but our results suggest that a lengthy treatment period would be necessary. After considering the dual treatment combinations we can formulate conclusions about the clinical potential for both AMPs and the antivirulence drug. In Chapter 2 we produced results that strongly supported the combined use of meropenem and AMPs to clear an antibiotic-susceptible bacterial population *in vitro* when growing in isolation with the treatment. Whilst we do not have experimental data to indicate the analogous result for a resistant strain, it is feasible that a resistant population could also be cleared with the antibiotic and AMPs in isolation. However, after including host defences and a combination of strains we find that the results do not strongly support the use of AMPs when used as part of a combined continuous therapeutic strategy. Our results suggest that the success of a combined treatment of an antibiotic and AMPs would depend on the effectiveness of the AMPs and the composition of the infection. For an antibiotic-susceptible infection with identical immunogenic properties, the combination of antibiotics and AMPs could decrease the treatment time needed to clear the infection by half compared to an antibiotic treatment alone if the AMPs could increase the spherical cell death 5-fold. However, a

treatment time of 100 days is still significant and could be threatening to the patients health. If the AMPs are too potent or if the phagocytosis rate of the spherical cells is slower than the corresponding rate for the rod-shaped population then we find that AMPs may only alter the composition of the population and have little impact on the treatment time. Similarly, we predict that the use of AMPs in conjunction with the antibiotic merely alters the composition of the resistant population and has no effect on bacterial load or on the treatment time.

We see that in the case of the spherical cells having a low phagocyte recruitment rate, the failed antibiotic-only treatment becomes successful if we add AMPs for both the susceptible and resistant populations. What we observe as a success for the AMPs is soon discounted as we remind ourselves that the predicted treatment period needed for clearance was extensive and not clinically feasible. Furthermore, as formerly mentioned, the effect of varying phagocytosis rates on the resistant population is unclear and we would need to know how resistant bacteria would adapt in response to immunogenic characteristics in order to know whether AMPs would be necessary or helpful. If the bacterial population is mixed and the phagocytosis rate of the spherical cells is low then it is possible that the use of AMPs could be detrimental and cause treatment failure. Overall, our results do not imply positive or conclusive hypotheses to support the use of AMPs as part of a combined treatment with antibiotic. Whilst our results do not condemn the use of AMPs they do emphasise the need for further investigation into their use. The results of the triple combination simulations unanimously support the potential of AMPs when used in a triple drug combination and we acknowledge the ability of the AMPs to clear the persistent spherical population. As with the antivirulence drug, we would need to obtain pharmacodynamic properties of AMPs for *P. aeruginosa* before convincing conclusions can be made regarding their use.

Throughout the results in this chapter, the antivirulence drug has shown potential as a single treatment, therapeutic aid of the antibiotic and as a component of the triple drug combination. However, in many cases we have observed long predicted treatment

times due to the spherical cell population that remains after the rod-shaped bacteria have been cleared by the antivirulence drug. If the antibiotic is withdrawn before this spherical population is cleared (via phagocytosis and cell lysis) then this could propose a hindrance to treatment success as we may expect the infection to regrow once the antibiotic is removed. We note that these predictions were obtained under the assumption that the antivirulence drug could only affect the rod-shaped cells. It is possible that the antivirulence drug could also increase the phagocytosis rates of the spherical cells. After further investigation, we can confirm that in all cases (single and mixed infections) the infection could be completely cleared within a week using the combined treatment of antibiotic and an antivirulence drug if the latter affected spherical cell and rod-shaped cell phagocytosis equally (results omitted). However, if experimental evidence suggested that the antivirulence drug only targeted the rod-shaped cells then we may still face long treatment periods unless it is possible to clear the spherical population faster. We propose that the need to reduce long treatment times could present an opportunity to use AMPs strategically in a more effective manner. If we can identify the time at which a combined dose of antibiotic and antivirulence drug clear the rod-shaped population, then it may be possible to predict a suitable time to add AMPs as part of a sequential drug strategy. The antibiotic and antivirulence drug could quickly remove the rod-shaped population and the AMPs could subsequently initiate rapid clearance of the remaining spherical cells and reduce the treatment time. We will consider this treatment strategy in the following chapter where we consider the impact of a persistent spherical population during the process of optimising antibiotic drug strategies.

CHAPTER 5

CONSIDERING THE MORPHOLOGICAL TRANSITION OF *P. AERUGINOSA* TO OPTIMISE ANTIBIOTIC USAGE

In the foregoing chapters we have formulated mathematical models of *P. aeruginosa* in order to consider how the morphological transition could impact bacterial growth when treated with meropenem. The majority of our results thus far have examined the growth of the population during a constant dose of antibiotic. Simulating a constant dose enables us to obtain the long term dynamics of the population more simply and in some cases has provided the opportunity for analytical analysis. Exploring the parameter space using a constant dose model has allowed us to investigate novel treatments and drug combinations. However, novel treatments may take years before becoming clinically available and combination strategies are not always financially feasible. It is crucial that we optimise the current use of available antibiotics in order to extend their life span.

Traditional treatment regimens usually consist of a fixed amount of antibiotic given at specific intervals. This type of treatment strategy offers practicability, due to the constant dose, but often lacks optimality and could help facilitate the spread of resistance. Mathematical modelling is increasingly being used to explore antibiotic dosing strategies and the effects of dosing on antibiotic resistance [17, 29, 39]. After formulating a mathematical model it is possible to simulate multiple doses of antibiotic by solving the model and adding antibiotic via a change in antibiotic concentration at prescribed time points.

Using this "manual" approach provides valuable insight into the effects of different dosing strategies. However, the antibiotic dose and duration is chosen by the person simulating the program and a disadvantage of this is that there is a limit to how many strategies can be explored.

Paterson et al. [86] explored a novel approach of using a genetic algorithm (GA) to search for optimal dosing strategies. In the study it was suggested that in user-controlled studies the person undertaking the investigation may only find "an *optimal* solution from a selection of sub-optimal treatments", due to the limits on how many dosing strategies can be explored. Using a GA makes it possible to explore a vast space of possible dosing strategies automatically in order to obtain the most optimal treatment regimen. In the study the authors analysed the effectiveness of traditional treatment regimens and compared them to the treatment regimes that were identified using the GA. A deterministic population dynamics model was formulated to describe the growth of a susceptible and a resistant strain of bacteria in isolation with an antibiotic treatment. Resistance was assumed to arise through HGT; as this process could result in small population densities a deterministic model may not always provide an accurate approximation. At low bacterial densities the randomness of biological processes can determine the survival of a population and therefore a stochastic framework was developed alongside the deterministic model to analyse bacterial growth during the dosing strategies. The stochastic model was used to obtain success rates, with confidence intervals, for each dosing strategy, in order to choose the most efficient. In addition to success rates, they also analysed the time taken to clear the infection and the amount of antibiotic in the system.

In [86], a traditional treatment regimen was initially investigate and simulated for 10 days. It was found that the antibiotic concentration fell between the MIC values for the susceptible and resistant bacteria for the first three days of treatment. Whilst the antibiotic concentration is within these two figures, the susceptible bacteria perish and leave the resistant bacteria in a favourable environment, thus facilitating their development. The GA then identified suitable treatment strategies that increased the success rate of

the treatment and decreased the treatment time. The optimal dosage vectors were found to exhibit the characteristics of a high dose followed by tapering lower doses. We will refer to this type of strategy as a high dose, tapered doses (HDTDs) strategy. The initially high dose causes the antibiotic concentration to quickly reach the MIC of the resistant bacteria and stop the initial facilitation of resistant bacteria that was found to occur in the traditional regimen. Additionally, the optimal treatment strategies often required a lower total amount of antibiotic over the course of the treatment compared to the traditional regimen. Overall, the GA found suitable treatments that were shorter, more effective and less toxic.

In this chapter we will explore optimal dosing strategies for *P. aeruginosa* by applying a similar methodology to that used in [86]. Instead of considering the emergence of resistance within a population, we will turn our focus to how the morphological transition could impact the results of the GA. We assume that antibiotic exposure will trigger an *en masse* transition within the bacterial population and therefore a deterministic model will provide a suitable approximation to the system.

5.1 Model formulation

In keeping with our previous models, we formulate a system of equations to describe the dynamics of a population of rod-shaped cells (H) and spherical cells (L). Additionally, we describe the concentration of antibiotic (A). We are interested in the role of the spherical population and its effects on treatment strategies; therefore, we do not include a resistant population or a population of rod-shaped cells with bound antibiotic and return to the simpler set-up from Chapter 2.

The mechanisms included in this model are similar to those in Model I and Figure 2.2 can be used for reference of the interactions in this model. The only distinctions that can be made between Model I and the current model is a change to the method used to describe bacterial growth and the reverse transition of the bacteria. For mathematical simplicity

we choose to model bacterial growth using a logistic term, with carrying capacity k and growth rate r. Natural cell death was found to be negligible in the parametrisation results in Chapter 2, we omit it from this model.

Following from Models I-III, we assume that the spherical bacteria cannot proliferate but can die naturally at a rate, ψ. We model the transition to the spherical shape using a saturating term with maximum rate γ and concentration needed for half maximal transition T_{50}. We assume that the reverse transition will only occur at low antibiotic concentrations and model this transition using a hyperbolic tangent function with slope parameter b and critical threshold concentration A_c.

We maintain the assumption that the spherical cells evade antibiotic effects completely and model the effect of the antibiotic on the rod-shaped cells using a nonlinear term with maximum death rate ρ and concentration at which half maximal killing occurs A_{50}. Following from [86] we assume that antibiotic doses are added to the system daily and we introduce the dosage vector, $D = (D_1, D_2, ..., D_{10})$, where at time $\hat{t}_i$ the antibiotic is replenished with an amount D_i ($i \in (1, 2, ..., 10)$). Finally, we assume that antibiotic decay follows first order kinetics. In Chapter 2 we also included antibiotic degradation due to bacterial death within the model yet we found both antibiotic-associated parameters to be unidentifiable. Therefore, we choose to simplify the mechanisms involved in antibiotic decay.

Following mass action kinetics we produce Model IV:

$$\begin{aligned}
\frac{dH}{dt} &= rH\left(1-\frac{H}{k}\right) - \left(\frac{\rho A}{A_{50}+A}\right)H - \left(\frac{\gamma A}{T_{50}+A}\right)H \\
&\quad + \frac{\delta}{2}\left(1+\tanh\left(\frac{A_c-A}{b}\right)\right)L, \qquad (5.1)\\
\frac{dL}{dt} &= \left(\frac{\gamma A}{T_{50}+A}\right)H - \psi L - \frac{\delta}{2}\left(1+\tanh\left(\frac{A_c-A}{b}\right)\right)L, \qquad (5.2)\\
\frac{dA}{dt} &= \sum_{n=1}^{10} D_n \delta(t-\hat{t}_n) - \alpha A, \qquad (5.3)
\end{aligned}$$

with initial conditions

$$H(0) = 10^3, \quad L(0) = 0, \quad A(0) = 0. \tag{5.4}$$

Variable definitions are given in Table 5.1 and parameter definitions and default parameter values are displayed in Table 5.2. We note that the initial condition for the antibiotic, $A(0) = 0$, as we choose to add the first initial antibiotic dose on day 1.

Table 5.1: Definitions and units for the variables in Model IV, described by equations (5.1)-(5.4).

Variable	**Definition**	**Units**
H	Antibiotic-susceptible rod-shaped cells	cells cm^{-3}
L	Spherical shaped cells	cells cm^{-3}
A	Antibiotic concentration	$\mu\text{g}\,\text{ml}^{-1}$

Parameters were chosen following the previous models where possible. Some parameters have been chosen as to suitably predict the dynamics required. In [86], the MIC values of the susceptible and resistant strain were used to model antibiotic death and having these parameter values allowed for analysis of the predicted antibiotic concentration over the time course of the treatment. As the parameters in our model are not all parametrised using experimental data, they are not all specific to a strain of bacteria and antibiotic. Therefore we will not aim to suggest MIC values and thereon formulate conclusions based on the antibiotic concentration. Instead we focus on the total amount of antibiotic used and the time taken to clear the infection.

5.2 Detail of the genetic algorithm

The tailored treatment methods were obtained using the built-in MATLAB function *ga*, which uses a GA to find a local minimum to a function. By choosing a suitable objective function that relates to the number of bacteria and the amount of antibiotic used over a 10 day dosing period, we can use the GA to find local minima that represent the optimal

Table 5.2: Definitions and units for the parameters in Model IV, described by equations (5.1)-(5.4).

Parameter	**Description**	**Units**	**Default value**
α	Antibiotic decay rate.	day^{-1}	1
r	Growth rate of rod-shaped bacteria.	day^{-1}	2
k	carrying capacity of rod-shaped bacteria	cells cm^{-3}	10^6
γ	Transition rate from rod to spherical shape.	day^{-1}	1
δ	Transition rate from spherical to rod shape.	day^{-1}	1
A_c	critical antibiotic concentration threshold for reversion of spherical cells	$\mu\text{g ml}^{-1}$	0.5
b	smoothed step function slope parameter	$\mu\text{g ml}^{-1}$	1
ρ	Death rate of rod-shaped bacteria due to antibiotic.	day^{-1}	5
ψ	Death rate of spherical bacteria.	day^{-1}	0.017
T_{50}	Antibiotic concentration required for half maximal killing effect	$\mu\text{g ml}^{-1}$	0.47
A_{50}	Antibiotic concentration required for half maximal transition effect	$\mu\text{g ml}^{-1}$	10

dosing strategies. Following [86], we choose the objective function:

$$F = n_1 \sum_{i=1}^{10} D_i + n_2 \int_0^{30} H(t)dt. \tag{5.5}$$

This represents a multicriteria objective function. The first term in our objective function represents the sum of doses over a 10 day dosing period. We wish to minimise the total amount of antibiotic in order to reduce antibiotic exposure (and hence the likelihood that resistance may emerge). Following from [86], we constrain the antibiotic concentration at any given time to be less than $60\mu\text{g ml}^{-1}$ due to the toxicity of antibiotic and we test maximum daily doses of $40, 50$ and $60\mu\text{g ml}^{-1}$.

Whilst we wish to minimise the amount of antibiotic used, if less antibiotic is added then the bacterial population may increase. Therefore we also choose to minimise the

total bacterial load to ensure treatment success; the second term in our objective function calculates the total bacterial load from the day before the inital dose ($t = 0$ days) to just under 3 weeks after the final dose ($t = 30$ days). Note that we calculate the total bacterial load over the extended period after the dosing regimen is complete as we wish to consider regrowth of the infection within our minimising function. By including the possibility of regrowth we hope to reject treatment strategies that result in failed treatment in the long-term. Weighting coefficients were used in [86]. We choose to balance the terms equally by scaling appropriately: we normalise both terms in the objective function using the scaling factors, n_1 and n_2, that scale the terms to values that are approximately $O(1)$. To scale the total amount of antibiotic we choose a scaling factor equal to a typical total amount of antibiotic allowed over the dosing regimen. For example, for a typical daily antibiotic dose of $14\mu\text{g}\,\text{ml}^{-1}$, the scaling factor is $n_1 = \frac{1}{140}$. Similarly, we scale the total bacterial load over the 30 day time period using the total bacterial load achieved with a dosing strategy that minimises the second term in the fitness function, with the constraint that the total antibiotic used cannot exceed $140\mu\text{g}\,\text{ml}^{-1}$; this gives $n_2 = \frac{1}{7.5\times10^3}$. This approach roughly balances the two terms in the fitness function. Varying this balance would lead to either unnecessarily large quantities of antibiotic being used or treatments that don't eradicate the bacteria. The default options in Matlab for *ga* were used meadning that new generations were produced from a combination of elite children, crossover children (recombination) and mutation children. The GA was implemented with a population size of 100, for 200 generations and repeated 10 times.

5.3 Results

5.3.1 Investigating antibiotic dosing regimens for a rod-shaped population

Initially we assume that the bacteria do not transition to spherical cells during exposure to antibiotics to attempt to reproduce some of the results obtained in [86] (where no transition was considered), i.e. $\gamma = 0$ day^{-1}. We obtain the reduced version of Model IV,

$$\frac{dH}{dt} = rH\left(1 - \frac{H}{k}\right) - \left(\frac{\rho A}{A_{50} + A}\right)H, \tag{5.6}$$

$$\frac{dA}{dt} = \sum_{n=1}^{10} D_n \delta(t - \hat{t}_n) - \alpha A, \tag{5.7}$$

with initial conditions

$$H(0) = 10^3, \quad A(0) = 0. \tag{5.8}$$

Traditional treatment regimens

Following [86] we begin by looking for a traditional treatment regimen that is able to clear the infection within a 10 day treatment period. For the traditional regimen we assume that the antibiotic doses are equal such that $D_1 = D_2 = ... = D_{10}$. If we simulate a 10 day traditional treatment strategy of a constant dose then we predict that a minimum dose of 14μg ml^{-1} per day would be required to clear the population in 10.97 days (Figure 5.1).

Tailored treatment regimens

To clear the infection we have shown that a total of 140μg ml^{-1} must be administered over a 10 day period if the doses are equal. The most effective solutions chosen by the GA are displayed in Table 5.3. In agreement with [86], the GA selects dosage vectors that have a high initial dose followed by lower doses that taper off towards the end of

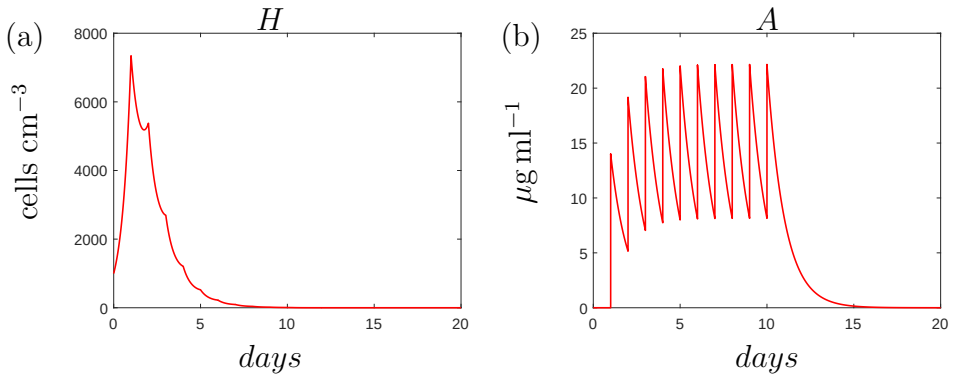

Figure 5.1: The solution to the system (5.6)-(5.7), with initial conditions (5.8) with dosing vector $D = (D_1, D_2, ..., D_{10})$, with $D_i = 10\,\forall i \in [1, 10]$. In (a) the bacterial concentration is given and in (b) the antibiotic concentration.

the treatment (HDTDs). The total amount of antibiotic can be reduced from $140\mu\text{g}\,\text{ml}^{-1}$ in the traditional regimen to as low as $124\mu\text{g}\,\text{ml}^{-1}$ in $R1$ and the time it takes to clear the infection can also be decreased. Previously we found that it would take 10.97 days to eradicate the population and with the tailored treatments we find that it is possible to clear the infection in as little as 6.35 days ($R3$).

Table 5.3: Dosage vectors chosen by the GA to treat an infection of rod-shaped bacteria. We constrain the total amount of antibiotic available to $140\mu\text{g}\,\text{ml}^{-1}$ and employ the objective function (5.5).

	Dosage vector	**Total antibiotic (μg ml^{-1})**	**Time to clear infection (days)**
$R1$	$(40, 19, 16, 18, 15, 16, 0, 0, 0, 0)$	124	7.31
$R2$	$(50, 18, 19, 11, 18, 12, 0, 0, 0, 0)$	128	7.10
$R3$	$(50, 17, 21, 26, 15, 0, 0, 0, 0, 0)$	129	6.35
$R4$	$(46, 18, 13, 19, 21, 9, 0, 0, 0, 0)$	126	7.04
$R5$	$(50, 17, 11, 24, 13, 13, 0, 0, 0, 0)$	128	7.04
$R6$	$(56, 15, 14, 14, 15, 16, 0, 0, 0, 0)$	130	7.2
$R7$	$(51, 11, 17, 13, 19, 13, 4, 0, 0, 0)$	128	7.56

We have obtained similar predictions to those in [86] and would support the use of a HDTDs treatment regimen for a population of rod-shaped cells that cannot transition. Our aim is to now consider whether a HDTDs strategy is advisable for an infection that utilises the shape transition.

5.3.2 Investigating antibiotic dosing regimens for a population that utilises the antibiotic-induced morphological transition

Traditional treatment regimen

The full model, described by equations (5.1)-(5.4), is used if we assume that the bacteria can employ the morphological transition. Following from Section 5.3.1 we attempt to find a traditional regimen that could clear the infection within 10 days. Figure 5.2 displays the populations of rod-shaped spherical cells one day after the final dose of antibiotic is administered (Figures 5.2 (a) and (b)) and three weeks after the final dose is administered (Figures 5.2 (c) and (d)) with varied antibiotic doses. The day after we add the final dose we find that the rod-shaped population is cleared for repeated doses of $6\mu g\,ml^{-1}$ and higher (Figure 5.2 (a)) but a spherical population remains regardless of the antibiotic dose.

After three weeks of no antibiotic exposure we see changes to both populations of cells. For all antibiotic concentrations we find that most of the spherical cells will return to the rod-shape and resume proliferation. Regardless of the dose used for the traditional treatment regimen, we would expect the population to regrow to the steady state population.

We note that the range of doses tested is large and that for the higher concentrations it is likely that the antibiotic concentration within the body at the end of the treatment could be high and potentially toxic.

Applying the GA

Our results suggest that it is not possible to clear the infection using a traditional 10 day dosing regimen with equal doses. Therefore we do not have a total amount of antibiotic to use as a constraint in the GA. To obtain the GA results we set the maximum daily dose to $40\mu g\,ml^{-1}$ and do not limit the total amount of antibiotic used over the treatment or the concentration of antibiotic during the treatment. The dosage vectors chosen by

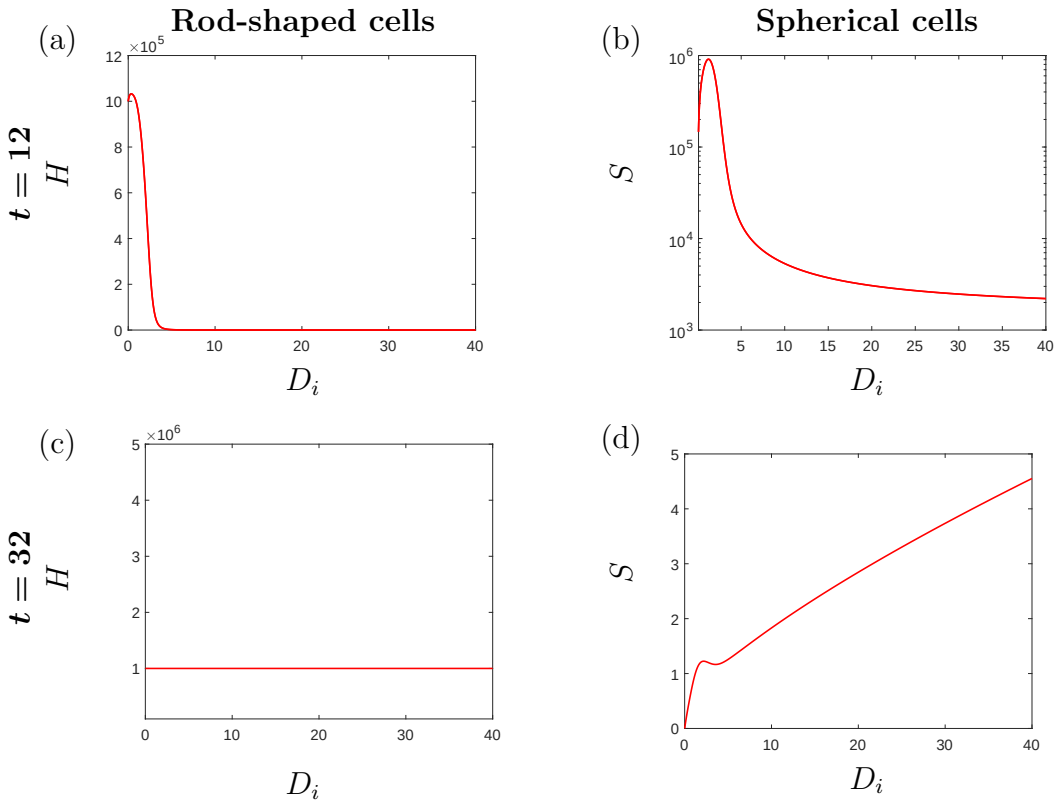

Figure 5.2: The populations of rod-shaped cells ((a) and (c)) and spherical cells ((b) and (d)), the day after ((a)-(b)) and two weeks after ((c)-(d)) the final dose of a traditional treatment for a fixed dose for 10 days with varied dose, D_i.

the GA are displayed in Table 5.4. The most efficient dosage vectors exhibit a trend of a high initial dose and high final dose but between these doses there is no significant trend.

If it is not possible to clear the infection during the 10 day treatment period then the population will grow to the carrying capacity once the antibiotic has degraded. The contribution of population growth to the total bacterial load term post-antibiotic exposure becomes very large. Therefore, we find that any change to the bacterial load term, caused by alterations in the dosage vector over the first 10 days, will have a negligible effect on the objective function compared to the bacterial load that grows in the remainder of time after the treatment. As a result, we find that the GA chooses treatment strategies that do not utilise the total amount of antibiotic available as it attempts to minimise the objective function by reducing the second term of (5.5) that corresponds to the total amount of antibiotic used. If we amend the objective function to only minimise the bacterial load or add in constraints to the total amount of antibiotic used and the antibiotic concentration during treatment we still find that the GA does not predict the HDTDs strategy we predicted for the infection that can be cleared within 10 days.

Table 5.4: Dosage vectors chosen by the GA to treat an infection that utilises the morphological transition ($\gamma = 1$ day^{-1}). The total amount of antibiotic available is unconstrained and we employ the objective function (5.5). The concentrations of both bacterial populations are recorded for each treatment strategy 24 hours after the final dose is administered.

	Dosage vector	**Total antibiotic** (μg ml^{-1})	**Concentration at** $t = 12$	
			H	S
$R1$	$(11, 4, 4, 3, 3, 4, 3, 3, 2, 11)$	48	788	0.95×10^4
$R2$	$(12, 3, 3, 3, 4, 3, 4, 2, 3, 11)$	48	877	1.02×10^4
$R3$	$(12, 3, 3, 4, 3, 3, 4, 3, 2, 11)$	48	822	0.98×10^4
$R4$	$(12, 3, 4, 4, 3, 4, 2, 3, 2, 12)$	49	853	0.902×10^4
$R5$	$(11, 3, 3, 5, 2, 4, 3, 3, 3, 10)$	47	827	1.08×10^4

Our results suggest that if a bacterial infection cannot be cleared using a traditional treatment strategy that the GA will not advise towards a HDTDs strategy as the algorithm struggles to substantially minimise the total bacterial load. The same result is obtained if we use the GA to identify the most effective dosing strategy for a population with no

spheres that is not cleared using the prescribed traditional dosing regimen. For example, if we apply a $12\mu g\,ml^{-1}$ dose each day for 10 days then, following from our results in Section 5.3.1, we would not clear the bacterial population and the GA would not suggest the HDLDs strategy (results omitted).

If the population of spherical cells is not cleared then we do not obtain a clear trend within the most effective treatment strategies suggested by the GA. This result highlights the importance of considering phenotypic variants when using this method to choose treatment strategies. The spherical population and the reverse transition enable the population to survive high dosage treatment strategies and therefore the GA finds it hard to substantially minimise the objective function. If we can successfully remove the persistent population then it may be possible to once again get a strong conclusion regarding suitable treatment strategies using the GA.

Considering the use of AMPs

In Chapter 4 we analysed the effects of using AMPs in conjunction with the antibiotic and concluded that the use of AMPs may not be beneficial during treatment. We briefly considered that they could propose a suitable treatment option once the rod-shaped population has been cleared. Here, we assume that the spherical population that persists and enables population recovery after the antibiotic dosing strategy has finished, can be cleared using AMPs alone using a sequential treatment strategy. To simplify investigating this we set the reverse transition rate $\delta = 0$ day^{-1}. By removing the reverse transition we provide the GA with the chance to optimise clearance of the rod-shaped population without being affected by the spherical population that previously enabled population regrowth after the treatment period. We assume that AMPs will subsequently be added to eradicate the remaining spherical population following the final dose of antibiotic.

We find that the rod-shaped population can be cleared using a traditional strategy with a 10 day repeated dose of $7\mu g\,ml^{-1}$ (results omitted). This is a lower dose than estimated was necessary for the population of cells that do not alter their morphology

(Figure 5.1) but we note that the bacteria are transitioning to spheres and being killed by the antibiotic so the rod-shaped population will decrease faster and as a result are cleared faster. If we subsequently apply the GA with the total amount of antibiotic as $70\mu g\,ml^{-1}$, using the objective function (5.5), we obtain the tailored treatment strategies shown in Table 5.5. The GA chooses treatment strategies that exhibit the HDTDs trend and the amount of antibiotic and time taken to clear the infection decreases from the traditional treatment regimen.

Table 5.5: Dosage vectors chosen by the GA to treat an infection that utilises the morphological transition but does not revert back to the rod-shape in the absence of antibiotic. We constrain the total amount of antibiotic available to $70\mu g\,ml^{-1}$ and we employ the objective function (5.5).

	Dosage vector	**Total antibiotic ($\mu g\,ml^{-1}$)**	**Time to clear infection (days)**
$R1$	$(27, 7, 8, 8, 7, 0, 0, 0, 0, 0)$	59	6.34
$R2$	$(29, 7, 8, 8, 7, 0, 0, 0, 0, 0)$	60	6.17
$R3$	$(32, 4, 10, 9, 5, 0, 0, 0, 0, 0)$	59	6.89
$R4$	$(28, 5, 8, 9, 5, 4, 0, 0, 0, 0)$	59	6.24
$R5$	$(28, 9, 9, 7, 6, 0, 0, 0, 0, 0)$	59	6.1

Whilst the GA has suggested suitable treatment strategies, recall that there will be a large spherical population present during and after the antibiotic treatment. If we simulate a sequential treatment strategy of antibiotic dosing regimen $R1$ from Table 5.5 followed by a constant dose of AMPs, administered for 5 days starting from the day after the last nonzero antibiotic dose, we obtain the results in Figure 5.3. Previously we set the reverse transition rate $\delta = 0\ day^{-1}$ in order to apply the GA to the population with rod-shaped and spherical cells. To simulate the chosen strategies we do not need to maintain this assumption and we reset the reverse transition rate to its default value, $\delta = 1\ day^{-1}$. The results suggest that the AMPs could quickly clear the spherical population before they transition back to rod-shaped cells and resume proliferation. As the antibiotic has not degraded fully from the system we see that the spherical cells may not transition back to the rod-shape before the AMPs are added. The spherical population is rapidly cleared and total clearance occurs before the antibiotic has fully degraded.

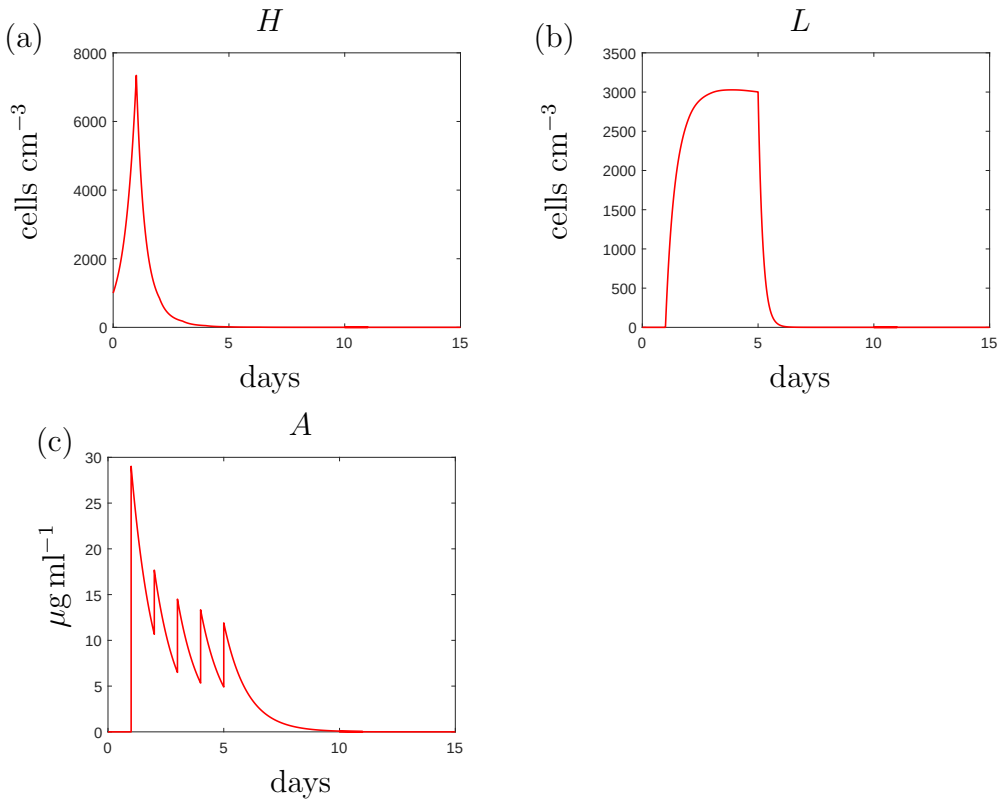

Figure 5.3: The individual variable solutions to the system (5.1)-(5.3) with initial conditions (5.4). For $t \in [1, 5]$ we simulate the antibiotic dosage vector $D = (27, 7, 8, 8, 7)$. For $t \in [6, 11]$ we change the death rate of the spherical cells, ψ from its default value of $0.017\,\text{day}^{-1}$ to $\psi = 5\ \text{day}^{-1}$ to simulate the addition of AMPs. For $t > 11$ we return to the value of $\psi = 0.017\ \text{day}^{-1}$ in order to simulate the removal of the AMPs.

5.4 Discussion

In this chapter we have shown that the presence of phenotypic variants, such as the spherical cells, could impact the dosing strategies obtained using a GA. As the cells lie dormant and possess the ability to transition back to the rod shape, a HDTDs strategy would not clear the infection. It is likely that this result would be similar for populations that include persister cells and highlights the need to consider these phenotypes when searching for optimal treatment strategies.

The model formulated for this chapter was simplified in order to observe the basic impact of morphological heterogeneity on optimal dosing strategies. We could apply the genetic algorithm to a more complex model such as Model III to see if the HDTDs strategy is optimal in the presence of an immune response. Using Model III we could attempt to reproduce the results in [86] using the mixed strain model and include a stochastic framework to evaluate treatment success.

If the morphological transition facilitates treatment failure then we predict that it may still be able to obtain a successful treatment strategy if we include addition of AMPs following the final antibiotic dose. In Chapter 4 we found that AMPs could be ineffective if used simultaneously with antibiotic to treat an *in vivo* infection but here we highlight their potential as part of a sequential treatment strategy. Further optimisation attempts could be made to predict the optimal dosing frequency (we only considered one dose each day) and at which time to add the AMPs. We note that we have only considered a constant dose of AMPs; we could extend the model to incorporate the AMP concentration in order to optimise the dosage and number of doses required to effectively remove the spherical population. Finally, we could apply the GA to optimise the simultaneous use of antibiotics and an antivirulence drug and investigate the use of the triple drug combination we considered in Chapter 4.

CHAPTER 6

DISCUSSION

This thesis has comprised a number of mathematical models that have been formulated to investigate the role of the antibiotic-induced morphological transition witnessed in populations of *P. aeruginosa*. We have investigated the potential threat of the cell wall deficient forms that are observed in populations of *P. aeruginosa* but whose characteristics, clinical significance and cause have not yet been established.

Research suggests that the formation of spheroplasts, with a depleted peptidoglycan layer and unstable osmotic properties, may be the final structural change witnessed before lysis, implying that the transition may be due to antibiotic effects and not an intrinsic mechanism. However, the results in [75], which we were able to reproduce experimentally, show a clear indication of the reverse transition and its ability to replenish the population after antibiotic exposure, suggesting that it is in fact a purposeful evasion mechanism, induced by antibiotic exposure, yet ultimately implemented by a responsive cellular mechanism.

Using Model I (to describe the *in vitro* growth of a single susceptible strain) we can attempt to address the ambiguity surrounding the cause of structural changes to the bacterial population. By assuming that the change in bacterial morphology occurs due to the presence of antibiotic exposure, whether the transition is an intrinsic internal response of the bacteria or a result of antibiotic action, the model formulated allows for both of these possibilities. The death rate of the bacillary cells due to antibiotic can be

seen to represent those cells that are eliminated by the antibiotic before any significant changes in morphotype occur. Those that do display changes in their ultrastructure undergo transition into the spherical population and are then subject to a higher death rate; however this mechanism is not explicitly dependent on antibiotic. Another way of looking at this would be to suggest that if the shift in population structure is solely the result of peptidoglycan inhibition, induced by the antibiotic, then once a bacterium has converted into a spherical form the bactericidal damage has already been induced and lysis is no longer dependent on antibiotic presence. Similarly, allowing for a reverse transition would suggest that the damage made by the antibiotic is reversible.

Much of our results in Chapter 2, however, support the hypothesis proposed by Monahan et al. [75] that this transition is in fact a purposeful mechanism used to evade antibiotic effects. Under the assumption that spherical cells are immune to antibiotic effects, and by using suitable parameters, we have shown that the transition may lead to the recovery of population levels in the absence of meropenem, which we have seen in both our microscopy results and growth curves using low antibiotic concentrations. Although these results are restricted by limited data, the repercussions of this theory could give insight into the persistent characteristics of *P. aeruginosa* and explain its ability to sometimes withstand high levels of carbapenems.

Our experimental results provide evidence for the morphological transition when the bacteria are grown in isolation with the antibiotic. Following from our results in Chapter 2, we extended Model I to formulate Model II, which was used to describe the growth of a single strain of *P. aeruginosa* and included the possibility of efflux pump upregulation. We subsequently developed Model III to further investigate the potential threat of the morphological transition *in vivo*. By including host defences, we recognised the significant contribution of the immune response to treatment; the presence of a persistent subpopulation did not always hinder treatment success due to the efforts of the immune response. However, after further investigation into the immunogenic properties we proposed that the persistent spherical population could be the cause of treatment failure if they are

less immunogenic. Following from [7, 40], we find that our results highlight the need to include population heterogeneity and the immune response within infection level models to truly explore novel treatment approaches.

Related cell morphologies have been shown to play a role in *in vivo* infections, for example, L-forms have been detected in the urine and blood of patients suffering from recurrent renal diseases and urinary tract infections [35, 36]. Our results have detailed the impact that a population of spherical cells would have on a *P. aeruginosa* infection and led to multiple hypotheses regarding novel treatments and potential treatment strategies. To better our predictions we would require further evidence of the characteristics of the spherical cells, including their immunogenic and virulence properties and their growth capabilities. We have assumed throughout that a cell with a disrupted cell wall would be unable to grow. It has been suggested that the spherical cells may be able to proliferate through blebbing or explode in order to produce membrane vesicles that can contribute to biofilm formation and virulence [73, 106]. If so then our results here would possibly present the best case scenario as it is likely that additional proliferation would only exaggerate the potential threat of the spherical cells.

Using Models I-IV we have been able to test an array of treatment strategies *in silico*. In Chapter 2 we hypothesised the use of two novel treatments that could inhibit either the forward or reverse transition. We predicted that a drug that could inhibit the transition to spherical cells could cause higher bacterial loads but would leave the population more vulnerable to the antibiotics resulting in fast clearance of the population. It is also worth noting here that if the morphological changes witnessed are a result of antibiotic action then inhibiting the transition mechanism could be counter-productive to the application of meropenem. Envisaging a drug that could inhibit the bacterium from shedding the cell membrane, thus keeping it intact, could work directly against the mechanism of action of the antibiotic. Furthermore, if a resistant bacteria emerged that could evade the effects of the transition-inhibiting drug then the resistance genes could be directly selected for as the resistant bacteria would be able to transition to the spherical form and have an

increased chance of survival.

Alternatively, we simulated the use of a drug that could inhibit the reverse transition. Whilst the viability of this type of drug is unclear, the results suggested that a drug of this type may not help to eradicate the population but could instead prevent the bacteria from regrowing by forcing the bacteria to remain as spheres. Additionally, we proposed that the reverse transition inhibiting drug would work synergistically with AMPs and help decrease the treatment time needed to clear the population.

The use of AMPs as a supporting drug for antibiotics has been investigated throughout this thesis. *In vitro* results supported the theory that AMPs could clear spherical populations when added with antibiotics and using Model I we were able to simulate their use and reinforce the potential of AMPs [75]. Using Model III we simulated the combined use of AMPs and antibiotic as a treatment for an infection of *P. aeruginosa* at a site of infection. By including host defences we produced results that differed from our previous conclusions. If used simultaneously with the antibiotic we predicted that AMPs could decrease treatment times. However, this result was dependent on specific levels of drug effectiveness and the strain of bacteria. For higher levels of potency we predicted that the AMPs could be ineffective at best, and in the worst case scenario, they could lead to higher levels of virulence and a more resistant infection. *In vivo* testing of AMP usage could be performed to examine whether the results of the drug combination are congruent to the *in vitro* or *in silico* predictions and could determine their potential. Nonetheless, our results indicate that we should not disregard the potential for using AMPs to remove cell wall deficient subpopulations. We previously mentioned the combined use of antibiotics and AMPs with a drug that could inhibit the reverse transition. In addition, we have estimated that a triple combination of antibiotics, AMPs and an antivirulence treatment may clear bacterial infections within a clinically feasible time frame regardless of the immunogenic properties of the spherical cells and the presence of resistance. Furthermore, in Chapter 5 we appraised the use of AMPs as a sequential treatment after a tailored antibiotic dosing regimen. By implementing the GA with an infection level model

we could test whether the immune response impacts the synergism between the antibiotic and AMPs, as we previously found in Chapter 4.

As with all potential treatment options, further investigation into the resultant impact that AMP usage may have on the emergence of resistance would be needed. The use of AMPs would impose a direct fitness cost on the spherical cells that could impact selection for resistant phenotypes. However, due to the already-depleted cell wall and lowered natural survival rate of the spherical cells, it is uncertain whether imposing a further fitness cost on the bacteria would impact the possible emergence of resistance.

The final treatment tested was an antivirulence drug that could prevent the bacteria from evading host defences and increase their vulnerability. We incorporated the effects of an antivirulence drug into Model IV by increasing the susceptibility of the rod-shaped cells to immune cells and found that in all cases the antivirulence drug helped clear the rods faster than using antibiotic alone. If used alone, our predictions suggested that the antivirulence drug may be able to clear the infection yet we acknowledge that a high potency level is needed to achieve this. Furthermore, our predictions were obtained under the assumption that only the rod-shaped cells were targeted by the antivirulence drug; if all cell types were affected by the drug then its effects would be drastically increased.

Resistance to an antivirulence drug could develop and we discussed antivirulence drug resistance in Section 1.4.3. To consider resistance to a drug that increases bacterial vulnerability to host defences would require knowledge of the specific mechanism that the drug inhibited. There are multiple ways in which bacteria evade host defences and resistance would only emerge if the inhibited mechanism had a direct impact on bacterial fitness.

In Chapter 5 we investigated the impact of a spherical subpopulation on the optimised treatment strategies chosen by the GA. As the threat of resistance develops and the need to optimise antibiotic usage increases, tailored treatment regimens may become a viable option. As we have shown, treatment strategies that are suggested for non-transitioning populations may not be successful in clearing populations that include spherical cells.

The presence of any persistent subpopulation would need to be considered when obtaining tailored treatment strategies; if we ignore persistence then tailored treatment regimens may be ineffective. Furthermore, the results in Chapter 4 indicate that a slight change to the immune response could significantly impact treatment success and therefore patient immunity must be considered when choosing a personalised treatment strategy.

If we wish to combat the threat of antibiotic resistance then we must gain a complete understanding of bacterial species, virulence and the mechanisms that enable antibiotic evasion. In this thesis we have detailed how mathematical modelling can be used to simplify complex biological systems and describe bacterial growth in order to obtain predictions that could be used as a basis for experimental investigation. The presence of cell wall deficient *P. aeruginosa* cells could enable antibiotic evasion and increase the threat of recurrent infection that comes along with phenotypic persistence. By exploring parameter spaces we have investigated novel treatment strategies and using a genetic algorithm we have shown that the presence of a spherical population could change treatment strategies chosen by the algorithm. We have highlighted the importance of including host defences in mathematical models of bacterial growth as the contribution of the immune response and the interplay between the persistent population and immune cells could have serious consequences for personalised medicine approaches. To further investigate tailored treatments, the GA could be applied to the infection level model, Model III. It is possible that the GA could successfully select optimal treatments (without AMPs) for an infection with a spherical cell subpopulation if host defences are incorporated. It would be vital to investigate weak immune responses and the immunogenic properties of the spherical cells to gauge a better understanding of the viability of tailored antibiotic regimens. Furthermore, experimental validation of spherical cell properties would be integral to establish the role of the morphological transition *in vivo* and refine our hypotheses.

APPENDIX A

MATERIALS AND METHODS

A.1 Staining and fluorescence microscopy

Single colonies of the *P. aeruginosa* strain PA1008, a meropenem susceptible isolate derived from a hospital burn unit [90], were inoculated into LB broth and grown for around 16 hours at 37°C , shaking at 200 rpm.

A.1.1 Microscopy images for displaying transition

Cultures were normalised to an optical density at 600 nm (OD_{600}) of 0.2 in 20 ml LB broth containing the desired concentration of meropenem. Cultures were incubated at 37°C, 200 rpm in between time points.

At each time point, 1 ml of bacteria was removed from each flask and the OD_{600} measured. A sample from each flask was then normalised to an OD_{600} of 1 by centrifuging the sample and re-suspending in the appropriate volume of PBS. 500 μl of each sample was stained with 1.5 μl of LIVE/DEAD BacLight stain mixture and incubated for 15 minutes at room temperature, in the dark. Samples were centrifuged and re-suspended in 4% PFA for 10 minutes at room temperature to fix the samples. Samples were washed three times with PBS to remove the fixative, and re-suspended in 500 μl of PBS following the final wash.

5 μl of stained culture was loaded onto a microscope slide and allowed to air dry. Once dry, one drop of antifade gold mounting solution was loaded onto the sample and covered with a cover slip. These were left overnight to set in the dark. Microscope slides were examined using a Zeiss Axio Observer microscope. Images were taken using the 63× oil immersion objective and exposure to transmitted light, red and green fluorescence. For fluorescence an exposure of 500 ms was used.

A.1.2 Microscopy images for parameter testing

Cultures were normalised to an optical density at 600 nm (OD_{600}) of 0.4 in LB broth after 16 hours of growth. Meropenem dilutions were made at twice the desired final concentration in LB. 50 μl of the normalised PA1008 culture was added to a 96-well plate followed by 50 μl of the meropenem dilution. For each condition, 6 wells were prepared so that the contents could be pooled together to increase the yield of cells. Between time points the 96-well plate was incubated in a plate reader, shaking at 200 rpm, 37°C. OD_{600} was measured from the samples every 10 minutes to allow the OD of the samples to be monitored over the course of the experiment (thus ensuring bacterial load is comparable to that of our growth curves – see below).

At each time point, the contents of the appropriate wells were removed and pooled together for each concentration in separate microcentrifuge tubes. 600 μl of 4% PFA was added directly and incubated for 30 minutes at room temperature to fix the samples. Samples were washed three times with PBS to remove the fixative, and re-suspended in 50 μl of PBS following the final wash. Each sample was stained with 3 μl of LIVE/DEAD BacLight stain mixture and incubated for 15 minutes at room temperature, in the dark. Samples were washed three times with PBS to remove excess stain, and re-suspended in 50 μl of PBS following the final wash.

5 μl of stained culture was loaded onto a microscope slide and allowed to air dry. Once dry, one drop of antifade gold mounting solution was loaded onto the sample and covered with a cover slip. These were left overnight to set in the dark. Microscope slides were

examined using a Zeiss Axio Observer microscope. Images were taken using the 63× oil immersion objective and exposure to transmitted light, red and green fluorescence. For fluorescence an exposure of 100 ms was used. At least 5 images were obtained for each condition.

A.2 Growth curves for model parametrisation

Single colonies of the *P. aeruginosa* strain PA1008 were inoculated into 5 ml of LB broth and grown overnight at 37°C, shaking at 200 rpm. The following day, the cultures were diluted to an OD_{600} of 0.4, which would be diluted to 0.2 following the addition of the antibiotic. Dilutions of meropenem were made using LB broth to give final concentrations. 50 μl of bacteria culture was added to the appropriate wells of a sterile, 96 well, flat bottom microtitre plate, followed by 50 μl of the appropriate meropenem dilution. Media controls were then added to the plate for each meropenem concentration, consisting of 50 μl of each meropenem dilution plus 50 μl of LB broth. The OD_{600} of each well was taken using a FLUOstar Omega plate reader every 30 minutes for 24 hours. Between OD readings the plate was shaken for 27 minutes. The temperature was set to 37°C for the duration of the assay.

LIST OF REFERENCES

[1] P Abel zur Wiesch, S Abel, S Gkotzis, P Ocampo, J Engelstädter, T Hinkley, C Magnus, MK Waldor, K Udekwu, and T Cohen. Classic reaction kinetics can explain complex patterns of antibiotic action. *Sci. Transl. Med.*, 7:287RA73, 2015.

[2] M Alcalde-Rico, S Hernando-Amado, P Blanco, and JL Martínez. Multidrug efflux pumps at the crossroad between antibiotic resistance and bacterial virulence. *Front. Microbiol.*, 7:1483, 2016.

[3] R Allen, R Popat, S Diggle, and S Brown. Targeting virulence: can we make evolution-proof drugs? *Nature Rev. Microbiol.*, 12:300–308, 2014.

[4] RI Aminov. A brief history of the antibiotic era: lessons learned and challenges for the future. *Front. Microbiol*, 1:134, 2010.

[5] K Anguige, JR King, and JP Ward. Modelling antibiotic-and anti-quorum sensing treatment of a spatially-structured *Pseudomonas aeruginosa* population. *J. Math. Biol.*, 51:557–594, 2005.

[6] K Anguige, JR King, JP Ward, and P Williams. Mathematical modelling of therapies targeted at bacterial quorum sensing. *Math. Biosci.*, 192:39–83, 2004.

[7] P Ankomah and BR Levin. Exploring the collaboration between antibiotics and the immune response in the treatment of acute, self-limiting infections. *Proc. Natl. Acad. Sci. U.S.A.*, 111:8331–8338, 2014.

[8] DJ Austin and RM Anderson. Studies of antibiotic resistance within the patient, hospitals and the community using simple mathematical models. *Philos. Trans. R. Soc. Lond., B, Biol. Sci.*, 354:721–738, 1999.

[9] DJ Austin, M Kakehashi, and RM Anderson. The transmission dynamics of antibiotic–resistant bacteria: the relationship between resistance in commensal organisms and antibiotic consumption. *Proc. R. Soc. Lond. [Biol.]*, 264:1629–1638, 1997.

[10] M Baker, JL Hobman, CER Dodd, SJ Ramsden, and DJ Stekel. Mathematical modelling of antimicrobial resistance in agricultural waste highlights importance of gene transfer rate. *FEMS Microbiol. Ecol.*, 92:fiw040, 2016.

[11] NQ Balaban, J Merrin, R Chait, L Kowalik, and S Leibler. Bacterial persistence as a phenotypic switch. *Science*, 305:1622–1625, 2004.

[12] P Ball, F Baquero, O Cars, T File, J Garau, K Klugman, DE Low, E Rubinstein, R Wise, Consensus Group on Resistance, and The Prescribing in Respiratory Tract Infection. Antibiotic therapy of community respiratory tract infections: strategies for optimal outcomes and minimized resistance emergence. *J. Antimicrob. Chemother.*, 49:31–40, 2002.

[13] J Baranyi and TA Roberts. A dynamic approach to predicting bacterial growth in food. *Int. J. Food Microbiol.*, 23:277–294, 1994.

[14] C Baron. Antivirulence drugs to target bacterial secretion systems. *Curr. Opin. Microbiol.*, 13:100–105, 2010.

[15] JW Bigger. Treatment of staphylococcal infections with penicillin by intermittent sterilisation. *Lancet*, pages 497–500, 1944.

[16] IA Bliziotis, G Samonis, KZ Vardakas, S Chrysanthopoulou, and ME Falagas. Effect of aminoglycoside and β-lactam combination therapy versus β-lactam monotherapy on the emergence of antimicrobial resistance: a meta-analysis of randomized, controlled trials. *Clin. Infect. Dis.*, 41:149–158, 2005.

[17] S Bonhoeffer, M Lipsitch, and BR Levin. Evaluating treatment protocols to prevent antibiotic resistance. *Proc. Natl. Acad. Sci.*, 94:12106–12111, 1997.

[18] A Brauner, O Fridman, O Gefen, and NQ Balaban. Distinguishing between resistance, tolerance and persistence to antibiotic treatment. *Nat. Rev. Microbiol.*, 14:320, 2016.

[19] SP Brown, DM Cornforth, and N Mideo. Evolution of virulence in opportunistic pathogens: generalism, plasticity, and control. *Trends. Microbiol.*, 20:336–342, 2012.

[20] L Cegelski, G Marshall, G Eldridge, and S Hultgren. The biology and future prospects of antivirulence therapies. *Nature Rev. Microbiol.*, 6:17–27, 2008.

[21] E Chain, HW Florey, AD Gardner, NG Heatley, MA Jennings, J Orr-Ewing, and AG Sanders. Penicillin as a chemotherapeutic agent. *Lancet*, 236:226–228, 1940.

[22] E Chamot, EB El Amari, P Rohner, and C Van Delden. Effectiveness of combination antimicrobial therapy for *Pseudomonas aeruginosa* bacteremia. *Antimicrob. Agents Chemother.*, 47:2756–2764, 2003.

[23] P Christie, K Atmakuri, V Krishnamoorthy, S Jakubowski, and E Cascales. Biogenesis, architecture, and function of bacterial type iv secretion systems. *Annu. Rev. Microbiol.*, 59:451–485, 2005.

[24] ARM Coates, G Halls, and Y Hu. Novel classes of antibiotics or more of the same? *Br. J. Pharmacol.*, 163:184–194, 2011.

[25] NG Cogan. Effects of persister formation on bacterial response to dosing. *J. Theor. Biol.*, 238:694–703, 2006.

[26] NG Cogan. Incorporating toxin hypothesis into a mathematical model of persister formation and dynamics. *J. Theor. Biol.*, 248:340–349, 2007.

[27] MM Curtis, R Russell, CG Moreira, AM Adebesin, C Wang, NS Williams, R Taussig, D Stewart, P Zimmern, B Lu, et al. Qsec inhibitors as an antivirulence approach for gram-negative pathogens. *MBio*, 5:e02165–14, 2014.

[28] T Cushnie, NH ODriscoll, and AJ Lamb. Morphological and ultrastructural changes in bacterial cells as an indicator of antibacterial mechanism of action. *Cell. Mol. Life Sci.*, 73:4471–4492, 2016.

[29] EMC D'Agata, M Dupont-Rouzeyrol, P Magal, D Olivier, and S Ruan. The impact of different antibiotic regimens on the emergence of antimicrobial-resistant bacteria. *PLoS One*, 3:e4036, 2008.

[30] EMC D'Agata, G Webb, and M Horn. A mathematical model quantifying the impact of antibiotic exposure and other interventions on the endemic prevalence of vancomycin-resistant enterococci. *J. Infect. Dis.*, 192:2004–2011, 2005.

[31] VN De Groote, N Verstraeten, M Fauvart, CI Kint, AM Verbeeck, S Beullens, P Cornelis, and J Michiels. Novel persistence genes in *Pseudomonas aeruginosa* identified by high-throughput screening. *FEMS microbiol. lett.*, 297:73–79, 2009.

[32] CA DeRyke, SY Lee, JL Kuti, and DP Nicolau. Optimising dosing strategies of antibacterials utilising pharmacodynamic principles. *Drugs*, 66:1–14, 2006.

[33] GH Dibdin, SJ Assinder, WW Nichols, and PA Lambert. Mathematical model of β-lactam penetration into a biofilm of *Pseudomonas aeruginosa* while undergoing simultaneous inactivation by released β-lactamases. *J. Antimicrob. Chemother.*, 38:757–769, 1996.

[34] JD Dockery and JP Keener. A mathematical model for quorum sensing in *Pseudomonas aeruginosa*. *Bull. Math. Biol.*, 63:95–116, 2001.

[35] GJ Domingue and HB Woody. Bacterial persistence and expression of disease. *Clin. Microbiol. Rev.*, 10:320–344, 1997.

[36] J Errington, K Mickiewicz, Y Kawai, and LJ Wu. L-form bacteria, chronic diseases and the origins of life. *Phil. Trans. R. Soc. B*, 371:20150494, 2016.

[37] A Fleming. On the antibacterial action of cultures of a penicillium, with special reference to their use in the isolation of *B. influenzae*. *Brit. J. Exp. Pathol.*, 10:226, 1929.

[38] David Gammack, Suman Ganguli, Simeone Marino, Jose Segovia-Juarez, and Denise E Kirschner. Understanding the immune response in tuberculosis using different mathematical models and biological scales. *Multiscale Model. Simul.*, 3:312–345, 2005.

[39] P Geli, R Laxminarayan, M Dunne, and DL Smith. one-size-fits-all? optimizing treatment duration for bacterial infections. *PloS ONE*, 7:e29838, 2012.

[40] E Gjini and PH Brito. Integrating antimicrobial therapy with host immunity to fight drug-resistant infections: classical vs. adaptive treatment. *PLoS Comput. Biol.*, 12:e1004857, 2016.

[41] B Gompertz. Xxiv. on the nature of the function expressive of the law of human mortality, and on a new mode of determining the value of life contingencies. *Philos. Trans. R. Soc. Lond.*, 115:513–583, 1825.

[42] Z Han, JS Pinkner, B Ford, E Chorell, JM Crowley, CK Cusumano, S Campbell, JP Henderson, SJ Hultgren, and JW Janetka. Lead optimization studies on fimh

antagonists: discovery of potent and orally bioavailable ortho-substituted biphenyl mannosides. *J. Med. Chem.*, 55:3945–3959, 2012.

[43] REW Hancock. Resistance mechanisms in *Pseudomonas aeruginosa* and other nonfermentative gram-negative bacteria. *Clin. Infect. Dis.*, 27:S93–S99, 1998.

[44] A Handel, E Margolis, and BR Levin. Exploring the role of the immune response in preventing antibiotic resistance. *J. Theor. Biol.*, 256:655–662, 2009.

[45] M Hentzer, K Riedel, TB Rasmussen, A Heydorn, JB Andersen, MR Parsek, SA Rice, L Eberl, S Molin, N Høiby, et al. Inhibition of quorum sensing in *Pseudomonas aeruginosa* biofilm bacteria by a halogenated furanone compound. *Microbiol.*, 148:87–102, 2002.

[46] M Hentzer, H Wu, JB Andersen, K Riedel, TB Rasmussen, N Bagge, N Kumar, MA Schembri, Z Song, P Kristoffersen, et al. Attenuation of *Pseudomonas aeruginosa* virulence by quorum sensing inhibitors. *EMBO J.*, 22:3803–3815, 2003.

[47] M Hilf, LY Victor, J Sharp, JJ Zuravleff, JA Korvick, and RR Muder. Antibiotic therapy for *Pseudomonas aeruginosa* bacteremia: outcome correlations in a prospective study of 200 patients. *Am. J. Med.*, 87:540–546, 1989.

[48] NHG Holford and LB Sheiner. Kinetics of pharmacologic response. *Pharmacol. Therapeut.*, 16:143–166, 1982.

[49] B Huttner, H Goossens, T Verheij, S Harbarth, et al. Characteristics and outcomes of public campaigns aimed at improving the use of antibiotics in outpatients in high-income countries. *Lancet Infect. Dis.*, 10:17–31, 2010.

[50] CB Inderlied, MG Lancero, and LS Young. Bacteriostatic and bactericidal invitro activity of meropenem against clinical isolates, including *Mycobacterium avium* complex. *J. Antimicrob. Chemother.*, 24:85–99, 1989.

[51] S Jabbari, JR King, AJ Koerber, and P Williams. Mathematical modelling of the *agr* operon in *Staphylococcus aureus*. *J. Math. Biol.*, 61:17–54, 2010.

[52] TH Jakobsen, M van Gennip, RK Phipps, MS Shanmugham, LD Christensen, M Alhede, ME Skindersoe, TB Rasmussen, K Friedrich, F Uthe, et al. Ajoene, a sulfur rich molecule from garlic, inhibits genes controlled by quorum sensing. *Antimicrob. Agents Chemother.*, pages AAC–05919, 2012.

[53] AM Jarrett, NG Cogan, and ME Shirtliff. Modelling the interaction between the host immune response, bacterial dynamics and inflammatory damage in comparison with immunomodulation and vaccination experiments. *Math. Med. Biol.*, 32:285–306, 2014.

[54] F Kargi. Re-interpretation of the logistic equation for batch microbial growth in relation to monod kinetics. *Lett. Appl. Microbiol.*, 48:398–401, 2009.

[55] AM Kauppi, R Nordfelth, H Uvell, H Wolf-Watz, and M Elofsson. Targeting bacterial virulence: inhibitors of type iii secretion in *Yersinia*. *Chem. Biol.*, 10:241–249, 2003.

[56] D Kim, S Chung, S Lee, and J Choi. Relation of microbial biomass to counting units for *Pseudomonas aeruginosa*. *Afr. J. Microbiol. Res.*, 6:4620–4622, 2012.

[57] E Klieneberger. The natural occurrence of pleuropneumonia-like organism in apparent symbiosis with *Streptobacillus moniliformis* and other bacteria. *J. Pathol.*, 40:93–105, 1935.

[58] AM Krachler, H Ham, and K Orth. Outer membrane adhesion factor multivalent adhesion molecule 7 initiates host cell binding during infection by gram-negative pathogens. *Proc. Natl. Acad. Sci. U.S.A.*, 108:11614–11619, 2011.

[59] AM Krachler and K Orth. Functional characterization of the interaction between bacterial adhesin multivalent adhesion molecule 7 (mam7) protein and its host cell ligands. *J. Biol. Chem.*, 286:38939–38947, 2011.

[60] AM Krachler and K Orth. Targeting the bacteria–host interface: strategies in anti-adhesion therapy. *Virulence*, 4:284–294, 2013.

[61] JC Lagarias, JA Reeds, MH Wright, and PE Wright. Convergence properties of the nelder–mead simplex method in low dimensions. *SIAM J. Optimiz.*, 9:112–147, 1998.

[62] AB Lang, MP Horn, MA Imboden, and AW Zuercher. Prophylaxis and therapy of *Pseudomonas aeruginosa* infection in cystic fibrosis and immunocompromised patients. *Vaccine*, 22:S44–S48, 2004.

[63] BR Levin and C Svanborg Edén. Selection and evolution of virulence in bacteria: an ecumenical excursion and modest suggestion. *Parasitology*, 100:S103–S115, 1990.

[64] M Lipsitch and BR Levin. The population dynamics of antimicrobial chemotherapy. *Antimicrob. Agents Chemother.*, 41:363–373, 1997.

[65] C-I Liu, GY Liu, Y Song, F Yin, ME Hensler, W-Y Jeng, V Nizet, AH-J Wang, and E Oldfield. A cholesterol biosynthesis inhibitor blocks *Staphylococcus aureus* virulence. *Science*, 319:1391–1394, 2008.

[66] DM Livermore. Of *Pseudomonas*, porins, pumps and carbapenems. *J. Antimicrob. Chemother.*, 47:247–250, 2001.

[67] DM Livermore. Multiple mechanisms of antimicrobial resistance in *Pseudomonas aeruginosa*: our worst nightmare? *Clin. Infect. Dis.*, 34:634–640, 2002.

[68] T Maeda, R García-Contreras, M Pu, L Sheng, LR Garcia, M Tomás, and TK Wood. Quorum quenching quandary: resistance to antivirulence compounds. *ISME J.*, 6:493–501, 2012.

[69] DE Mager, E Wyska, and WJ Jusko. Diversity of mechanism-based pharmacodynamic models. *Drug Metab. and Dispos.*, 31:510–518, 2003.

[70] R Marcus, M Paul, H Elphick, and L Leibovici. Clinical implications of β-lactam–aminoglycoside synergism: systematic review of randomised trials. *Int. J. Antimicrob. Agents*, 37, 2011.

[71] Mariana Ruiz Villarreal. Average prokaryote cell. `https://commons.wikimedia.org/wiki/File:Average_prokaryote_cell-_en.svg` - Last accessed January 9th, 2019.

[72] B Mellbye and M Schuster. The sociomicrobiology of antivirulence drug resistance: a proof of concept. *MBio*, 2:e00131–11, 2011.

[73] R Mercier, Y Kawai, and J Errington. General principles for the formation and proliferation of a wall-free (l-form) state in bacteria. *Elife*, 3:e04629, 2014.

[74] S Michelson and D Slate. A mathematical model of the p-glycoprotein pump as a mediator of multidrug resistance. *Bull. Math. Biol.*, 54:1023–1038, 1992.

[75] L Monahan, L Turnbull, S Osvath, D Birch, I Charles, and C Whitchurch. Rapid conversion of *Pseudomonas aeruginosa* to a spherical cell morphotype facilitates

tolerance to carbapenems and penicillins but increases susceptibility to antimicrobial peptides. *Antimicrob. Agents Ch.*, 58:1956–1962, 2014.

[76] J Monod. The growth of bacterial cultures. *Annu. Rev. Microbiol.*, 3:371–394, 1949.

[77] JW Mouton and MF Michel. Pharmacokinetics of meropenem in serum and suction blister fluid during continuous and intermittent infusion. *J. Antimicrob. Chemother.*, 28:911–918, 1991.

[78] LR Mulcahy, JL Burns, S Lory, and K Lewis. Emergence of *Pseudomonas aeruginosa* strains producing high levels of persister cells in patients with cystic fibrosis. *J. Bacteriol.*, 192:6191–6199, 2010.

[79] H Nikaido and REW Hancock. Outer membrane permeability of *Pseudomonas aeruginosa*. *The bacteria*, 10:145–193, 1986.

[80] R Nordfelth, AM Kauppi, HA Norberg, H Wolf-Watz, and M Elofsson. Small-molecule inhibitors specifically targeting type iii secretion. *Infect. Immun.*, 73:3104–3114, 2005.

[81] AS Novozhilov, GP Karev, and EV Koonin. Mathematical modeling of evolution of horizontally transferred genes. *Mol. Biol. Evol.*, 22:1721–1732, 2005.

[82] SK Olofsson and Otto Cars. Optimizing drug exposure to minimize selection of antibiotic resistance. *Clin. Infect. Dis.*, 45:S129–S136, 2007.

[83] ME Onwuamaegbu, RA Belcher, and C Soare. Cell wall-deficient bacteria as a cause of infections: a review of the clinical significance. *J. Int. Med. Res.*, 33:1–20, 2005.

[84] World Health Organization. Antimicrobial resistance: global report on surveillance 2014. *WHO*, 2014.

[85] World Health Organization et al. Who global strategy for containment of antimicrobial resistance. *WHO*, 2001.

[86] IK Paterson, A Hoyle, G Ochoa, C Baker-Austin, and NGH Taylor. Optimising antibiotic usage to treat bacterial infections. *Sci. Rep.*, 6, 2016.

[87] JS Pinkner, H Remaut, F Buelens, E Miller, V Åberg, N Pemberton, M Hedenström, A Larsson, P Seed, G Waksman, et al. Rationally designed small compounds inhibit pilus biogenesis in uropathogenic bacteria. *Proc. Natl. Acad. Sci. U.S.A.*, 103:17897–17902, 2006.

[88] AM Queenan and K Bush. Carbapenemases: the versatile β-lactamases. *Clin. Microbiol. Rev.*, 20:440–458, 2007.

[89] AM Queenan, W Shang, R Flamm, and K Bush. Hydrolysis and inhibition profiles of β-lactamases from molecular classes a to d with doripenem, imipenem, and meropenem. *Antimicrob. Agents Chemother.*, 54:565–569, 2010.

[90] J Quick, N Cumley, CM Wearn, M Niebel, C Constantinidou, CM Thomas, MJ Pallen, NS Moiemen, A Bamford, B Oppenheim, et al. Seeking the source of *Pseudomonas aeruginosa* infections in a recently opened hospital: an observational study using whole-genome sequencing. *BMJ open*, 4, 2014.

[91] F Rafii, J Sutherland, and C Cerniglia. Effects of treatment with antimicrobial agents on the human colonic microflora. *Ther. Clin. Risk Manag.*, 4:1343, 2008.

[92] TB Rasmussen, ME Skindersoe, T Bjarnsholt, RK Phipps, KB Christensen, PO Jensen, JB Andersen, B Koch, TO Larsen, M Hentzer, et al. Identity and effects of quorum-sensing inhibitors produced by penicillium species. *Microbiology*, 151:1325–1340, 2005.

[93] FJ Richards. A flexible growth function for empirical use. *J. Exp. Bot.*, 10:290–301, 1959.

[94] PA Roberts, RM Huebinger, E Keen, A Krachler, and S Jabbari. Predictive modelling of a novel anti-adhesion therapy to combat bacterial colonisation of burn wounds. *PLoS Comput. Biol.*, 14, 2018.

[95] R Rosqvist, S Håkansson, Å Forsberg, and H Wolf-Watz. Functional conservation of the secretion and translocation machinery for virulence proteins of yersiniae, salmonellae and shigellae. *EMBO J.*, 14:4187, 1995.

[96] CT Rueden, J Schindelin, MC Hiner, BE DeZonia, AE Walter, ET Arena, and KW Eliceiri. Imagej2: Imagej for the next generation of scientific image data. *BMC Bioinformatics*, 18:529, 2017.

[97] J Schindelin, I Arganda-Carreras, E Frise, V Kaynig, M Longair, T Pietzsch, S Preibisch, C Rueden, S Saalfeld, B Schmid, et al. Fiji: an open-source platform for biological-image analysis. *Nat. Methods*, 9:676–682, 2012.

[98] AM Smith, JA McCullers, and FR Adler. Mathematical model of a three-stage innate immune response to a pneumococcal lung infection. *J. Theor. Biol.*, 276:106–116, 2011.

[99] C Spalding, E Keen, DJ Smith, A-M Krachler, and S Jabbari. Mathematical modelling of the antibiotic-induced morphological transition of *Pseudomonas aeruginosa*. *PLoS Comput. Biol.*, 14, 2018.

[100] M Subbiah, EM Top, DH Shah, and DR Call. Selection pressure required for long-term persistence of blacmy-2-positive inca/c plasmids. *Appl. Environ. Microbiol.*, 77, 2011.

[101] Y Sumita, M Fukasawa, and T Okuda. Comparison of two carbapenems, sm-7338 and imipenem: affinities for penicillin-binding proteins and morphological changes. *J. Antibiot.*, 43:314–320, 1990.

[102] L Ternent, RJ Dyson, AM Krachler, and S Jabbari. Bacterial fitness shapes the population dynamics of antibiotic-resistant and susceptible bacteria in a model of combined antibiotic and anti-virulence treatment. *J. Theor. Biol.*, 372:1–11, 2015.

[103] F Thalhammer, F Traunmüller, I El Menyawi, M Frass, UM Hollenstein, GJ Locker, B Stoiser, T Staudinger, R Thalhammer-Scherrer, and H Burgmann. Continuous infusion versus intermittent administration of meropenem in critically ill patients. *J. Antimicrob. Chemother.*, 43:523–527, 1999.

[104] M Trautmann, M Heinemann, R Zick, A Möricke, M Seidelmann, and D Berger. Antibacterial activity of meropenem against *Pseudomonas aeruginosa*, including antibiotic-induced morphological changes and endotoxin-liberating effects. *Eur. J. Clin. Microbiol. Infect. Dis.*, 17:754–760, 1998.

[105] J Trias and H Nikaido. Outer membrane protein d2 catalyzes facilitated diffusion of carbapenems and penems through the outer membrane of *Pseudomonas aeruginosa*. *Antimicrob. Agents Chemother.*, 34:52–57, 1990.

[106] L Turnbull, M Toyofuku, AL Hynen, M Kurosawa, G Pessi, NK Petty, SR Osvath, G Cárcamo-Oyarce, ES Gloag, R Shimoni, et al. Explosive cell lysis as a mechanism

for the biogenesis of bacterial membrane vesicles and biofilms. *Nat. Commun.*, 7:11220, 2016.

[107] LS Tzouvelekis, A Markogiannakis, M Psichogiou, PT Tassios, and GL Daikos. Carbapenemases in *Klebsiella pneumoniae* and other enterobacteriaceae: an evolving crisis of global dimensions. *Clin. Microbiol. Rev.*, 25:682–707, 2012.

[108] LR Usher, RA Lawson, I Geary, CJ Taylor, CD Bingle, GW Taylor, and MKB Whyte. Induction of neutrophil apoptosis by the *Pseudomonas aeruginosa* exotoxin pyocyanin: a potential mechanism of persistent infection. *J. Immunol.*, 168:1861–1868, 2002.

[109] T Vogwill, M Kojadinovic, and RC MacLean. Epistasis between antibiotic resistance mutations and genetic background shape the fitness effect of resistance across species of *Pseudomonas*. *Proc. R. Soc. B*, 283, 2016.

[110] VV Volkova, C Lanzas, Z Lu, and YT Gröhn. Mathematical model of plasmid-mediated resistance to ceftiofur in commensal enteric *Escherichia coli* of cattle. *PLoS ONE*, 7:e36738, 2012.

[111] JP Ward, JR King, AJ Koerber, P Williams, JM Croft, and RE Sockett. Mathematical modelling of quorum sensing in bacteria. *Math. Med. Biol.*, 18:263–292, 2001.

[112] DJ Waxman and JL Strominger. Penicillin-binding proteins and the mechanism of action of β-lactam antibiotics. *Annu. Rev. Biochem.*, 52:825–869, 1983.

[113] JE Wigginton and D Kirschner. A model to predict cell-mediated immune regulatory mechanisms during human infection with *Mycobacterium tuberculosis*. *J. Immunol.*, 166, 2001.

[114] K Wolf, HJ Betts, B Chellas-Géry, S Hower, CN Linton, and KA Fields. Treatment of *Chlamydia trachomatis* with a small molecule inhibitor of the yersinia type iii secretion system disrupts progression of the chlamydial developmental cycle. *Molec. Microbiol.*, 61:1543–1555, 2006.

[115] KJ Wright, PC Seed, and SJ Hultgren. Development of intracellular bacterial communities of uropathogenic *Escherichia coli* depends on type i pili. *Cell. Microbiol.*, 9:2230–2241, 2007.

[116] Y Yamagishi, M Hagihara, H Kato, J Hirai, N Nishiyama, Y Koizumi, D Sakanashi, H Suematsu, H Nakai, and H Mikamo. In vitro and in vivo pharmacodynamics of colistin and aztreonam alone and in combination against multidrug-resistant *Pseudomonas aeruginosa*. *Chemotherapy*, 62, 2017.

[117] P Yeh, AI Tschumi, and R Kishony. Functional classification of drugs by properties of their pairwise interactions. *Nat. Genet.*, 38:489, 2006.

[118] MH Zwietering, Il Jongenburger, FM Rombouts, and K van't Riet. Modeling of the bacterial growth curve. *Appl. Environ. Microbiol.*, 56:1875–1881, 1990.